

Adam Mickiewicz University in Poznań

Faculty of Physics

**Experimental studies of particle-covered droplets in electric fields:
Mechanical and rheological properties of droplets and interfacial
particle organization**

A dissertation submitted for the Degree of Doctor of Philosophy in Physics

by

Khobaib Khobaib

supervised by:

Prof. UAM dr hab. Tomasz Hornowski

co-supervised by:

Prof. UAM dr hab. Zbigniew Rozynek



Poznań 2021

Acknowledgments

I would like to thank my supervisor, Prof. Tomasz Hornowski, for his considerable enthusiasm, encouragement, help and scientific input throughout my PhD. I deeply appreciate the guidance from my co-supervisor Prof. Zbigniew Rozynek. I have been in touch with him from the first day of my PhD, and he has consistently inspired me to become a better communicator and devoted scientist. I feel incredibly grateful for his mentorship. His encouragement and backing were crucial to make the PhD one of my most satisfying experiences so far.

I would like to express gratitude to Dr. Alexander Mikkelsen, who also supported me unconditionally during my PhD. He always shared his insight and challenged what I thought and what I knew about the topics. Our discussions typically left me with a more profound comprehension of physics and new ideas, I am truly grateful for his guidance and excellent support at all time. I would like to thank Prof. Arkadiusz Józefczak for giving me an opportunity to be his teaching assistant, and also for his kind support in many aspects during my PhD.

I would like to thank Prof. Knut Jørgen Måløy and Dr. Michał Rajńák for their productive collaboration and for allowing me to conduct the experiments in their laboratories. I would also like to thank Prof. Vinothan Manoharan for hosting me as a visiting researcher and allowing me to observe research at Harvard University closely. I would like to thank members of Manoharan Lab for showing me the laboratory and for the fruitful discussions.

I also give thanks to former and current colleagues at UAM: Dr. Tomasz Kubiak, Dr. Peter Keša, Joanna Banaszak, Dawid Surdeko, Yaroslav Harkavyi, Rafał Bielas, and Bassam Jamil. Thanks for the companionship, encouragement, support, productive conversations and the wonderful time we had together. I am additionally grateful to the Faculty of Physics administration for the help and for replying all my non-physics related inquiries.

I also want to thank several friends for being a source of joy. Maragadham Selvakumar, you are my oldest friend. Thank you for being constant in my life and for being there when I need you. Alauddin Khan, thank you for your warm friendship; your guidance is immensely appreciated. Yaroslav Harkavyi, Viktoriia Drushlyak, Manjunath Bhat, Nandan Babu, and Vishal Vashistha, thank you for your honest companionship and for staying in touch. I would also like to say special thanks to Dr. Agnieszka Magdziarz for treating me like a family member.

Ultimately and in particular, I would like to thank my family for their help and faith in me at each phase of my life and the tremendous sacrifices they have made to make sure I accomplish my dreams and objectives. For that, I am grateful beyond words.

I thank the Polish National Science Centre for financial support through the research project within the OPUS funding scheme (2015/19/B/ST3/03055: *Mechanical properties, specific release and motility of patchy colloidosomes—an emerging class of structures*), and PRELUDIUM funding scheme (2019/35/N/ST5/02821: *Electric-field-induced deformation and crumpling of non-spherical particle shells formed on droplets*).



Table of contents

Abstract	vii
Abstract in Polish	ix
List of publications constituting the dissertation	xi
Declarations of authorship contribution	xiii
Chapter 1 Introduction	- 1 -
Chapter 2 Particle-free droplet in electric fields	- 4 -
2.1. Droplet deformation under uniform electric field	- 4 -
2.2. Governing equations for the pure dielectric droplet model (PDM)	- 4 -
2.3. Governing equations for the leaky dielectric droplet model (LDM)	- 7 -
2.4. Electrohydrodynamic convective flow	- 12 -
2.5. Corrections to the LDM	- 12 -
2.6. Droplet in moderate and strong electric fields	- 14 -
2.6.1. Electrorotation	- 14 -
2.6.2. Stability and break up	- 16 -
Chapter 3 Particle-covered droplet in electric fields	- 18 -
3.1. Pickering droplet	- 18 -
3.2. Deformation of particle-covered droplet under electric field	- 19 -
3.3. Influence of surface particle on the EHD flows	- 20 -
3.4. Presence of particle shell alters electrorotation of a droplet	- 21 -
3.5. Nonspherical droplets in electric field	- 22 -
3.6. Structuring of the particles at droplet interface under electric field	- 23 -
Thesis development—introduction to the Papers	- 25 -
References	- 31 -
Publications constituting the dissertation	- 37 -
Appendix I: List of other publications	xv
Appendix II: List of significant conference presentations	xv
Appendix III: List of awards and distinctions	xvi

Abstract

This thesis contains fundamental experimental studies in soft matter physics, focusing on the understanding of mechanical properties and kinetics of particle-covered droplets. In my research, I utilized electric field methods for the formation of particle-laden droplets and investigation of their mechanical and rheological properties. I also used different electric field approaches to study organization of the particles adsorbed at the droplet interfaces. These electric phenomena include electrohydrodynamic circulation flows, electrocoalescence, and dielectrophoretic and electrophoretic interactions.

My research concerns a single particle-covered droplet subjected to uniform DC and AC electric fields, although I also investigated the behavior of droplets in a non-uniform field. The results included in this thesis cover studies on the droplet's deformation and relaxation, electrorotation, and arrested coalescence, as well as the mechanics of a particle shell formed on the fluid–fluid interface. The knowledge gained from the experiments (supplemented by theoretical studies) on individual droplets will be useful in studying more complex systems, such as emulsions. This knowledge should also be valuable for designing new types of stable emulsions and microcapsules that can be used in various technological applications such as in food technology, pharmaceutical products, cosmetics and drug delivery. In addition, the results included in this thesis open a new route for assembly of colloidal and granular particles on fluid–fluid interfaces.

At the start of my Ph.D. work, the literature on droplets subjected to electric fields concerned mainly spherical droplets, either particle-free or fully covered by particles. Those fully-covered droplets typically had a homogenous shell. I decided to expand the previous studies by investigating droplets with different particle coverage, particle shell morphology and shape. I studied in detail the effects of several parameters (such as strength, frequency or uniformity of electric field; size and electrical properties of particles; viscosity and electrical conductivity of fluids, and more) on the deformation, and electrorotation of oil-in-oil emulsion droplets. In addition, I exploit the possibility of using different parameters of an electric field, for instance, to actively control the spatial arrangements of particles on the droplet's surface. Such new usage of an electric field to form an active smart structure may facilitate simple laboratory operations and can be used to manufacture new materials.

Abstract in Polish

Moja rozprawa doktorska zawiera wyniki badań podstawowych w zakresie fizyki materii miękkiej i wnosi wkład w zrozumienie mechanicznych właściwości oraz kinetyki zachowania kropeł pokrytych cząstkami stałymi. Do uzyskania takich kropeł i badania ich mechanicznych i reologicznych właściwości wykorzystywałem pole elektryczne, które umożliwiło mi także obserwowanie różnych form organizacji cząstek na powierzchni międzyfazowej kropeł. Mechanizm ich powstawania opierał się na zjawiskach elektrycznych, takich jak pływy elektrohydrodynamiczne, elektrokoalescencja, dielektroforeza czy elektroforeza.

Większość moich badań dotyczyła pojedynczej kropli pokrytej cząstkami stałymi poddanej działaniu jednorodnego stałego bądź zmiennego pola elektrycznego, choć obserwowałem także zachowanie kropli w niejednorodnym polu elektrycznym. Wyniki moich badań dotyczą deformacji, relaksacji, elektrorotacji kropeł, koalescencji oraz mechanizmu tworzenia się warstwy cząstek na powierzchni międzyfazowej. Wiedza zdobyta na podstawie doświadczeń przeprowadzanych na pojedynczych kroplach (podparta analizą teoretyczną) pozwala lepiej zrozumieć bardziej złożone układy, jak na przykład emulsje. Wyniki przedstawione w mojej rozprawie powinny okazać się przydatne przy opracowywaniu nowych rodzajów stabilnych emulsji lub mikrokapsuł, które mogą znaleźć różne zastosowanie w technologiach produkcji żywności, przemyśle farmaceutycznym, kosmetycznym czy sposobach dostarczania leków w terapiach celowanych. Ponadto wyniki zawarte w mojej rozprawie doktorskiej wskazują na nowe sposoby organizacji cząstek koloidalnych i ziarnistych na powierzchni międzyfazowej.

Gdy zaczynałem pracę nad swoją rozprawą, większość prac dotyczyła kropeł sferycznych, niepokrytych cząstkami lub pokrytych w całości. Krople pokryte całkowicie cząstkami zazwyczaj wytworzone są z jednorodnej warstwy cząstek stałych. W swojej pracy doktorskiej rozszerzyłem dotychczasowe badania na krople o różnym stopniu pokrycia cząstkami i o różnej budowie oraz kształcie warstwy cząstek otaczającej kroplę. Szczegółowo zbadałem wpływ kilku parametrów (takich jak między innymi natężenie, częstotliwość i niejednorodność pola elektrycznego; rozmiar, właściwości elektryczne cząstek oraz lepkość i przewodnictwo elektryczne cieczy tworzących kroplę i jej otoczenie) na deformację, elektrorotację kropli tworzących emulsję typu olej w oleju. Ponadto zbadałem możliwość wykorzystania różnych parametrów pola elektrycznego, na przykład do aktywnego kontrolowania przestrzennego ustawienia cząstek na powierzchni kropli. Tego rodzaju wykorzystanie pola elektrycznego do tworzenia aktywnych, inteligentnych struktur może ułatwić proste prace laboratoryjne oraz znaleźć zastosowanie w produkcji nowych materiałów.

List of publications constituting the dissertation

- I. Transient deformation dynamics of particle laden droplets in electric field
A Mikkelsen, Z Rozynek, **K Khobaib**, P Dommersnes and J O Fossum
Colloids and Surfaces A 532, 252–256 (2017)
- II. Electric field-driven assembly of sulfonated polystyrene microspheres
A Mikkelsen, J Wojciechowski, M Rajňák, J Kurimský, **K Khobaib**, A Kertmen and
Z Rozynek
Materials 10(4), 329 (2017)
- III. Particle-covered drops in electric fields: Drop deformation and surface particle
organization
A Mikkelsen, **K Khobaib**, F K Eriksen, K J Måløy and Z Rozynek
Soft Matter 14, 5442–5451 (2018)
- IV. Opening and closing of particle shells on droplets via electric fields and its
applications
Z Rozynek, **K Khobaib** and A Mikkelsen
ACS Appl. Mater. Interfaces 11, 22840–22850 (2019)
- V. Particle-covered droplet and a particle shell under compressive electric stress
K Khobaib, T Hornowski and Z Rozynek
Phys. Rev. E 103, 062605 (2021)
- VI. Electrorotation of particle-coated droplets: from fundamentals to applications
Z Rozynek, J Banaszak, A Mikkelsen, **K Khobaib** and A Magdziarz
Soft Matter 17, 4413–4425 (2021)
- VII. Electric-field-induced deformation, yielding, and crumpling of jammed particle
shells formed on non-spherical Pickering droplets
K Khobaib, A Mikkelsen, T Vincent-Dospital and Z Rozynek
Soft Matter 17, 5006–5017 (2021)

In preparation

- VIII. Mechanical properties of particle-covered droplets probed by non-uniform
electric field
K Khobaib and T Hornowski
To be submitted to Phys. Rev. E

Declarations of authorship contribution

My contribution to the papers

I hereby declare that I contributed to the following publications:

- Transient deformation dynamics of particle laden droplets in electric field, A Mikkelsen, Z Rozynek, K Khobaib, P Dommersnes and J O Fossum, *Colloids and Surfaces A* 532, 252–256 (2017) by co-performing experiments presented in Fig. 1, Fig. 2, and Fig. 3, and by taking part in discussions leading towards the finalization of the manuscript;
- Electric field-driven assembly of sulfonated polystyrene microspheres, A Mikkelsen, J Wojciechowski, M Rajňák, J Kurimský, K Khobaib, A Kertmen and Z Rozynek, *Materials* 10(4), 329 (2017) by co-performing experiments of which the results are presented in Fig. 5 and Fig.7, and by taking active part in discussions leading towards the finalization of the manuscript;
- Particle-covered drops in electric fields: Drop deformation and surface particle organization, A Mikkelsen, K Khobaib, F K Eriksen, K J Måløy and Z Rozynek, *Soft Matter* 14, 5442–5451 (2018) by co-performing experiments of which the results are presented in Fig. 2–6, by taking part in discussions leading towards the finalization of the manuscript;
- Opening and closing of particle shells on droplets via electric fields and its applications, Z Rozynek, K Khobaib and A Mikkelsen, *ACS Appl. Mater. Interfaces* 11, 25, 22840–22850 (2019) by co-designing all the experiments, performing the experiments of which the results are presented in Fig. 2, Fig. 3, Fig. 4, Fig. 5a, Fig. 5d, Fig. 6, Fig. 8, Fig. S1, Fig. S2, Fig. S3, and Figure S5, by contributing to data analysis and presentation, and by participating in writing and discussions towards the finalization of the manuscript together with all authors;
- Particle-covered droplet and a particle shell under compressive electric stress, K Khobaib, T Hornowski and Z Rozynek, *Phys. Rev. E* 103, 062605 (2021) by initiating the project, designing and performing all of the experiments, writing the first draft of the paper, and by participating in writing and discussions towards the finalization of the manuscript together with all authors;
- Electrorotation of particle-coated droplets: from fundamentals to applications, Z Rozynek, J Banaszak, A Mikkelsen, K Khobaib and A Magdziarz, *Soft Matter* 17, 4413–4425 (2021) by performing the experiments of which the results are presented in Fig. 7, Fig. 9 and Fig. S3, and by participating in writing and discussions towards the finalization of the manuscript together with all authors;
- Electric-field-induced deformation, yielding, and crumpling of jammed particle shells formed on non-spherical Pickering droplets, K Khobaib, A Mikkelsen, T Vincent-Dispotal and Z Rozynek, *Soft Matter* 17, 5006–5017 (2021) by conducting all the actual experiments of which the results are presented in Figs. 2–10, writing the first version of the manuscript, and by participating in writing and discussions towards the finalization of the manuscript together with all authors;
- Mechanical properties of particle-covered droplets probed by non-uniform electric field, K Khobaib and T Hornowski (*in preparation*) by initiating the project, designing and performing all of the experiments, writing the first draft of the manuscript.

Confirmed by:



Supervisor



Co-supervisor



Khobaib Khobaib

Alexander Mikkelsen
Ph.D.
Telephone no.: (+47) 41612999
Email: alexander.mikkelsen@ffi.no

Dated: 02/07/2021

Co-author statement

I hereby declare that I contributed to the following publications:

- Mikkelsen A, Wojciechowski J, Rajnak M, Kurimsky J, Khobaib K, Kertmen A, et al. Electric field-driven assembly of sulfonated polystyrene microspheres. *Materials* 10:329 (2017)
by co-performing experiments presented in Fig. 5 and Fig. 7, by taking part in discussions leading towards the finalization of the manuscript, and by co-authoring the paper;
- Mikkelsen A, Rozynek Z, Khobaib K, Dommersnes P, Fossum J O, Transient deformation dynamics of particle laden droplets in electric field. *Colloids and Surfaces A*, 532, 252–256 (2017)
by co-designing all experiments, co-performing experiments presented in Fig. 1–4, writing the first draft of the manuscript, and by taking part in discussions leading towards the finalization of the manuscript;
- Mikkelsen A, Khobaib K, Eriksen F K, Måløy K J, Rozynek Z, Particle-covered drops in electric fields: Drop deformation and surface particle organization. *Soft Matter* 14, 5442–5451 (2018)
by co-initiating the project, co-designing all experiments, co-performing experiments presented in Fig. 2–5, writing the first draft of the manuscript, and by taking part in discussions leading towards the finalization of the manuscript;
- Rozynek Z, Khobaib K, Mikkelsen A, Opening and Closing of Particle Shells on Droplets via Electric Fields and its Applications, *ACS Appl. Mater. Interfaces* 11, 25, 22840–22850 (2019) by assisting in the experiments of which the results were presented in Fig. 5d, Fig. 6, and Fig. S2, by contributing to data analysis and presentation, and by participating in writing and discussions towards the finalization of the manuscript together with all authors;
- Rozynek Z, Banaszak J, Mikkelsen A, Khobaib K, Magdziarz A, Electrorotation of particle-coated droplets: from fundamentals to applications, *Soft Matter* 17, 4413–4425 (2021) by co-initiating the project and co-designing the experiments, by performing the experiments of which the results were presented in Fig. 8, and by taking part in discussions leading towards the finalization of the manuscript;
- Khobaib K, Mikkelsen A, Vincent-Disptal T, Rozynek Z, Electric-field-induced deformation, yielding, and crumpling of jammed particle shells formed on non-spherical Pickering droplets, *Soft Matter* 17, 5006–5017 (2021) by co-initiating the project, performing the preliminary experiments, and by taking part in discussions leading towards the finalization of the manuscript.

Sincerely yours



Alexander Mikkelsen



UNIwersYTET
WARSAWski

Wydział Chemii



Warszawa, dnia 05.07.2021

Jarosław Wojciechowski
Uniwersytet Warszawski
Wydział Chemii

Oświadczam, że w pracy (Mikkelsen A, Wojciechowski J, Rajňák M, Kurimský J, Khobaib K, Kertmen A, et al. Electric field-driven assembly of sulfonated polystyrene microspheres. *Materials* 10:329, 2017) mój udział polegał na opracowaniu metody chemicznej modyfikacji powierzchni cząstek polistyrenowych wykorzystanych do eksperymentów, oraz na pomocy w pomiarach elektoreologicznych, których rezultaty zaprezentowano na ilustracji 3.

Jarosław Wojciechowski



Institute of Experimental Physics
Slovak Academy of Sciences
Watsonova 47, 040 01 Košice, SLOVAKIA
Tel.: +421-55-7922201, Fax: +421-55-6336292, E-mail:
rainak@saske.sk



Khobaib Khobaib
Uniwersytet im. Adama Mickiewicza
ul. Uniwersytetu Poznańskiego 2
61-614 Poznan, Poland

Košice, 30 June 2021

Michal Rajňák, doctor
Institute of Experimental Physics
Slovak Academy of Sciences

To whom it may concern

I hereby declare that I contributed to the following publication:

Mikkelsen A, Wojciechowski J, Rajňák M, Kurimský J, Khobaib K, Kertmen A, et al. Electric field-driven assembly of sulfonated polystyrene microspheres.

***Materials* 10:329 (2017)**

by co-performing electric conductance and dielectric constant experiments, and by analyzing the data presented in Table 2. I also took part in discussions leading towards the finalization of the manuscript.

Michal Rajňák



TECHNICAL UNIVERSITY OF KOŠICE



Faculty of Electrical Engineering and Informatics

Department of Electric Power Engineering

Dr.h.c. prof. Ing. Michal Kolcun, PhD., Head of Department

Mäsiarska 74

042 00 Košice, Slovakia

tel.: +421 55/602 3551

e-mail: michal.kolcun@tuke.sk
<http://www.tuke.sk/fei-kee>

Khobaib Khobaib
Uniwersytet im. Adama Mickiewicza
ul. Uniwersytetu Poznanskiego 2
61-614 Poznan, Poland

Code Number

Contact person/phone ext.
prof. Kurimský/3550

Košice
30 June 2021

Declaration of contribution

To whom it may concern

I hereby declare that I contributed to the following publications:

- Mikkelsen A, Wojciechowski J, Rajňák M, Kurimský J, Khobaib K, Kertmen A, et al.
Electric field-driven assembly of sulfonated polystyrene microspheres. *Materials*
10:329 (2017)

by co-performing electric conductance and dielectric constant experiments, and by analyzing the data presented in Table 2. I also took part in discussions leading towards the finalization of the manuscript.

Best regards



Prof. Ing. Juraj Kurimský, PhD.
Department of Electric Power Engineering
Technical University of Kosice



Paul Dommersnes
Department of Physics
Norwegian University of Science and Technology

July 6, 2021

Co-author statement

To whom it may concern

I hereby declare that I contributed to the following publication:

- Mikkelsen A, Rozynek Z, Khobaib K, Dommersnes P, Fossum JO. Transient deformation dynamics of particle laden droplets in electric field. *Colloids and Surfaces A*, 532, 252-256 (2017) by initiating the project together with Prof J.O. Fossum, by planning and designing all experiments, together with J.O. Fossum, A. Mikkelsen, and Z. Rozynek, by writing the first versions of the manuscript together with A. Mikkelsen and J.O. Fossum, by contributing to discussions leading towards the finalization of the manuscript together with all authors.

Sincerely yours

A handwritten signature in blue ink that reads "Paul Dommersnes". The signature is written in a cursive style with a large initial 'P'.

Paul Dommersnes



03.07.2021, Poznan

To whom it may concern

I hereby declare that I contributed to the following publication:

A. Mikkelsen; J. Wojciechowski; M. Rajnak, J. Kurimsky; K. Khobaib; A. Kertmen; Z. Rozynek.
Electric field-driven assembly of sulfonated polystyrene microspheres. *Materials* 2017
Apr; 10(4): 329.

by performing FTIR experiments, analyzing the results presented in Figure 1 and taking part
in discussions leading towards the finalization of the manuscript.

Dated: 30 June 2021

Contribution to publication

I hereby declare that I contributed to the following publication:

- Mikkelsen A, Khobaib K, Eriksen FK, Måløy KJ, Rozynek Z.

Particle-covered drops in electric fields: Drop deformation and surface particle organization.

Soft Matter doi: 10.1039/c8sm00915e (2018)

by co-designing the experiments on electrohydrodynamic flows, and co-performing experiments presented in Fig. 3 and Fig. 5, by taking part in discussions leading towards the finalization of the manuscript.

Sincerely yours,



Fredrik K. Eriksen





Knut Jørgen Måløy
Professor
Telephone no.: (+47) 22856524
Email: k.j.maloy@fys.uio.no

Dated: 01/07/2021

I hereby declare that I contributed to the following publication:

- Mikkelsen A, Khobaib K, Eriksen FK, Måløy KJ, Rozynek Z.
Particle-covered drops in electric fields: Drop deformation and surface particle organization.
Soft Matter doi: 10.1039/c8sm00915e (2018)
by co-designing the experiments on electrohydrodynamic flows, and co-performing experiments presented in Fig. 3 and Fig. 5, by taking part in discussions leading towards the finalization of the manuscript.

Sincerely Yours


Knut Jørgen Måløy



Dr. hab. Prof. UAM Tomasz Hornowski
hornaku@amu.edu.pl

July 5, 2021

Co-author statement

I hereby declare that I contributed to the following publications:

- Particle-covered droplet and a particle shell under compressive electric stress, K Khobaib, T Hornowski and Z Rozynek, Phys. Rev. E 103, 062605 (2021) by performing the theoretical calculations of which the results are presented in Fig. 4 and Fig. 6, and by participating in writing and discussions towards the finalization of the manuscript together with all authors;
- Mechanical properties of particle-covered droplets probed by non-uniform electric field, K Khobaib, Z Rozynek, and T Hornowski (*in preparation*) by performing the theoretical calculations of which the results are presented in Fig. 1, Fig. 2b, Fig. 3b, and Fig. 5b, and by participating in writing and discussions towards the finalization of the manuscript together with all authors.

Sincerely yours

Tomasz Hornowski



Dr. hab. Prof. UAM Zbigniew Rozynek
zbiroz@amu.edu.pl

July 4, 2021

Co-author statement

I hereby declare that I contributed to the following publications:

- Transient deformation dynamics of particle laden droplets in electric field, *Colloids and Surfaces A* 532, 252–256 (2017) by co-performing the experiments of which the results were presented in Fig. 1, Fig. 2 and Fig. 5;
- Electric field-driven assembly of sulfonated polystyrene microspheres, *Materials* 10(4), 329 (2017) by conducting the experiments of which the results were presented in Fig. 2, Fig. 4, and Fig. 6, and by participating in writing and discussions towards the finalization of the manuscript together with all authors;
- Particle-covered drops in electric fields: Drop deformation and surface particle organization, *Soft Matter* 14, 5442–5451 (2018) by conducting the experiments of which the results were presented in Fig. 6, Fig. S2, and supplementary Movies S1 and S2, and by participating in writing and discussions towards the finalization of the manuscript together with all authors;
- Opening and Closing of Particle Shells on Droplets via Electric Fields and its Applications, *ACS Appl. Mater. Interfaces* 11, 25, 22840–22850 (2019) by assisting in conducting the experiments of which the results were presented in Fig. 2, Fig. 4, Fig. 5a, Fig. 8, Fig. S1 and Fig. S5, by performing experiments of which the results were presented in Figs. 5b,c,e, Fig. 7, Fig. S4 and Fig. S6, and by participating in writing and discussions towards the finalization of the manuscript together with all authors;
- Particle-covered droplet and a particle shell under compressive electric stress, *Phys. Rev. E* 103, 062605 (2021) by participating in writing and discussions towards the finalization of the manuscript together with all authors;
- Electrorotation of particle-coated droplets: from fundamentals to applications, *Soft Matter* 17, 4413–4425 (2021) by performing the experiments of which the results were presented in Fig. 6, Fig. 10, Fig. S1, and Fig. S4. I wrote the first draft of the manuscript and participated in writing and discussions towards the finalization of the manuscript together with all authors;
- Electric-field-induced deformation, yielding, and crumpling of jammed particle shells formed on non-spherical Pickering droplets, *Soft Matter* 17, 5006–5017 (2021) by performing the preliminary experiments, and by participating in writing and discussions towards the finalization of the manuscript together with all authors;

Sincerely yours

Zbigniew Rozynek

Joanna Banaszak

Poznań, 02-07-2021

Co-author statement

I hereby declare that I contributed to the publication titled “Electrorotation of particle-coated droplets: from fundamentals to applications” published in *Soft Matter* 17, 4413–4425 (2021) by co-designing the experiments, performing the experiments of which the results are presented in Fig. 2–5 and Fig. S2, and by participating in writing and discussions towards the finalization of the manuscript together with all authors.

Sincerely yours



Joanna Banaszak



Dr. Agnieszka Magdziarz
agnmag1@amu.edu.pl

July 1, 2021

Co-author statement

I hereby declare that I contributed to the publication titled “Electrorotation of particle-coated droplets: from fundamentals to applications” published in *Soft Matter* 17, 4413–4425 (2021) by taking an active part in discussions on the interpretation of the data, and by participating in writing and discussions towards the finalization of the manuscript together with all authors.

Sincerely yours

Agnieszka Magdziarz

Dr. Tom Vincent-Dospital
Post-doctoral researcher at
PoreLab – Centre of Excellence

Dated: 30 June 2021

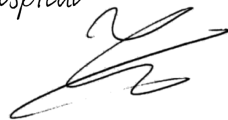
Contribution to publication

I hereby declare that I contributed to the following publication:

K Khobaib, A Mikkelsen, T Vincent-Dospital and Z Rozynek
Electric-field-induced deformation, yielding, and crumpling of jammed particle shells
formed on non-spherical Pickering droplets, *Soft Matter* 17, 5006–5017 (2021)
by performing data analysis (Fig. 8 and Fig. S3), and by participating in writing and
discussions towards the finalization of the manuscript together with all authors.

Sincerely yours,

Tom Vincent-Dospital



Tom Vincent-Dospital



Chapter 1 Introduction

Droplets with granular and colloidal particles at their interface have lately received significant research attention in both the applied and fundamental sciences [1–8]. This is because such droplets have characteristics that can be exploited for fabricating adaptive structures, porous materials [9], colloidal photonic crystals [10, 11], and responsive microcapsules [12]. In addition, the particle-covered droplet can be utilized as an experimental model for studying different phenomena and properties of the particle layer at droplet interface, for instance, particle structuring [4, 13], mechanical properties of particle layer [14], and wrinkling [15], folding [16], and buckling [17] on a droplet's curved interface. Particle-laden droplets are also considered as suitable materials to use in the biomedical and oil industries [18, 19], food technology [7], biofuel processing [20], pharmaceutical products [8], cosmetics [21] and drug delivery [22]. In this context, broadening the knowledge of mechanical and rheological properties of a particle-covered droplet and performance of a particle shell under applied force is crucial to further advancing the aforementioned research fields.

Experimental methodologies involved in research on pure droplets and particle-covered droplets include various mechanical [23–26], ultrasonic [27, 28], magnetic [29] and electric approaches. Electric fields have been demonstrated to be a suitable method for inducing and studying transient and steady-state deformations, rotation, as well as different kinds of instabilities of the droplets. Electric fields also enable structuring of particles at droplet interfaces by using electrohydrodynamic (EHD) circulation flows [4, 30, 31] and electric forces [32, 33].

The majority of studies on droplets subjected to electric fields concern spherical droplets, either particle-free or fully covered by particles. Those fully-covered droplets typically had a homogenous shell, i.e., one composed of particles of a single kind. In my work, I expand the previous studies by investigating droplets having different particle coverage and particle shell morphology. I use various electric field phenomena to prepare particle-covered droplets, including the EHD liquid flows and electrocoalescence. EHD liquid flows, dipolar interactions, electro-coalescence, and dielectrophoresis have been used to transport [34], sort or jam particles at the droplet's interface [35], and to remove particles from the droplet [36]. These phenomena can be also used to form droplets covered with desired concentration of particles, droplets with particles shells having distinct morphologies (homogenous or patchy shells), and stable non-spherical droplets, as demonstrated in the papers constituting this thesis.

Different electric field parameters, such as frequency, strength, mode (pulsating or continuous) or uniformity, and physical parameters of the fluids and particles, determine the dominant electrical mechanism in the systems that I study (i.e., an oil-in-oil emulsion droplet). For example, under direct current (DC) electric field, the electric stress compresses the droplet that acquires an oblate shape. On the other hand, if the same droplet is subjected to an alternating current (AC) electric field, the electric stress stretches the droplet that, in turn, acquires a prolate shape [37]. In my thesis, I study the effects of the above-listed parameters on the deformation, electrorotation and breakup of oil-in-oil emulsion droplets. In addition, I exploit the possibility of using different parameters of an electric field, for instance, to actively control the spatial arrangements of particles on the droplet's surface. Such new usage of an electric field to form an active smart structure may facilitate simple laboratory operations and can be used to manufacture new materials.

Deformation of particle-covered droplets under an electric field may provide information about their mechanical properties, such as elasticity and bending stiffness of the particle film, which depends on the particle size, shape, and three-phase contact angle. Relaxation of a deformed particle-covered droplet on releasing compressive stress is also an important mechanical property of the droplet. Several researchers have studied the relaxation of the particle-covered droplets after removing applied stress [24, 38]. Mikkelsen et al. [39] studied the relaxation dynamics of pure droplets and particle-covered droplets. The result showed that the particle-covered droplets relax more slowly than particle-free droplets. Rane et al. [26] studied the mechanical compression and decompression of liquid marble (droplet with a particle shell formed in air). After removing the compressive stress, they found that the droplets relax more slowly and exhibit hysteresis. Monteux et al. [40] and Xu et al. [41] also found a similar result by volume compression and relaxation of liquid marbles. In all these works, researchers studied droplets densely covered by particles. However, the influence of particle concentration or particle packing has not been studied extensively, creating a knowledge gap. In addition, different mechanisms of droplet compression and decompression were used in the abovementioned works. This may have certain consequences. For example, during the mechanical compression of a droplet by two flat slabs, the particles in the shell become loosely packed [26]. Whereas, in the electric method [39], the particles are kept tight during the application of the electric field. When the stress is removed, and the droplet returns to its original spherical shape, the particles need to rearrange on the droplet's surface.

I anticipated that the way particles rearrange during the healing of the particle shell determines the final particle shell morphology and ultimately the droplet shape in the absence of the external stress. This has not been studied before, therefore, I planned experiments to study how the particle-coverage influences the magnitude of droplet deformation and emergence of its deformation-hysteresis during compression and decompression of the droplet under an electric field.

In this thesis, I wanted to study particle-covered droplets and particle shells under applied electrical stress. I chose to work with an oil-in-oil emulsion droplet covered by either electrically conducting or insulating micro-particles and used uniform and non-uniform DC and AC electric fields. The primary experimental set-up used in most of the experiments was simple and rather inexpensive and was comprised of a sample cell placed on a mechanical XYZ translation stage, a digital microscope for viewing in the direction perpendicular to or along the electric field, a signal generator, a voltage amplifier for generating high-voltage signals, a light source, and a computer for data collection. Droplets with or without particles were simply made by using a mechanical pipette. The schematic illustration of the experimental set-up is presented in **Fig. 1**, and an example of a silicone oil droplet covered with polyethylene particles subjected under uniform DC electric field is shown in **Fig. 1b**. In all the experiments presented in the thesis, silicone oil constituted a droplet that was suspended in slightly more conductive castor oil. Various types of particles are used with a wide range of electrical conductivities from 10^{-11} to 10^7 S·m⁻¹, and sizes in a range of around 1–100 μ m.

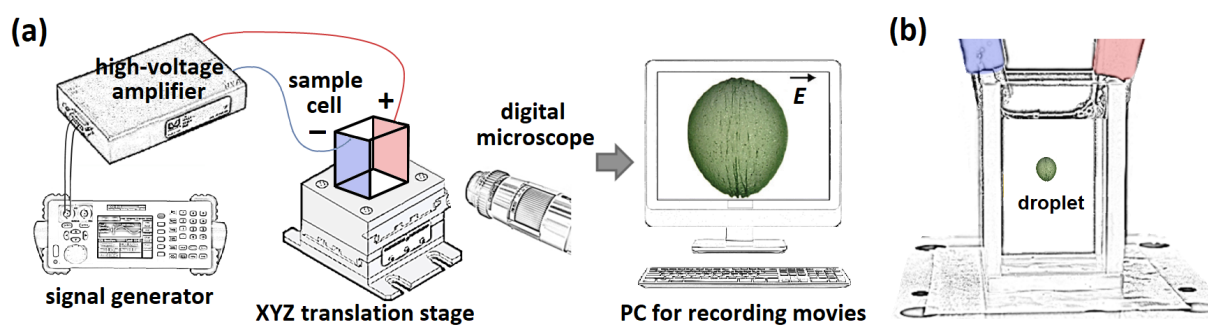


Fig. 1. Schematic figures illustrating the experimental setup used in most experiments: (a, b) The setup consisted of a sample cell placed on a mechanical XYZ translational stage, a digital microscope for viewing perpendicular to the direction of the applied electric field, a signal generator and a voltage amplifier for generating a high-voltage electric signal, which is provided to the electrodes inserted inside the sample cell via two crocodile clips, and a PC for data collection.

Chapter 2 Particle-free droplet in electric fields

2.1. Droplet deformation under uniform electric field

A bubble gas or liquid droplet suspended in another immiscible liquid may be deformed under electric field. The electric-field-induced deformation has been studied extensively both experimentally and theoretically. O'Konski and Thacher 1953 [42]; Taylor 1964 [43]; Garton and Krasucki 1964 [44]; Sherwood 1988 [45]; and Hua, Lim and Wang 2008 [46] described the prolate shape of the droplet deformation, i.e., the droplet deformed in the direction of the applied electric field. Whereas, Allan and Mason 1962 [47]; Torza, Cox and Mason 1971 [48]; Arp, Foister & Mason 1980 [49]; Vizika and Saville 1992 [50] and Ha and Yang 1995 [51] described the oblate deformation of the droplet, i.e., the droplet deformed perpendicular to the direction of the applied electric field.

Under the weak electric field, deformation of the droplet can be described by two different mathematical expressions: the pure dielectric droplet model (PDM) and the leaky dielectric droplet model (LDM). In the classical electrostatic model (PDM), both the droplet and the surrounding fluid are treated as perfectly insulating dielectrics. Therefore, the electric stress acting on a droplet only has a component normal to the droplet's surface, and only prolate deformation is allowed. To explain the deformation of the droplet in the direction of the electric field, the LDM was introduced. The LDM takes into account small conductivities of the fluids and enables relatively good prediction of the magnitude of droplet deformation when a droplet is either stretched or compressed by the electric field. As it will be discussed in Section 2.5, the LDM was further developed to better represent the experimental observations.

2.2. Governing equations for the pure dielectric droplet model (PDM)

Each fluid, including insulating oils, conducts electricity. However, a fluid (in the considered two-phase system) can be considered as a pure dielectric material, if it satisfies the condition $\tau_e \gg \tau_v$, ($\tau_e = \frac{\varepsilon}{\sigma}$ and $\tau_v = \frac{\rho_d L^2}{\mu}$) where τ_e is the Maxwell-Wagner charge relaxation time, τ_v is the time scale for the fluid motion that convect charge, ε is the permittivity of the fluid, σ is the conductivity of the fluid, ρ_d is the fluid density, μ is the fluid viscosity and L is the characteristics length scale [46]. The Maxwell–Faraday equation is:

$$\frac{\partial B}{\partial t} + \nabla \times E = 0, \quad (2.1)$$

when a droplet is placed in another immiscible liquid and subjected to an electric field.

Because the dynamic current in the considered system is very small, the magnetic induction effect is close to zero, and then Eq. (2.1) becomes:

$$\nabla \times E = 0. \quad (2.2)$$

Eq. (2.2) states that the electric field is irrotational, and the electric field potential in the form of the gradient of electric potential can be written as $E = -\nabla\phi$. According to the Gauss's law, the volume charge density is defined as:

$$\rho/\varepsilon_0 = \nabla \cdot (\varepsilon E). \quad (2.3)$$

In a pure dielectric medium, there is no free charge present in the medium. Therefore, Eq. (2.3) becomes:

$$\nabla \cdot (\varepsilon E) = 0. \quad (2.4)$$

As we know, $E = -\nabla\phi$. Therefore, Eq. (2.4) in terms of electric potential can be written as:

$$\nabla \cdot (\varepsilon \nabla\phi) = 0. \quad (2.5)$$

Because there are no free charges at the interface between the two fluids of different permittivities, the electric potential (ϕ) (Eq. (2.5)) can be reduced to the Laplace equation ($\nabla^2\phi = 0$).

The electric stress at droplet interface can be calculated by taking the divergence of the Maxwell stress tensor (T_m) [52], and written as:

$$F_{es} = \nabla \cdot T_m = -\frac{1}{2} E \cdot E \nabla \varepsilon + \rho E, \quad (2.6)$$

where E is the applied electric field, ε is the absolute permittivity or permittivity of the medium, and ρ is the volume charge density. For pure dielectric material, the volume charge density is zero and Eq. (2.6) can be reduced to:

$$F_{es} = -\frac{1}{2} E \cdot E \nabla \varepsilon. \quad (2.7)$$

Equations (2.4), (2.5) and (2.7) give the complete description of the pure dielectric model and show that, unlike in the LDM, electrical conductivity is not included in PDM.

Deformation of a pure dielectric droplet

In 1953, O'Konski and Thacher [42] predicted the first analytical result on the deformation of perfectly insulating droplets in a perfectly insulating medium under the application of the weak electric field. Later, in 1962 Allan and Mason [47] described the same model for

deformation expression by balancing the electric forces over surface tension and their result was similar to that of O'Konski and Thacher. When a pure dielectric droplet is suspended in a pure dielectric medium and subjected to an electric field (E_0), bound charges are formed at the interface between two mediums of different dielectric permittivities. The electric potential inside (ϕ_{in}) and outside (ϕ_{out}) of a sphere of radius a is given by [47]:

$$\phi_{in} = \left(\frac{3\varepsilon_{ex}}{\varepsilon_{in}+2\varepsilon_{ex}} \right) E_0 r \cos \theta, \quad (r < a) \quad (2.8)$$

$$\phi_{ex} = \left(1 - \frac{\varepsilon_{in}-\varepsilon_{ex}}{\varepsilon_{in}+2\varepsilon_{ex}} \frac{a^3}{r^3} \right) E_0 r \cos \theta, \quad (r > a) \quad (2.9)$$

where ε_{in} and ε_{ex} is the dielectric constant of the interior liquid (droplet) and exterior liquid (suspended fluid), respectively, (r, θ) are the polar coordinates, where r is the distance from the center of the sphere and θ is the angle between radius vector and the z-axis, see **Fig. 2**. The corresponding tangential and normal component of the electric field at the droplet interface is:

$$E_{t,ex} = \frac{1}{a} \left(\frac{\partial \phi_{ex}}{\partial \theta} \right) = - \left(\frac{3\varepsilon_{ex}}{\varepsilon_{in}+2\varepsilon_{ex}} \right) E_0 \sin \theta, \quad (r = a) \quad (2.10)$$

$$E_{n,ex} = \left(\frac{\partial \phi_{ex}}{\partial a} \right) = \left(\frac{3\varepsilon_{in}}{\varepsilon_{in}+2\varepsilon_{ex}} \right) E_0 \cos \theta, \quad (r = a) \quad (2.11)$$

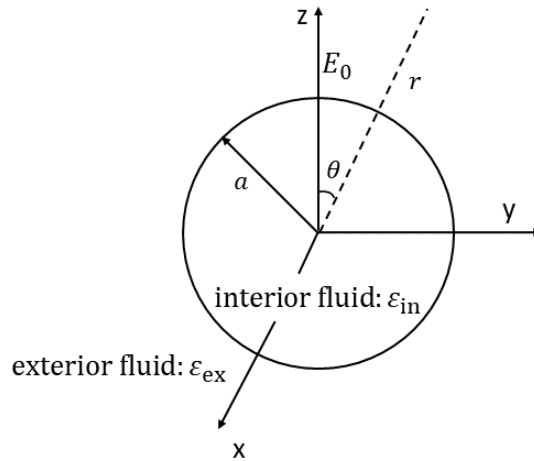


Fig. 2. Perfectly insulating droplet (ε_{in}) suspended in a perfectly insulating medium (ε_{ex}) and subjected to a uniform electric field of magnitude E_0 .

In order to characterize the magnitude of the droplet deformation under applied electric field, the degree of deformation is calculated by:

$$D = \left(\frac{d_{\parallel} - d_{\perp}}{d_{\parallel} + d_{\perp}} \right), \quad (2.12)$$

where d_{\parallel} is the length of the droplet parallel to the direction of the applied electric field and d_{\perp} is the length of the droplet perpendicular to the direction of the applied electric field. If the droplet is stretched along the direction of the applied electric field (acquires a prolate shape), the deformation magnitude is positive ($D > 0$); if the droplet is deformed perpendicular to the direction of the applied electric field (acquires an oblate shape), the deformation magnitude is negative ($D < 0$).

When a pure dielectric droplet is placed in a pure dielectric medium and subjected to an electric field, the electric field acts on the bound charges formed at droplet interface between two fluids of different dielectric permittivities. In a pure dielectric, the surface charge only has a normal stress component and is balanced by the interfacial tension. Due to the absence of tangential stress, no induced liquid flows inside and outside of the droplet are observed. The steady-state deformation of the droplet is obtained by balancing the normal stress with the interfacial tension. The magnitude of droplet's deformation is determined by O'Konski and Allan [42] as follows:

$$D = \frac{9 a \varepsilon_0 \varepsilon_{ex} E_0^2 (\varepsilon_{in} - \varepsilon_{ex})^2}{16 \gamma (\varepsilon_{in} + 2 \varepsilon_{ex})^2}, \quad (2.13)$$

where γ is the droplet interfacial surface tension and ε_0 is the vacuum permittivity. In the pure dielectric model, the droplet can only be stretched ($D > 0$) and acquire a prolate shape. For this model, the deformation of the droplet is only observed up to a critical electric field; above the critical electric field, the droplet breakup occurs.

2.3. Governing equations for the leaky dielectric droplet model (LDM)

In the leaky dielectric model, the suspended fluid and droplet both have free ions and exhibit finite conductivity to modify the fluid-fluid interface in an electric field, satisfying the condition $\tau_e \ll \tau_v$ [46]. When a leaky dielectric droplet is placed in a leaky dielectric medium and subjected to an electric field, free charges accumulate at the droplet interface faster than the time scale of the fluid motion to convect the charge from the droplet interface. Similar to the pure dielectric droplet model, the electric field is also irrotational ($\nabla \times E = 0$) in the leaky dielectric droplet model. The electric field potential in the form of the gradient of electric potential can be written as $E = -\nabla\phi$. According to the Gauss's law, volume charge density is defined as:

$$\rho/\varepsilon_0 = \nabla \cdot (\varepsilon E). \quad (2.14)$$

The charge conservation equation can be expressed as [46]:

$$\frac{D\rho}{Dt} = \frac{\partial\rho}{\partial t} + u \cdot \nabla\rho = -\nabla \cdot (\sigma E), \quad (2.15)$$

where $\frac{D}{Dt}$ is the material derivative, σ is the electrical conductivity, and u is the velocity of the fluid. If we assumed that the system is quasi-static, then the charge conservation equation (Eq. (2.15)) can be written as in term of divergence due to the electrical conduction:

$$\nabla \cdot (\sigma E) = 0. \quad (2.16)$$

As we know, $E = -\nabla\phi$. Therefore, Eq. (2.16) in terms of electric potential can be written as:

$$\nabla \cdot (\sigma \nabla\phi) = 0. \quad (2.17)$$

In a homogeneous medium, the electrical conductivity is the same within both fluids, the electric potential (ϕ) can then be reduced to the Laplace equation ($\nabla^2\phi = 0$). The electric stress at droplet interface can be calculated by taking the divergence of the Maxwell stress tensor (T_m) [52], and the expression for an electric force at droplet interface can be written as:

$$F_{es} = \nabla \cdot T_m = -\frac{1}{2} E \cdot E \nabla\epsilon + \rho E. \quad (2.18)$$

Equations (2.16), (2.17) and (2.18) give the complete description of the leaky dielectric model. The electric stress at the droplet can be calculated from Eq. (2.18) by inserting the electrical component from the Eqs. (2.19) and (2.20).

Deformation of leaky dielectric droplet

In 1966, Taylor introduced the leaky dielectric model to describe the electrohydrodynamic deformation (EHD) of a droplet. According to this model, a weakly conductive (also called leaky dielectric) droplet is suspended in another weakly conducting medium, the droplet can acquire either oblate or prolate shapes under applied electric field. Due to the (small) conductivity of the liquids, the free charges accumulate at the droplet interface in an electric field and compressive stress is exerted on the droplet. If σ_{in} is the conductivity of droplet and σ_{ex} is the conductivity of the suspended fluid, the electric potential inside and outside the droplets are [53]:

$$\phi_{in} = \frac{3 E_0 r \cos\theta}{2+R}, \quad (2.19)$$

$$\phi_{ex} = E_0 r \cos\theta \left(r + \frac{1-R}{2+R} \frac{a^3}{r^2} \right), \quad (2.20)$$

where $R = \frac{\sigma_{in}}{\sigma_{ex}}$; in a leaky dielectric material the potential inside and outside the droplet is similar to the pure dielectric material. The corresponding tangential and normal components of the electric field at the interface of the droplet ($r = a$) are:

$$E_{t,ex} = \frac{1}{a} \left(\frac{\partial \phi_{ex}}{\partial \theta} \right) = - \left(\frac{3E_0 \sin \theta}{2+R} \right), \quad E_{n,out} = \left(\frac{\partial \phi_{ex}}{\partial a} \right) = \frac{3RE_0 \cos \theta}{2+R}, \quad (2.21)$$

$$E_{t,in} = \frac{1}{a} \left(\frac{\partial \phi_{in}}{\partial \theta} \right) = - \left(\frac{3E_0 \sin \theta}{2+R} \right), \quad E_{n,in} = \left(\frac{\partial \phi_{in}}{\partial a} \right) = \frac{3E_0 \cos \theta}{2+R}. \quad (2.22)$$

The electric stress component exerted at the droplet interface can be calculated by inserting the above electric field component into the Maxwell stress tensor (Eq. (2.18)). For a droplet under applied electric field, the timescale for the accumulation of charges at droplet interface can be obtained by the Maxwell-Wagner charge relaxation time (τ_{mw}) [54, 55]:

$$\tau_{mw} = \frac{\varepsilon_{in} + 2\varepsilon_{ex}}{\sigma_{in} + 2\sigma_{ex}}. \quad (2.23)$$

Once the charges build up at the droplet interface, three different types of deforming forces act on the droplet [56], which are (i) due to the difference in the dielectric permittivities of both liquids, the electric force acts on the bound charges similar to a pure dielectric system, (ii) the induced free charges at the droplet interface have normal and tangential force, the tangential force brings the fluid (inside and outside of the droplet) in motion, (iii) the flow at the droplet's interface yields small viscous stresses. Taylor has predicted both oblate and prolate droplet deformations by balancing between these three forces and the interfacial tension, which depends on the properties of both fluids. The magnitude of the droplet deformation depends on the stability between surface tension (γ) and normal stress ($\varepsilon_{ex} \cdot E_0^2$); and can be calculated as [53]:

$$D = \frac{9a\varepsilon_0\varepsilon_{ex}E_0^2}{16\gamma S(2+R)^2} \left[S(R^2 + 1) - 2 + 3(RS - 1) \frac{2\lambda+3}{5\lambda+5} \right], \quad (2.24)$$

where the dimensionless numbers S , R and λ are the dielectric constant, conductivity, and viscosity ratios, respectively, and are defined as: $S = \frac{\varepsilon_{ex}}{\varepsilon_{in}}$; $R = \frac{\sigma_{in}}{\sigma_{ex}}$; $\lambda = \frac{\mu_{ex}}{\mu_{in}}$. According to Taylor's LDM, the shape of the droplet deformation is defined by the product of R and S , i.e. $RS = \frac{\tau_{e,ex}}{\tau_{e,in}}$, where $\tau_{e,in} = \frac{\varepsilon_{in}}{\sigma_{in}}$, $\tau_{e,ex} = \frac{\varepsilon_{ex}}{\sigma_{ex}}$ and $\tau_{e,ex}$ are the Maxwell-Wagner relaxation times of the droplet and suspended fluid, respectively. τ_e measures the characteristics time for the charges to build up at the droplet interface. If the droplet fluid is more conductive than

the suspended fluid (and their dielectric constants are equal), the product of R and S is greater than 1 ($RS > 1, \tau_{e,in} < \tau_{e,ex}$), and the charge distribution at the droplet interface is dominated by charges from the interior liquid (droplet); as a result, the droplet acquires a dipole moment in the direction of the applied electric field. Whereas, if the suspended fluid is more conductive than the droplet, the product of R and S is less than 1 ($RS < 1, \tau_{e,in} > \tau_{e,ex}$), and the charge distribution at the droplet interface is dominated by charges in the exterior fluid. As a result, the dipole moment is oriented opposite to the direction of the applied electric field, see **Fig. 3**.

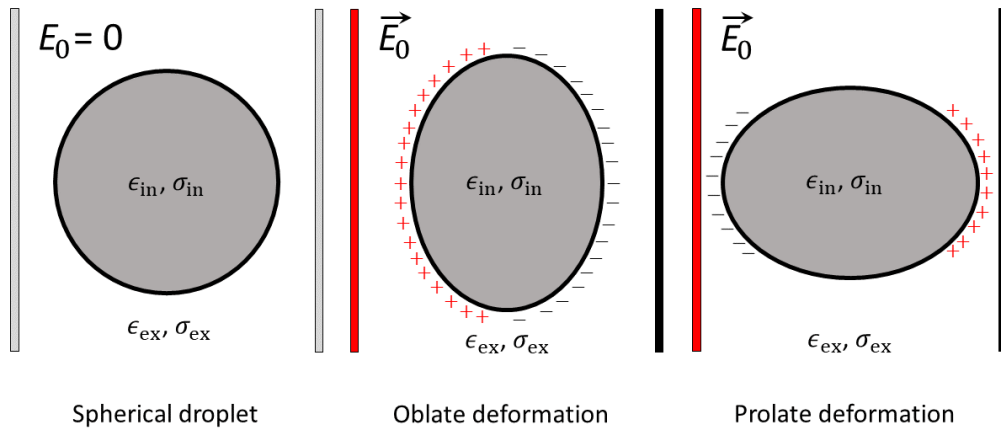


Fig. 3. Schematic figure illustrating the deformation of a droplet in a two-phase system. The droplet is suspended in another immiscible liquid and subjected to an electric field E_0 . In the absence of an electric field, the droplet was spherical in shape (left panel). Under the applied electric field, there are two possible steady-state deformations of droplet. Oblate and prolate shapes are depicted in the middle and right panel, respectively.

In **Fig. 4**, I estimated the deformation of the droplet numerically by using Taylor's equation (Eq. (2.24)). In the calculation, silicone oil droplet is suspended in castor oil and subjected to an electric field of strength 250 V mm^{-1} . The magnitude of prolate and oblate droplet deformations are plotted against the applied electric field (**Fig. 4a**). For the red curve, the castor oil droplet is suspended in silicone oil and subjected to an electric field. Due to the stronger conductivity of castor oil ($RS > 1, \tau_{e,in} < \tau_{e,ex}$), the droplet acquires a dipole moment in the direction of the electric field. The charges at droplet poles are pulled by the electrodes and deformed in a prolate shape. When the system is reversed ($RS < 1, \tau_{e,in} > \tau_{e,ex}$), i.e., silicone oil is formed in castor oil, the droplet acquires an oblate shape and the magnitude of droplet deformation is negative, see black curve in **Fig. 4a**.

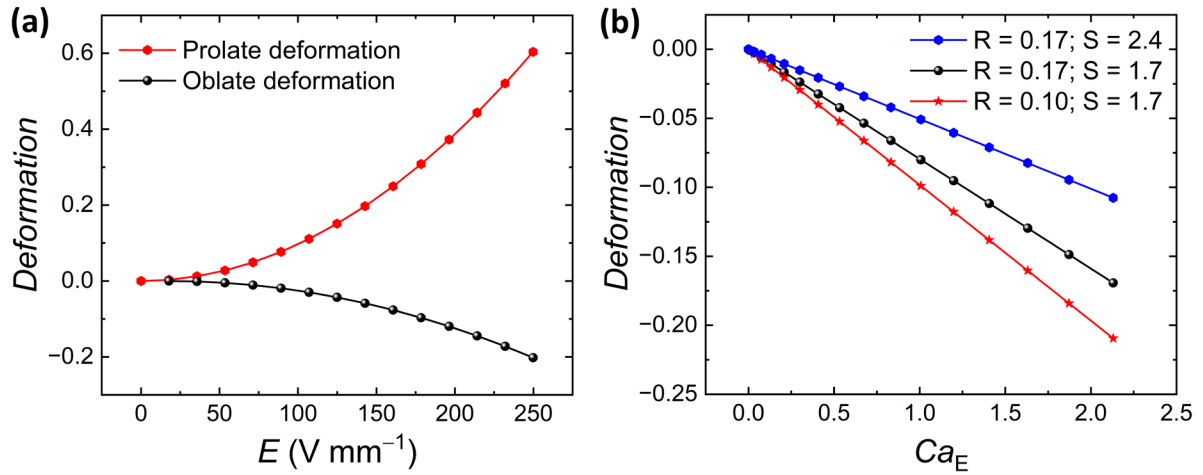


Fig. 4. Theoretical result for the droplet deformation. **(a)** The magnitude of the droplet deformation plotted as a function of the applied electric field. **(b)** The magnitude of the droplet deformation plotted as a function of the electric capillary number (Ca_E) for different ratios of conductivities (R) and permittivities (S).

The electric capillary number (Ca_E) measures the magnitude of the interaction between applied electric field and interfacial tension. The electric stress acts to deform the droplet, whereas the surface tension acts to make the droplet spherical. The electric capillary number is defined as:

$$Ca_E = \frac{a \epsilon_{ex} \epsilon_0 E_0^2}{\gamma}. \quad (2.25)$$

If the applied electric stress ($\epsilon_{ex} \cdot E_0^2$) becomes greater than the critical capillary stress ($\frac{\gamma}{a}$), the surface tension is no longer balanced, and droplet breakup occurs.

In **Fig. 4b**, a silicone oil droplet is suspended in castor oil, and the deformation of the droplet is calculated for the different ratios of conductivities (R in the range 0.1–0.17) and permittivities (S in the range 1.7–2.4) (the ratio of the conductivity and permittivities was changed by the changing of the conductivity and permittivity of the silicone oil droplet) by using Eq. (2.25) under an applied electric field. In **Fig. 4b**, the deformation of the droplet is plotted against the electric capillary number. The magnitude of droplet deformation is linear with electric capillary number for all different conductivities and permittivities ratios. Moreover, the results also demonstrate that at a higher permittivity ratio, the magnitude of droplet deformation is decreased, whereas at a higher conductivity ratio, the magnitude of droplet deformation increased. This is because at higher conductivity ratio, the droplet experienced stronger electric stress due to higher number of charges at the droplet interface.

2.4. Electrohydrodynamic convective flow

When a leaky dielectric droplet is suspended in another leaky dielectric medium and subjected to an electric field, the induced charges accumulate at the droplet interface due to their contrast in electrical conductivity and dielectric permittivity. The induced surface charge has two types of stress components, (i) normal stress balanced by the surface tension, and (ii) tangential stress which induces electrohydrodynamic (EHD) circulation flow inside and outside the droplet; see **Fig. 5**. The direction of the induced flow either can be from the droplet's electric pole to equator, or from the equator to pole, depending on the product of R and S . If $RS < 1$, the droplet undergoes oblate deformation and the flow is directed from pole to equator, whereas if $RS > 1$, the droplet undergoes prolate deformation and the flow is directed from equator to pole. The EHD flow velocity (U_θ) at the droplet interface is given by [4, 53]:

$$U_\theta = \frac{9 a \varepsilon_0 \varepsilon_{ex} E_0^2}{10 \mu} \frac{R(RS-1)}{(1+\lambda)(2R+1)^2} \sin(2\theta). \quad (2.26)$$

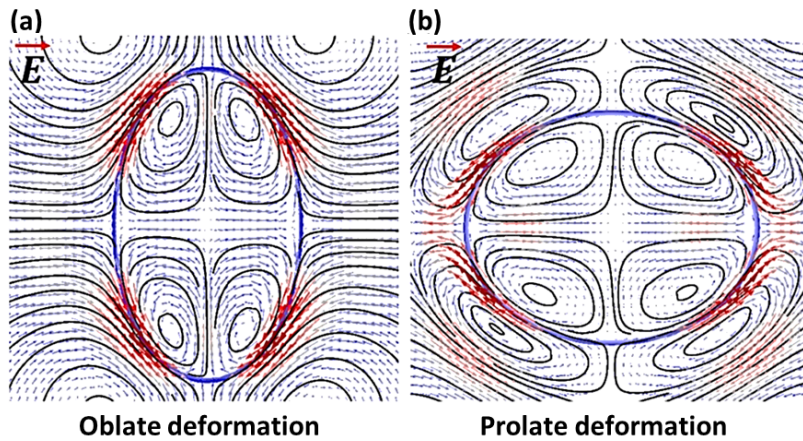


Fig. 5. Simulated results for the flow inside and outside of a droplet. **(a)** Oblate deformation of the droplet and the flow is directed from the droplet's poles to the equator ($RS < 1$). **(b)** Prolate deformation of the droplet and the flow is directed from the droplet's equator to the poles ($RS > 1$). Figure adapted with permission from [3].

2.5. Corrections to the LDM

Taylor's leaky dielectric model does not consider all the physical phenomena that have been observed experimentally. In 1971, Torza et al. [48] experimentally studied the deformation of a silicone oil droplet in castor oil under the applied electric field and compared the result with Taylor's leaky dielectric model. They found that the magnitude of the droplet deformation was consistently less than the theoretical prediction. After the observation of quantitative discrepancy between theoretical and experimental analysis of the droplet deformation, the leaky dielectric model was studied by several other researchers. Vizika and

Saville [50], Ha and Yang [57], Salipante and Vlahovska [55], and Dommersnes et al. [4], experimentally verified Taylor's model; the results showed good agreement with theoretical prediction only for small deformation at weaker electric field. Based on the leaky dielectric model, Benteitis and Krause [58] introduced an extended leaky dielectric model to study highly deformed droplets in a strong electric field but below the critical electric field to avoid droplet breakup. The authors found that the extended leaky dielectric model could be used to predict the behavior of the droplet, such as continuous deformation at high electric field strength, based on S , R , and λ . The authors also compared the leaky dielectric model and the extended leaky dielectric model with experimental data. They found that for prolate deformation, the extended leaky dielectric model was in qualitative and quantitative agreement with the data from other studies and within the experimental errors. Whereas, for oblate deformation, the extended leaky dielectric model overestimated the results.

In 1978, Ajayi [59] extended the Taylor theory to study droplet deformation up to the second-order correction. However, he did not consider the charge convection in his correction model, and the result was not sufficiently strong to remove the complete discrepancy between the experimental result and theoretical prediction. Feng and Scott (1996) [60] employed the Galerkin finite-element method to study the deformation of a leaky dielectric droplet under a uniform electric field. The result was considerably improved, and the analysis gives a better understanding of the EHD behavior of leaky dielectric droplet. Later, Feng (1999) [61] extended the work of Feng and Scott (1996) by considering the effect of charge convection on droplet deformation due to the EHD circulation around the droplet. The result demonstrates that charge convection plays an important role in the magnitude of the droplet deformation. They concluded that in case of the prolate deformation (when $RS > 1$) the surface charge convection enhances the deformation, whereas in the case when droplet is compressed (oblate deformation), the charge convection decreases the deformation. In recent years, Supeene (2007) [62], Herrera (2010) [63], Lanauze (2015) [64], Das (2017) [65], and Sengupta et al. (2017) [66], studied the deformation of the droplet by taking into account of charge convection and the result was similar to Feng's (1999) result. They estimated that without charge convection the magnitude of the oblate deformation increases about 30 to 50%; see **Fig. 6** [65].

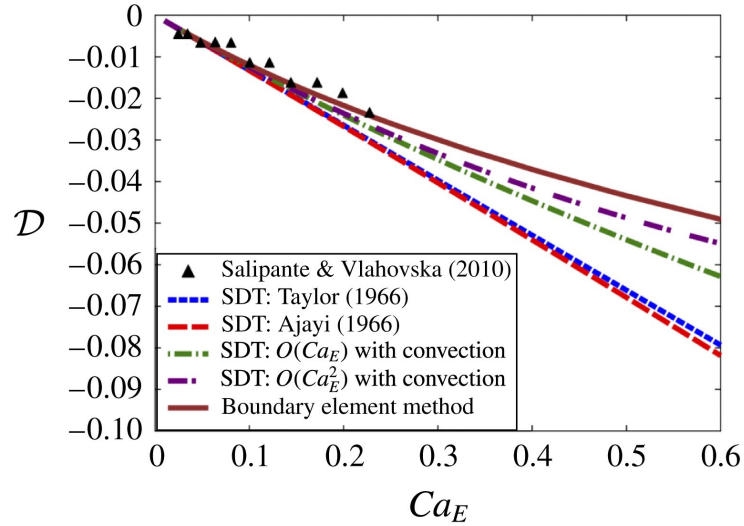


Fig. 6. Steady-state droplet deformation D as a function of electric capillary number Ca_E . The various models are compared to the experimental measurements of Salipante & Vlahovska (2010). Figure and caption adapted with permission from [65].

2.6. Droplet in moderate and strong electric fields

2.6.1. Electrorotation

All aforementioned studies are limited to the axisymmetric shape of the droplet; the non-axisymmetric shape arises when the droplet is subjected to a stronger electric field, and the breaking of symmetry leads to droplet rotation. Electric fields provide a contactless approach to rotate a weakly conductive droplet suspended in another weakly conducting medium ($RS < 1$). Under the application of a strong electric field, a perturbation in the orientation of the charges at the droplet interface creates torque, and the droplet starts spontaneous rotation. The Quincke rotation was first discovered by Quincke in 1896 [67], who studied the motion of solid particles. Later, the influence of an object's shape, size and electrical properties on the rotation rate was studied more thoroughly [68–70].

Several experimental and theoretical studies were performed on electrorotation of pure droplets. Ha and Yang [71], Salipante and Vlahovska [55] experimentally investigated the electric-field-induced rotation of deformable pure liquid droplets. In their studies, a weakly conducting droplet was suspended in fluid with slightly higher electrical conductivity and subjected to an electric field. The result demonstrated that the critical electric field strength depends on the size of the droplet and the viscosity ratio. The authors also stated that the highly viscous droplet or very small droplet behaves similar to the rigid body, and the deviation from the rigid body theory is small. Krause and Chandratreya [72] demonstrated that

electrorotation alters the deformation of the droplet and especially suppresses the oblate deformation. He et al. [73] developed a three-dimensional model to describe the electrorotation of a viscous droplet in a uniform DC electric field. The result shows that, if the surface charge convection is dominated due to the rotation, the critical electric field for the onset of rotation is similar to the rigid body sphere.

For a weakly conductive spherical droplet immersed in a weakly conducting medium ($RS < 1$) and subjected to a uniform electric field; the charges are accumulated at the droplet interface and induce a dipole moment. Based on the charge relaxation time, there are certain conditions to electrorotate the droplet. When the charge relaxation time of the interior liquid (droplet) is smaller than that of the exterior liquid ($\tau_{e,in} < \tau_{e,ex}$), the dipole moment is stable and aligned parallel with the direction of the electric field, and no rotation will take place. On the other hand, if $\tau_{e,in} > \tau_{e,ex}$, then the dipole moment itself is reversed, see **Fig. 7**. In this case, below the critical electric field, the droplet is in axisymmetric deformation, whereas above the critical electric field, the configuration becomes unfavorable and breaks the axisymmetry of the droplet. Thus, the major axis of the droplet inclined at an angle with respect to the applied electric field, resulting in induced torque and leading to the spontaneous rotation of the droplet, similar to that described by Quincke [54].

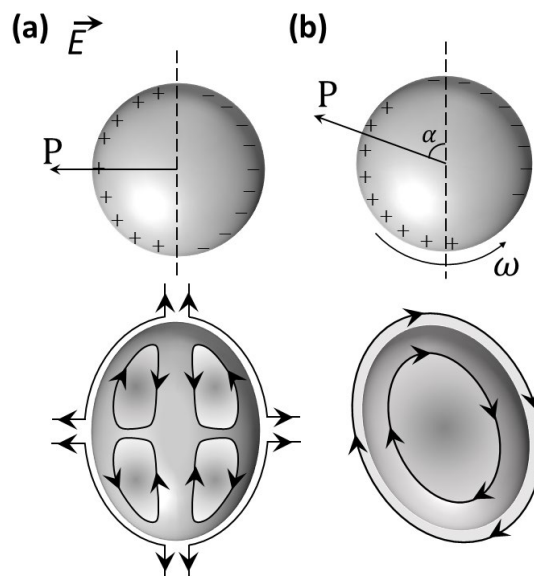


Fig. 7. Schematic diagram illustrating the droplet polarization for $RS < 1$ and $\tau_{e,in} > \tau_{e,ex}$, under uniform DC electric field. (a) At weaker electric field, when $E_0 < E_Q$, induced pure straining flow and axisymmetric oblate deformation (b) In strong electric field, when $E_0 > E_Q$, non-axisymmetric oblate deformation and the droplet inclined at an angle α with respect to the applied electric field, induced torque leads to droplet rotation. The droplet dipole moment P electrorotates to align itself in the direction of the applied electric field.

The critical electric field and the rotation rate for the Quincke rotation of the rigid body sphere can be compared to the electrorotating droplet, for which the E_Q and ω are described as following [54, 73]:

$$E_Q^2 = \frac{2\sigma_{ex}\mu_{ex}(R+2)^2}{3\epsilon_{ex}\epsilon_{in}(1-RS)}, \quad (2.29)$$

where E_Q is the critical electric field above which the droplet starts rotating and the rotation rate ω of the droplet is given by:

$$\omega = \pm \frac{1}{\tau_{mw}} \sqrt{\frac{E_0^2}{E_Q^2} - 1}. \quad (2.30)$$

The angle between the induced charge at droplet interface and applied electric field (see **Fig. 7**) is given by:

$$\alpha = \tan^{-1}\left(\frac{1}{\omega\tau_{mw}}\right). \quad (2.31)$$

Unlike a rigid sphere, a weakly conductive droplet deforms at any strength of the applied electric field. At lower electric field strength, $E_0 \leq E_Q$, the droplet deformed axisymmetric, which is described by Taylor's leaky-dielectric model. At a stronger electric field strength where $E_0 > E_Q$, the droplet starts to rotate and drag the exterior fluid, which acquires a rotational component. The rotational straining flow affects the charge convection at the droplet interface, and thus it affects the critical electric field E_c for the droplet's rotation compared to the critical electric field E_Q for the rigid body's Quincke rotation.

2.6.2. Stability and break up

Electrohydrodynamic (EHD) breakup phenomena for a leaky dielectric droplet suspended in another leaky dielectric medium and subjected to a uniform electric field are studied using the LDM. The breakup mode of the droplet appears when the electric stress ($\epsilon_{ex} \cdot E_0$) becomes larger than the critical capillary stress ($\frac{\gamma}{a}$) and the surface tension can no longer balance the electric stress. As a result, the droplet breaks into different sizes of daughter droplets. Various breakup modes and steady-state deformation of axisymmetric droplets were investigated experimentally and by numerical simulation under a uniform applied electric field. In 1988, Sherwood [45] studied the stability of droplet based on the leaky dielectric model. He demonstrated two distinct mechanisms of droplet breakup, depending on the permittivity and conductivity of the interior and exterior fluids. He showed if the permittivity of the droplet is higher than the surrounding fluid, the droplet undergoes tip-streaming, if the conductivity of the droplet is higher than the surrounding fluid, the droplet undergoes blob division.

In recent years, Sherwood's work was explored more deeply by other researchers to obtain a complete understanding of the drop behavior based on leaky dielectric liquids and flow motion around the droplet. Ha (2000) [57], Dubash (2007) [74], Lac (2007) [75], Shivraj (2013) [76], and Dong et al. (2019) [77] studied the effect of electric stress on droplet deformation and various modes of breakup under an applied electric field. They explored different ratios of conductivity, viscosity, permittivity as well as the applied electric field to observe the different mode of breakup. They reported that the deformation and breakup of droplet depend not only on the permittivity and conductivity of the droplet and surrounding liquid but also on the applied electric field strength as well as the viscosity ratio of the droplet and surrounding liquid. Brosseau and Vlahovska [78] demonstrated the two different modes of droplet breakup at electric field $E \geq 3 \text{ kV cm}^{-1}$, (i) equatorial streaming mode, and (ii) droplet dimpling mode. In the equatorial streaming mode, the droplet flattens and forms a sharp edge at its equator and eventually breaks into smaller droplets via capillary instability, see **Fig. 8**. In this process, the micron size daughter droplets are beautifully arranged in the equatorial plane of the parent droplet. The equatorial streaming mode occurs when $\lambda < 0.1, Ca_E \geq 4, R \ll 1$ ($\lambda = \frac{\mu_{in}}{\mu_{ex}}$, and $R = \frac{\sigma_{in}}{\sigma_{ex}}$). In the dimpling mode, the droplet deforms into a biconcave disk and forms a torus shape; the torus shape eventually breaks into comparatively larger droplets. The torus mode appears when $\lambda > 0.1, R \ll 1$. The droplet breakup through dimpling is uncontrolled, whereas the equatorial streaming is a controlled process that is easily triggered and interrupted.

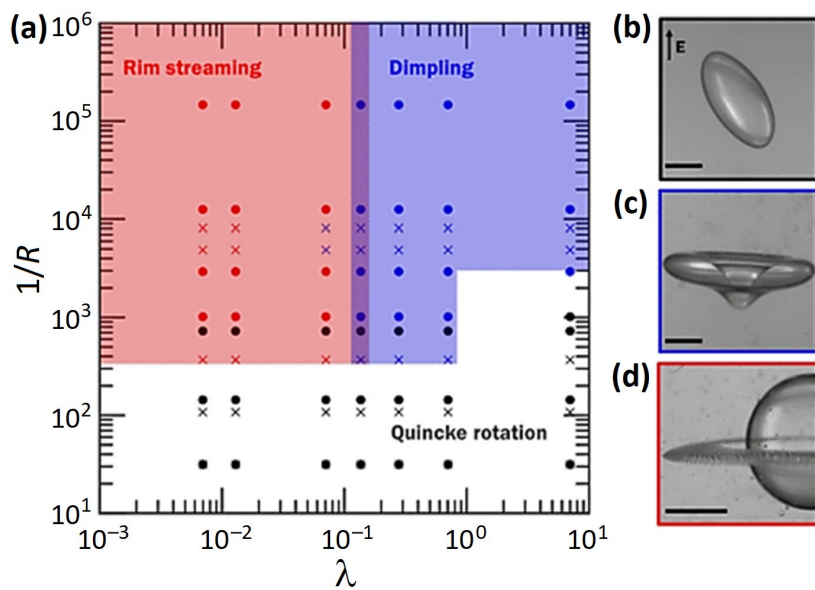


Fig. 8. Phase diagram of the drop dynamics in a strong uniform dc electric field: Quincke electroration (black), dimpling (blue) for $\lambda > 0.1$, EHD equatorial streaming (red) for $\lambda < 0.1$. The conductivity of the suspending oil is modified by the addition of the electrolyte TBAB (the dots) or AOT (the crosses). $E \geq 3 \text{ kV cm}^{-1}$. The scale bar is $500 \mu\text{m}$. Images (b)–(d) illustrate the drop behaviors. Figure and caption adapted with permission from [78].

Chapter 3 Particle-covered droplet in electric fields

Particles at the droplet interface may modify the behavior and characteristics of the droplet, such as compression, relaxation, mechanics and rotation under an applied electric field. Droplets with densely packed particles (also called Pickering droplets) have several advantages that can be put in practice. For instance, the particle shell can help to minimize the possibility of coalescence during droplet collisions, leading to formation of a stable emulsion. The stability of particle-laden droplets is greatly affected by the mechanical properties of their particle film (Young moduli, bending stiffness and Poisson ratio) and partial wettability of particles with the fluids (droplet and suspended fluid). Inter-inter particle interactions, shape, size, and particle concentrations also play roles in the stability of the droplet.

Particles at the droplet interface can also be used to form responsive droplets with various functionalities and can be controlled by the external stimuli. For example, they can form plasmonic-based mechanochromic microcapsules [79], self-healing capsules [80], and microcapsules for targeted drug delivery [1]. In addition, by adequately choosing the properties of the particles, it is possible to design a droplet with functional characteristics such as conductivity, porosity and responsiveness, etc.

In the following sections, I will explain the fundamental features of the particle-covered droplets and the differences in the behavior of pure and particle-covered droplets subjected to electric fields, and I will highlight the knowledge gaps that were to be explored when I started my research.

3.1. Pickering droplet

Pickering droplets (comprising a Pickering emulsion) are formed by the assembly of colloidal or granular particles at the interfaces of two immiscible liquids. They were first recognized by Ramsden in 1903 [81], and later the phenomenon was described by Pickering in 1907 [82]. Under large deformation, Pickering droplets are able to recover without breaking of the droplet and due to the three-face contact angle, the particles at the droplet interface bound very strongly; see **Fig. 9**. Thus, high desorption energy is required to detach the particles at the droplet interface. The energy needed for the desorption of a single particle from the oil-water interface is given by [83]:

$$E = \pi r_0^2 \gamma_{ow} (1 \pm \cos \theta_{ow})^2, \quad (2.27)$$

where r_0 is the radius of the particle, γ_{ow} is the oil-water interfacial tension, the positive sign inside the bracket refers to the desorption of particle from the droplet, the negative sign is for transfer of particle into the droplet, and θ_{ow} is the contact angle of the particles with the interface. The binding energy is maximum (and for microparticles can reach $E \approx 10^7 k_B T$) when the contact angle $\theta = 90^\circ$ and the spherical particle is protruding halfway into the oil-water interface [84]. The three-phase contact angle is governed by the different interfacial energies in the system and defined by Young's equation:

$$\cos \theta = \frac{\gamma_{po} - \gamma_{pw}}{\gamma_{ow}}, \quad (2.28)$$

where γ_{po} and γ_{pw} are the energy per unit area of the particle-oil interface, and particle-water interface, respectively.

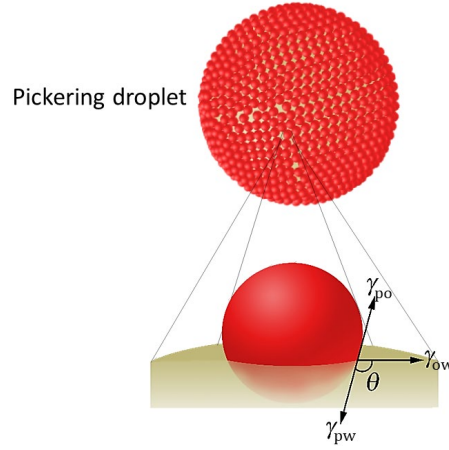


Fig. 9. Schematic diagram of solid particle at water-oil interface. γ represents the interfacial tension between particle-oil, oil-water and particle-water.

Within this thesis, I research Pickering droplets, that is, droplets with a monolayer particle shell made of densely packed particles, and also droplets partially covered by particles with different particle concentration.

3.2. Deformation of particle-covered droplet under electric field

Several theoretical and experimental studies have demonstrated the deformation of pure droplets. The literature is less extensive on the deformation of the particle-covered droplets. Ouriemi and Vlahovska [30, 31] investigated the effect of particle coverage on the magnitude of the droplet deformation. Their results demonstrate that the deformation of the droplet is enhanced with the particle coverage ($\varphi = 0$ to 90 %). Experimentally and theoretically,

Mikkelsen et al. [32] and Abbasi et al. [3] studied the deformation of a pure silicone oil droplet and a fully-covered silicone oil droplet (Pickering droplet) in a uniform DC electric field. Their results demonstrate that the Pickering droplet deformed more than the pure silicone oil droplet. The increase in the magnitude of the droplet deformation is mainly due to two reasons: (i) as the particles coverage at the droplets' interface increases, the effective electrical conductivity of the droplet decreases, and (ii) the particles at the droplet interface reduce the EHD circulation flows around the droplet that convects the charges from the droplet interface. Because of the above two reasons, a higher number of charges accumulates at the droplet interface and stronger electric stress acts on the droplet. The strength of the EHD flows depends upon many parameters, but primarily it depends upon the applied electric field strength and the particle coverage. In the case of pure silicone oil droplets, the EHD flows are strong and convect more charges, whereas in the case of the Pickering droplets, the EHD flows are nearly non-existent [30, 32, 85].

The magnitude of the droplet deformation and its sign (prolate vs. oblate) should also be affected by the size and the electrical conductivity of the particles covering the droplet. However, little is known about the effect of these parameters on the droplet response to the electric field. In my studies, I focused on studying the mechanics of particle-covered droplets and how the particle coverage, size, electrical conductivity and the strength of the applied electric field affect the magnitude of the droplets' steady-state deformation.

For investigating the mechanics of particle-covered silicone oil drops suspended in castor oil, as well as particle assembly at the droplet interface, I used a wide range of electrically conductive particles ranging from insulating polystyrene to highly conductive silver. I also studied the effect of electrohydrodynamic flows on the magnitude of droplet deformation. The presence of particles on the droplet interface may also affect the dynamics of the droplet deformation. There was not much known about the dynamic deformation of particle-covered droplets under an applied electric field. My aim was to fill the gap and study the dynamics of the droplet with different particle coverage under a uniform electric field.

3.3. Influence of surface particle on the EHD flows

In Section 2.4., I described the origin of EHD flows. The strength of the straining flows depends upon many parameters, but primarily it depends on the surface particle coverage and applied electric field strength. When pure silicone oil droplets are subjected to an electric

field, the EHD flows are strongest. On the other hand, when a Pickering droplet is subjected to an electric field, the straining flows are nearly non-existent, this is because the particle layer behaves like a solid droplet. Ouriemi et al. [30] studied the EHD deformation of a particle-covered droplet and they observed that the flow was suppressed when the droplet was almost fully covered. Mikkelsen et al. [32] also claimed that the EHD flow is zero for a fully covered droplet. But there was still missing research in the literature about the influence of the particles' electrical properties, particle size and particle coverage on the strength of the EHD flows. I aimed to study how the different particle coverage and different electrical properties of the particles influence the induced EHD flows at the droplet interface.

3.4. Presence of particle shell alters electroration of a droplet

In Section 2.6., I described the electroration of particle-free droplets. Adding particles to the droplet interface may change the critical electric field of the electroration. Unlike particle-free droplets, electroration of the particle-covered droplet has not been studied extensively. Only a few research groups studied the effect of particles coverage and its electric properties on the onset field for the electroration. Dommersnes et al. [85] studied the electroration of a pure droplet and a fully covered droplet. They claimed that the critical electric field for electroration of particle-covered droplet is almost less than twice that of the particle-free droplet. Brosseau et al. [68] studied the electroration of prolate droplets; they characterized the rotation of the droplet on the basis of the orientation. When the droplet was oriented in the direction of the electric field, it was spinless, and the spinning only occurred when the droplet was oriented perpendicular to the direction of the electric field.

Ouriemi and Vlahovska [30] contributed significantly to this research topic. They performed several experiments on particle-covered droplets and provided new insight into this research area and raised questions, for example on the role of important parameters (such as droplet size, particle type, and particle shell morphology and composition) affecting the electroration of particle-covered droplets or the fluid-solid transition of rotating particle shells. In my thesis, I address many of these questions, and also go a step further by demonstrating new applications of electroration of particle-covered droplets.

The behavior of a Pickering droplet can be defined in three different regimes with respect to the applied electric field. At lower electric field strength $E_0 \leq E_c$, the droplet simply follows an axisymmetric deformation regime; at electric field $E_T > E_0 > E_c$, the droplet is in an

electrorotation regime; and at electric field $E_0 \geq E_T$, the droplet is in the tank-treading regime. E_T is the critical electric field above which the Pickering droplet starts tank-treading. In the tank-treading regime, the major axis of the Pickering droplet is inclined at a constant angle with respect to the applied electric field, whereas the particles flow at the droplet interface. This can be used for the mixing of the particles at droplet interface, as presented in a paper on droplet electrorotation, which constitutes this thesis.

3.5. Nonspherical droplets in electric field

Unlike pure droplets, particle-covered droplets may acquire stable non-spherical shapes. This is because high concentration of particles on the droplet interface may jam the particle shell of the droplet and oppose the action of surface tension and Laplace pressure, leading to formation of a stable non-spherical Pickering droplet. When the Pickering droplet is jammed and forms an arrested shell, the particles at the droplet interface behave like an elastic sheet that may support anisotropic stresses and strains [15, 41]. Recently, Mikkelsen et al. [86] studied the wrinkling and mechanics of particle shells formed on curved interfaces under the application of an electric field. They showed that on a curved interface, wrinkles are formed with a different characteristic wavelength compared to those occurring at a flat interface.

In the last few decades, several studies have been devoted to describing the behavior of elastic capsules in the presence of extensional flow [87], shear flow [88–91] or other external forces [92]. When an elastic capsule is subjected to an electric field, the induced electric stress acting at the capsule's interface acts to deform it. During the deformation, the capsule generates the restoring elastic stress to balance the electric stress. There are several models to describe the deformation of elastic capsules under an electric field. Ha and Yang [93] (employed Hookean model) studied the combined effect of electric field and shear flow on the deformation and orientation of capsule. Das et al. [94, 95] (employed Skalak's model) studied the deformation of an elastic capsule in an AC and DC electric field. Karyappa et al. [96] (employed Hookean model, Skalak's model, and Mooney-Rivlin model) and Randall et al. [97] (employed Hookean model) studied the deformation and formation wrinkling on elastic capsules made of polysiloxane membranes and protein-coated capsules using the electric fields.

When I began this PhD, most of the research in the field concerned the deformation of spherical Pickering droplets under an electric field. My aim was to study the electric-field-

induced deformation of arrested nonspherical particle shell formed on droplets. The questions of primary interest were how the arrested-particle-shell behave under applied electric field, how particle shell geometry affects the critical electric field strength for arrested Pickering droplets to collapse, and how particle size and droplet size affect the collapsing mechanism of non-spherical Pickering droplets.

3.6. Structuring of the particles at droplet interface under electric field

Electric fields have been established as an easy method for both deforming droplets and structuring particles at droplet interfaces. In recent years, the research interest in particle manipulation on droplet interfaces has increased [98–100]. Particle structuring on droplet interfaces has a vast range of applications; for example, self-assembly of colloidal particles [98], formation of hetero- and homogeneous shells [101, 102], stabilization of emulsions [103], and fabrication of novel materials [104, 105].

As described before in Section 2.4., when a droplet is suspended in another immiscible leaky dielectric medium and subjected to an electric field, Maxwell stress arises due to free charge accumulation at the droplet interface and induces liquid flows (EHD flows) inside and outside of the droplet. If the particles are adsorbed at the droplet interface, the EHD flows are capable of guiding the surface particles from the droplet's pole to the equator, or the equator to its pole, depending on the resultant shape of the droplet. If the droplet is deformed perpendicular to the direction of the electric field, the particles are aggregated at the droplet equator. On the other hand, if the droplet is deformed parallel to the direction of the electric field, the particles are aggregated at the droplet poles. Nudurupati et al. [106] and Amah et al. [36] demonstrated that particles adsorbed at a droplet's interface can be transported to its electric equator or electric pole via electrophoretic force. Ouriemi and Vlahovska [30, 31] conduct a systematic experimental study for manipulation of particles (for a wide range of particle sizes, conductivities and shapes) at droplet interface under uniform electric field for $RS < 1$. They demonstrate that, at moderate coverage ($\varphi \sim 0.5$), the particles have different assemblies at the lower applied electric field. For example, less conductive particles form "belt", whereas highly conductive particles form pole-to-pole chains. The particles may also form static belts or dynamic sinusoid belts depending on the particle properties and the applied electric field strength, whereas higher particle-covered droplets undergo drum-like shape and implosion. Abbasi et al. [3] also demonstrated particle structuring at the droplet

interface in increasing electric field. At weaker electric fields, particles formed a belt-like structure; when the electric field increased, the particles formed a helmet-like structure, whereas at the stronger electric field, the particles separated into two portions and formed a cap-like structure.

In another experiment, Dommersnes et al. [4] showed that non-conductive particles at the droplet interface aggregated at the droplet's equator and formed a ribbon-like structure via EHD flows; whereas, for the same system, conductive particles formed chains from the droplet's pole-to-pole via dipolar-dipolar interactions. In their work, the authors also demonstrated that controlling electric field strength made it possible to actively structure and redistribute non-ohmic (i.e. having a non-linear relationship between the electric current and the voltage) clay mineral particles at the droplet interface. In our work, we expanded the structuring to ohmic conductive particles, and show how to actively structure conductive particles and locally change their concentration and packing on the interface of a droplet. The research hypothesis was that tuning the electric field frequency enables the switching between two physical mechanisms: particle–particle dipolar interactions and EHD flows.

Thesis development—introduction to the Papers

In spring 2017, I started my PhD research. I was hired under the research project (*Mechanical properties, specific release and motility of patchy colloidosomes—an emerging class of structures*) led by Prof. Zbigniew Rozynek. My first task was to assist in studies on transient deformation dynamics of particle-laden droplets subjected to a uniform DC electric field. I co-performed the experiments, the results of which are presented in *Fig. 1*, *Fig. 2*, and *Fig. 3* in **Paper 1**. The research work conducted in **Paper 1** is an extension of preceding work in Prof. Jon Otto Fossum's laboratory at NTNU, Trondheim, Norway, where researchers studied extensively the deformation of silicone oil droplets in castor oil under an applied electric field. In **Paper 1**, we present our studies on the effect of the particle concentration on the electric-field-induced transient deformation of droplets. We prepared silicone oil droplets covered by polyethylene particles ($\sim 50 \mu\text{m}$) with different particle coverage (φ) from 0 to 1, where $\varphi = 0$ represents a particle-free silicone oil droplet and $\varphi = 1$ represents a fully covered silicone oil droplet. Our objective was to see how the surface particles affect transient droplet deformation, steady-state deformation and prolate-oblate anomalies. We also studied the effect of droplet size and applied electric field strengths on droplet deformation.

The experimental result showed that the deformation time increases with increased particle coverage because of the particle-capillary interactions. Moreover, we found that just after turning on the electric field, the droplet was for a short moment stretched before the droplet compression occurred. This anomaly was found to be caused by a delay in the interfacial charging. The experimental results also showed that the particles at the droplet interface influenced the magnitude of the droplet deformation significantly, and the fully covered droplet deformed more than the particle-free silicone oil droplet. We attributed that to the reduced charge convection due to the decrease of the electrohydrodynamic circulation flow owing to the presence of the surface particles. In addition, the electrically insulating particles at the droplet interface also reduced the electrical conductivity of the droplet, affecting the magnitude of the droplet's deformation.

The experiments performed within the research on the transient deformation led us to new scientific questions, for example on the effect of a particle's conductivity on the steady-state deformation of the droplet and the particle arrangement of the fluid–fluid interface.

Therefore, we decided to conduct experiments using particles with different values of electrical conductivity.

Particles with different conductivity values were not available commercially. That is why we had to produce them ourselves. We decided to modify polystyrene particles using a chemical approach. With the help of a chemist, we prepared several batches of polystyrene particles with different conductivities by sulfonation. Particle sulphonation yielded polymeric particles with a large range of electrical properties related to the degree of sulphonation, which could be controlled by several reaction conditions, including the reaction time, temperature, or concentration of sulphuric acid. In **Paper 2**, we present the results of particle sulfonation. The particles were characterized by different techniques, including FTIR, optical microscopy, and scanning electron microscopy, and we also took measurements of dielectric constant and electric conductivity. To determine the dielectric constant and the electrical conductance of the powder samples, we carried out capacitance measurements by means of an LCR meter. I performed those measurements in collaboration with colleagues from the Slovak Academy of Science in Košice. The characterized samples were then used in the actual experiments, in which we studied the assembly of sulfonated and non-sulfonated PS microparticles at a droplet interface in an applied electric field.

We first studied the formation of chains at the droplet interface in an AC electric field. We used different sulfonation reaction times of PS particles (from 0 to 32 minutes) at the droplet interface, whereas other parameters such as both the fluids, electric field strength, and frequency were kept constant. We found that the PS particles sulfonated for a longer time (32 min) formed a longer chain at the droplet interface in comparison to the PS particles sulfonated for a shorter time. We found that the change in the particle's electrical properties affected the dipolar interaction between the particles. In another experiment, we studied how the non-sulfonated PS particles at the droplet interface were structured at a constant electric field strength but at different frequencies. At high frequency (100 Hz), the particles formed small chains and moved toward the droplet's electric pole due to the dielectrophoretic (DEP) forces. On the other hand, when we decreased the frequency from 5 to 1 Hz, the particles moved toward the droplet's electric equator. We found that, at a lower frequency, the free charges had enough time to accumulate at the droplet interface and induce the electrohydrodynamic (EHD) flows. These EHD flows convected the particles from the droplet's pole to the equator, where they formed a ribbon-like structure. In another experiment, we

used different properties of sulfonated PS particles at the droplet interface and subjected them to constant DC electric fields of strength 150 V mm^{-1} . We found that the formation of the chain at the droplet interface depended on the sulfonation time of the PS particles. Those PS particles which were sulfonated for 32 minutes formed longer chains (pole-to-pole), whereas those PS particles sulfonated for a shorter time (4 minutes) did not form chains. We found that for the pure PS particles, the dipolar-dipolar force was weaker than the EHD drag force, preventing them from forming chains. When PS particles were sulfonated for a longer time, the dielectric constant and electric conductivities increased, resulting in dipolar-dipolar forces that exceeded the EHD drag force and formed longer chains.

In **Paper 2**, we demonstrated qualitatively how the conductive and non-conductive surface particles organized at the droplet interface under AC and DC electric fields. In **Paper 3**, we showed qualitative and quantitative data on the effect of the particles' conductivity and its concentration on the magnitude of the droplet deformation. We found that when the pure silicone oil droplet and the non-conductive PS particle-covered silicone droplet were subjected to the uniform DC electric field, they underwent oblate deformation. This is because the free charges accumulated at the droplet interfaces and created the dipole moment opposite to the applied electric field. However, the steady-state deformation of the pure PS particle-covered droplet was deformed slightly more compared to the particle-free silicone oil droplet. On the other hand, we found that when the silicone oil droplet was fully covered by the highly conductive particles (more conductive than both oils) and subjected to the DC electric field, the droplet underwent prolate deformation. This is because when the silicone oil droplet was fully covered with the highly conductive particles, it behaved like a conductive droplet and the dipole moment oriented in the direction of the applied electric field. In another experiment, we studied the influence of particle coverage and its conductivity on the magnitude of the droplet deformation when the droplet was subjected to a DC electric field of strength 170 V mm^{-1} . The experimental result showed that the silicone oil droplet covered by the non-conductive PS particle compressed more (oblate deformation) with the particle coverage. On the other hand, the droplet covered by the conductive particles became less compressed with the particle's coverage, and at some critical coverage the deformation of the droplet changed the shape from oblate to prolate. We also studied the effect of particle coverage on EHD flows, and we found that the induced EHD flows at the droplet interface were reduced by the surface particles.

In **Paper 3**, we studied droplets subjected to low and moderate strengths of an electric field. This is because the particle-covered droplet at a stronger electric field strength (above $\sim 150 \text{ Vmm}^{-1}$) starts electrorotating. To study the droplet at higher electric field strengths we had to prevent its electrorotation. In **Paper 4**, we resolved the problem by docking the droplet into an O-ring attached to one of the electrodes. In this way, the droplet could not translate in the sample cell (due to the convective flows typically present in the cell), nor could it electrorotate, and we were able to study the behavior of the droplets comparatively at stronger electric field strengths.

In **Paper 4**, we investigated how electric field strength (increasing and decreasing electric fields in a cycle) influenced the steady-state magnitude of the droplets' deformation, their relaxation, and arrangements of surface particles on such droplets by controlling EHD flows. We also quantified the droplet deformation and opening area at the droplet pole by stepwise increasing and decreasing the applied electric field. Interestingly, we found that both the deformation magnitude of the particle-covered droplet and the opening area exhibited hysteresis. In another experiment, we demonstrated three examples of applications based on the reversible opening and closing of the particle shell at the droplet's electrical pole by using the electric field. In this research, I co-designed all the experiments, performed the majority of the experiments and helped greatly in writing the first draft of the paper.

In **Paper 4**, we studied the deformation of the fully covered droplet during the electric field sweeping. In **Paper 5**, the objective was to show how the particle coverage, particle size, and strength of the electric field influence the magnitude of steady-state droplet deformation. In addition, we studied how the particle size, cohesiveness, and strength of the applied electric field affect the recovery of a particle shell and the particles' arrangement at the droplet interface. Our experimental results showed that adding non-conductive particles to a droplet interface significantly changed the magnitude of the droplet deformation. We also found that the magnitude of the droplet deformation was not retraceable during the electric field sweeping, and the curves exhibited hysteresis. We determined that this was possibly due to two reasons: (i) as the surface particle coverage increases, the EHD circulation flows decrease, and thus the charge convection may decrease, leading to the accumulation of a greater number of charges at the droplet interface. As a result, stronger electrical stress acts on the droplet. And (ii) the particle at the droplet interface may decrease the effective conductivity of the droplet, leading to the stronger electrical stress acting on the droplet. In addition, the

magnitude of the hysteresis area is sensitive to the particle coverage above $\varphi \approx 0.65$, due to the stronger energy dissipation. Moreover, we found that, after the electric field was turned off, the shells made of smaller particles were more prone to jamming and formation of arrested shells. In **Paper 5**, I was the initiator of the project, the main driver of the research, and I authored the first draft of the manuscript.

Unlike in **Paper 5**, where we intentionally prevented electrorotation of the droplet, in **Paper 6** we focused on the droplet rotation and tank-threading. We demonstrated that the particle at the droplet interface changes the critical electric field (for the electrorotation) compared to the particle-free droplets. This is because in the case of the particle-free droplets, the EHD circulation flows are stronger and convect the higher number of charges from the droplet interface; as a result, the critical electric field (for the electrorotation) of the droplet increases. On the other hand, the EHD flows are almost zero for the Pickering droplets, which leads to a stronger electric stress on the droplet interface compared to the same size and viscosity of the droplet, and thus the droplet starts rotating at the lower electric field. We also demonstrated that the rotation rate of the droplet is strongly affected by the presence of particles. This is because particles at the droplet interface provided a viscous effect and slowed down the droplet rotation. We also showed the importance of the electrical parameters of the surface particles by comparing the behavior of droplets covered by non-conductive PE particles and droplets covered by the clay particles. Moreover, we demonstrated examples of applications based on electrorotation of the particle-covered droplet shell by using a uniform electric field.

In **Papers 1–6**, the studies concerned spherical droplets. In **Paper 7**, we studied the behavior of non-spherical Pickering droplets with arrested particle shells under compressive electric stress. Here, we used an electric field to induce electric stress on a particle shell, which enabled non-contact exertion of force on it and measurements of numerous mechanical and rheological properties of the particle-covered droplet. We found that the non-spherical Pickering droplets with arrested particle shells under compressive electric stress resembled a Bingham plastic material, i.e. it behaves like a solid material at low applied stresses, and when the applied stress exceeds a yield stress point it becomes liquid-like. Our experimental results also revealed that the particles' shell geometry, size, as well as the particle size and applied electric field strength, strongly influenced the deformation, yielding the non-spherical particle shell. The non-spherical Pickering droplet absorbed electric stress differently and depending

on the strength of the applied electric field. Interestingly we also found that the curvature of the droplet significantly influences the yielding of the non-spherical Pickering droplet and it follows $E_y \propto \sqrt{\kappa}$, where E_y is the electric field threshold and is referred to as the critical yield point of the droplet, and κ is the curvature at the droplet's electric pole. In another experiment, we found that the wrinkling wavelength of the particle film depended on the diameter of the particle, and the wrinkling wavelength scaled as $\lambda \propto \sqrt{d}$, where d is the particle diameter. Finally, we studied the absorption of electric stress by asymmetric Pickering droplets. We found that particle shells can deform either through folding or through inward indentation. In this research, I co-designed all the experiments, performed all the actual experiments and wrote the first draft of the paper.

In all the experiments performed within **Papers 1–7**, we tested the behavior of droplets subjected to a uniform electric field. In the last contribution, **Paper 8** (*in preparation*), we studied mechanical properties of particle-covered droplets probed by a non-uniform electric field. We created electric fields with different intensities and field gradients by changing the shape of the signal electrode and its position with respect to the stationary plate-shaped electrode. The experimental results on droplet deformation are compared with the theoretical calculations obtained through modelling of the distribution of a non-uniform electric field around a cylindrical electrode using the finite element method. We found quite good agreement between the experimental results and the theoretical predictions for droplet deformations, especially for moderate electric potentials, up to 1 kV. In this research, I designed all the experiments, initiated the project, performed all the actual experiments and wrote the first draft of the paper.

References

- [1] T. Bollhorst, K. Rezwani, M. Maas, Colloidal capsules: nano- and microcapsules with colloidal particle shells, *Chemical Society Reviews*, **46** (2017) 2091–2126.
- [2] T. Brugarolas, F. Tu, D. Lee, Directed assembly of particles using microfluidic droplets and bubbles, *Soft Matter*, **9** (2013) 9046–9058.
- [3] M.S. Abbasi, H. Farooq, H. Ali, A.H. Kazim, R. Nazir, A. Shabbir, S. Cho, R. Song, J. Lee, Deformation of emulsion droplet with clean and particle-covered interface under an electric field, *Materials*, **13** (2020) 2984.
- [4] P. Dommersnes, Z. Rozynek, A. Mikkelsen, R. Castberg, K. Kjerstad, K. Hersvik, J.O. Fossum, Active structuring of colloidal armour on liquid drops, *Nature Communications*, **4** (2013).
- [5] T. Kubiak, J. Banaszak, A. Józefczak, Z. Rozynek, Direction-specific release from capsules with homogeneous or Janus shells using an ultrasound approach, *ACS Applied Materials & Interfaces*, **12** (2020) 15810–15822.
- [6] R. Bielas, D. Surdeko, K. Kaczmarek, A. Józefczak, The potential of magnetic heating for fabricating Pickering-emulsion-based capsules, *Colloids and Surfaces B: Biointerfaces*, **192** (2020) 111070.
- [7] E. Dickinson, Food emulsions and foams: Stabilization by particles, *Current Opinion in Colloid & Interface Science*, **15** (2010) 40–49.
- [8] M.H. Asfour, H. Elmotasem, D.M. Mostafa, A. Salama, Chitosan based Pickering emulsion as a promising approach for topical application of rutin in a solubilized form intended for wound healing: In vitro and in vivo study, *International Journal of Pharmaceutics*, **534** (2017) 325–338.
- [9] V.O. Ikem, A. Menner, T.S. Horozov, A. Bismarck, Highly permeable macroporous polymers synthesized from Pickering medium and high internal phase emulsion templates, *Advanced Materials*, **22** (2010) 3588–3592.
- [10] E. Sowade, T. Blaudeck, R.R. Baumann, Self-assembly of spherical colloidal photonic crystals inside inkjet-printed droplets, *Crystal Growth & Design*, **16** (2016) 1017–1026.
- [11] J.H. Lee, G.H. Choi, K.J. Park, D. Kim, J. Park, S. Lee, H. Yi, P.J. Yoo, Dual-colour generation from layered colloidal photonic crystals harnessing “core hatching” in double emulsions, *Journal of Materials Chemistry C*, **7** (2019) 6924–6931.
- [12] Z. Yu, Y. Lan, R.M. Parker, W. Zhang, X. Deng, O.A. Scherman, C. Abell, Dual-responsive supramolecular colloidal microcapsules from cucurbit[8]uril molecular recognition in microfluidic droplets, *Polymer Chemistry*, **7** (2016) 5996–6002.
- [13] V. Liljeström, C. Chen, P. Dommersnes, J.O. Fossum, A.H. Gröschel, Active structuring of colloids through field-driven self-assembly, *Current Opinion in Colloid & Interface Science*, **40** (2019) 25–41.
- [14] A. Mikkelsen, Z. Rozynek, Mechanical properties of particle films on curved interfaces probed through electric field-induced wrinkling of particle shells, *ACS Applied Materials & Interfaces*, **11** (2019) 29396–29407.
- [15] P. Erni, H.A. Jerri, K. Wong, A. Parker, Interfacial viscoelasticity controls buckling, wrinkling and arrest in emulsion drops undergoing mass transfer, *Soft Matter*, **8** (2012) 6958–6967.
- [16] P. Lipowsky, M.J. Bowick, J.H. Meinke, D.R. Nelson, A.R. Bausch, Direct visualization of dislocation dynamics in grain-boundary scars, *Nature Materials*, **4** (2005) 407–411.
- [17] F. Sicard, A. Striolo, Buckling in armored droplets, *Nanoscale*, **9** (2017) 8567–8572.
- [18] E.L. Chaikof, Engineering and material considerations in islet cell transplantation, *Annual Review of Biomedical Engineering*, **1** (1999) 103–127.
- [19] B. Peng, L. Zhang, J. Luo, P. Wang, B. Ding, M. Zeng, Z. Cheng, A review of nanomaterials for nanofluid enhanced oil recovery, *RSC Advances*, **7** (2017) 32246–32254.
- [20] S. Drexler, J. Faria, M.P. Ruiz, J.H. Harwell, D.E. Resasco, Amphiphilic nanohybrid catalysts for reactions at the water/oil interface in subsurface reservoirs, *Energy & Fuels*, **26** (2012) 2231–2241.

- [21] J. Tang, P.J. Quinlan, K.C. Tam, Stimuli-responsive Pickering emulsions: recent advances and potential applications, *Soft Matter*, **11** (2015) 3512–3529.
- [22] G. Xiuqing, P. Suili, W. Weijia, S. Ping, L. Weihua, Design and fabrication of magnetically functionalized core/shell microspheres for smart drug delivery, *Advanced Functional Materials*, **19** (2009) 292–297.
- [23] S.-Y. Tan, R.F. Tabor, L. Ong, G.W. Stevens, R.R. Dagastine, Nano-mechanical properties of clay-armoured emulsion droplets, *Soft Matter*, **8** (2012) 3112–3121.
- [24] L. Bécu, L. Benyahia, Strain-induced droplet retraction memory in a Pickering emulsion, *Langmuir*, **25** (2009) 6678–6682.
- [25] I. Koleva, H. Rehage, Deformation and orientation dynamics of polysiloxane microcapsules in linear shear flow, *Soft Matter*, **8** (2012) 3681–3693.
- [26] Y. Rane, E. Foster, M. Moradiafrapoli, J.O. Marston, Compressive deformation of liquid marbles, *Powder Technology*, **338** (2018) 7–16.
- [27] M. Alghane, Y.Q. Fu, B.X. Chen, Y. Li, M.P.Y. Desmulliez, A.J. Walton, Streaming phenomena in microdroplets induced by Rayleigh surface acoustic wave, *Journal of Applied Physics*, **109** (2011) 114901.
- [28] D. Zang, J. Li, Z. Chen, Z. Zhai, X. Geng, B.P. Binks, Switchable opening and closing of a liquid marble via ultrasonic levitation, *Langmuir*, **31** (2015) 11502–11507.
- [29] Q. Xie, G.B. Davies, J. Harting, Direct assembly of magnetic Janus particles at a droplet interface, *ACS Nano*, **11** (2017) 11232–11239.
- [30] M. Ouriemi, P.M. Vlahovska, Electrohydrodynamic deformation and rotation of a particle-coated drop, *Langmuir*, **31** (2015) 6298–6305.
- [31] M. Ouriemi, P.M. Vlahovska, Electrohydrodynamics of particle-covered drops, *Journal of Fluid Mechanics*, **751** (2014) 106–120.
- [32] A. Mikkelsen, J. Wojciechowski, M. Rajňák, J. Kurimský, K. Khobaib, A. Kertmen, Z. Rozynek, Electric field-driven assembly of sulfonated polystyrene microspheres, *Materials*, **10** (2017) 329.
- [33] S. Nudurupati, M. Janjua, N. Aubry, P. Singh, Concentrating particles on drop surfaces using external electric fields, *Electrophoresis*, **29** (2008) 1164–1172.
- [34] A. Ramos, H. Morgan, N.G. Green, A. Castellanos, The role of electrohydrodynamic forces in the dielectrophoretic manipulation and separation of particles, *Journal of Electrostatics*, **47** (1999) 71–81.
- [35] M. Li, D. Li, Redistribution of charged aluminum nanoparticles on oil droplets in water in response to applied electrical field, *Journal of Nanoparticle Research*, **18** (2016) 120.
- [36] E. Amah, K. Shah, I. Fischer, P. Singh, Electrohydrodynamic manipulation of particles adsorbed on the surface of a drop, *Soft Matter*, **12** (2016) 1663–1673.
- [37] Z. Rozynek, P. Dommersnes, A. Mikkelsen, L. Michels, J.O. Fossum, Electrohydrodynamic controlled assembly and fracturing of thin colloidal particle films confined at drop interfaces, *Eur. Phys. J.-Spec. Top.*, **223** (2014) 1859–1867.
- [38] P. Siahcheshm, F. Goharpey, R. Foudazi, Droplet retraction in the presence of nanoparticles with different surface modifications, *Rheologica Acta*, **57** (2018) 729–743.
- [39] A. Mikkelsen, P. Dommersnes, Z. Rozynek, A. Gholamipour-Shirazi, M.d.S. Carvalho, J.O. Fossum, Mechanics of Pickering drops probed by electric field-induced stress, *Materials*, **10** (2017) 436.
- [40] C. Monteux, J. Kirkwood, H. Xu, E. Jung, G.G. Fuller, Determining the mechanical response of particle-laden fluid interfaces using surface pressure isotherms and bulk pressure measurements of droplets, *Physical Chemistry Chemical Physics*, **9** (2007) 6344–6350.
- [41] H. Xu, S. Melle, K. Golemanov, G. Fuller, Shape and buckling transitions in solid-stabilized drops, *Langmuir*, **21** (2005) 10016–10020.
- [42] C.T. O'Konski, H.C. Thacher, The distortion of aerosol droplets by an electric field, *The Journal of Physical Chemistry*, **57** (1953) 955–958.
- [43] G. I. Taylor, Disintegration of water drops in an electric field, *Proceedings of the Royal Society of London. Series A. Mathematical and Physical Sciences*, **280** (1964) 383–397.

- [44] C.G. Garton, Z. Krasucki, Bubbles in insulating liquids: stability in an electric field, *Proceedings of the Royal Society of London. Series A. Mathematical and Physical Sciences*, **280** (1964) 211–226.
- [45] J.D. Sherwood, Breakup of fluid droplets in electric and magnetic fields, *Journal of Fluid Mechanics*, **188** (1988) 133–146.
- [46] J. Hua, L.K. Lim, C.-H. Wang, Numerical simulation of deformation/motion of a drop suspended in viscous liquids under influence of steady electric fields, *Physics of Fluids*, **20** (2008) 113302.
- [47] R.S. Allan, S.G. Mason, L.E. Marion, Particle behaviour in shear and electric fields I. Deformation and burst of fluid drops, *Proceedings of the Royal Society of London. Series A. Mathematical and Physical Sciences*, **267** (1962) 45–61.
- [48] S. Torza, R. G. Cox, S.G. Mason, Electrohydrodynamic deformation and bursts of liquid drops, *Philosophical Transactions of the Royal Society of London. Series A*, **269** (1971) 295–319.
- [49] P.A. Arp, R.T. Foister, S.G. Mason, Some electrohydrodynamic effects in fluid dispersions, *Advances in Colloid and Interface Science*, **12** (1980) 295–356.
- [50] O. Vizika, D.A. Saville, The electrohydrodynamic deformation of drops suspended in liquids in steady and oscillatory electric fields, *Journal of Fluid Mechanics*, **239** (1992) 1–21.
- [51] H. Jong-Wook, Y. Seung-Man, Effects of surfactant on the deformation and stability of a drop in a viscous fluid in an electric field, *Journal of Colloid and Interface Science*, **175** (1995) 369–385.
- [52] D.A. Saville, Electrohydrodynamics: The Taylor-Melcher Leaky Dielectric Model, *Annual Review of Fluid Mechanics*, **29** (1997) 27–64.
- [53] G. Taylor, Studies in electrohydrodynamics. I. The circulation produced in a drop by electrical field, *Proceedings of the Royal Society of London. Series A. Mathematical and Physical Sciences*, **291** (1966) 159–166.
- [54] T.B. Jones, Quincke rotation of spheres, *IEEE Transactions on Industry Applications*, **IA-20** (1984) 845–849.
- [55] P.F. Salipante, P.M. Vlahovska, Electrohydrodynamics of drops in strong uniform dc electric fields, *Physics of Fluids*, **22** (2010) 112110.
- [56] E.K. Zholkovskij, J.H. Masliyah, J.A.N. Czarnecki, An electrokinetic model of drop deformation in an electric field, *Journal of Fluid Mechanics*, **472** (2002) 1–27.
- [57] J.W. Ha, S.M. Yang, Deformation and breakup of Newtonian and non-Newtonian conducting drops in an electric field, *Journal of Fluid Mechanics*, **405** (2000) 131–156.
- [58] N. Benteinis, S. Krause, Droplet deformation in DC electric fields: The extended Leaky Dielectric Model, *Langmuir*, **21** (2005) 6194–6209.
- [59] O.O. Ajayi, T.G. Cowling, A note on Taylor's electrohydrodynamic theory, *Proceedings of the Royal Society of London. A. Mathematical and Physical Sciences*, **364** (1978) 499–507.
- [60] J.Q. Feng, T.C. Scott, A computational analysis of electrohydrodynamics of a leaky dielectric drop in an electric field, *Journal of Fluid Mechanics*, **311** (1996) 289–326.
- [61] J.Q. Feng, Electrohydrodynamic behaviour of a drop subjected to a steady uniform electric field at finite electric Reynolds number, *Proceedings of the Royal Society of London. Series A: Mathematical, Physical and Engineering Sciences*, **455** (1999) 2245.
- [62] G. Supeene, C.R. Koch, S. Bhattacharjee, Deformation of a droplet in an electric field: nonlinear transient response in perfect and leaky dielectric media, *Journal of colloid and interface science*, **318** (2008) 463–476.
- [63] J.M. López-Herrera, S. Popinet, M.A. Herrada, A charge-conservative approach for simulating electrohydrodynamic two-phase flows using volume-of-fluid, *Journal of Computational Physics*, **230** (2011) 1939–1955.
- [64] J.A. Lanauze, L.M. Walker, A.S. Khair, Nonlinear electrohydrodynamics of slightly deformed oblate drops, *Journal of Fluid Mechanics*, **774** (2015) 245–266.
- [65] D. Das, D. Saintillan, A nonlinear small-deformation theory for transient droplet electrohydrodynamics, *Journal of Fluid Mechanics*, **810** (2017) 225–253.
- [66] R. Sengupta, L.M. Walker, A.S. Khair, The role of surface charge convection in the electrohydrodynamics and breakup of prolate drops, *Journal of Fluid Mechanics*, **833** (2017) 29–53.

- [67] G. Quincke, Ueber Rotationen im constanten electrischen Felde, *Annalen der Physik*, **295** (1896) 417-486.
- [68] Q. Brosseau, G. Hickey, P.M. Vlahovska, Electrohydrodynamic Quincke rotation of a prolate ellipsoid, *Physical Review Fluids*, **2** (2017) 014101.
- [69] E. Lemaire, L. Lobry, Chaotic behavior in electro-rotation, *Physica A: Statistical Mechanics and its Applications*, **314** (2002) 663–671.
- [70] Y. Gu, H. Zeng, Optically tunable Quincke rotation of a nanometer-thin oblate spheroid, *Physical Review Fluids*, **2** (2017) 083701.
- [71] J.-W. Ha, S.-M. Yang, Electrohydrodynamics and electrorotation of a drop with fluid less conductive than that of the ambient fluid, *Physics of Fluids*, **12** (2000) 764–772.
- [72] S. Krause, P. Chandratreya, Electrorotation of deformable fluid droplets, *Journal of Colloid and Interface Science*, **206** (1998) 10–18.
- [73] H. He, P.F. Salipante, P.M. Vlahovska, Electrorotation of a viscous droplet in a uniform direct current electric field, *Physics of Fluids*, **25** (2013) 032106.
- [74] N. Dubash, A.J. Mestel, Behaviour of a conducting drop in a highly viscous fluid subject to an electric field, *Journal of Fluid Mechanics*, **581** (2007) 469–493.
- [75] E. Lac, G.M. Homsy, Axisymmetric deformation and stability of a viscous drop in a steady electric field, *Journal of Fluid Mechanics*, **590** (2007) 239–264.
- [76] S.D. Deshmukh, R.M. Thaokar, Deformation and breakup of a leaky dielectric drop in a quadrupole electric field, *Journal of Fluid Mechanics*, **731** (2013) 713–733.
- [77] Q. Dong, A. Sau, Breakup of a leaky dielectric drop in a uniform electric field, *Physical Review E*, **99** (2019) 043106.
- [78] Q. Brosseau, P.M. Vlahovska, Streaming from the equator of a drop in an external electric field, *Physical Review Letters*, **119** (2017) 034501.
- [79] C.A.S. Burel, A. Alsayed, L. Malassis, C.B. Murray, B. Donnio, R. Dreyfus, Plasmonic-based mechanochromic microcapsules as strain sensors, *Small*, **13** (2017).
- [80] P. Sanders, A.J. Young, Y. Qin, K.S. Fancey, M.R. Reithofer, R. Guillet-Nicolas, F. Kleitz, N. Pamme, J.M. Chin, Stereolithographic 3D printing of extrinsically self-healing composites, *Sci Rep*, 2019, pp. 388.
- [81] W. Ramsden, F. Gotch, Separation of solids in the surface-layers of solutions and suspensions; (observations on surface-membranes, bubbles, emulsions, and mechanical coagulation), *Proceedings of the Royal Society of London*, **72** (1903) 156–164.
- [82] S.U. Pickering, Emulsions, *Journal of the Chemical Society, Transactions*, **91** (1907) 2001–2021.
- [83] S. Levine, B.D. Bowen, S.J. Partridge, Stabilization of emulsions by fine particles I. Partitioning of particles between continuous phase and oil/water interface, *Colloids and Surfaces*, **38** (1989) 325–343.
- [84] R. McGorty, J. Fung, D. Kaz, V.N. Manoharan, Colloidal self-assembly at an interface, *Materials Today*, **13** (2010) 34–42.
- [85] P. Dommersnes, A. Mikkelsen, J.O. Fossum, Electro-hydrodynamic propulsion of counter-rotating Pickering drops, *The European Physical Journal Special Topics*, **225** (2016) 699–706.
- [86] A. Mikkelsen, P. Dommersnes, J.O. Fossum, Electric stress-induced slip lines in jammed particle monolayers, *Revista Cubana de Física*, **33** (2016) 3.
- [87] K.S. Chang, W.L. Olbricht, Experimental studies of the deformation of a synthetic capsule in extensional flow, *Journal of Fluid Mechanics*, **250** (1993) 587–608.
- [88] D. Barthes-Biesel, A. Diaz, E. Dhenin, Effect of constitutive laws for two-dimensional membranes on flow-induced capsule deformation, *Journal of Fluid Mechanics*, **460** (2002) 211–222.
- [89] A. Walter, H. Rehage, H. Leonhard, Shear-induced deformations of polyamide microcapsules, *Colloid and Polymer Science*, **278** (2000) 169–175.
- [90] S. Ramanujan, C. Pozrikidis, Deformation of liquid capsules enclosed by elastic membranes in simple shear flow: large deformations and the effect of fluid viscosities, *Journal of Fluid Mechanics*, **361** (1998) 117–143.

- [91] M. Kaganyuk, A. Mohraz, Shear-induced deformation and interfacial jamming of solid-stabilized droplets, *Soft Matter*, **16** (2020) 4431–4443.
- [92] R.M. Hochmuth, R.E. Waugh, Erythrocyte membrane elasticity and viscosity, *Annual Review of Physiology*, **49** (1987) 209–219.
- [93] J.-W. Ha, S.-M. Yang, Electrohydrodynamic effects on the deformation and orientation of a liquid capsule in a linear flow, *Physics of Fluids*, **12** (2000) 1671–1684.
- [94] S. Das, R.M. Thaokar, Large deformation electrohydrodynamics of a Skalak elastic capsule in AC electric field, *Soft Matter*, **14** (2018) 1719–1736.
- [95] S. Das, R.M. Thaokar, Large-deformation electrohydrodynamics of an elastic capsule in a DC electric field, *Journal of Fluid Mechanics*, **841** (2018) 489–520.
- [96] R.B. Karyappa, S.D. Deshmukh, R.M. Thaokar, Deformation of an elastic capsule in a uniform electric field, *Physics of Fluids*, **26** (2014) 122108.
- [97] G.C. Randall, Electric field deformation of protein-coated droplets in thin channels, *Langmuir*, **34** (2018) 10028–10039.
- [98] A. Toor, T. Feng, T.P. Russell, Self-assembly of nanomaterials at fluid interfaces, *The European Physical Journal E*, **39** (2016) 57.
- [99] E.C. Amah, K. Shah, I.S. Fischer, P. Singh, Self-assembly and manipulation of particles on drop surfaces, *ASME proceedings*, doi: 10.1115/FEDSM2014-21792(2014).
- [100] M. Cui, T. Emrick, T.P. Russell, Stabilizing liquid drops in nonequilibrium shapes by the interfacial jamming of nanoparticles, *Science*, **342** (2013) 460–463.
- [101] Z. Rozynek, A. Mikkelsen, P. Dommersnes, J.O. Fossum, Electroformation of Janus and patchy capsules, *Nature Communications*, **5** (2014) 6.
- [102] Z. Rozynek, A. Józefczak, Patchy colloidosomes - an emerging class of structures, *The European Physical Journal Special Topics*, **225** (2016) 741–756.
- [103] Z. Rozynek, R. Bielas, A. Józefczak, Efficient formation of oil-in-oil Pickering emulsions with narrow size distributions by using electric fields, *Soft Matter*, **14** (2018) 5140–5149.
- [104] A.R. Studart, H.C. Shum, D.A. Weitz, Arrested coalescence of particle-coated droplets into nonspherical supracolloidal structures, *The Journal of Physical Chemistry B*, **113** (2009) 3914–3919.
- [105] J. Wang, M. Jin, Y. Gong, H. Li, S. Wu, Z. Zhang, G. Zhou, L. Shui, J.C.T. Eijkel, A. van den Berg, Continuous fabrication of microcapsules with controllable metal covered nanoparticle arrays using droplet microfluidics for localized surface plasmon resonance, *Lab on a Chip*, **17** (2017) 1970–1979.
- [106] S. Nudurupati, M. Janjua, P. Singh, N. Aubry, Effect of parameters on redistribution and removal of particles from drop surfaces, *Soft Matter*, **6** (2010) 1157–1169.

Publications constituting the dissertation

Paper I

Transient deformation dynamics of particle laden droplets in electric field

A Mikkelsen, Z Rozynek, K Khobaib, P Dommersnes and J O Fossum

Colloids and Surfaces A **532**, 252–256 (2017)



Transient deformation dynamics of particle laden droplets in electric field



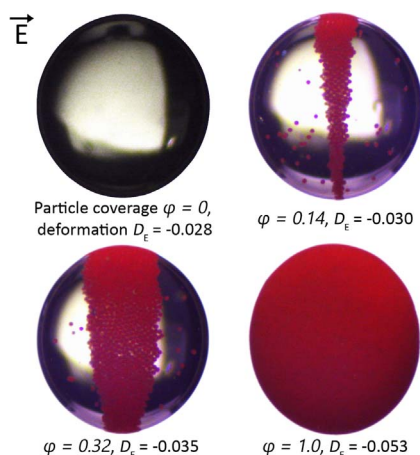
Alexander Mikkelsen^{a,b,*,1}, Zbigniew Rozynek^{a,1}, Khobaib Khobaib^a, Paul Dommersnes^b,
Jon Otto Fossum^{b,c}

^a Adam Mickiewicz University, Faculty of Physics, Umultowska 85, 61-614 Poznań, Poland

^b Department of Physics, Norwegian University of Science and Technology, Høgskoleringen 5, 7491 Trondheim, Norway

^c Institut Pierre-Gilles de Gennes, 6-12 rue Jean Calvin, Paris 75005, France

GRAPHICAL ABSTRACT



ARTICLE INFO

Keywords:

Particle laden droplets
Electric field
Deformation
Particle structuring
Electrohydrodynamics
Colloidal particles

ABSTRACT

We study the transient deformation dynamics after application of uniform DC electric fields to particle laden droplets with different polyethylene particle coverage. Presence of interfacial particles result in reduced electrohydrodynamic circulation flows and charge convection, which in turn result in slower transient droplet deformation compared to pure uncovered droplets, and as well to increased steady-state droplet deformation. A prolate-oblate deformation transition is observed immediately after the application of the electric field. This anomaly is not visible or greatly reduced for droplets fully covered by particles.

1. Introduction

The dynamics of soft materials subjected to electric fields have lately attracted much attention in a variety of areas such as the dynamics of pendant and sessile droplets [1,2], electrorheological response in

emulsions [3–5], vesicle manipulation [6–8] and colloidal particle manipulation at droplet interfaces [9–13]. Deformation of droplets plays key roles in many industrial applications and/or natural processes such as microfluidic systems (chemical reactors), combustion systems, electrohydrodynamic ink-jet printers, emulsification, mixing processes,

* Corresponding author at: Adam Mickiewicz University, Faculty of Physics, Umultowska 85, 61-614 Poznań, Poland.

E-mail address: alexam@amu.edu.pl (A. Mikkelsen).

¹ These authors contribute equally.

biological cell systems or enhanced oil recovery [14–17].

It is energetically favourable for particles to bind at droplet interfaces, thus confining particle movement to within the interface. This has proven essential for a variety of studies and applications, including material development [10,18,19], emulsions stabilization [20–22], two-dimensional particle systems [23–25] and particle structuring [9,13,26]. The deformation of particle-free and particle laden droplets has previously been investigated by mechanical compression [27,28], microfluidics focusing devices [29], in hydrodynamic shear flows [30–33] and by magnetic or electric fields [9–12,34–38].

To understand the electric response of such complex systems, it is important to quantify the dynamics and time scales of simpler systems, for instance single droplets, for which the surface particle coverage φ is systematically increased from zero to full particle coverage. Here we study the transient deformation of weakly conductive droplets of silicone oil with different particle coverages. The electrohydrodynamic deformation of weakly conducting droplets without particles is described by Taylor's model [39], which has subsequently been developed by Melcher [40] and others [41–43]. The model is based on the assumptions that the two fluids have finite electric conductivities which yields a charge build-up at the droplet interface creating an interfacial electrical shear stress. In addition to a normal stress component balanced by the droplet surface tension, the electric stress has a tangential component that sets up viscous electrohydrodynamic flows.

Assuming that the deformations are small, and that the time required for the interface to acquire its steady-state surface charge density distribution, is much shorter than the convective time, the Taylor-model deformation is proportional to the applied electric field squared, and the droplet deformation is given by the electric properties of the fluids [39]:

$$D_E = \frac{d_{||} - d_{\perp}}{d_{||} + d_{\perp}} = \frac{9a\epsilon_0\epsilon_{ex}E_0^2}{16\gamma S(2+R)^2} \left[S(R^2 + 1) - 2 + 3(RS - 1) \frac{2\lambda + 3}{5\lambda + 5} \right],$$

where $d_{||}$ and d_{\perp} respectively are the droplet axis parallel and perpendicular with the electric field direction, ϵ_0 the vacuum permittivity, ϵ_{ex} the relative dielectric constant of the surrounding exterior fluid, a the droplet radius, γ the interfacial surface tension between the droplet and exterior fluid, while the dimensionless numbers R , S and λ are the conductivity, dielectric constant and viscosity ratios, respectively: $R = \sigma_{in}/\sigma_{ex}$, $S = \epsilon_{ex}/\epsilon_{in}$, $\lambda = \mu_{ex}/\mu_{in}$. Dimensional and dimensionless parameters for our system (silicone oil suspended in castor oil) are listed in Table 1 in the Materials section.

Since Taylor's pioneering work on electro-hydrodynamics [39], which is considering small deformations, several theoretical and computational investigations have been worked out to predict the transient deformation observed in experiments. Due to the challenges in coupling the interfacial charge distribution to the induced fluid flow, the transient charge relaxation and the charge convection driven by the interfacial flow are most often neglected in models. Taylor's model predicts both prolate and oblate steady-state deformations, but does not include charge convection and transient deformation effects. These effects are important to predict the right droplet shape evolution and to improve the accuracy of predictions [44,45].

For particle covered droplets, the electric properties of the surface particles are of importance, as they may suppress DC electric field induced electrohydrodynamic flows and stretch the droplet if the

Table 1

Set of parameters for a silicone oil droplet suspended in castor oil. The top section of the table lists dimensional parameters for the droplet and the bath medium, while the bottom section lists dimensionless groups. The electric field is set to 200 V mm⁻¹.

Phase	ϵ_r	σ (S m ⁻¹)	μ (Pa s)	ρ (kg m ⁻³)	a (mm)	γ (mN m ⁻¹)
Droplet (silicone oil)	2.8	5.6×10^{-12}	0.05	959	1.0	4.5
Medium (castor oil)	4.7	5.6×10^{-11}	0.75	960		
	Ca_E	Re_E	Sa_{ex}	S	λ	R
	0.4	1.3	4.5	1.7	15	0.1

electrical conductivity of the particles is sufficiently high [9]. Suppression of electrohydrodynamic flows is also expected and observed in this case if the particle surface coverage is high (φ approximately or above 90%) [11,35]. For sufficiently low particle concentration, the particles form thin electric-equatorial ribbons at the droplet surface in applied DC electric field, however in this case there may still be circulation flows in the particle-free electric-polar areas. For fully covered droplets, a capsule type model has to be used, for example an elastic model [11] or a fluid shell description [35].

Here we investigate how surface particles influence transient droplet deformation by both weakening the charge convection and by strengthening the charge relaxation. We quantify the effects of surface particles on droplet deformation times, steady-state deformation and prolate-oblate anomalies for a range of droplet sizes, coverages and applied electric field strengths.

2. Material and methods

The current experiments were performed in an optical square acrylic cuvette (10 × 10 × 45 mm), with two copper plates constituting electrodes. The distance between the electrodes was 7.8 mm. Castor oil (Sigma-Aldrich 83912, density 0.961 g cm⁻³ at 25 °C, electrical conductivity ~60 pS m⁻¹, relative permittivity 4.7 at 25 °C, and viscosity 0.75 Pa s) was poured in the cuvette, and silicone oil (VWR Chemicals, Rhodorsil® 6678.1000, density 0.96 g cm⁻³, electrical conductivity ~5–6 pS m⁻¹, relative permittivity 2.8 at 25 °C, and viscosity 0.05 Pa s) droplets without and with red polyethylene particles (REDPMS-0.98 45–53 μm, relative permittivity 2.1 and density ~0.98 g cc⁻¹ purchased from Cospheric LLC) were placed inside the castor oil using a micropipette. The polyethylene particles were dispersed in the silicone oil, and the concentration was numerically characterized by weight percent. To avoid aggregation, the samples were placed in an ultrasonic bath for 5 min and mechanically shaken. There is a small density difference between the fluids, as well as between the fluids and the particles, however, the droplet sedimentation velocity was sufficiently small enough to enable us to neglect sedimentation effects. DC electric fields with strength between 0 and 300 V mm⁻¹ were applied by connecting the electrodes to a high voltage amplifier (5HVA24-BP1 Ultravolt®, Advanced Energy®), controlled by a voltage signal generator and monitored by an oscilloscope.

The droplet dynamics was studied and recorded through an IDS camera (UI-3590CP-C-HQ R2, IDS Imaging Development Systems GmbH) with magnifying lenses (Thorlabs, High-Magnification Zoom Lens Systems). Movies and images with a resolution of 1028 × 768 (XGA) and 50 fps framerate with uEye Cockpit software, were recorded.

The transient droplet deformations were estimated by analyzing 50 fps. The recorded movies were converted to frames by using a JPG converter software. In each frame, the edge of the droplets was recognized and fitted with an ellipse using ImageJ software. The axes of the droplets parallel and perpendicular to the electric field direction were measured from the fitting procedure. The droplet deformation is defined here as $D = (d_{||} - d_{\perp}) / (d_{||} + d_{\perp})$, where $d_{||}$ and d_{\perp} are the drop axes parallel and perpendicular to the electric field direction, respectively. We calculated the deformation for each frame and normalized it by the deformation before the electric field was turned on, by subtracting the average deformation of the first hundred frames. This latter procedure was necessary because the ImageJ software cannot distinguish the edge of the droplet from the edge of the surface particles and therefore measured some of the particle droplets to be slightly deformed (up to $D = 0.01$) even before the electric field was applied.

We define here the particle coverage of the droplets as $\varphi = S/A$, where A is the surface area of the droplet and $S = 2\pi ah$ [46] is the surface area of the particle ribbon film (a spherical segment defined by cutting a sphere with a pair of parallel planes), a the radius of the droplet and h the width of the ribbon. φ is defined as 1 when the droplet is fully covered by particles, and 0 when the droplet is particle-free.

3. Results and discussions

3.1. Transient deformation of particle laden droplets

We study the deformation of polyethylene laden silicone oil droplets

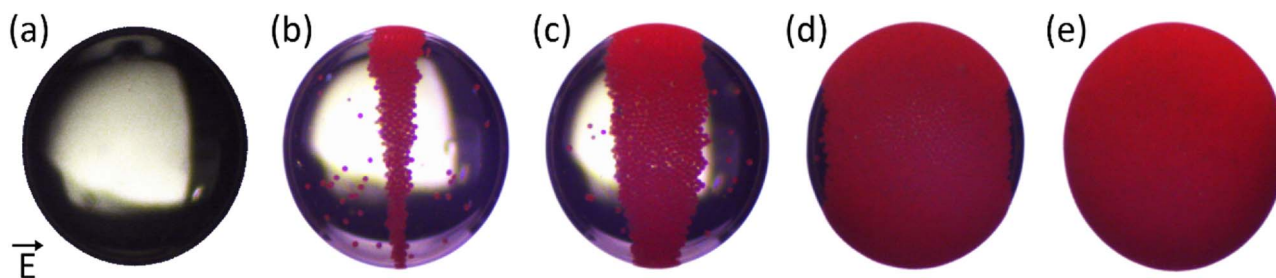


Fig. 1. Silicone oil droplets with different particle coverage and suspended in castor oil. Silicone oil droplets (diameters 2.0 mm) (a) without and (b)–(e) with red polyethylene particles subjected to a DC electric field of strength 200 V mm^{-1} . The particle coverage for the five droplets are respectively (a) 0, (b) 0.14, (c) 0.32, (d) 0.83 and (e) 1.

that are suspended in castor oil and subjected to DC electric fields. Fig. 1 presents images of five silicone oil droplets (diameters 2.0 mm) with various polyethylene particle coverages, where the ratio between the particle coverage ranges between 0 and 1, all subjected to a DC electric field of strength 200 V mm^{-1} . When uniform DC electric fields are applied in this way, charges accumulate at the interface between the two liquids [39] due their contrast in electric conductivities and dielectric permittivity. Depending on the relative electric properties of the fluids and particles, such a droplet can be stretched to a prolate, or compressed to an oblate shape [9,38] when subjected to an applied electric field. The polarity of the induced droplet surface charge depends on the charge relaxation time $\tau_{e,\text{in}} = \epsilon_0 \epsilon_{\text{in}} / \sigma_{\text{in}}$ of the droplet relative to that of the external fluid $\tau_{e,\text{ex}} = \epsilon_0 \epsilon_{\text{ex}} / \sigma_{\text{ex}}$ [40,42]. Since the surrounding castor oil conducts better than the silicone oil droplet, the dipole moment of the droplets in Fig. 1 is aligned antiparallel with the electric field direction and the electric stress exerts a compressive force on the droplets, i.e. an oblate (negative) deformation occurs ($d_{\perp} > d_{\parallel}$).

When electric charges reach the droplet interface, electrohydrodynamic circulation flows are induced by tangential electric stresses. The direction of the circulation flows is given by the relative magnitudes of the electric conductivities and dielectric constants of the fluids, and the induced flows can transport surface particles to the droplet electric equator area or to the electric pole areas [39] respectively. In our present oil in oil system, the polyethylene particles are structured in ribbons at the droplet surfaces where the particle packing increases with time and also with the applied electric field strength [36]. In the deformation experiments described in the following, we limited the applied electric field to 300 V mm^{-1} to avoid effects such as electrically induced Quincke rotation [11,12,47], droplet breakup [38,48,49] or spinning particle domains [9,11,12].

In Fig. 2 we display the transient deformation of the droplets in Fig. 1. The transient droplet deformation of a droplet is governed by three characteristic times: the charge relaxation time τ_e , which is the time scale for the interface to acquire its steady-state surface charge density distribution, the capillary time $\tau_c = \mu\alpha/\gamma$, which is the time scale for droplet relaxation due to capillary forces, and the flow time scale $\tau_f = \mu/(\epsilon_0 \epsilon_{\text{ex}} E^2)$, which is the time scale for transporting charges by hydrodynamic convection.

In the inset in Fig. 2a, shortly after the electric field is turned on, we observe a transient prolate to oblate anomaly, i.e. the measured droplet deformations evolve from positive (stretched out) to negative (compressed). This appears to be most pronounced for particle covered droplets that are not fully covered. A similar anomaly has been reported by computational studies of droplets in [50] and characterized by the Saville number Sa_{ex} , which is defined as the ratio $\tau_{e,\text{ex}}/\tau_{c,\text{ex}}$, and is a number characterizing the charge transport towards the droplet interface [42,50]. For the 2 mm sized pure silicone oil droplet used in our experiments, Sa_{ex} is about 4.5, indicating that it takes more time to accumulate charges at the interface than to transport charges away from the interface. Thus, at early times, the droplet behaves as a perfect dielectric, and the droplet deforms along the electric field direction.

For a given electric field, the drop deformation D_E increases with particle coverage ϕ (see Fig. 2a). A silicone oil droplet fully covered by polyethylene particles (violet diamonds) has a steady-state deformation D_E twice as large compared to a particle-free silicone oil droplet (red squares). This result could potentially be due to: (i) reduced resistance to deformation related to reduced surface tension, (ii) increased elastic

stress from the particle shell, or (iii) an increase in electrical stress. Since the contributions from (i) and (ii) can be neglected for Pickering shells that are not jammed [35], we are left with (iii) for the present situations. In numerical models [11,35,45], charge convection has been shown to weaken the steady-state oblate deformation by distorting the surface charge density profile and weaken tangential stress. The electric Reynolds number Re_E represents the ratio of the charge relaxation time scale τ_e to the flow time scale τ_f . A small electric Reynolds number (< 1) indicates that it takes more time to transport charges by convection than the time it takes to build up charges at the droplet interface. Since $Re_E \approx 1$ for the silicone oil in castor oil system, charge relaxation by convection influences the steady-state droplet deformation. Without electrohydrodynamic flow, no charge convection is present in and around the fully covered droplets, thus explaining the larger electric stress and droplet deformation. In addition, the insulating polyethylene particles at the droplet surface decrease the effective conductivity of the droplet which then leads to a larger charge accumulation at the droplet interface [35].

Esmaeli and Sharifi developed a simple model for the transient droplet deformation given by [51]: $D(t) = D_E [1 - \exp(-t/\tau_d)]$, where D_E is the steady-state deformation and τ_d is the time scale that governs the deformation dynamics: $\tau_d = \frac{\mu_{\text{ex}} \alpha (2\lambda + 3)(19\lambda + 16)}{40(\lambda + 1)}$. This model strictly applies to pure droplets not covered by particles.

In Fig. 2b, $\ln(1 - D(t)/D_E)$ is plotted versus time (after the application of an electric field of strength 200 V mm^{-1}) for the same droplets in Fig. 1 and Fig. 2a. The plots are linearly fitted to calculate the slope (which is the inverse of τ_d). We note the observed exponential relaxation also for particle laden drops. For a more complete model, charge convection, finite charge relaxation and transient fluid inertia has to be included. Here we can only refer to computational and numerical work [44,45,50], since to the best of our knowledge, there are currently no particle-interface models available for the time dependent deformation of particle covered droplets. However, some capsule models have been used to describe the steady-state deformation of particle laden droplets, for instance elastic models where the particle layer has shear elasticity [11,52,53] or a fluid shell description where the particle layer can be considered fluid during deformation [35].

3.2. Effect of surface particles on droplet deformation time

The time for charges to accumulate at interfaces of layered or inhomogeneous dielectrics is given by the Maxwell-Wagner charge relaxation time, which is independent of the applied electric field [54]: $\tau_{\text{MW}} = \frac{\epsilon_{\text{in}} + 2\epsilon_{\text{ex}}}{\sigma_{\text{in}} + 2\sigma_{\text{ex}}}$, τ_{MW} is approximately 0.9 s for a silicone oil droplet in castor oil system. Because the silicone oil and the polyethylene particles have much smaller electric conductivities than the castor oil, and their dielectric constants are similar, the Maxwell-Wagner charge relaxation time of the particle laden droplets will be approximately the same as the particle-free droplets in castor oil. For the silicone oil droplet (red squares) in Fig. 2a, the deformation time t_D , defined as the time for droplets to reach the arbitrarily set threshold of 95% of their steady-state deformation D_E , is measured to be $t_D \approx 1.9$ s.

Fig. 3 shows the deformation time plotted versus the particle coverage for droplets with diameters ranging from 1.0–2.5 mm and subjected to a DC electric field of strength 200 V mm^{-1} . The deformation time increases when

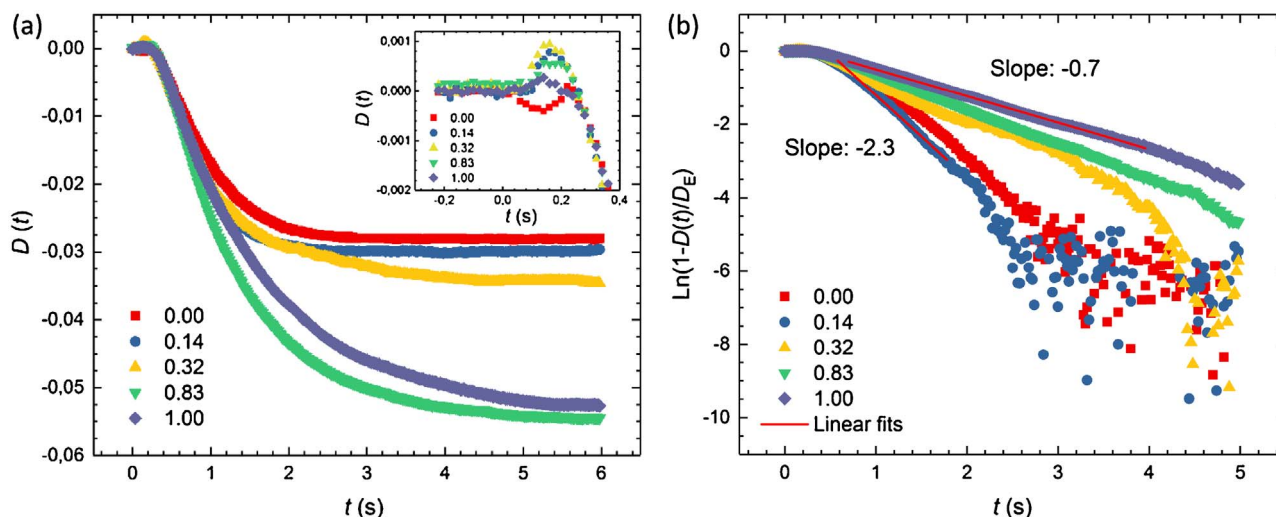


Fig. 2. Transient droplet deformation. (a) Transient deformation of 2 mm sized silicone oil droplets without and with surface particles when subjected to a 200 V mm^{-1} electric field (see Materials and Methods section for details on the measurements). The particle coverage ϕ ranges between 0 and 1. (b) $\ln(1-D(t)/D_E)$ plotted versus time.

more polyethylene particles are added to the droplet surface, which can be attributed to changes in the electric properties (conductivity and dielectric constant) of the droplet interface by the added particles. In a recent work, we concluded that the electric conductivity of a polyethylene Pickering droplet (fully particle covered droplet) is approximately 30% of a silicone oil droplet when using particles that are $50 \mu\text{m}$ (the same size as we use in the present work) [35]. Viscous dissipation due to the presence of the polyethylene particle layer might also contribute to the increased deformation time [55]. Similar to the experimental work reported in ref. [56] dealing with particle-free silicone oil droplets, we also find that the deformation time of particle covered droplets decreases with the applied electric field strength.

3.3. Deformation versus electric capillary number

The electric capillary number Ca_E is the ratio of the electric stress $\epsilon_{\text{ex}} E_0^2$ to the capillary stress γ/a . For Taylor's model to be valid, Ca_E must be sufficiently small for the deformation to be linear in Ca_E . If the electric stress becomes larger than a critical capillary stress (which is working to restore the deformed droplet to a spherical shape), the surface tension can no longer balance the electric stress and the droplet

breaks up into smaller droplets [48]. Fig. 4 displays the steady-state deformation of different sized silicone oil droplets with particle coverage ranging from 0 (no surface particles) to 1 (fully covered droplets) plotted versus the electric capillary number. As expected, the droplet deformation for all the droplets is linear with Ca_E (i.e. proportional to the droplet radius and electric field squared) for small deformations when surface tension is strong enough to overcome deformations due to electric stresses. For larger Ca_E values, the droplet deformations start to deviate from Taylor's theory. It is also observed that particle-free droplets deform less than particle covered droplets.

4. Conclusions

We show that electrically insulating polyethylene particles at the interface of silicone oil droplets results in a larger deformation compared to particle-free droplets. We conclude that this can be caused by reduced charge convection and reduced electric conductivity of the interface when the polyethylene surface coverage is high. We also find that the deformation time increases with increasing particle coverage. This may not only be caused by diminished electrohydrodynamic flows and interfacial charge convection, but can possibly also be due to particle capillary interactions. Immediately after the electric field is turned on, we observe a transient prolate to oblate anomaly, possibly caused by a delay in the interfacial charging.

Author contributions

A.M., Z.R., P.D. and J.O.F. planned all experiments. A.M. and Z.R. performed the experiments at NTNU, Norway. A.M., Z.R. and K.K. performed the experiments at AMU, Poland. A.M. wrote the manuscript. A.M., Z.R., P.D. and J.O.F. contributed in all discussions towards the finalization of the manuscript.

Competing financial interests

The authors declare no competing financial interests.

Acknowledgements

Z.R. acknowledges financial support of the Polish National Science Centre through FUGA4 programme (2015/16/S/ST3/00470). Z.R., A.M. and K.K. acknowledge financial support of the Polish National Science Centre through OPUS programme (2015/19/B/ST3/03055). A.M., P.D. and J.O.F. thank the Norwegian University of Science and Technology (NTNU) for PhD grant support. A.M. acknowledges financial support from the European Union's Horizon 2020 research and innovation

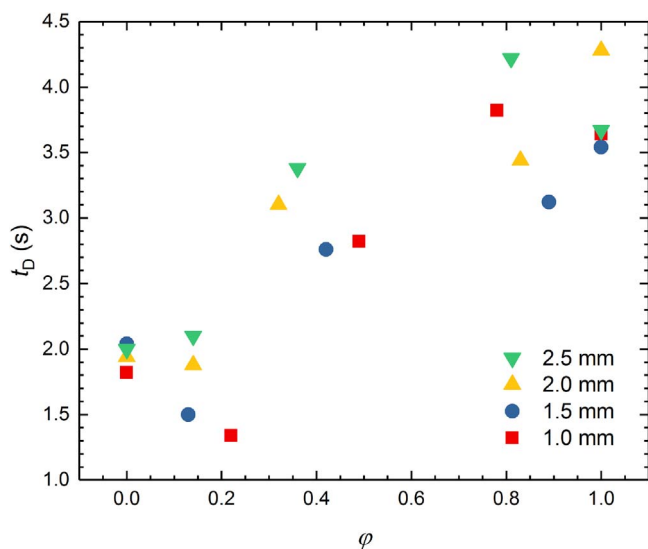


Fig. 3. (a) Deformation time (time for droplets to reach the arbitrarily set threshold of 95% of their steady-state deformation D_E) plotted versus the particle coverage ϕ (particle covered surface area/droplet surface area) for droplets with diameters ranging from 1.0–2.5 mm and subjected to a DC electric field of strength 200 V mm^{-1} .

Paper II

Electric field-driven assembly of sulfonated polystyrene microspheres

A Mikkelsen, J Wojciechowski, M Rajňák, J Kurimský, K Khobaib,
A Kertmen and Z Rozynek

Materials **10(4)**, 329 (2017)

Article

Electric Field-Driven Assembly of Sulfonated Polystyrene Microspheres

Alexander Mikkelsen ¹, Jarosław Wojciechowski ², Michal Rajňák ^{3,4}, Juraj Kurimský ⁴, Khobaib Khobaib ¹, Ahmet Kertmen ⁵ and Zbigniew Rozynek ^{1,*}

¹ Faculty of Physics, Adam Mickiewicz University, Umultowska 85, 61-614 Poznań, Poland; alexam@amu.edu.pl (A.M.); khobaib@amu.edu.pl (K.K.)

² Department of Chemistry, University of Warsaw, Ludwika Pasteura 1, 02-093 Warsaw, Poland; jaroslaww@chem.uw.edu.pl

³ Institute of Experimental Physics SAS, Watsonova 47, 040-01 Kosice, Slovakia; rajnak@saske.sk

⁴ Faculty of Electrical Engineering and Informatics, Technical University of Košice, Letná 9, 04200 Košice, Slovakia; juraj.kurimsky@tuke.sk

⁵ Faculty of Chemistry, Gdańsk University of Technology, Narutowicza 11/12, 80-233 Gdańsk, Poland; ahmet.kertmen@pg.gda.pl

* Correspondence: zbiroz@amu.edu.pl; Tel.: +48-503-775-401

Academic Editors: Andrei V. Petukhov and Gert Jan Vroege

Received: 11 February 2017; Accepted: 21 March 2017; Published: 23 March 2017

Abstract: A designed assembly of particles at liquid interfaces offers many advantages for development of materials, and can be performed by various means. Electric fields provide a flexible method for structuring particles on drops, utilizing electrohydrodynamic circulation flows, and dielectrophoretic and electrophoretic interactions. In addition to the properties of the applied electric field, the manipulation of particles often depends on the intrinsic properties of the particles to be assembled. Here, we present an easy approach for producing polystyrene microparticles with different electrical properties. These particles are used for investigations into electric field-guided particle assembly in the bulk and on surfaces of oil droplets. By sulfonating polystyrene particles, we produce a set of particles with a range of dielectric constants and electrical conductivities, related to the sulfonation reaction time. The paper presents diverse particle behavior driven by electric fields, including particle assembly at different droplet locations, particle chaining, and the formation of ribbon-like structures with anisotropic properties.

Keywords: microparticles; sulfonation; spherical polystyrene particles; electric fields; self-assembly; electric conductance; dielectric constant; electro-rheology; droplets

1. Introduction

Nano- and micrometer particles have become very important in today's technological world. Though not visible to the naked eye, they interact and dictate mechanisms in various systems, ranging from cosmetic products to food. Due to their small size and large numbers, the self-organization and assembly of particles are required to further develop new technology which is reliant on smaller structures and complex materials.

Droplets are important in a vast range of areas, both in nature and industrially, involving phenomena such as capillarity, wetting, hydrodynamics, and materials such as emulsions and colloidosomes [1–3]. By decreasing the interfacial free energy of the system, particles find it energetically favorable to adsorb to fluid-fluid interfaces of droplets [4]. Particles may move in the plane of the interface, but movement normal to the interface is limited. Such a configuration is useful for numerous studies, including an experimental model system for basic questions of

statistical mechanics [4,5], material development [6–8], particle structuring [9], and stabilizing emulsions by preventing drop coalescence [10–12]. The assembly of particles on drops is particularly attractive for the development of materials due to the architectural control it offers, together with the wide range of particles and solvents that can be used. Droplets covered with particles have been studied in different setups, including shear flows, where the particles affect drop deformation, inclination, and relaxation [13–15], and in magnetic or electric fields for manipulating fluids and particle dynamics [16–20].

In this work, we study the electric field-driven assembly of polystyrene (PS) microparticles located in the bulk of oil droplets, before being transported to droplet surfaces, and on drop surfaces. It has been reported that particle structuring and assembly depend on the type (DC or AC) and strength of the applied electric field, and the dielectric properties and electrical conductivity of the particles [9,21–23]. While it is simple to adjust the applied electric field, changing the properties of the particles is more challenging. Adjusting the electrical properties of PS particles is possible through sulfonation. Here, we investigate particle sulfonation as a method to produce PS particles with an increased dielectric constant and electric conductivity. This allows for different structuring and organization of PS particles at droplet interfaces. Particle sulfonation yields polymeric particles with a large range of electrical properties that are related to the degree of sulfonation, which can be controlled by several reaction conditions, including the reaction time, temperature, or concentration of sulfuric acid. Other physical properties may also change when PS particles are sulfonated for long periods of time, i.e., sulfonated PS particles become sticky, and this property can be used to create composite microcapsules with varied morphologies [24,25].

In this paper, we use electric fields to study the behavior of particles in the bulk of droplets and at droplet interfaces. The application of external electric fields has proven to be a flexible method for particle structuring and manipulation of droplets. When a weakly conductive droplet is subjected to a uniform electric field, charges build up at the interface of the droplet, resulting in electric stress that induces electrohydrodynamic (EHD) flows [16]. EHD flows can be used to indirectly structure particles at drop interfaces [23,26], for colloidal assembly [17], to fabricate patchy colloidal capsules [7], and to improve particle packing [27]. Particles can also be manipulated directly, by electric forces such as electrophoresis [28] or dielectrophoresis (DEP) [29–31], e.g., to separate particles at drop interfaces via gradients in the electric field [22] or to remove particles from drop surfaces using a tip streaming mechanism [32,33]. The structuring of particles can also occur via dipole-dipole interactions between particles, resulting in electrorheological chain formation [23,34,35] at drop interfaces.

In certain systems, both dielectrophoretic and EHD effects may be present, and depend on the applied electric field. By adjusting the frequency of the applied electric field, Amah and co-workers [21] demonstrated that the motion of particles can be switched between EHD flows transporting particles towards the drop equator, and DEP moving particles towards the drop poles. In our previous work, we discovered the “pupil effect”, where weakly conductive clay particles assemble at the drop equator and form a ribbon-like structure. The particle concentration and the ribbon width can be controlled by the electric field strength, i.e., at weak electric field strengths, EHD flows dominate and compress the ribbon, whereas at strong electric field strengths, particle dipolar interactions stretch the particle ribbon in direction towards the drop electric poles [23]. However, the effect was only achievable for particles with certain electrical properties: if the surface particles were too conductive, they only formed chain-like structures, while insulating particles only formed equatorial ribbons. This result motivated us to prepare a set of particles of the same size, shape, and material, but with different electrical properties. We have produced such a set of particles by sulfonating PS particles, which is an efficient, fast, and cheap method for modifying low-priced polystyrene particles.

The electrical properties of particles are also important in electrorheological (ER) fluids: colloidal or granular dispersions consisting of particles with a high dielectric constant or conductivity in an insulating (or weakly conductive) liquid. When subjected to external electric fields, the structure of the particles and the rheological properties of the ER fluids, such as the yield stress, apparent viscosity, storage, and loss moduli, may change drastically [36,37], allowing some ER fluids to change from a liquid to a gel and back, in time scales typically of the order of milliseconds. These characteristics make ER fluids useful in applications in microfluidic devices [38] and systems like hydraulic valves, clutches [39], brakes, and dampers [40,41]. In this work, we measure the flow of ER dispersions of modified PS particles in silicone oil, in response to applied electric fields at different strengths. We investigate how sulfonated PS particles change the electrorheological properties of PS suspensions, including the shear stress. The purpose of the ER experiments is not to pursue materials with high yield stresses, but rather to relate the electrorheological properties of PS suspensions with particle structuring inside droplets and at their interfaces. In addition, we perform Fourier transform infrared (FTIR) studies, measurements of particle dielectric constants and electrical conductance. These measurements complement and support the experiments on the electric field-driven assembly of particles. In short, all of the experiments demonstrate how sulfonation can be used to tailor electrical properties of PS particles and the importance of such properties in particle structuring in the bulk of droplets and at their interfaces.

2. Results

We use PS particles (mean diameter around 40 μm) sulfonated at incremental reaction times (2, 4, 8, 16, 32, 64, 128, and 256 min) to study the influence of the reaction time on the final physical properties of the sulfonated PS particles, and their electric field-driven assembly capabilities in an oil-in-oil system. The untreated PS particles, from which the sulfonated particles were made, are also studied here as a reference sample.

2.1. FTIR Studies

To recognize the chemical changes of particles due to the sulfonation procedure, we collected FTIR spectra of the modified PS samples. Figure 1 shows a stacked view of the measured FTIR transmission data in the 900–1250 cm^{-1} region. The line at 1046 cm^{-1} indicates the asymmetric stretching vibrations of the SO_3^- groups, whereas the lines at 1180 cm^{-1} and 1224 cm^{-1} indicate the symmetric stretching vibrations of the SO_3^- groups [42,43]. The appearance of a 1130 cm^{-1} band for sulfonated polystyrene samples indicates the presence of sulfonate groups attached to phenyl rings, i.e., attributed to ring deformations [42–44]. Table 1 lists the calculated values of the transmittance ratios between the 1180 cm^{-1} and 1153 cm^{-1} bands (red dashed lines in Figure 1), where the latter band is either attributed to the C–H bending of the aromatic ring or the CH–CH₂ stretching vibrations [45]. The increase of the transmittance ratio values with sulfonation time is correlated with the increased number of sulfonated groups. In short, the FTIR data consistently confirm that our sulfonation procedures impart sulfate groups to the surface of the PS particles.

Table 1. Lists of the calculated values of the transmittance ratios between the bands at 1180 cm^{-1} and 1153 cm^{-1} . The increase of the transmittance ratio values with sulfonation time is correlated with the increased number of the sulfonated groups imparted to the surface of the PS particles.

Reaction Time (min)	0	2	4	8	16	32	64
Transmittance Ratio	1	1	1	1.001	1.002	1.007	1.009

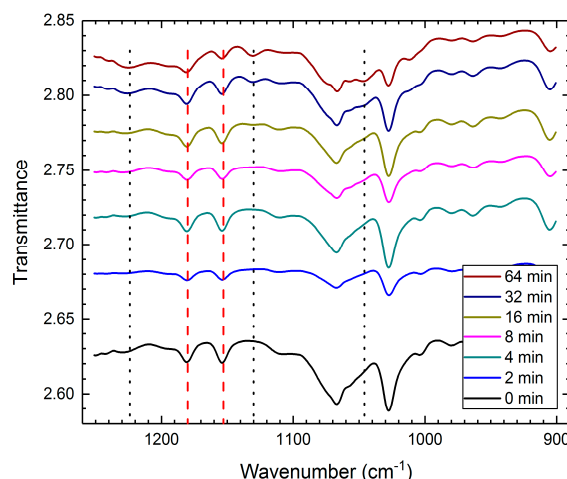


Figure 1. Stacked view of the FTIR transmission data. The line at 1046 cm^{-1} indicates the asymmetric stretching vibrations of the SO_3^- groups, whereas the lines at 1180 and 1224 cm^{-1} indicate the symmetric stretching vibrations of the SO_3^- groups. The appearance of a 1130 cm^{-1} band for the sulfonated polystyrene samples indicates the presence of sulfonate groups attached to phenyl rings. The red dashed lines indicate the bands used for calculating the transmittance ratio values.

2.2. Optical Photography and Electron Microscopy Examination of Sulfonated PS Particles

Optical photography and scanning electron microscope (SEM) images of both the pure and sulfonated PS particles are presented in Figure 2, in the top and bottom rows, respectively. Dry PS samples were placed in $10\text{ mm} \times 10\text{ mm}$ plastic cuvettes and photographed. The PS particles sulfonated for short periods of time (up to around 32 min) resemble non-modified PS particles in appearance: they remain white and powdery (hard particles that do not adhere to one another) after the chemical treatment, see Figure 2a–c. The PS particles sulfonated for longer periods of time appear progressively more yellowish and tend to aggregate and form chunks, as shown in Figure 2d,e. They are also much more difficult to disperse in oil because they become more hydrophilic [46,47], aggregate, and adhere to one another. The yellow color is caused by the degradation of PS molecules at the surface of the microspheres. Previously, such a color change has been reported to increase with both the reaction time and the temperature [48,49].

SEM was used to study the surface morphology of the PS samples. The images in Figure 2f–j show that all of the modified PS particles remain spherical and have sizes similar to the untreated PS particles. The surface morphology of the particles sulfonated for 8 and 16 min look similar to that of the non-modified PS particles (Figure 2f–h). The particles sulfonated for around 1 h and longer, develop inhomogeneous surfaces in the form of rough spots—marked with black arrows in Figure 2i,j. The PS particles that are sulfonated for long periods of time start to fuse, form necks between each other, and eventually form aggregated structures. When such structures and interparticle necks break (for instance during sample preparation for SEM imaging), the detached particles are left with neck residuals. Adhesion between sulfonated particles has been observed by other researchers [24], and is generally expected for particles exposed to sulfonation for a long period of time [46].

For electro-rheological investigations and experiments focusing on electric field-driven particle assembly, we chose to use particles that were modified for no longer than 32 min, i.e., we used particles without significant morphological surface modifications. These particles disperse in oil more readily because they do not form large aggregates and are less hydrophilic than particles modified for longer periods of time.

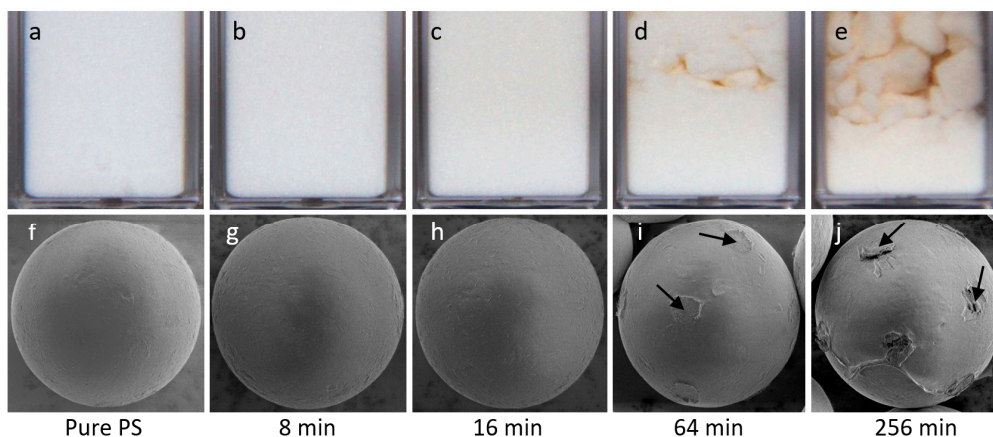


Figure 2. Optical photography (a–e) and scanning electron microscope (f–j) images of pure and sulfonated PS particles. The PS particles that were sulfonated for short periods of time remain white and powdery, resembling non-modified PS particles (a–c). When the PS particles are sulfonated for longer periods of time (64 and 256 min), they become yellowish, and during the washing and drying steps of particle sulfonation, they aggregate (d,e). Electron microscope images show that all the modified PS particles remain spherical and have sizes similar to non-modified PS particles (f–j). The PS particles modified for longer than around 1 h display inhomogeneities on their surfaces in the form of spots, some of them marked with black arrows (i,j). These spots are residuals of “necks” that were formed between fused PS spheres forming aggregated structures. During sample preparation for SEM imaging, the aggregated particles detach and the necks between the spheres break, leaving spots at the particle surfaces.

2.3. Electrical Conductance and Dielectric Constant

To determine the electrical properties of the PS particles, including the dielectric constant (ϵ) and electrical conductivity (σ), we carried out capacitance measurements using an LCR meter at a frequency (f) of 100 Hz. The LCR meter was set to capacitor mode, where the capacitance (C) and the dissipation factor ($\tan \delta$) were recorded. The dielectric constant and electrical conductance (G) values were calculated using equation: $\epsilon = C / C_0$, $G = 2\pi f C \tan \delta$ (for details see Section 4). The conductance was then converted to conductivity. Table 2 lists the calculated values of ϵ and σ . The dielectric constant increases with the sulfonation reaction time, starting from the sample sulfonated for 4 min and reaching a maximum value for the PS sample modified for 32 min, which is one order of magnitude higher than that of pure PS particles. A similar trend applies to the measured conductivity values. The highest electrical conductivity value is obtained for the sample sulfonated for 32 min, and is three orders of magnitude higher than that of the pure PS particles. This is expected because the degree of sulfonation increases with the reaction time [50], allowing more water to be absorbed on the PS samples [25,51], thus enhancing the protonic conductivity [52]. To test this assumption, we dried the sulfonated PS particles by lyophilisation and measured the electrical properties of the lyophilized samples. The results of these measurements are included in Table 2. Both the dielectric constant and electrical conductivity values of all the lyophilized PS sulfonated particles are significantly smaller than those of the initial PS sulfonated samples, but are still larger than non-modified PS particles. This indicates that water content plays an important role in the electrical conductivity and polarization of the sulfonated PS particles. Previously, such water dependency on the dielectric properties of sulfonated PS films has been reported [53]. To produce a broad distribution of particles in terms of the electrical properties, we decided to use the initial sulfonated PS particles (not lyophilized) for further experiments on electro-rheology and electric field-driven particle assembly.

Table 2. Lists of the calculated electrical values, including the particle dielectric constant (ϵ) and electrical conductivity (σ) measured at a frequency of 100 Hz.

Reaction Time (min)	0	2	4	8	16	32
Dielectric constant, ϵ	1.5	1.4	2.2	4.5	8.1	19.5
Dielectric constant, ϵ (lyophilized)	1.3	1.3	1.4	1.4	1.8	3.0
Electrical conductivity, σ (nS/m)	0.08	3.9	9.3	31.0	95.9	107.5
Electrical conductivity, σ (nS/m) (lyophilized)	0.08	0.8	1.6	1.6	8.5	30.1

2.4. Electro-Rheology

Figure 3a–d presents the flow curves for silicone oil dispersion with non-modified PS particles, and three dispersions with PS particles sulfonated for 2, 4, and 8 min, respectively. The particle concentration in all dispersions is 0.5% by weight, similar to the particle concentration in silicone oil dispersions utilized for the electric field-driven assembly experiments, described in the next section.

When no electric field is applied, the dispersions behave as Newtonian fluids, i.e., their shear stress values increase linearly with the shear rate (remark: Two electrical grounding brushes connected to the measuring bob may induce an artificial yield stress of up to 0.05 Pa). At low shear rates, we observe small non-Newtonian behavior (nonlinear), as seen in Figure 3a,b. The dispersions behave as Bingham fluids when subjected to DC electric fields of strengths 0.5, 1, 2, 4, 6, and 8 kV/mm, i.e., a viscoelastic material that acts as a rigid body when subjected to low stresses and flows as a viscous fluid when subjected to high stresses [54]. This behavior is particularly apparent for dispersions in strong electric fields.

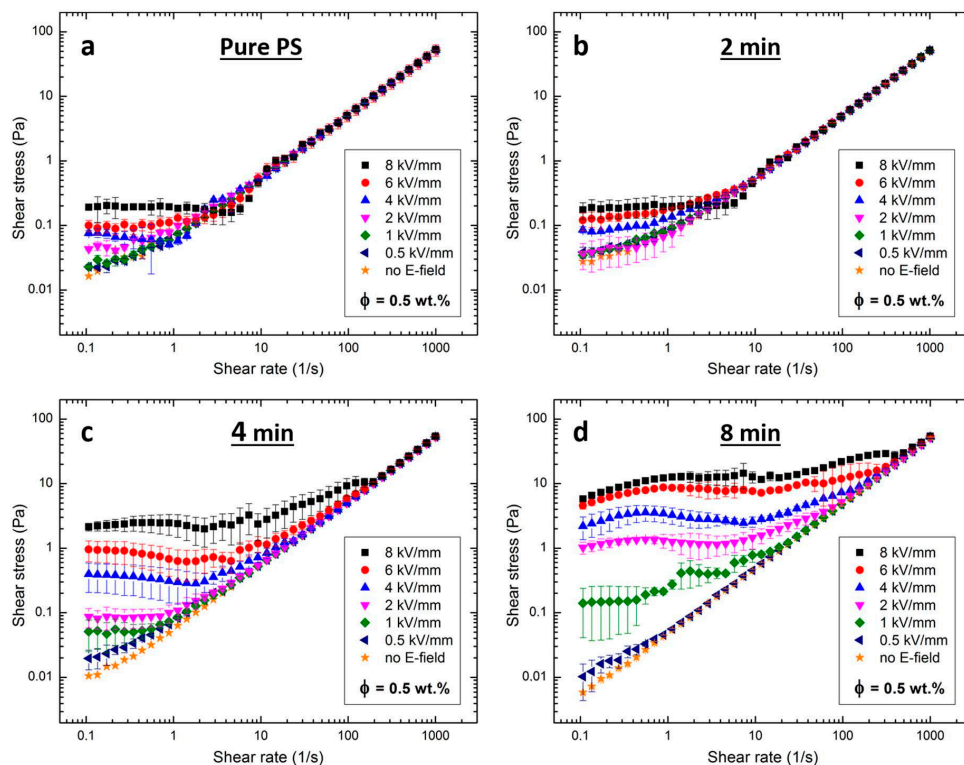


Figure 3. Log-log plots of flow curves of silicone oil dispersions with non-modified PS particles (a); and with PS particles sulfonated for 2 min (b); 4 min (c); and 8 min (d). The silicone oil dispersions are subjected to electric field strengths between 0.5 and 8 kV/mm, and a particle concentration of ~0.5% by weight was used to prepare all the silicone oil (50 cSt) dispersions.

Table 3 lists the shear stress values of dispersions measured at a shear rate equal to 0.1 s^{-1} and subjected to different electric field strengths. At the strongest electric field strength (8 kV/mm), the PS particles sulfonated for 8 min exhibit the largest electrorheological response, and the yield stress value is nearly 30 times higher than that observed for the pure PS particle dispersion. The values of the shear stress generally increase with applied electric field strength and sulfonation time. For electrorheological fluids, this behavior is usually attributed to either differences in dielectric properties, and/or conductivities between the particles and carrier liquid, and simple polarization or conduction models apply [55–57]. The electrorheological results presented here are consistent with measurements of the dielectric constant and electrical conductance shown in the previous section.

Table 3. Shear stress values (τ) measured at shear rate 0.1 s^{-1} .

Silicone Oil Dispersions with:	E (kV/mm)	0.5	1	2	4	6	8
pure PS particles	τ (Pa)	~0.02	~0.02	~0.04	~0.07	~0.10	~0.19
PS particles sulfonated for 2 min	τ (Pa)	~0.03	~0.03	~0.03	~0.08	~0.11	~0.18
PS particles sulfonated for 4 min	τ (Pa)	~0.02	~0.05	~0.08	~0.40	~1.00	~2.00
PS particles sulfonated for 8 min	τ (Pa)	~0.01	~0.13	~1.00	~2.00	~4.00	~5.50

2.5. Electric Field-Driven Particle Assembly

We use electric fields to manipulate particles both inside the droplet and at the droplet surfaces. The particles are set in motion and assemble either by: (i) direct interaction of the applied electric field, i.e., through electrophoresis and/or dielectrophoresis; or (ii) indirectly, through circulating liquid flows induced by DC or low frequency AC electric fields. Here, we qualitatively demonstrate how the dipolar interaction force between modified particles changes with the particle sulfonation reaction time. We show interesting interactions between viscous forces (induced by EHD flows) and dipolar forces, creating different particle assemblies.

We apply AC electric fields to observe whether (and how fast) the PS particles form dipolar chains. This gives an indication of the dipolar forces acting on the different PS particles. The electric field frequency was set to 100 Hz, a value far above the critical frequency at which EHD liquid flows occur in this system (few Hz) [23]. Four silicone oil droplets with radii of around 1 mm were suspended in castor oil, each containing particles with different degrees of sulfonation, including non-modified PS particles and PS particles sulfonated for 2, 8, and 16 min. Initially, the particles in each droplet are randomly dispersed, and the majority of them are located in the bulk of a droplet (Figure 4a,d,g,j). Each droplet is subjected to an AC electric field of 600 V/mm. The non-modified PS particles (Figure 4b,c) and the PS particles sulfonated for 2 min (Figure 4e,f) do not experience any significant motion within the time frame of the experiment. Only a few short particle chains are observed, approximately aligned in the direction of the electric field lines. The PS particles sulfonated for 8 min clearly interact with one another, forming short chains visible 10 s after the application of the electric field (Figure 4h,i). The highest number of dipolar chains are formed for the dispersion containing PS particle sulfonated for 16 min. The interactions between these particles are very strong, and the long chains are formed in just a few seconds (Figure 4k,l). Such particle behavior is consistent with the results presented in previous Sections 2.2 and 2.3. For the sake of image clarity, we did not include the experiment for droplets with samples sulfonated for 4 min (particle behavior is qualitatively similar to that of the sample modified for 2 min) and for 32 min (particle behavior is qualitatively similar to that of the sample modified for 16 min).

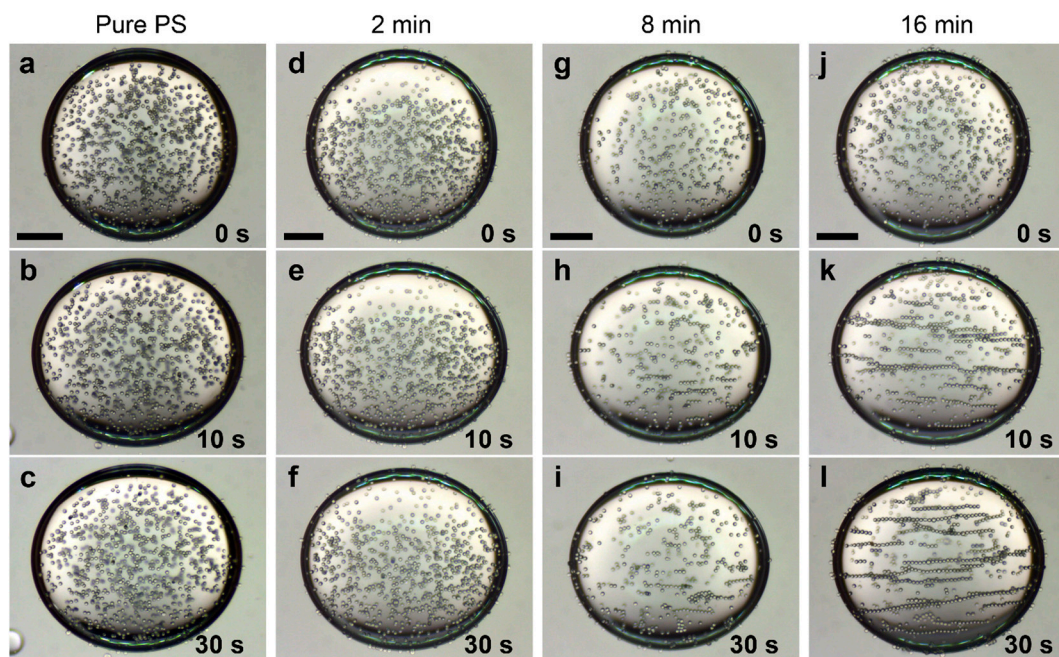


Figure 4. Four silicone oil droplets suspended in castor oil, each containing different particles, from left to right column: non-modified PS particles, and PS particles sulfonated for 2, 8, and 16 min. Initially, the particles in each droplet are randomly dispersed, and the majority of the particles are in the droplet bulk (a,d,g,j). The electric field is zero at $t = 0$ s (first row), then a 100 Hz square wave electric field of strength 600 V/mm is applied (rows 2 and 3). The non-modified PS particles do not experience any significant motion after the application of the electric field (b,c). The same applies for the PS particles sulfonated for 2 min (e,f). The PS particles sulfonated for 8 min clearly interact with one another, and short chains are present 10 s after the application of the electric field (h,i). Dipolar chaining is most distinct for the PS particle sulfonated for 16 min (k,l). Scale bars are 500 μm .

In Figure 5, we plot the average chain length versus time for the four droplets with different PS particles (presented in Figure 4). In the absence of an electric field, the average chain length is around two particles for the chains present in all four droplets. After the electric field is applied, the PS particles interact via dipolar interactions and the length of the chains increases. The pure PS particles (red squares) and PS particles sulfonated for 2 min (blue circles) form short chains (average chain length after 30 s is around 2.5 particles), while the PS particles sulfonated for 8 min (yellow triangles) and 16 min (green down pointing triangles) form longer chains, and the average chain length after 30 s is around four to five particles, respectively. Quantitatively, this consistently shows that the dipolar force between the PS particles increases with sulfonation time, allowing particles to form longer chains in the droplet. We attribute this result to the increased electrical properties of the particles obtained through sulfonation (see Table 2). For AC electric fields, the dipolar force between two particles is proportional to the complex particle polarizability [58]: $Q^2 = (\sigma_p^* - \sigma_{in}^*) / (\sigma_p^* + 2\sigma_{in}^*)$, where $\sigma_p^* = \sigma_p + i\omega\epsilon_0\epsilon_p$ and $\sigma_{in}^* = \sigma_{in} + i\omega\epsilon_0\epsilon_{in}$ are the complex conductivities, σ_p and σ_{in} are the conductivities of the particles and droplet, ω is the angular frequency of the electric field, ϵ_0 is the vacuum permittivity, and ϵ_p and ϵ_{in} are the dielectric constant of the particles and the droplet. If we insert numbers and compare the Q^2 values of the non-modified PS particles (0 min) and particles sulfonated for the longest time (32 min), we obtain: $Q_{32}^2 / Q_0^2 \approx 2.3$. This calculation shows that the increased electrical properties of the PS particles (through sulfonation) can double the dielectric force, supporting our observations.

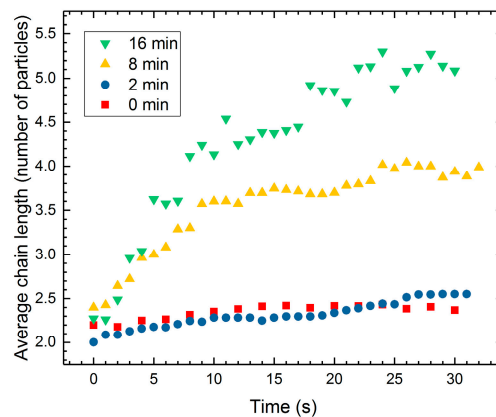


Figure 5. Average length of chains plotted against time for PS particles used in the four droplets presented in Figure 4.

As mentioned above and demonstrated in Figure 4, we apply AC electric fields with a frequency of 100 Hz to prevent the induction of EHD flows. We observe similar particle chaining effects, as presented in Figure 4, when we apply AC electric fields with higher frequencies, i.e., up to around 5 kHz, which is the limit of our voltage amplifier. However, if we decrease the frequency of the electric field, different phenomena take place. Figure 6 shows a silicone oil droplet with pure PS particles adsorbed at the interface. The particles were brought to the droplet interface and then gently dispersed by mechanical stirring using a pipette tip. As a result, the majority of the particles are initially randomly dispersed at the droplet interface, before the application of an electric field (Figure 6a). When an electric field (600 V/mm) with a frequency of 100 Hz is applied, all of the particles are guided towards the electric poles through the action of DEP (Figure 6b–d) [21]. The direction of the DEP force is determined by the sign of $\beta\hat{\beta} = \text{Re}\left(\frac{\epsilon_{\text{in}}^* - \epsilon_{\text{ex}}^*}{\epsilon_{\text{in}}^* + 2\epsilon_{\text{ex}}^*}\right)\text{Re}\left(\frac{\epsilon_{\text{p}}^* - \epsilon_{\text{ex}}^*}{\epsilon_{\text{p}}^* + 2\epsilon_{\text{ex}}^*}\right)$, the Clausius-Mossotti factor of the droplet and particle with respect to the exterior fluid [21]. The complex permittivity is $\epsilon^* = \epsilon - i\sigma/\omega$, where ω is the angular frequency of the applied electric field. If $\beta\hat{\beta} < 0$, the particles aggregate at the equator, and if $\beta\hat{\beta} > 0$, the particles aggregate at the droplet poles. Inserting numbers yields $\beta\hat{\beta} \approx 0.05$ for the studied silicone-castor oil system (with pure PS particles), which is consistent with the DEP force direction observed in our experiments. The interparticle dipolar forces are sufficiently strong (compared to the DEP force) for the PS particles to form chains. Note that the dipolar interaction of particles at the droplet interface is stronger than when they are in the bulk of the droplet, and even non-modified PS particles form chains in the presence of an AC electric field. After we decrease the frequency of the electric field to 5 Hz, the particles are transported in the opposite direction, i.e., towards the electric equator (Figure 6e,f). This is due to induced EHD flows, which arise when free charges accumulate on the interface of the droplet [16,59,60]. In this silicone oil droplet in castor oil system, the direction of these flows is directed from the electric poles to the electric equator of the droplet. Experimentally, we observe that the drag force on a particle due to the EHD flows dominates the DEP force for frequencies below ~ 10 Hz. The EHD drag force increases with a decreasing frequency, as $1/\omega^2$ [21]. At 5 Hz, the EHD flows are weak because the charges do not have sufficient time to accumulate at the droplet interface (for a silicone oil droplet in castor oil system, the time for the interface to acquire its steady-surface charge distribution is around 1 s). If we decrease the frequency to 1 Hz, the particles move towards the electric equator more rapidly (Figure 6g,h), where they stay and form an equatorial ribbon-like structure (Figure 6h). At this frequency, the EHD drag force dominates both the DEP and dipolar force. As a result, the particle chains made of non-modified PS particles are broken into smaller chains or single particles. When applying AC electric fields with low frequencies or DC fields, the modified PS particles may form a compacted ribbon-like structure, or short dipolar chains assembled at the electric equator of a droplet, or make long dipolar chains. The particle organization depends on the dielectric properties and electric conductivity of the PS particles (presented in Figure 7).

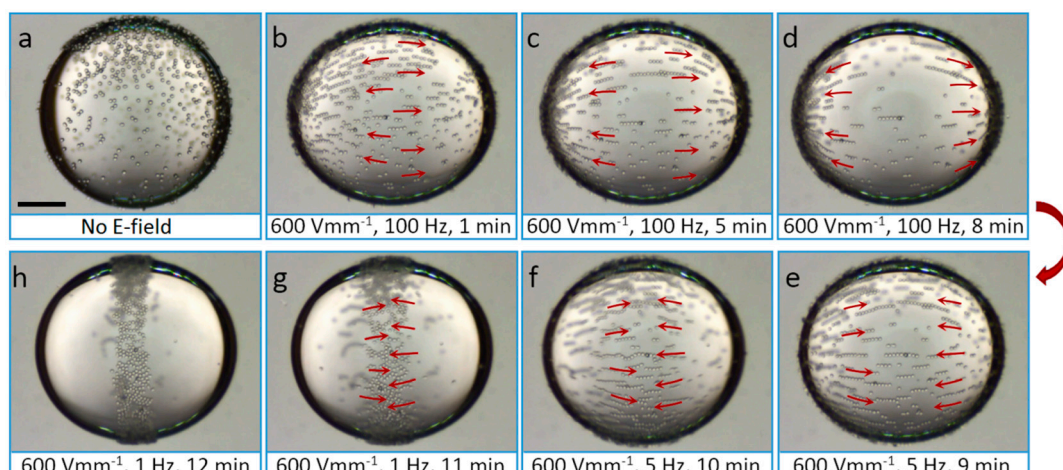


Figure 6. A silicone oil droplet containing pure PS particles and suspended in castor oil. The majority of particles are at the interface, randomly dispersed (a). An electric field of strength 600 V/mm is applied through the whole experiment, and the frequency is adjusted between 100 Hz (b–d), 5 Hz (e,f), and 1 Hz (g,h). By tuning the frequency of the electric field, it is possible to change the surface particle arrangements. Scale bar is $500 \mu\text{m}$, and the droplet radius around 1 mm .

Figure 7 shows three silicone oil droplets suspended in castor oil (same oils and droplet sizes as used in Figure 4), each covered by particles with different degrees of sulfonation, including PS particles sulfonated for 4, 8, and 32 min. The particles were brought to the interface and then gently dispersed by mechanical stirring using a pipette tip. As a result, a majority of the particles are randomly dispersed at the droplet interface (Figure 7a,c,e). In this system, the particle density is similar to those of both oils, so the gravitational force (vertical direction in all images) can be neglected. Each droplet is subjected to a DC electric field, initiating particle movement. We use an electric field strength of 150 V/mm , not 600 V/mm as in the experiments with AC fields, because the EHD flows that are present in DC electric fields generate instabilities on the droplet surface, which may lead to the formation of spinning domains [23,61], as presented in Figure S1.

In addition to the gravitational force, the PS particles at the droplet interface experience three different forces when subjected to a DC electric field: EHD drag, DEP and dipolar forces. In Section 2.3, we ascertained that the electrical properties of the PS particles increase with the sulfonated time. For the particles sulfonated for short periods of time, the low dielectric constant and electric conductivity (Table 2) yield DEP and dipolar forces that are $\sim 2\text{--}3$ orders of magnitude smaller than the EHD drag force. Consequently, EHD circulation flows govern the dynamics of PS particles sulfonated for short periods of time (4 min), i.e., the particles follow the EHD flows and are brought to the droplet equator where they form a ribbon-like structure (Figure 7b) [23,62]. For these particles, we do not observe any direct electrical interactions (e.g., electrophoretic motion or dipolar interaction between the particles). A similar behavior is observed for pure PS particles and PS particles sulfonated for 2 min (not shown here). The direction of the EHD flows and the droplet deformation are determined by the ratios between the conductivities and dielectric constant of the fluids [23,63,64]. In our case, the surrounding castor oil conducts approximately 10 times better than the silicone oil, thus resulting in an oblate deformation (droplet axis perpendicular to the electric field direction is larger than the axis parallel to the electric field direction), and the EHD flows are directed from droplet electric poles to the electric equator [16]. The PS particles sulfonated for longer periods of time have higher dielectric constants and conductivities (than the PS particles sulfonated for shorter times), resulting in stronger dipolar interactions.

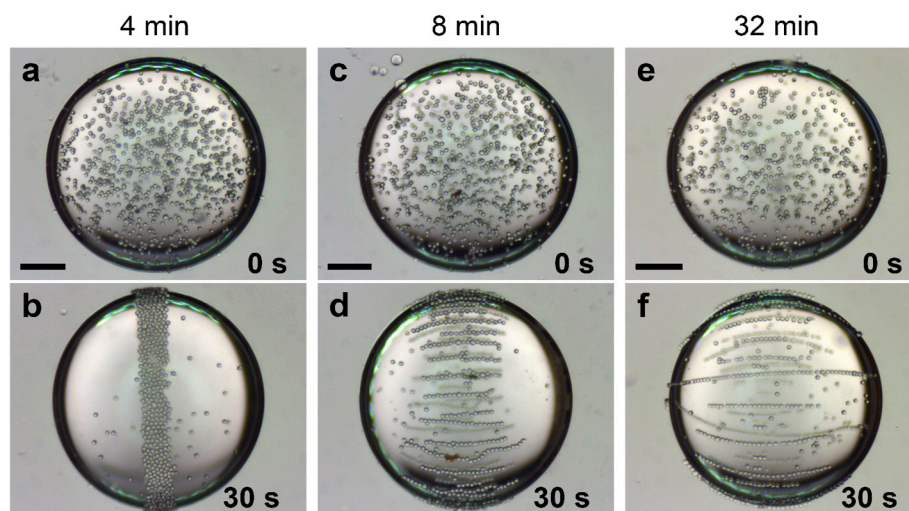


Figure 7. Three silicone oil droplets suspended in castor oil, each covered by particles with different degrees of sulfonation, including PS particles sulfonated for 4, 8, and 32 min. The majority of particles are at the interface, randomly dispersed (**a,c,e**). Each droplet is subjected to a DC electric field of 150 V/mm, initiating particle movement. The PS particles sulfonated for 4 min are carried by circulating EHD flows towards the electric equator and assemble into a “ribbon-like” structure (**b**). For the PS particles sulfonated for the longest time, i.e., with the largest dielectric constant and electrical conductance, we observe particle chain-structures that align along the electric field lines and span the entire droplet (**f**). Interesting particle organization takes place for the PS particles modified for 8 min. Due to the combined action of EHD flows and dipolar attractive interactions between the particles, chain like assemblies form and are structured at the electric equator (**d**). Scale bars are 500 μm and the droplet radii are around 1 mm.

For DC electric fields, the dipolar force between two particles is proportional to the factor [65]: $\beta^2 = (\sigma_p - \sigma_{in})^2 / (\sigma_p + 2\sigma_{in})^2$, involving the conductivities of the particles σ_p and the surrounding fluid σ_{in} . If we insert numbers and compare β between the non-modified PS particles (0 min) and the particles sulfonated for the longest time (32 min), we get: $\beta_{32}^2 / \beta_0^2 \approx 360$. This shows that the sulfonation process results in larger interparticle dipolar forces. Particles are able to form chains when the dipolar force exceeds the EHD drag force. This is the case for the PS particles modified for 8 min, where the combined action of the EHD flows and dipolar forces between the particles leads to chain-like assemblies being formed and structured at the electric equator of the droplet (Figure 7d). The dipolar force between the particles is attractive when they are aligned parallel to the electric field direction, and repulsive when aligned perpendicular to the electric field direction. That is why the particle chains are separated.

If the dipolar force is sufficiently strong compared to the EHD drag force, the particles can form chains from droplet pole to droplet pole (Figure 7f), and suppress or remove the EHD flows by short cutting the electric poles [23]. These chains conduct electric current much better than oils and form electrical short cuts between the two droplet electric poles. As a result, the droplet becomes less oblate (Figure 7f) and can even stretch and acquire a prolate shape if the particle concentration and electric field are higher.

The DEP force on the particles also increases with the dielectric constant and electric conductivity of the particles. However, the increase in the DEP force between non-modified particles (0 min) and particles sulfonated for a long time (32 min) is only one order of magnitude (for equations see [21]). The DEP force is thus dominated by both EHD and dipolar forces, and it is safe to neglect DEP forces in this experiment.

3. Discussion and Conclusions

In this work, we have investigated how sulfonation changes the electrical properties of PS particles and how this modification affects particle organization at the interfaces and bulk of droplets subjected to electric fields. To study how our sulfonation procedure changes the properties of the PS particles, the particles were sulfonated for different lengths of time and compared. FTIR studies of the sulfonated PS particles show that our sulfonation procedures impart sulfate groups to the surface of the PS particles.

We measured the electric conductivity and dielectric constant of pure and modified PS particles. The measurements consistently show that these electric parameters increase with sulfonation time. Electro-rheology experiments were also performed on pure and sulfonated PS particles dispersed in silicone oil. Consistent with the measured electrical properties, we find that the shear stress value of the particle dispersions increases with the sulfonation reaction time. We can thus conclude that our sulfonation procedure brings sulfate groups to the surface of the PS particles, and that the degree of sulfonation increases the dielectric constants and electric conductivities of the PS particles.

We also studied how these modified particles organize in the bulk and interfaces of droplets, when subjected to electric fields. PS particles with different degrees of sulfonation were placed in silicone oil droplets and suspended in castor oil. First, we applied AC electric fields to study the formation of particle chains and structuring of particles at droplet poles. The electric field strength, frequency, and fluids were kept constant, with particle properties being the only variable parameters. We observed that the PS particles sulfonated for long periods of time (32 min) form longer chains compared to PS particles sulfonated for shorter periods of time (0 min). This is attributed to the change in the electrical properties, affecting the dipolar force between particles. Next, we studied how PS particle organization changes with the frequency of the applied electric field. When we apply an electric field with a high frequency (100 Hz), the PS particles form chains and move towards the droplet poles. This movement is caused by DEP forces. When we decrease the frequency (to 5 and 1 Hz), the particles move in the opposite direction, towards the droplet equator. This is because free charges have time to accumulate at the droplet interface, inducing EHD flows with a direction from the droplet poles to the droplet equator. The EHD drag force experienced by the particles increases with the electric angular frequency as $1/\omega^2$, and becomes stronger than both the DEP and dipolar forces when the electric field frequency is sufficiently low. Particles chains are then broken into smaller chains or individual particles, and assemble in a ribbon at the droplet equator.

In the last part of the paper, we utilized DC electric fields. With particle properties as the only variables, we observed that PS particles sulfonated for longer periods of time form long chains, while PS particles sulfonated for shorter periods of time do not form chains at all. Our calculations show that the dipolar force between particles can increase by three orders of magnitude when we compare pure PS particles with PS particles sulfonated for 32 min. The dipolar force is weaker than the EHD drag force for the pure PS particles, preventing them from forming chains. When PS particles are sulfonated, the dielectric constant and electric conductivities increase, resulting in dipolar forces that exceed the EHD drag force.

In the future, we plan to extend these studies to mixtures of particles with different electrical properties, and also vary both the strengths and frequencies of the electric fields. We foresee that by doing so, it will be possible to obtain new particle architectures at droplets surfaces. PS particles can be easily sintered and this allows us to permanently lock the assembled structure formed, for example, Janus shells with anisotropic properties.

We note that the PS particles in the bulk of the droplet arrive at the droplet interface much faster than particles of the same size made of polyethylene particles that we studied before [23]. This is possibly due to charges that sulfonated particles acquire. It was demonstrated that the values of the zeta potential increase as the sulfonation reaction progresses to up to few hours [24].

As a final remark, we discuss the importance of the wettability of PS particles. Once the sulfonated PS particles are brought to a drop surface, they bind to it with a binding energy proportional to $a^2\gamma(1 \pm \cos \theta)^2$, where a is the particle radius, γ is the surface tension between the drop and

surrounding fluids, and θ is the contact angle. The sign inside the bracket is defined as positive for the removal of particles into the outer surrounding liquid. The particle binding energy to the interface is maximum when the contact angle is equal to 90° . Generally, PS particles with a high degree of sulfonation become more hydrophilic than non-modified PS particles, and thus have a higher affinity towards castor oil than silicone oil. Experimentally, we observe that the sulfonated PS particles bind weakly to droplet interfaces and may detach due to strong EHD flows or dipolar interactions, as presented in Figure S2.

4. Materials and Methods

4.1. Sulfonation of PS Particles

The PS particles were purchased from Microbeads AS, Skedsmokorset, Norway (Dynoseeds TS40 6317) with mean diameters of around $40\ \mu\text{m}$, a density of around $1.05\ \text{g}\cdot\text{cm}^{-3}$, and without cross-linking. The general preparation route for the chemical modification of PS particles was as follows. Firstly, sulfuric acid (5 mL, 98%, 231-639-5, Chempur, Piekary Śląskie, Poland) was poured into a glass vial filled with polystyrene powder (5 g). During the chemical reaction, the temperature was maintained at $50\ ^\circ\text{C}$ by placing the vial into a water bath. The powder dispersion was continuously stirred using a magnetic stirrer. After the respective stirring time, the dispersion was neutralized using a concentrated potassium hydroxide water solution. Subsequently, the dispersion was poured into a sintered glass funnel (connected to a side-arm flask with a tube leading to a vacuum pump), and the sulfonated polystyrene particles were rinsed thoroughly with distilled water. Finally, the sulfonated particles were dried at $75\ ^\circ\text{C}$ for 24 h. To study the influence of the reaction time on the final physical properties of the sulfonated particles, we made eight samples prepared at incremental reaction times: 2, 4, 8, 16, 32, 64, 128, 256 min, respectively. The schematic representation of the sulfonation procedure is presented in Figure S3. We studied the influence of water content on the electrical properties of sulfonated PS particles by lyophilization conducted in a freeze dryer (IlshinEurope TFD5503) at $-50\ ^\circ\text{C}$ and 50 mTorr for 24 h. Before the lyophilization, the samples were stored in a freezer at $-20\ ^\circ\text{C}$ for 24 h.

4.2. FTIR Studies

A Tensor 27 FTIR spectrometer (Bruker Optics, Ettlingen, Germany) equipped with a single reflection diamond ATR unit was utilized for the IR analyses. Before each spectral acquisition session, the background was recorded and the background spectra were subtracted from the FTIR spectrum of each sample. The FTIR-ATR spectra were then recorded in the $900\text{--}1250\ \text{cm}^{-1}$ range by running 512 scans with a resolution of $2\ \text{cm}^{-1}$.

4.3. Optical Photography and Scanning Electron Microscopy Imaging

The dry samples in Figure 2 (top row) were photographed using a digital camera (Canon EOS 700D, Tokyo, Japan). The structural surface characterization of the sulfonated PS particles presented in Figure 2 (bottom row) was performed by scanning electron microscopy, using a JEOL JSM-7001F TTLS (JEOL Ltd., Tokyo, Japan). We prepared the powder samples by spreading a thin layer of the powder onto a double-sided conductive carbon tape. The surface of the uncoated samples was imaged via secondary electron imaging and observed at an accelerating voltage of 1 kV, to avoid a charging effect.

4.4. Measurements of Dielectric Constant and Electric Conductivity

To determine the dielectric constant and the electrical conductance of the powder samples, we carried out capacitance measurements by means of an LCR meter (Agilent E4980A, Santa Clara, CA, USA) at a frequency (f) of 100 Hz. A home-made cylindrical capacitor (with dimensions depicted in Figure S4) was used as a sample holder, where the separation distance between the inner and outer cylindrical electrode was 1.4 mm, which gives a capacitance value of the empty capacitor (C_0) equal to

2.78 pF. The studied sample was poured into the cylindrical gap, while the homogenous filling was provided by shaking the capacitor. We performed measurements with an effective voltage value of 1 V at room temperature (24 °C) and an ambient pressure. The LCR meter was set to parallel mode, where the capacity (C) and the dissipation factor ($\tan \delta$) were recorded. Then, the dielectric constant (ϵ) and conductance (G) values were calculated by: $\epsilon = C/C_0$, $G = 2\pi f C \tan \delta$. Finally, the conductance was converted to the electrical conductivity (σ).

4.5. Rheometry

The electro-rheological properties of the sulfonated PS particle dispersions were measured under direct current (DC) electric fields using a Physica MCR300 Rotational Rheometer equipped with a coaxial cylinder Physica ERD CC/27 (Malvern Instruments Ltd., Malvern, UK). Silicone oil (Dow Corning, Auburn, AL, USA) with a viscosity of 50 cSt, an electrical conductivity of approximately 3–5 pS·m⁻¹, and a relative permittivity of around 2.8, was used for the experiments. All the rheological measurements were performed at a constant temperature of 23 °C. The flow curves were collected in the shear rate range between 0.1 and 1000 s⁻¹, and at different electric field strengths, namely 0.5, 1, 2, 4, 6, and 8 kV/mm, respectively.

4.6. Experimental Set-Up for Electric Field-Driven Particle Assembly

The experimental set-up for the electric field-driven particle assembly of PS particles consisted of a sample cell placed on a mechanical x-y-z translational stage, a digital microscope, a signal generator, a voltage amplifier, an oscilloscope for monitoring signal shape and amplitude, and a PC for recording images. We used 10 mm × 10 mm plastic cuvettes (typically used for light spectroscopy) with two copper plates constituting electrodes, as a sample cell. Castor oil (83912, Sigma-Aldrich, St. Louis, MO, USA, density of 0.961 g·cm⁻³ at 25 °C, electrical conductivity of around 60 pS·m⁻¹, relative permittivity 4.7, and viscosity of around 700 cSt) was poured into the cell. Silicone oil droplets containing PS particles were introduced into the castor oil by a mechanical pipette. To minimize the buoyancy force on the droplet with particles, two silicone oils (200/10 cSt and 200/100 cSt, Dow Corning, Auburn, AL, USA, electrical conductivity approximately 3–5 pS·m⁻¹, relative permittivity 2.8) with densities of 0.960 and 0.965 g·cm⁻³ (measured at 25 °C) were adequately mixed, to match the castor oil density. The AC electric signal was always square-shaped and bipolar, and its RMS value (i.e., half of the peak-to-peak value) was provided in the text and figure captions. Optical microscopy observations of the electric field-driven particle assembly of PS particles presented in Figures 4, 6 and 7, were performed using a CMOS camera (UI-3590CP-C-HQ, IDS Imaging Development Systems GmbH, Obersulm, Germany) mounted on a high-magnification zoom lens system (MVL12X3Z, Thorlabs, Inc., Newton, NJ, USA). The experimental set-up is presented in Figure S5. All droplets have similar radii (~1 mm), and the small differences in their size do not affect the observed effects of particle structuring.

Supplementary Materials: The following are available online at www.mdpi.com/1996-1944/10/4/329/s1. Figure S1: Instabilities on droplet interface at high DC electric fields, Figure S2: Particle detachment from a silicone oil droplet suspended in castor oil, Figure S3: Schematic illustration of the sulfonation process of spherical PS particles, Figure S4: A home-made cylindrical capacitor used as a sample holder for measuring electrical capacitance and dielectric constants, Figure S5: Experimental set-up for the electric field-driven particle assembly of PS particles consisted of a CMOS camera.

Acknowledgments: Zbigniew Rozynek acknowledges financial support of the Foundation for Polish Science (Homing Plus/2013-7/13) and of the Polish National Science Centre through OPUS programme (2015/19/B/ST3/03055). Juraj Kurimský acknowledges Slovak Research and Development Agency under the contract No. APVV-15-0438. Ahmet Kertmen acknowledges financial support of the Polish National Science Centre through PRELUDIUM programme (2015/17/N/NZ7/01087). This work was also supported by the Slovak Academy of Sciences and Ministry of Education in the framework of project VEGA 2/0141/16. We thank Zuzanna Pietralik from the Department of Macromolecular Physics at Adam Mickiewicz University in Poznań, Poland, for assisting the FTIR measurements. We thank J.O. Fossum for use of laboratory facilities for the experiments shown in Figure 3.

Author Contributions: Zbigniew Rozynek (50%) initiated the project and designed all of the experiments. Jarosław Wojciechowski (15%) modified polystyrene particles and took part in electro-rheology experiments. Michal Rajňák (5%) and Juraj Kurimský (5%) performed the electric conductance and dielectric constant experiments, analyzed the data, and contributed to the presentation of the results in Table 2. Ahmet Kertmen (5%) performed the FTIR experiments, analyzed the data, and contributed to the presentation of the results in Figure 1. Khobaib Khobaib (5%) and Alexander Mikkelsen (15%) performed part of the experiments related to the electric field-driven particle assembly of polystyrene particles and contributed to the presentation of the results in Figures 5 and 7. All authors took part in discussions towards the finalization of the manuscript. Alexander Mikkelsen and Zbigniew Rozynek authored the paper.

Conflicts of Interest: The authors declare that the research was conducted without any commercial or financial relationships that could be construed as a potential conflict of interest.

References

1. Brochard-Wyart, F.; Quéré, D.; De Gennes, P.G. *Capillarity And Wetting Phenomena: Drops, Bubbles, Pearls, Waves*; Springer: New York, NY, USA, 2003.
2. Dinsmore, A.D.; Hsu, M.F.; Nikolaidis, M.G.; Marquez, M.; Bausch, A.R.; Weitz, D.A. Colloidosomes: Selectively Permeable Capsules Composed of Colloidal Particles. *Science* **2002**, *298*, 1006–1009. [[CrossRef](#)] [[PubMed](#)]
3. Tabeling, P. *Introduction to Microfluidics*; Oxford University Press: New York, NY, USA, 2010.
4. Pieranski, P. Two-Dimensional Interfacial Colloidal Crystals. *Phys. Rev. Lett.* **1980**, *45*, 569–572. [[CrossRef](#)]
5. Lipowsky, P.; Bowick, M.J.; Meinke, J.H.; Nelson, D.R.; Bausch, A.R. Direct Visualization of Dislocation Dynamics in Grain-Boundary Scars. *Nat. Mater.* **2005**, *4*, 407–411. [[CrossRef](#)] [[PubMed](#)]
6. Zeng, C.; Bissig, H.; Dinsmore, A.D. Particles on Droplets: From Fundamental Physics to Novel Materials. *Solid State Commun.* **2006**, *139*, 547–556. [[CrossRef](#)]
7. Rozynek, Z.; Mikkelsen, A.; Dommersnes, P.; Fossum, J.O. Electroformation of Janus and Patchy Capsules. *Nat. Commun.* **2014**, *5*, 3945. [[CrossRef](#)] [[PubMed](#)]
8. Brugarolas, T.; Tu, F.; Lee, D. Directed Assembly of Particles Using Microfluidic Droplets and Bubbles. *Soft Matter* **2013**, *9*, 9046–9058. [[CrossRef](#)]
9. Dommersnes, P.; Fossum, J.O. Surface Structuring of Particle Laden Drops Using Electric Fields. *Eur. Phys. J. Spec. Top.* **2016**, *225*, 715–728. [[CrossRef](#)]
10. Ashby, N.P.; Binks, B.P. Pickering Emulsions Stabilised by Laponite Clay Particles. *Phys. Chem. Chem. Phys.* **2000**, *2*, 5640–5646. [[CrossRef](#)]
11. Aveyard, R.; Binks, B.P.; Clint, J.H. Emulsions Stabilised Solely by Colloidal Particles. *Adv. Colloid Interface Sci.* **2003**, *100*, 503–546. [[CrossRef](#)]
12. Tang, J.; Quinlan, P.J.; Tam, K.C. Stimuli-Responsive Pickering Emulsions: Recent Advances and Potential Applications. *Soft Matter* **2015**, *11*, 3512–3529. [[CrossRef](#)] [[PubMed](#)]
13. Frijters, S.; Gunther, F.; Harting, J. Effects of Nanoparticles and Surfactant on Droplets in Shear Flow. *Soft Matter* **2012**, *8*, 6542–6556. [[CrossRef](#)]
14. Mei, Y.; Li, G.; Moldenaers, P.; Cardinaels, R. Dynamics of Particle-Covered Droplets in Shear Flow: Unusual Breakup and Deformation Hysteresis. *Soft Matter* **2016**, *12*, 9407–9412. [[CrossRef](#)] [[PubMed](#)]
15. Bécu, L.; Benyahia, L. Strain-Induced Droplet Retraction Memory in a Pickering Emulsion. *Langmuir* **2009**, *25*, 6678–6682. [[CrossRef](#)] [[PubMed](#)]
16. Taylor, G. Studies in Electrohydrodynamics. I. The Circulation Produced in a Drop by Electrical Field. *Proc. R. Soc. Lond. A* **1966**, *291*, 159–166. [[CrossRef](#)]
17. Van Blaaderen, A.; Dijkstra, M.; van Roij, R.; Imhof, A.; Kamp, M.; Kwaadgras, B.; Vissers, T.; Liu, B. Manipulating the Self Assembly of Colloids in Electric Fields. *Eur. Phys. J. Spec. Top.* **2013**, *222*, 2895–2909. [[CrossRef](#)]
18. Dorvee, J.R.; Derfus, A.M.; Bhatia, S.N.; Sailor, M.J. Manipulation of Liquid Droplets Using Amphiphilic, Magnetic One-Dimensional Photonic Crystal Chaperones. *Nat. Mater.* **2004**, *3*, 896–899. [[CrossRef](#)] [[PubMed](#)]
19. Hwang, K.; Singh, P.; Aubry, N. Destabilization of Pickering Emulsions Using External Electric Fields. *Electrophoresis* **2010**, *31*, 850–859. [[CrossRef](#)] [[PubMed](#)]
20. Cui, M.M.; Emrick, T.; Russell, T.P. Stabilizing Liquid Drops in Nonequilibrium Shapes by the Interfacial Jamming of Nanoparticles. *Science* **2013**, *342*, 460–463. [[CrossRef](#)] [[PubMed](#)]

21. Amah, E.; Shah, K.; Fischer, I.; Singh, P. Electrohydrodynamic Manipulation of Particles Adsorbed on the Surface of a Drop. *Soft Matter* **2016**, *12*, 1663–1673. [[CrossRef](#)] [[PubMed](#)]
22. Nudurupati, S.; Janjua, M.; Singh, P.; Aubry, N. Effect of Parameters on Redistribution and Removal of Particles from Drop Surfaces. *Soft Matter* **2010**, *6*, 1157–1169. [[CrossRef](#)]
23. Dommersnes, P.; Rozynek, Z.; Mikkelsen, A.; Castberg, R.; Kjerstad, K.; Hersvik, K.; Otto Fossum, J. Active Structuring of Colloidal Armour on Liquid Drops. *Nat. Commun.* **2013**, *4*, 2066. [[CrossRef](#)] [[PubMed](#)]
24. Fan, X.; Niu, L.; Xia, Z. Preparation of Raspberry-Like Silica Microcapsules via Sulfonated Polystyrene Template and Aniline Medium Assembly Method. *Colloid Polym. Sci.* **2014**, *292*, 3251–3259. [[CrossRef](#)]
25. Fan, X.; Niu, L.; Wu, Y.H.; Cheng, J.; Yang, Z.R. Assembly Route toward Raspberry-Like Composite Particles and Their Controlled Surface Wettability through Varied Dual-Size Binary Roughness. *Appl. Surf. Sci.* **2015**, *332*, 393–402. [[CrossRef](#)]
26. Ouriemi, M.; Vlahovska, P.M. Electrohydrodynamics of Particle-Covered Drops. *J. Fluid Mech.* **2014**, *751*, 106–120. [[CrossRef](#)]
27. Rozynek, Z.; Dommersnes, P.; Mikkelsen, A.; Michels, L.; Fossum, J.O. Electrohydrodynamic Controlled Assembly and Fracturing of Thin Colloidal Particle Films Confined at Drop Interfaces. *Eur. Phys. J. Spec. Top.* **2014**, *223*, 1859–1867. [[CrossRef](#)]
28. Li, M.; Li, D. Redistribution of Charged Aluminum Nanoparticles on Oil Droplets in Water in Response to Applied Electrical Field. *J. Nanopart. Res.* **2016**, *18*, 120. [[CrossRef](#)]
29. Nudurupati, S.; Janjua, M.; Aubry, N.; Singh, P. Concentrating Particles on Drop Surfaces Using External Electric Fields. *Electrophoresis* **2008**, *29*, 1164–1172. [[CrossRef](#)] [[PubMed](#)]
30. Amah, E.C.; Fischer, I.S.; Singh, P. Transient Electrohydrodynamic Manipulation of Particles on the Surface of a Drop. *Am. Soc. Mech. Eng.* **2016**. [[CrossRef](#)]
31. Aubry, N.; Singh, P. Control of Electrostatic Particle-Particle Interactions in Dielectrophoresis. *Europhys. Lett.* **2006**, *74*, 623. [[CrossRef](#)]
32. Nudurupati, S.; Janjua, M.; Singh, P.; Aubry, N. Electrohydrodynamic Removal of Particles from Drop Surfaces. *Phys. Rev. E* **2009**, *80*, 4. [[CrossRef](#)] [[PubMed](#)]
33. Sherwood, J.D. Breakup of Fluid Droplets in Electric and Magnetic Fields. *J. Fluid Mech.* **1988**, *188*, 133–146. [[CrossRef](#)]
34. Sheng, P.; Wen, W. Electrorheological Fluids: Mechanisms, Dynamics, and Microfluidics Applications. *Annu. Rev. Fluid Mech.* **2012**, *44*, 143–174. [[CrossRef](#)]
35. Fossum, J.O.; Meheust, Y.; Parmar, K.P.S.; Knudsen, K.D.; Maloy, K.J.; Fonseca, D.M. Intercalation-Enhanced Electric Polarization and Chain Formation of Nano-Layered Particles. *Europhys. Lett.* **2006**, *74*, 438–444. [[CrossRef](#)]
36. Wang, B.X.; Zhou, M.; Rozynek, Z.; Fossum, J.O. Electrorheological Properties of Organically Modified Nanolayered Laponite: Influence of Intercalation, Adsorption and Wettability. *J. Mater. Chem.* **2009**, *19*, 1816–1828. [[CrossRef](#)]
37. Méheust, Y.; Parmar, K.; Schjelderupsen, B.; Fossum, J. The Electrorheology of Suspensions of Na-Fluorohectorite Clay in Silicone Oil. *J. Rheol.* **2011**, *55*, 809–833. [[CrossRef](#)]
38. Wang, L.; Gong, X.; Wen, W. Electrorheological Fluid and Its Applications in Microfluidics. In *Microfluidics*; Springer: New York, NY, USA, 2011; pp. 91–115.
39. Madeja, J.; Keszy, Z.; Keszy, A. Application of Electrorheological Fluid in a Hydrodynamic Clutch. *Smart Mater. Struct.* **2011**, *20*, 105005. [[CrossRef](#)]
40. Furusho, J.; Sakaguchi, M.; Takesue, N.; Koyanagi, K.I. Development of Er Brake and Its Application to Passive Force Display. *J. Intell. Mater. Syst. Struct.* **2002**, *13*, 425–429. [[CrossRef](#)]
41. Petek, N.K.; Romstadt, D.J.; Lizell, M.B.; Weyenberg, T.R. *Demonstration of an Automotive Semi-Active Suspension Using Electrorheological Fluid*; SAE Technical Paper 950586; SAE INTERNATIONAL: Warrendale, PA, USA, 1995. [[CrossRef](#)]
42. Weiss, R.A.; Sen, A.; Willis, C.L.; Pottick, L.A. Block Copolymer Ionomers. 1. Synthesis and Physical-Properties of Sulfonated Poly(Styrene Ethylene/Butylene Styrene). *Polymer* **1991**, *32*, 1867–1874. [[CrossRef](#)]
43. Barreira, S.V.P.; Garcia-Morales, V.; Pereira, C.M.; Manzanares, J.A.; Silva, F. Electrochemical Impedance Spectroscopy of Polyelectrolyte Multilayer Modified Electrodes. *J. Phys. Chem. B* **2004**, *108*, 17973–17982. [[CrossRef](#)]

44. Martins, C.R.; Ruggeri, G.; de Paoli, M.-A. Synthesis in Pilot Plant Scale and Physical Properties of Sulfonated Polystyrene. *J. Braz. Chem. Soc.* **2003**, *14*, 797–802. [[CrossRef](#)]
45. Zhang, L.; Wu, Z.L.; Nelson, N.C.; Sadow, A.D.; Slowing, I.I.; Overbury, S.H. Role of CO₂ as a Soft Oxidant for Dehydrogenation of Ethylbenzene to Styrene over a High-Surface-Area Ceria Catalyst. *ACS Catal.* **2015**, *5*, 6426–6435. [[CrossRef](#)]
46. Hazarika, M.; Malkappa, K.; Jana, T. Particle-Size-Dependent Properties of Sulfonated Polystyrene Nanoparticles. *Polym. Int.* **2012**, *61*, 1425–1432. [[CrossRef](#)]
47. Siqueira-Petri, D.F.; Wenz, G.; Schunk, P.; Schimmel, T.; Bruns, M.; Dichtl, M.A. Surface Modification of Thin Polystyrene Films. *Coll. Polym. Sci.* **1999**, *277*, 673–679. [[CrossRef](#)]
48. Coughlin, J.E.; Reisch, A.; Markarian, M.Z.; Schlenoff, J.B. Sulfonation Of Polystyrene: Toward The “Ideal” Polyelectrolyte. *J. Polym. Sci. Pol. Chem.* **2013**, *51*, 2416–2424. [[CrossRef](#)]
49. Bekri-Abbes, I.; Bayoudh, S.; Baklouti, M.; Papon, E.; Leclercq, D. Converting Waste Polystyrene into Adsorbent: Optimisation of Reaction Parameters and Properties. *Prog. Rubber Plast. Recycl. Technol.* **2006**, *22*, 179–193.
50. Kucera, F.; Jancar, J. Preliminary Study of Sulfonation of Polystyrene by Homogeneous and Heterogeneous Reaction. *Chem. Pap.* **1996**, *50*, 224–227.
51. Benavides, R.; Oenning, L.W.; Paula, M.M.S.; Da Silva, L. Properties of Polystyrene/Acrylic Acid Membranes after Sulphonation Reactions. *J. New Mater. Electrochem. Syst.* **2014**, *17*, 85–90.
52. Wallace, R.A. Electrical-Conduction in Sulfonated Polystyrene Films. *J. Appl. Polym. Sci.* **1973**, *17*, 231–238. [[CrossRef](#)]
53. Wallace, R.A. Dielectric Behavior of Sulfonic Acid Polystyrene Films. *J. Appl. Polym. Sci.* **1973**, *17*, 223–230. [[CrossRef](#)]
54. Barnes, H.A. The Yield Stress—A Review Or ‘Pi Alpha Nu Tau Alpha Rho Epsilon Iota’—Everything Flows? *J. Non-Newton. Fluid* **1999**, *81*, 133–178. [[CrossRef](#)]
55. Hao, T. Electrorheological Suspensions. *Adv. Colloid Interface Sci.* **2002**, *97*, 1–35. [[PubMed](#)]
56. Rozynek, Z.; Wang, B.; Fossum, J.O.; Knudsen, K.D. Dipolar Structuring of Organically Modified Fluorohectorite Clay Particles. *Eur. Phys. J. E* **2012**, *35*, 9. [[CrossRef](#)] [[PubMed](#)]
57. Davis, L.C. Polarization Forces and Conductivity Effects in Electrorheological Fluids. *J. Appl. Phys.* **1992**, *72*, 1334–1340. [[CrossRef](#)]
58. Pan, X.D.; Mckinley, G.H. Characteristics of Electrorheological Responses in an Emulsion System. *J. Colloid Interface Sci.* **1997**, *195*, 101–113. [[CrossRef](#)] [[PubMed](#)]
59. Das, D.; Saintillan, D. A Nonlinear Small-Deformation Theory for Transient Droplet Electrohydrodynamics. *J. Fluid Mech.* **2017**, *810*, 225–253. [[CrossRef](#)]
60. Lanauze, J.A.; Walker, L.M.; Khair, A.S. Nonlinear Electrohydrodynamics of Slightly Deformed Oblate Drops. *J. Fluid Mech.* **2015**, *774*, 245–266. [[CrossRef](#)]
61. Vlahovska, P.M. Electrohydrodynamic Instabilities of Viscous Drops. *Phys. Rev. Fluids* **2016**, *1*, 060504. [[CrossRef](#)]
62. Rozynek, Z.; Kaczmarek-Klinowska, M.; Magdziarz, A. Assembly and Rearrangement of Particles Confined at a Surface of a Droplet, and Intruder Motion in Electro-Shaken Particle Films. *Materials* **2016**, *9*, 679. [[CrossRef](#)]
63. Ouriemi, M.; Vlahovska, P.M. Electrohydrodynamic Deformation and Rotation of a Particle-Coated Drop. *Langmuir* **2015**, *31*, 6298–6305. [[PubMed](#)]
64. Salipante, P.F.; Vlahovska, P.M. Electrohydrodynamics of Drops in Strong Uniform Dc Electric Fields. *Phys. Fluids* **2010**, *22*. [[CrossRef](#)]
65. Lu, K.; Wen, W.; Li, C.; Xie, S. Frequency Dependence of Electrorheological Fluids in an Ac Electric Field. *Phys. Rev. E* **1995**, *52*, 6329–6332. [[CrossRef](#)]



Supplementary Materials: Electric Field-Driven Assembly of Sulfonated Polystyrene Microspheres

Alexander Mikkelsen ¹, Jarosław Wojciechowski ², Michal Rajňák ^{3,4}, Juraj Kurimský ⁴, Khobaib Khobaib ¹, Ahmet Kertmen ⁵ and Zbigniew Rozynek ^{1,*}

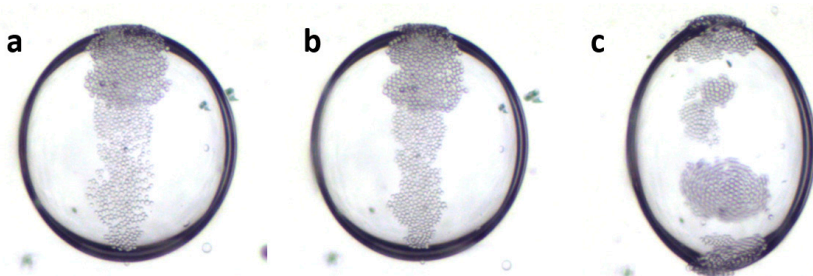


Figure S1. Instabilities on droplet interface at high DC electric fields. A silicone oil droplet containing pure PS particles (diameter 40 μm) and suspended in castor oil. The particles are at the droplet interface. A DC electric field of strength 100 V/mm (a), 200 V/mm (b) and 600 V/mm (c) is applied in horizontal direction. When a strong electric field is applied, instabilities develop at the droplet interface, leading to the formation of spinning particle domains (c). The droplet radius is around 1 mm.

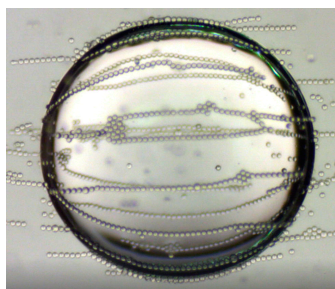


Figure S2. Particle detachment from a silicone oil droplet suspended in castor oil. The droplet is covered with 40 μm PS particles sulfonated for 32 min. An AC electric field (100 Hz) of strength 400 V/mm is applied in horizontal direction. The dipolar interactions between particles forming chains are strong, and some of the particles eventually detach from the droplet interface. This is because the particles have high affinity to the surrounding castor oil, resulting in low binding energy to the drop interface.

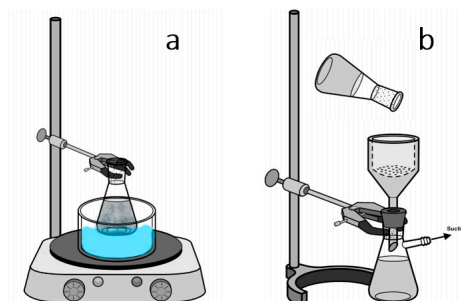


Figure S3. Schematic illustration of the sulfonation process of spherical PS particles. PS particles were placed in a small Erlenmeyer flask with sulphuric acid at 50 $^{\circ}\text{C}$ (placed in a water bath) and stirred using a magnetic stirrer (a). After the specific reaction periods, sulfonated polystyrene particles were filtrated by suction through a filter (b). Once the sulphuric acid was filtered out, the particles were washed with deionized water, saturated in KOH solution and then washed with deionized water again. Finally, the PH value was measured to control that the particles were properly neutralized.

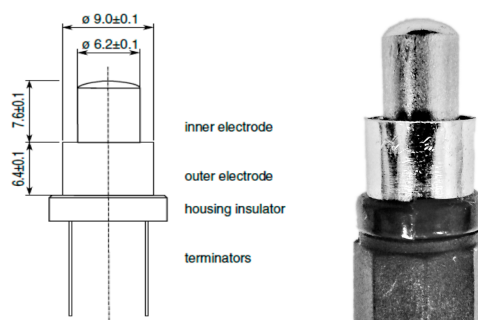


Figure S4. A home-made cylindrical capacitor used as a sample holder for measuring electrical capacitance and dielectric constants. The separation distance between the inner and outer cylindrical electrode was 1.4 mm, which gives a capacity value of the empty capacitor (C_0) equal to 2.78 pF. PS samples were poured into the cylindrical gap, while a homogenous filling of the cell was ensured by properly shaking of the capacitor.

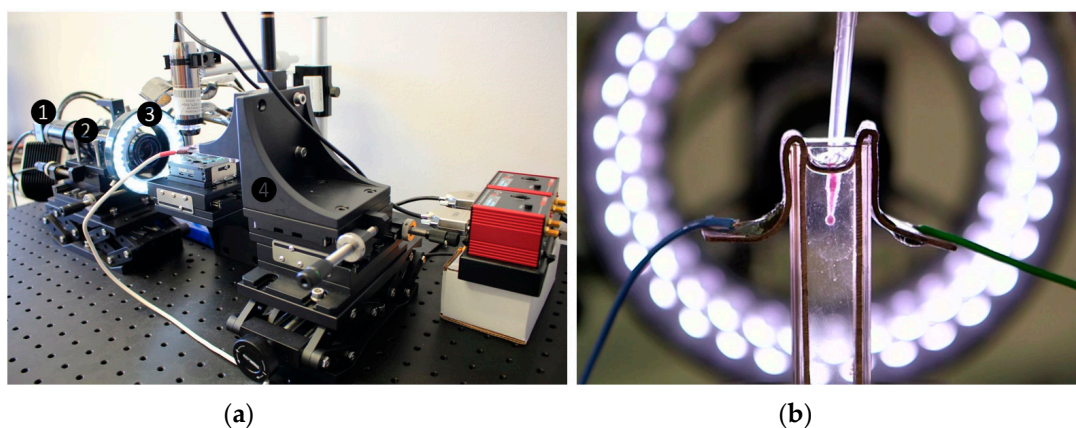


Figure S5. Experimental set-up for the experiments on electric field-driven particle assembly of PS particles consisted of a CMOS camera ① mounted on a high-magnification zoom lens system ②, a light source ③, a sample cell placed on a mechanical x-y-z translational stage ④, a voltage amplifier, an oscilloscope, and a PC for recording images (a). As sample cells, we used 10 mm × 10 mm plastic cuvettes (typically used for light spectroscopy) with two copper plates constituting electrodes (b).

Paper III

Particle-covered drops in electric fields: Drop deformation and surface particle organization




A Mikkelsen, K Khobaib, F K Eriksen, K J Måløy and Z Rozynek

Soft Matter **14**, 5442–5451 (2018)



Cite this: *Soft Matter*, 2018, 14, 5442

Particle-covered drops in electric fields: drop deformation and surface particle organization†

A. Mikkelsen, *^a K. Khobaib, ^a F. K. Eriksen,^b K. J. Måløy^b and Z. Rozynek [‡]^a

Drops covered by adsorbed particles are a prominent research topic because they hold promise for a variety of practical applications. Unlocking the enormous potential of particle-laden drops in new material fabrication, for instance, requires understanding how surface particles affect the electrical and deformation properties of drops, as well as developing new routes for particle manipulation at the interface of drops. In this study, we utilized electric fields to experimentally investigate the mechanics of particle-covered silicone oil drops suspended in castor oil, as well as particle assembly at drop surfaces. We used particles with electrical conductivities ranging from insulating polystyrene to highly conductive silver. When subjected to electric fields, drops can change shape, rotate, or break apart. In the first part of this work, we demonstrate how the deformation magnitude and shape of drops, as well as their electrical properties, are affected by electric field strength, particle size, conductivity, and coverage. We also discuss the role of electrohydrodynamic flows on drop deformation. In the second part, we present the electric field-directed assembly and organization of particles at drop surfaces. In this regard, we studied various parameters in detail, including electric field strength, particle size, coverage, and electrical conductivity. Finally, we present a novel method for controlling the local particle coverage and packing of particles on drop surfaces by simply tuning the frequency of the applied electric field. This approach is expected to find uses in optical materials and applications.

Received 3rd May 2018,
Accepted 26th May 2018

DOI: 10.1039/c8sm00915e

rsc.li/soft-matter-journal

1 Introduction

Drops covered by micro- and nanoparticles have recently received considerable research interest.^{1–4} This is because they are promising for a variety of practical applications, such as in food technology,⁵ the oil industry,⁶ biofuel processing,⁷ and for improving pharmaceutical products.⁸ Moreover, such drops possess characteristics that make them useful as experimental model systems for studying, for example, particle effects on interfacial tension,⁹ particle crystal growth and ordering or particle layer buckling on curved interfaces,^{10–13} particle assembly and rearrangement on drop surfaces,^{14,15} and particle detachment from drops.¹⁶ Particle-covered drops can additionally be employed for fabricating porous structures,¹⁷ granular or colloidal capsules of different mechanical properties, morphologies, or shapes,^{18,19} and adaptive structures.²⁰ In this context, broadening knowledge of particle-covered drop stability, deformation, and surface

particle manipulation is essential to further developing the abovementioned research areas.

The deformation of drops can be induced and investigated using various experimental tools, including atomic force microscopes,^{21,22} microfluidic devices,^{23–25} and by utilizing mechanical shearing^{26,27} or electric fields.^{28–32} For manipulating particles at drop surfaces or in the bulk of a drop, there are many physical or chemical approaches, such as pH-controlled particle assembly,³³ acoustic wave-induced bulk and surface particle convection,³⁴ magnetic field-directed particle assembly,³⁵ and electric field-assisted particle arrangements.³⁶

In this work, we explore the possibilities of employing electric fields as a contactless method for both drop deformation and the manipulation of particles at drop interfaces. In our experiments, no mechanical shearing or microfluidic flow was required to induce drop deformation, and the electric stresses imposed on the drops were axisymmetric. For that reason, the studied drops were stationary in the sample cell, which facilitated the experimental observation of the drops.

Particle organization at the surface of drops is achievable by various electric field phenomena. Electric fields can manipulate particles by exerting forces that are acting on them either directly, *e.g.* through particle motion *via* dipolar forces, or indirectly, *e.g.* by particle convection through electric field-induced liquid flows. Electrohydrodynamic (EHD) liquid flows,^{37,38}

^a Institute of Acoustics, Faculty of Physics, Adam Mickiewicz University, Umultowska 85, 61-614 Poznań, Poland. E-mail: alexam@amu.edu.pl; Tel: +48 608 179 539

^b PoreLab, The Njord Centre, Department of Physics, University of Oslo, P.O. Box 1048, Blindern, N 0316, Oslo, Norway

† Electronic supplementary information (ESI) available: Two supplementary movies. See DOI: 10.1039/c8sm00915e

‡ These authors contributed equally to this work.



dipolar interactions,³⁹ dielectrophoresis (DEP),^{40,41} electrostatics,³⁶ or electrocoalescence¹⁹ can be utilized to transport, assemble, or sort particles at drop interfaces. Removing particles from a drop is also possible through tip-streaming mechanisms⁴² and strong EHD flows.¹⁴ The applicability of the abovementioned approaches depends on the electric properties of both the particles and the liquids. For example, the dielectrophoretic force (force exerted on an object subjected to a non-uniform electric field) acting on drop surface particles is very small (and cannot be used to manipulate particles) when the dielectric properties of those particles are similar to those of the drop and surrounding liquid.⁴¹

We performed experiments on silicone oil drops suspended in castor oil (weakly conductive liquids) that were covered by microparticles with a broad spectrum of electrical conductivities and subjected to uniform electric fields. We present our investigations and conclusions on drop deformation and stability affected by the applied electric field strength, surface particle size, and electrical properties (Section 3.1); as well as surface particle coverage (Section 3.2). Moreover, we show how surface particles can be assembled and structured at drop interfaces (Section 3.3). In addition, we demonstrate an approach for actively controlling local particle coverage and packing at drop interfaces (Section 3.4). Before investigating particle-covered drops, let us first discuss the behaviour of a corresponding and simplified system, namely, a particle-free silicone oil drop formed in castor oil and subjected to electric fields.

1.1 Behaviour of particle-free silicone oil drops in electric fields

The electric conductivity and dielectric constant of a silicone oil drop is smaller than those of the surrounding castor oil. When subjected to a direct current (DC) electric field, free charges (ionic impurities) in the oils accumulate at the drop interface. This results in the formation of a drop dipole moment directed in the opposite direction of the electric field. The action of the applied DC electric field on the free charges at the silicone oil drop yields electric stresses. At the electric poles of the drop (surface areas closest to the electrodes), electric stress has only a normal component that is balanced by capillary forces and the pressure difference across the drop interface. There are no free charges at the electric equator of the drop, and thus there is no electric stress at this area of the drop. Everywhere else at the drop interface, electric stress has two components: normal and tangential to the drop interface. As a result of normal electric stress, the drop is compressed along the electric field direction, obtaining (within a second) an oblate shape. Tangential electric stress induces electrohydrodynamic flows at the drop interface that shear the liquids inside and outside the drop. In general, the direction of these EHD flows depends on the free charge distribution at the drop interface. In the case of a silicone oil drop suspended in castor oil, the EHD flows at the drop surface are directed from the drop poles to the drop equator (for more details, see ref. 43). As long as the applied electric field strength is weak (typically $< 200 \text{ V mm}^{-1}$), the induced EHD liquid flows can be used to convect and eventually

assemble surface particles, as we discuss later in this section. At strong DC electric fields, weakly-conductive drops may undergo electrorotation^{44–46} or break apart.⁴⁷

The accumulation of free charges at the interface of a drop requires finite time. For the drop system studied here, the time for free charges to build up at the drop interface (the Maxwell–Wagner relaxation time)⁴³ was $\sim 1 \text{ s}$. Therefore, when applying alternating current (AC) electric fields with sufficiently high frequencies, the electric field changes direction so quickly that no free charges accumulate at the drop interface. Experimentally, we observed no EHD flows for electric field frequencies above 100 Hz. At such electric field conditions, the drop behaves as a dielectric drop, *i.e.* there are only polarization charges present and no free charges. The dipole moment of the drop is now in the same direction as the applied electric field, unlike the situation when a DC field is applied. Accordingly, the drop stretches along the electric field direction, acquiring a prolate shape, and no EHD flows are present. Drop deformation is defined as $D = (d_{\parallel} - d_{\perp}) / (d_{\parallel} + d_{\perp})$, where d_{\parallel} and d_{\perp} are the drop axes parallel and perpendicular to the electric field direction, respectively. For small deformations, the drop deformation scales as E^2 for both DC and AC electric fields.⁴³

1.2 Behaviour of particle-covered silicone oil drops in electric fields

Adding particles to the drop surface may alter drop behaviour and characteristics in electric fields. The deformation,^{48–50} mechanics,^{32,51,52} relaxation,²⁶ or rotation⁵³ of particle-covered drops can differ from those of a pure drop. The surface particle's size, concentration, and electrical properties can influence the properties of the drop. The deformation of a pure silicone oil drop subjected to a DC electric field is affected by the amount of free charges built up at its interface. The addition of particles may influence the free charge accumulation and lead to an increase of the drop deformation in either direction (oblate or prolate configurations) or decrease the drop deformation magnitude. Furthermore, the addition of particles may also affect the magnitude of EHD flows, change drop conductivity, or influence drop stability. We describe these situations in the first part of this work.

1.3 Assembly of surface particles and their active structuring

Previous work showed that non-conductive (polymeric) particles assemble at the drop equator in the form of a ribbon *via* EHD flows, whereas for the same silicone oil–castor oil system, conductive (silver-coated) particles formed longitudinal particle chains *via* dipolar interactions.²⁰ Particles that are similar except for their dielectric properties may be transported either to the electric poles or electric equator of the drop by dielectrophoretics.⁴² These examples demonstrate the importance of the electrical properties of surface particles for particle assembly. Besides their electrical properties, we also investigated the influence of particle coverage and particle size on their organization at drop interfaces.

The family of electrokinetic phenomena offers different types of mechanisms that also enable the formation of active materials. Previous work demonstrated that controlling electric



field strength made it possible to actively structure and redistribute non-ohmic (*i.e.* having a non-linear relationship between the electric current and the voltage) clay mineral particles at the drop interface.²⁰ In the current study, we expanded the structuring to ohmic conductive particles. By utilizing the knowledge gained from the experiments presented in the first parts of this paper, we were able to actively structure conductive particles and to locally change their concentration and packing. Such smart material is easily controlled by tuning the electric field frequency, enabling the switching between two physical mechanisms: particle–particle dipolar interactions and EHD flows.

2 Materials and methods

2.1 Experimental set-up

Fig. 1 shows a schematic illustration of the set-up used in the experiments. The set-up consisted of a sample cell placed on a mechanical *x–y–z* translational stage, a signal generator (SDG1025, Sigilent), a high-voltage bipolar amplifier (10HVA24-BP1, HVP), two digital microscopes (AM7115MZTL, DINO-LITE) for front and side viewing (perpendicular and parallel to the electric field direction), and a PC for recording movies and images. The sample cell was made of glass with two of the inside walls coated with conductive indium tin oxide (ITO) constituting electrodes. A high-voltage signal was provided to the sample cell *via* two crocodile clips attached to the ITO-coated glass electrodes. The AC electrical signals used in the experiments presented in Section 3.4 were square-shaped and bipolar, and the provided signal values were root-mean-square values.

2.2 Oils and particles

The sample cell was filled with castor oil (83912, Sigma-Aldrich, density of $\sim 0.96 \text{ g cm}^{-3}$ at $25 \text{ }^\circ\text{C}$, electrical conductivity of $\sim 50\text{--}100 \text{ pS m}^{-1}$, relative permittivity ~ 4.7 , and viscosity of $\sim 700 \text{ mPa s}$ at $25 \text{ }^\circ\text{C}$). Silicone oil (6678.1000, Rhodorsil Oils 47, density of $\sim 0.96 \text{ g cm}^{-3}$ at $25 \text{ }^\circ\text{C}$, electrical conductivity of $\sim 5\text{--}10 \text{ pS m}^{-1}$, relative permittivity ~ 2.8 , and viscosity of $\sim 50 \text{ mPa s}$ at $25 \text{ }^\circ\text{C}$) drops with or without particles were made

in castor oil using a mechanical pipette, as presented in Fig. 1b. Particles in the bulk of the silicone oil drops were brought to the drop interface by applying a DC electric field and/or by particle sedimentation.

Different particle materials were used in the experiments, including conductive silver-coated hollow glass microspheres (M-40-0.67 and M-60-0.17, with an average size of $15 \text{ }\mu\text{m}$ and $55 \text{ }\mu\text{m}$, both with electrical conductivities of $\sim 10^7 \text{ S m}^{-1}$, purchased from Cospheric LLC) and polystyrene (PS) particles with an average size of $\sim 40 \text{ }\mu\text{m}$ (Dynoseeds TS40 6317, electrical conductivity of $\sim 10^{-11} \text{ S m}^{-1}$, density of $\sim 1.05 \text{ g cm}^{-3}$, purchased from Microbeads AS, Norway). The pristine PS particles were chemically treated (sulfonated, as described by Mikkelsen *et al.*⁵⁴) to increase their electrical conductivities to $\sim 5 \times 10^{-9} \text{ S m}^{-1}$. The PS particles were labelled PS0, PS16, and PS32, where the numbers refer to the sulfonation reaction time in minutes.

2.3 PIV experiments

The flowlines around drops were traced using particle image velocimetry (PIV). Fluorescent PE particles (UVPMS-BY2-1.00, size of $\sim 35 \text{ }\mu\text{m}$, Cospheric LLC) were dispersed in castor oil (0.3% by weight) and poured in the sample cell. A $500 \text{ }\mu\text{m}$ thin sheet of particles was selected by focusing a 532 nm laser light (COM-09906-5 mW, SparkFun Electronics) from above the sample cell through a laser line generator lens (Powell lens), as presented in Fig. S1 (ESI[†]). Silicone oil drops with or without surface particles were created in the castor oil using a mechanical pipette and brought to the drop interface, as explained above. During the experiments, the laser sheet was always aligned in the middle of the drop and oriented along the electric field direction and perpendicular to the view direction of the microscope. Movies (5 fps) were recorded for each experiment with a 1920×1080 pixel resolution (1 pixel $\sim 6.2 \text{ }\mu\text{m}$). 25 sequential frames were then compared and analysed using PIVlab (v.1.41, Matlab toolbox application),⁵⁵ yielding flow velocities for each interrogation area (the frames were split into a number of interrogation areas of size 64×64 pixels, which were then individually cross-correlated with the previous frame to obtain displacement vectors). Matlab (v.R2017b, MathWorks) was then used to plot the flow velocities, while Adobe Photoshop CC2018 (v.19.0, Adobe Systems) was utilized to create masks and add images of the analysed drops on top of the flow velocity figures.

3 Results

3.1 Electric field-induced deformation of Pickering drops

Initially, we investigated how the deformation of Pickering drops (drops fully covered by particles) is influenced by the strength of an applied DC electric field, as well as the size and electrical conductivity of surface particles. Silicone oil drops (size $\sim 2 \text{ mm}$) covered by particles were formed in castor oil and subjected to DC electric fields ranging from 0 to 200 V mm^{-1} . Fig. 2a presents images of five silicone oil drops covered by particles with electrical conductivities ranging from 10^{-11} to

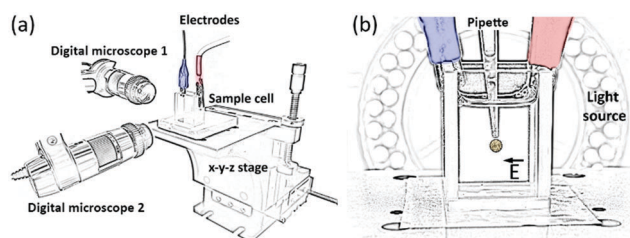


Fig. 1 (a) A schematic illustration of the set-up used in all experiments. The set-up consisted of a sample cell placed on a mechanical *x–y–z* translational stage, two digital microscopes for front and side viewing (perpendicular and parallel to the electric field direction), a signal generator, and a voltage amplifier for generating high-voltage bipolar signals provided to the cell *via* two crocodile clips. (b) The sample cell was made of glass with two of the walls coated with electrically-conductive ITO layers. The transparent ITO-covered glass electrodes allowed for observation in a direction along the electric field. Drops with or without particles were made using a mechanical pipette.



10^7 S m^{-1} and sizes between 15 and 55 μm . The drops were densely covered by particles (we estimated the particle coverage to be around 0.8, which is close to the maximum theoretical packing fraction).⁵⁶ As a reference, the deformation of a pure silicone oil drop is also included. Note that all drops were spherical before the application of electric fields, indicating that there was no particle jamming. This is important because the rigidity of jammed elastic shells increases with asphericity, and higher rigidity makes the particle-covered drop more difficult (requiring higher electric stress) to deform.⁵⁷

Fig. 2b presents quantitative data on drop deformation *versus* the applied electric field strength for the drops imaged in Fig. 2a. The particle-free silicone oil drop (pink triangles) and the drop covered by non-conductive PS0 particles (cyan diamonds) deformed into oblate shapes (compressed in the direction of the electric field). That is because the free charges accumulated at the drop surfaces created a drop dipole moment oriented in the opposite direction of the electric field. However, the steady state deformation of the PS0-covered drop was slightly larger than that of the particle-free silicone oil drop.

Supported by our previous work, we propose two origins for the increased drop deformation. First, the insulating particles reduced the electrical conductivity of the drop interface, allowing more free charges from the oils to accumulate on the drop interface, hence increasing the electric stress on the drop. Second, the induced EHD flows were greatly diminished or absent when the drop was covered by particles.³² EHD flows have been reported to weaken the steady-state deformation of particle-free drops by removing free charges from the drop interface by convection, thus decreasing the charge accumulation at drop surfaces (and the electric stress acting on the drops).⁵⁸

We decided to perform experiments to study the effect of particle coverage on EHD flows (their patterns and strengths). Fig. 3 presents the results of PIV experiments performed on

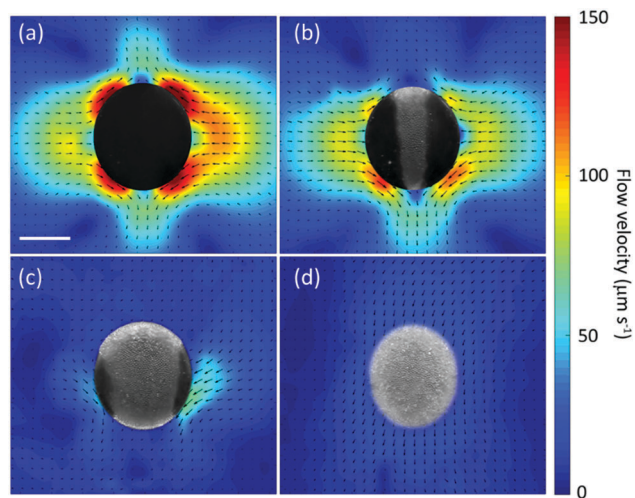


Fig. 3 (a–d) PIV images of (a) a particle-free silicone oil drop and silicone oil drops covered by non-modified PS particles with particle coverages (b) ~ 0.2 , (c) ~ 0.48 , and (d) ~ 0.81 . The drops were subjected to a DC electric field of 170 V mm^{-1} (in the horizontal direction), yielding steady-state drop deformations of (a) -0.023 , (b) -0.026 , (c) -0.028 , and (d) -0.04 . All drops had diameters equal to 2 mm and the scale bar is 1 mm. The asymmetry of the flow fields in (a–c) was caused by downward drop sedimentation, drop motion towards one of the electrodes, and, in (b and c), by non-uniform particle distribution. The masks in the middle of the flow fields are figures created from images of the drops used in the experiments.

silicone oil drops with PS0 surface particles at different particle coverages subjected to a DC electric field of 170 V mm^{-1} . The results from the PIV experiments confirm that the induced EHD flows at drop interfaces are indeed reduced by surface particles. When the particle coverage was increased from 0 (particle-free drop) to around 0.8 (drop fully covered by particles), the maximum EHD flow velocity around the drop

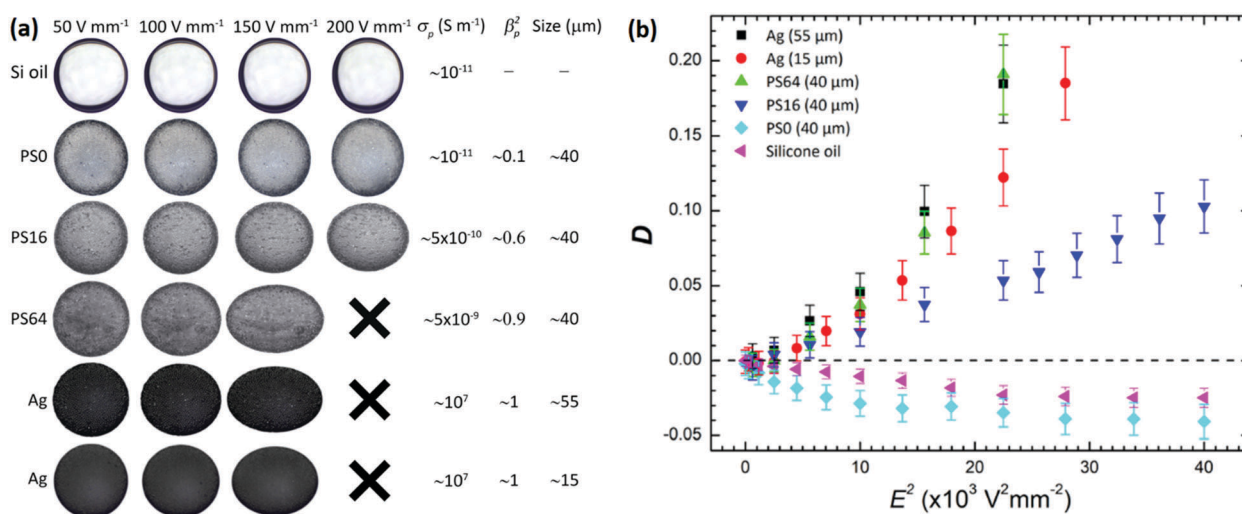


Fig. 2 (a) Electric field-induced deformation of silicone oil drops covered by particles with different electrical properties and sizes. The size of the drops was 2 mm and the electric field was applied in the horizontal direction. The deformation of a pure silicone drop is also included as a reference. Values of the electrical conductivity of the particles (σ_p), the conductivity mismatch between particles and castor oil ($\beta_p = (\sigma_p - \sigma_{ex})/(\sigma_p + 2\sigma_{ex})$), and the size of the particles are provided. The crosses indicate drop breakup. (b) Steady-state deformation *versus* applied electric field squared for the drops imaged in (a).



decreased from 150 to nearly $0 \mu\text{m s}^{-1}$, verifying that EHD flows surrounding a silicone oil drop in castor oil are suppressed when the drop is fully covered by particles. Moreover, Fig. 3b and c shows that EHD flows exist near the particle-free regions of the drop, and that these flows are asymmetric, *i.e.* the flow magnitude is stronger at the drop sides where there are less particles. The particle layer gives the drop surface shear elasticity (it behaves like an elastic sheet), which immobilizes the drop surface and greatly suppresses the EHD flows around particle-covered areas at the drop interface.^{59,60}

We found that silicone oil drops behaved as conductive drops and stretched in the direction of the applied electric field (prolate deformation) when they were fully covered by particles that were more conductive than both oils. In fact, the results presented in Fig. 2b are in accordance with previous work on the deformation of conducting drops.⁴⁷ In DC electric fields, drops behaving as conductors acquire a free charge distribution that sets up a drop dipole moment oriented in the same direction as the electric field, *i.e.* the dipole moment of these drops is oriented in the opposite direction to the dipole moment of the pure silicone oil drop (or the drops covered by PS0 particles).⁶¹ Accordingly, the electric stress at the drop surface deforms the conductive drop to a prolate shape. The next section presents more about drop stretching and our study of the influence of particle coverage on drop deformation.

3.2 Influence of particle coverage on drop deformations

Fig. 4a presents images of silicone oil drops covered by five types of particles (the same particles shown in Fig. 2) with different particle coverages. The drops were subjected to a DC electric field of 170 V mm^{-1} . Fig. 4b displays quantitative data on drop deformation against particle coverage (ϕ) for the drops imaged in Fig. 4a.

We found that the drops covered by PS0 particles compressed more (higher negative values of deformation, cyan diamonds in

Fig. 4b) when the particle coverage value increased. The drops covered by other particles became less compressed by increasing the particle coverage, and at certain particle coverage the deformation changed from oblate to prolate. Such a drop deformation transition occurred at lower particle coverage values for drops covered by more conducting particles (*e.g.* compare PS16 and PS64 in Fig. 4b), or by bigger particles (compare the drops covered by $55 \mu\text{m}$ vs. $15 \mu\text{m}$ Ag-coated glass spheres displayed in the bottom rows in Fig. 4a).

We observed that the particles formed chains when the particles at the drop interface were more conductive than the drop fluid (all particles except PS0). In addition to particle conductivity, chain formation also depends on particle size and particle coverage. The drop oblate–prolate transition occurs when the surface particles form chains spanning from drop pole to pole. The particle chains affect drop deformation by altering the build-up of free charges at the drop surface, owing to the faster conduction of charges through the chains compared to through the drop fluid. This also influences the EHD flows, as supported by the results in Fig. 5. The figure displays PIV images of silicone oil drops with and without PS64 particles subjected to a DC electric field of 170 V mm^{-1} . The figure shows that for a silicone oil drop covered with particles (PS64) that are more conductive than the drop and exterior oil, low particle coverage ($\phi \sim 0.13\text{--}0.17$) is sufficient to form pole–pole particle chains and suppress EHD flows (maximum flow velocity goes from $150 \mu\text{m s}^{-1}$ to almost zero, as shown in Fig. 5a and d, respectively). Furthermore, Fig. 5b and c demonstrate the influence of particle chain distribution on the EHD flow fields, *i.e.* EHD flows may exist outside drop domains that are free of particle chains, whereas flows near drop regions with particles are very weak. The EHD flows weaken due to the fast conduction of charges through particle chains at the drop surface. The particle chains redistribute the free charges at

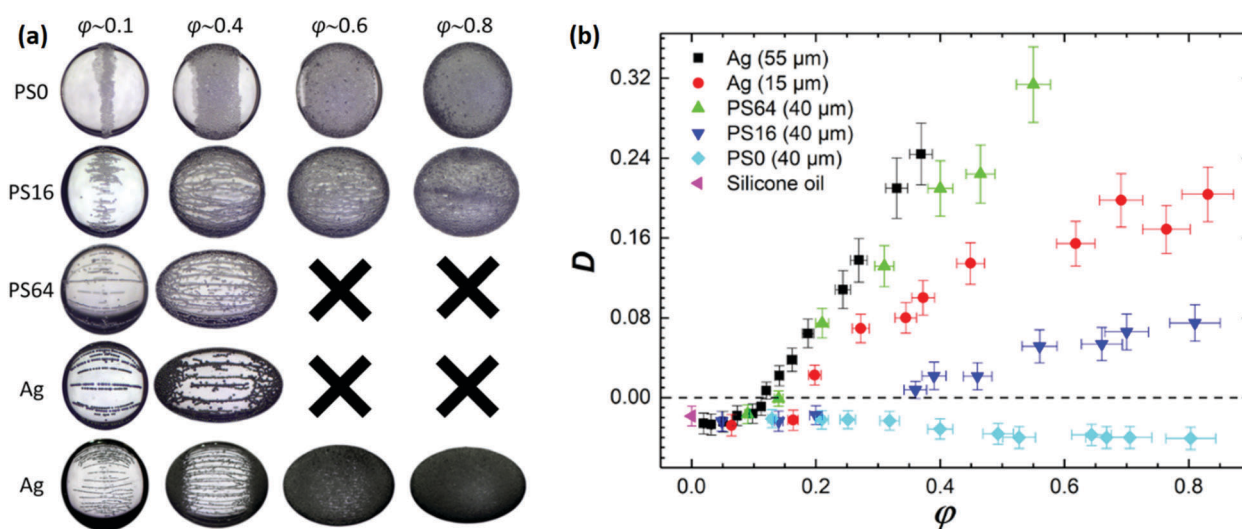


Fig. 4 (a) Electric field-induced deformation of silicone oil drops covered by non-modified and modified PS particles ($40 \mu\text{m}$) and silver coated glass spheres (15 and $55 \mu\text{m}$). The size of the drops was 2 mm , and the direction of the applied 170 V mm^{-1} DC electric field was horizontal. (b) Steady-state deformation of silicone oil drops as a function of particle coverage (ϕ ranges from $0\text{--}0.85$) the images in (a) correspond to respective data points in (b), and the crosses in (a) indicate drop breakup.



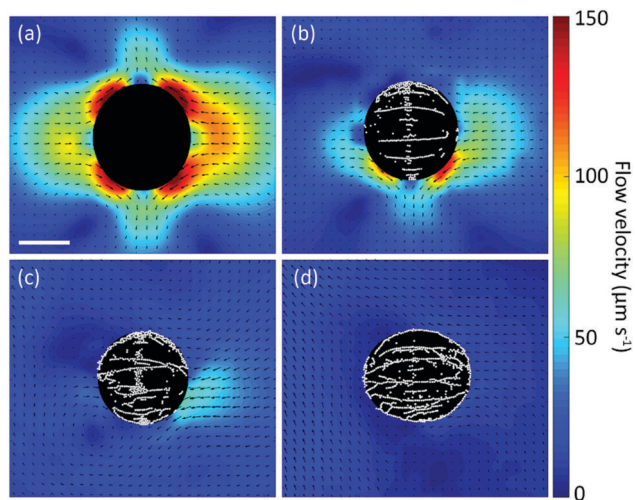


Fig. 5 PIV images of (a) a particle-free silicone oil drop and silicone oil drops covered by modified PS particles (PS64) with particle coverages: (b) ~ 0.08 , (c) ~ 0.13 , and (d) ~ 0.17 . The drops were subjected to a DC electric field of 170 V mm^{-1} (in the horizontal direction), yielding drop steady-state deformations of (a) -0.023 , (b) -0.023 , (c) -0.013 , and (d) 0.07 . All drops had diameters equal to 2 mm with a scale bar of 1 mm . The asymmetry of the flow fields in (a) was caused by downward drop sedimentation, drop motion towards one of the electrodes, and, in (b and c), by non-uniform particle distribution. The masks in the middle of the flow fields are figures created from real images of the drops used in the experiments.

the drop interface until the electric field component, which is parallel to the drop surface, becomes zero. In a steady state, the area of the drop containing conductive particles behaves as a conductor, *i.e.* the electric field has only a component perpendicular to the drop interface (because the electric field lines outside the drop are perpendicular to the drop surface and zero inside).⁶²

We also found that the magnitude of prolate deformation consistently increased with particle coverage, conductivity, and size (see Fig. 4b). For instance, at the same particle coverage, drops covered by PS64 particles of size $40 \mu\text{m}$ deformed less than drops covered by Ag-coated glass spheres that were slightly more conductive and larger. Moreover, drops covered by PS64 particles exhibited larger prolate deformations compared to drops covered by smaller, though more conductive, Ag particles.

3.3 Particle structuring at drop interfaces

Fig. 4a shows that at low particle coverages ($\varphi \sim 0.1$), all types of particles were transported towards the drop equator by EHD convective flows. However, only the PS0 particles formed a compacted particle ribbon. All other particles structured into chains because of particle–particle dipolar interactions. The dipolar force between particles (all types except PS0) was strong enough to resist the present EHD flows, and to eventually form dipolar chains along the electric field lines. For a particle with radius R subjected to a DC electric field of strength E_0 , the dipolar force F_D (between two particles) is given by the equation:⁶³ $F_D = 24\pi\epsilon_0\epsilon_{\text{ex}}R^6E_0^2\beta_p^2/(2R + s)^4$, where ϵ_0 is the vacuum permittivity, ϵ_{ex} the dielectric constant of the exterior

fluid, $\beta_p = (\sigma_p - \sigma_{\text{ex}})/(\sigma_p + 2\sigma_{\text{ex}})$ is the particle's Clausius–Mossotti factor, σ_p and σ_{ex} are the conductivities of the particles and the exterior fluid, respectively, and s is the edge-to-edge separation distance between particles. Note that the above-mentioned dipolar force equation is valid for a two-phase system. Here, we studied a three-phase system. However, because the surface particles on the drops had higher affinity to the surrounding castor oil (*i.e.*, a larger part of each particle was immersed in castor oil), it was justifiable to consider the system a two-phase system and employ the simplified dipolar force equation.

The dipolar force between two PS16 particles is around six times larger than the dipolar force between two non-modified PS0 particles ($\beta_{\text{p,PS16}}^2/\beta_{\text{p,PS0}}^2 \approx 6$), even though the difference in conductivity is small, *i.e.* PS16 particles are two times more conductive than the PS0 particles. Particles that are more conductive than the PS16 particles form longer chains, owing to the increased dipolar force. Interestingly, although the Ag-coated glass spheres used in these experiments were 15 orders of magnitude more conductive than the PS64 particles, the dipolar force between a pair of Ag-coated glass spheres was comparable to that of a pair of PS64 particles (of similar size) ($\beta_{\text{p,Ag}}^2/\beta_{\text{p,PS64}}^2 \approx 1.1$).

Furthermore, for drops with high particle coverage subjected to a DC electric field of 170 V mm^{-1} , we observed that the surface particles (all types except PS0) concentrated at the drop poles (Fig. 4a). We propose that the particle concentration at the drop poles was caused by electrorheological chaining, where the formed chains grew towards the drop poles due to their locally-strong electric fields (the increased curvature resulted in a higher free charge density at the drop poles). Dielectrophoresis (forces acting on a particle when the electric field is non-uniform) could also be a possible explanation for the observed particle accumulation. Other researchers have demonstrated that surface particles can be transported towards drop poles and agglomerate there *via* dielectrophoresis.^{15,42} However, according to our theoretical calculations, this could not have been the case here. We found that for all the different particles utilized in the experiments (except PS0), the dielectrophoretic (DEP) force on the particles was directed towards the drop equator rather than towards the drop poles. The term $\beta'\beta(2 + \beta)$ in the equation for the DEP force determines the force direction.⁶⁴ Here $\beta' = (\sigma_p - \sigma_{\text{ex}})/(\sigma_p + 2\sigma_{\text{ex}})$ is the particle's Clausius–Mossotti factor, $\beta = (\sigma_{\text{in}} - \sigma_{\text{ex}})/(\sigma_{\text{in}} + 2\sigma_{\text{ex}})$ is the drop's Clausius–Mossotti factor, and σ_p , σ_{in} , and σ_{ex} are the conductivities of the particles, drop fluid, and surrounding fluid, respectively. For all the drops except those covered by PS0, $\beta'\beta(2 + \beta) < 0$, indicating that any DEP force acting on the surface particles would move them towards the drop equator.⁶⁴

We validated the direction of the DEP force on the particles experimentally by forming a silicone oil drop covered by $15 \mu\text{m}$ silver-coated spheres and a silicone oil drop covered by PS0 particles. The particle coverages were low, and the drops were exposed to an AC electric field at 200 Hz and 300 V mm^{-1} . A DC electric field could not be used in this experiment because the induced EHD flows would have dominated the DEP force experienced by the particles (flow velocity ratio $\nu_{\text{EHD}}/\nu_{\text{DEP}} \approx 10^3$).



As explained in the Introduction section, when an AC electric field at such a high frequency (200 Hz) is applied, the electric field changes direction too fast for free charges in the oils to accumulate at the drop interface and for EHD flows to be induced. In the absence of EHD flows, it is possible to observe particle movement by DEP. Note that for an AC electric field, the previously-described Clausius–Mossotti terms used in the equation to determine the DEP force direction change. The conductivities are replaced by permittivity terms, yielding: $\beta_{AC}' = (\epsilon_p - \epsilon_{ex})/(\epsilon_p + 2\epsilon_{ex})$ and $\beta_{AC} = (\epsilon_{in} - \epsilon_{ex})/(\epsilon_{in} + 2\epsilon_{ex})$, where ϵ_p , ϵ_{in} , and ϵ_{ex} are the permittivities of the particles, drop fluid, and surrounding fluid, respectively.⁶⁵ For the fluids and particles used in this work, we calculated that the direction of the DEP force acting on the surface particles is the same whether the applied electric field is DC or AC. For all the particle-covered drops except those covered by PS0, $\beta_{AC}'\beta_{AC}(2 + \beta_{AC}) < 0$, indicating that the DEP force brings the particles to the drop equator. This was confirmed experimentally: when the AC electric field was turned on, the silver particles moved towards the drop equator and formed chains, whereas at the surface of the other drop, the PS0 particles translated much more slowly towards the drop poles. The PS0 particles also served as tracing particles, proving that there were no EHD flows present while the electric field of frequency 200 Hz was applied. Movie S1 (ESI[†]) presents the results of these experiments. Based on these results, we excluded the possibility of DEP interactions causing particle agglomeration at drop poles. Note that the silicone oil drops stretched (prolate deformation) in the direction of the applied AC electric field. That is because there were no free charges present, and the resulting drop dipole moment polarized by the electric field was oriented in the same direction as the electric field.⁶⁶

3.4 Manipulating interfacial particles by EHD flows and dipolar interactions

In this section, we demonstrate the possibilities of particle manipulation at drop interfaces by employing EHD flows and particle dipolar interactions. We utilize the knowledge gained from the previous sections about the influence of the particles' properties, their coverage, and the electric field strength on the magnitude of EHD flows and drop deformation.

During the experiments and for all particles (except PS0), we observed that the growth of particle chains started from the drop equator and extended towards the drop poles (see Movie S1, ESI[†]), irrespective of the electric field frequency used (within the studied frequency range, *i.e.* from 0 to 1 kHz). The more particles present at the drop interface, the longer the chains became (until the particles started to agglomerate at the drop poles at high particle coverages).

We took advantage of this observation to create an adaptive structure in which particle packing, coverage, and structuring were easily controlled by only changing the frequency of the applied electric field. Fig. 6 shows a silicone oil drop (size of ~ 3 mm) formed in castor oil and covered by $15 \mu\text{m}$ Ag-coated glass spheres ($\phi \sim 0.15$). The drop was subjected to an electric field of 170 V mm^{-1} and viewed parallel (Fig. 6a and b) and

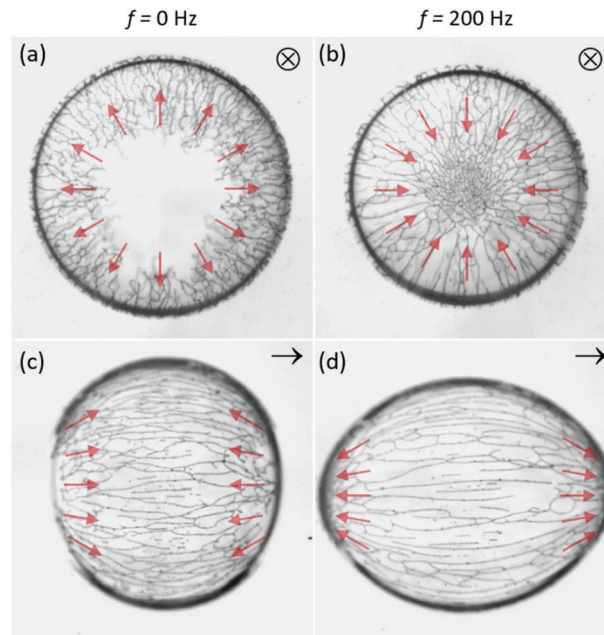


Fig. 6 (a–d) Actively arranging surface-adsorbed conductive particles by switching the electric field frequency from 0 Hz (EHD flow regime) to 200 Hz (particle dipolar interaction regime). A silicone oil drop with diameter ~ 3 mm is viewed (a and b) along and (c and d) perpendicular to the electric field direction, as indicated by the symbols. Ag-coated glass microspheres with mean diameters of $\sim 20 \mu\text{m}$ were used in this experiment, in which $E = 200 \text{ V mm}^{-1}$ was fixed. The structuring process is reversible, and the switching between two particle conformations occurred in seconds, as shown in Movie S2 (ESI[†]).

perpendicular (Fig. 6c and d) to the electric field direction. When a DC electric field was applied, the particles formed chains *via* particle–particle dipolar interactions. However, the growth of the chains was limited (and thus also their lengths) by the induced EHD flows, *i.e.* the chains were not rigid enough to withstand the strain imposed by the EHD flows, and the electric poles of the drop became particle-free (Fig. 6a and c). As demonstrated in Movie S2 (ESI[†]), the EHD flows bend the ends of the particle chains, and sometimes even break and push the chains back towards the drop's electric equator (as indicated by the red arrows in Fig. 6a and c). To disable the EHD flows and allow the particle chains to grow towards the drop poles, we simply increased the electric field frequency to a value far above the critical frequency for EHD flow induction. As demonstrated in Fig. S2 (ESI[†]), a frequency of 200 Hz satisfies this condition. After changing the frequency from 0 to 200 Hz, the particles redistributed at the surface of the drop and locally changed the particle coverage, *i.e.* both drop poles were densely covered by particles at the cost of the particle coverage around the equatorial area. The direction of particle transport is indicated by the red arrows in Fig. 6b and d. After the frequency of the AC electric field was decreased from 200 to 0 Hz, EHD flows were induced (free charges had sufficient time to accumulate at the drop interface) to transport the particles located at the drop electric poles back to the drop electric equator.

For the current drop–particle system, the whole structuring process is reversible, as demonstrated in Movie S2 (ESI[†]).



However, it is worth mentioning that the reversibility and feasibility of the approach depend on particle size, material, and concentration. When the experiment shown in Fig. 6 was repeated for drops covered by larger particles of the same type (55 μm silver-coated microspheres, $\phi \sim 0.1$), the process was irreversible, *i.e.* the particle-covered drop remained prolately deformed when the electric field was changed from AC to DC. The dipolar force between surface particles on a drop is proportional to the particle radius squared. As a consequence, the dipolar force between 55 μm sized particles is significantly larger compared to the force between 15 μm particles, considerably increasing the chain stiffness. The increased dipolar force between the 55 μm particles was sufficiently strong to keep the particles in the chain structures together by resisting the EHD shear stress induced at the drop surface when the applied electric field changed from AC to DC. Note that the surface particle rearrangement was accompanied with changes in the drop shape (compare Fig. 6c and d), and that the timescale for switching between the two particle conformations was on the order of seconds.

4 Conclusions and discussions

In conclusion, we studied both the behaviour of particle-covered drops and particle organization at drop interfaces by employing external electric fields. Here, we discuss our results and the underlying mechanisms, especially how particles on drop interfaces affect drop deformation, EHD flows, and particle structuring.

4.1 Surface particles and their effect on drop deformation

We found, that, besides the applied electric field strength, the particle material, particle coverage and size affect the deformation and electrical properties of silicone oil drops when subjected to electric fields. Our experiments show that the addition of particles to drop surfaces enhances the deformation magnitude of the drops, suppresses EHD flows, and alters drop shapes. For example, by adding conductive particles to the surface of a silicone oil (which is weakly-conductive), the drop geometry changes from oblate to prolate (from compressed to stretched in the direction of the electric field). Particles adsorbed at a drop interface may alter the surface tension, interfacial viscosity, or electric properties (conductivity and permittivity) of the drop.^{32,53} Because the surface tension works against drop compression or stretching (trying to make the drop spherical and reduce the energy of the system), a change in surface tension can affect the deformation magnitude, but does not determine whether the drop is prolate or oblate. Besides, as observed in previous experiments on particle-covered silicone oil drops in castor oil, adding particles to the drop surfaces has an insignificant effect on the surface tension of the drops, and thus also a negligible effect on the deformation magnitude of such drops.³²

Similarly, an increase of the effective interfacial viscosity (expected after adding particles to the liquid interface)⁶⁷ affects only the magnitude of the drop deformation⁴³ and cannot cause

the oblate-to-prolate shape transition. We therefore attribute the oblate–prolate deformation transition to changes in the electric properties of the drop interface. In the case of a silicone oil drop in castor oil, adding particles to the drop interface that are more conductive than the silicone and castor oil reverses the free charge distribution. The dipole moment of the drop (formed by free charges at the surface) changes direction from opposite of to similar to the electric field direction.

4.2 Suppression of EHD flows

Qualitative results from previous studies suggest that if the interfacial viscosity of a particle-covered silicone oil drop in castor oil is sufficiently large (high particle coverage), the particle layer can suppress electric field-induced EHD flows.^{32,53} In this research, we performed both qualitative (*e.g.* presence and direction) and quantitative (flow magnitude) studies on EHD flows. Our experiments show that the addition of surface particles on a silicone oil drop in castor oil leads to a reduction of the electric field-induced EHD flow velocities around the drop, irrespective of the electrical conductivity of the surface particles. A monolayer of packed particles at a liquid interface behaves like an elastic sheet that can support stresses and strain.^{59,60} For that reason, the shear elasticity of the particle layer immobilizes the drop interface and suppresses the EHD flows. However, the electrical properties of the surface particles do determine the critical particle concentration at which EHD flows are suppressed, as is explicitly shown in Fig. 3 and 5. Particles at the drop surface can form particle chains *via* dipole–dipole interactions (due to particle polarization), where the force between the particles depends on parameters such as particle size, electrical conductivity (for DC fields), and permittivity (for AC fields).⁶³ The presence of conductive particle chains affects the distribution of free charges at the drop interface by conducting charges faster through the particle chains than through the silicone oil drop (which is weakly conductive). If the concentration of particle chains at the drop surface is high, the drop behaves as a conductive drop with no electric stress component acting parallel to the drop interface.

4.3 Particle organization at drop surfaces

We also observed that particles at drop surfaces subjected to a constant DC electric field exhibit different structuring depending on their electrical properties and coverage. For instance, at the same low particle coverage, insulating surface particles assemble at the equator of silicone oil drops, forming ribbon-like structures composed of densely-packed particles, while silver-coated particles form short chains aligned with the electric field. We conclude that particle structuring is determined by the competition between EHD flows and particle–particle dipolar interactions. When the dipolar interactions between particles are strong, the particles can form long chains that cannot be broken by the EHD flows. Additionally, if the particle concentration is high, the chains can span the whole drop and particles concentrate at the drop poles. When the dipolar interactions between particles are weak, the EHD flows can be utilized to structure particles at drop poles or at the drop



equator, depending on the electric properties of the drop and surrounding fluid.²⁰ For the system studied in our research (silicone oil drop in castor oil), the EHD flows were directed from drop poles to drop equator.

4.4 Method for manipulating conductive particles at drop surfaces

Furthermore, we present a novel method for manipulating conductive particles at drop surfaces. By applying an AC electric field and tuning the frequency, we actively structured surface particles and locally changed their concentration and packing. The adaptive particle structure is organized by dipolar interactions and EHD flows. When the frequency of the applied electric field is high, the particles form long chains *via* dipolar interactions and concentrate at the drop poles. Switching the electric field to DC induces EHD flows that move the particles from the drop poles towards the drop equator. The method resembles the pupil effect reported by Dommersnes *et al.*,²⁰ where the strength of the applied DC electric field was used to control the coverage of clay particles at a drop surface. The new method presented in this article is not limited to clay particles, it also allows for using surface particles of different conductive materials. A subtle point is that the size of particles and their concentrations must be chosen so that the dipolar forces are strong enough to assemble particles at drop poles under electric fields at high frequencies, and weak enough to allow for the formed chains to be broken by EHD flows at DC electric fields. It is worth pointing out that by reducing the viscosity of the liquids, the time for actively stretching the particle chains can be as small as micro-seconds, just by reducing the viscosity of the liquids to that of water. The electrical conductivities of the oils could also be tuned (*e.g.* by adding inorganic salts) to speed up this process. Another note is that from the frequency tuning experiments (demonstrated in Movie S2, ESI[†]), we learn that it is possible to control the packing density and likely also the characteristic periodicity between the particle chains. We envisage the possibility to further investigate these effects in respect to optical materials and applications.

4.5 Outlook

We believe the findings of this work are important for developing advanced structures, such as patchy microcapsules. With a myriad of applications ranging from energy storage to the encapsulation of an extensive range of materials, homogenous and patchy microcapsules have received considerable research interest in this decade. It has been reported that the target microencapsulated product will be worth around \$9.25 billion by 2020.⁶⁸ To succeed in implementing these microcapsules, we need to precisely control the mechanical stability and structural properties of their shells.

Author contributions

Z. R. and A. M. initiated the project and designed all the experiments. F. K. E. and K. J. M. contributed to the design of

the PIV measurements. A. M. and K. K. performed the experiments on drop deformation and contributed to data analysis and presentation. A. M., K. K., F. K. E., and K. J. M. performed the experiments on tracing EHD flows and contributed to data analysis and presentation. Z. R. and K. K. conducted the experiments on particle manipulation and contributed to data analysis and presentation. All authors took part in discussions on the finalization of the manuscript. A. M. and Z. R. authored the paper. A. M. administered the submission and the review process.

Conflicts of interest

There are no conflicts of interest to declare.

Acknowledgements

A. M. acknowledges financial support from the European Union's Horizon 2020 research and innovation framework programme under the M. Skłodowska-Curie grant agreement no. 752896. Z. R. and K. K. were supported by the Polish National Science Centre through OPUS programme (2015/19/B/ST3/03055). The contributions from K. J. M. and F. K. E. were supported by the Research Council of Norway through its Centres of Excellence funding scheme, project number 262644 (PoreLab). The authors thank Prof. Eirik Grude Flekkøy and Prof. Tomasz Hornowski for a careful reading of the manuscript and useful feedback.

References

- 1 A. Maestro, E. Santini, D. Zabiegaj, S. Llamas, F. Ravera, L. Liggieri, F. Ortega, R. G. Rubio and E. Guzman, *Adv. Condens. Matter Phys.*, 2015, 17.
- 2 T. Bollhorst, K. Rezwan and M. Maas, *Chem. Soc. Rev.*, 2017, **46**, 2091–2126.
- 3 R. Urbas, R. Milošević, N. Kašiković, Ž. Pavlović and U. S. Elesini, *Iran. Polym. J.*, 2017, **26**, 541–561.
- 4 T. Brugarolas, F. Tu and D. Lee, *Soft Matter*, 2013, **9**, 9046–9058.
- 5 E. Dickinson, *Curr. Opin. Colloid Interface Sci.*, 2010, **15**, 40–49.
- 6 B. Peng, L. Zhang, J. Luo, P. Wang, B. Ding, M. Zeng and Z. Cheng, *RSC Adv.*, 2017, **7**, 32246–32254.
- 7 S. Drexler, J. Faria, M. P. Ruiz, J. H. Harwell and D. E. Resasco, *Energy Fuels*, 2012, **26**, 2231–2241.
- 8 M. H. Asfour, H. Elmotasem, D. M. Mostafa and A. A. Salama, *Int. J. Pharm.*, 2017, **534**, 325–338.
- 9 N. G. Vilkoova and A. V. Nushtaeva, *Mendeleev Commun.*, 2013, **23**, 155–156.
- 10 W. T. M. Irvine, V. Vitelli and P. M. Chaikin, *Nature*, 2010, **468**, 947–951.
- 11 V. N. Manoharan, *Science*, 2015, **349**, 942.
- 12 F. Sicard and A. Striolo, *Nanoscale*, 2017, **9**, 8567–8572.
- 13 J. Hegemann, S. Knoche, S. Egger, M. Kott, S. Demand, A. Unverfehrt, H. Rehage and J. Kierfeld, *J. Colloid Interface Sci.*, 2018, **513**, 549–565.



- 14 Z. Rozynek, M. Kaczmarek-Klinowska and A. Magdziarz, *Materials*, 2016, **9**, 679.
- 15 E. Amah, K. Shah, I. Fischer and P. Singh, *Soft Matter*, 2016, **12**, 1663–1673.
- 16 R. Ettelaie and S. V. Lishchuk, *Soft Matter*, 2015, **11**, 4251–4265.
- 17 V. O. Ikem, A. Menner, T. S. Horozov and A. Bismarck, *Adv. Mater.*, 2010, **22**, 3588.
- 18 Z. Rozynek and A. Józefczak, *Eur. Phys. J. B*, 2016, **225**, 741–756.
- 19 Z. Rozynek, A. Mikkelsen, P. Dommersnes and J. O. Fossum, *Nat. Commun.*, 2014, **5**, 3945.
- 20 P. Dommersnes, Z. Rozynek, A. Mikkelsen, R. Castberg, K. Kjerstad, K. Hersvik and J. O. Fossum, *Nat. Commun.*, 2013, **4**, 2066.
- 21 S. Y. Tan, R. F. Tabor, L. Ong, G. W. Stevens and R. R. Dagastine, *Soft Matter*, 2012, **8**, 3112–3121.
- 22 J. K. Ferri, P. Carl, N. Gorevski, T. P. Russell, Q. Wang, A. Boker and A. Fery, *Soft Matter*, 2008, **4**, 2259–2266.
- 23 M. K. Mulligan and J. P. Rothstein, *Langmuir*, 2011, **27**, 9760–9768.
- 24 S. She, C. Xu, X. Yin, W. Tong and C. Gao, *Langmuir*, 2012, **28**, 5010–5016.
- 25 D. F. do Nascimento, J. A. Avendano, A. Mehl, M. J. B. Moura, M. S. Carvalho and W. J. Duncanson, *Sci. Rep.*, 2017, **7**, 11898.
- 26 L. Bécu and L. Benyahia, *Langmuir*, 2009, **25**, 6678–6682.
- 27 I. Koleva and H. Rehage, *Soft Matter*, 2012, **8**, 3681–3693.
- 28 J. W. Ha and S. M. Yang, *Phys. Fluids*, 2000, **12**, 1671–1684.
- 29 M. Ouriemi and P. M. Vlahovska, *J. Fluid Mech.*, 2014, **751**, 106–120.
- 30 R. B. Karyappa, S. D. Deshmukh and R. M. Thaokar, *Phys. Fluids*, 2014, **26**, 122108.
- 31 M. Ouriemi and P. M. Vlahovska, *Langmuir*, 2015, **31**, 6298–6305.
- 32 A. Mikkelsen, P. Dommersnes, Z. Rozynek, A. Gholamipour-Shirazi, M. d. S. Carvalho and J. O. Fossum, *Materials*, 2017, **10**, 436.
- 33 C. Huang, Z. Sun, M. Cui, F. Liu, B. A. Helms and T. P. Russell, *Adv. Mater.*, 2016, **28**, 6612–6618.
- 34 M. Alghane, Y. Q. Fu, B. X. Chen, Y. Li, M. P. Y. Desmulliez and A. J. Walton, *Jpn. J. Appl. Phys.*, 2011, **109**, 114901.
- 35 Q. Xie, G. B. Davies and J. Harting, *ACS Nano*, 2017, **11**, 11232–11239.
- 36 M. Li and D. Li, *J. Nanopart. Res.*, 2016, **18**, 120.
- 37 Z. Rozynek, P. Dommersnes, A. Mikkelsen, L. Michels and J. O. Fossum, *Eur. Phys. J.-Spec. Top.*, 2014, **223**, 1859–1867.
- 38 Z. Rozynek, R. Bielas and A. Józefczak, *Soft Matter*, 2018, DOI: 10.1039/C8SM00671G.
- 39 P. Sheng and W. Wen, *Annu. Rev. Fluid Mech.*, 2012, **44**, 143–174.
- 40 E. Amah, K. Shah, I. Fischer and P. Singh, *Soft Matter*, 2016, **12**, 1663–1673.
- 41 S. Nudurupati, M. Janjua, N. Aubry and P. Singh, *Electrophoresis*, 2008, **29**, 1164–1172.
- 42 S. Nudurupati, M. Janjua, P. Singh and N. Aubry, *Soft Matter*, 2010, **6**, 1157–1169.
- 43 G. Taylor, *Philos. Trans. R. Soc., A*, 1966, **291**, 159–166.
- 44 P. F. Salipante and P. M. Vlahovska, *Phys. Fluids*, 2010, **22**, 112110.
- 45 D. Das and D. Saintillan, *J. Fluid Mech.*, 2017, **829**, 127–152.
- 46 P. Dommersnes, A. Mikkelsen and J. O. Fossum, *Eur. Phys. J.-Spec. Top.*, 2016, **225**, 699–706.
- 47 Rahul B. Karyappa, Shivraj D. Deshmukh and Rochish M. Thaokar, *J. Fluid Mech.*, 2014, **754**, 550–589.
- 48 R. B. Karyappa, S. D. Deshmukh and R. M. Thaokar, *Phys. Fluids*, 2014, **26**, 122108.
- 49 A. Mikkelsen, Z. Rozynek, K. Khobaib, P. Dommersnes and J. O. Fossum, *Colloids Surf., A*, 2017, **532**, 252–256.
- 50 M. Ouriemi and P. M. Vlahovska, *J. Fluid Mech.*, 2014, **751**, 106–120.
- 51 A. Mikkelsen, P. Dommersnes and J. O. Fossum, *Rev. Cubana Fis.*, 2016, **33**, 47–49.
- 52 M. M. Cui, T. Emrick and T. P. Russell, *Science*, 2013, **342**, 460–463.
- 53 M. Ouriemi and P. M. Vlahovska, *Langmuir*, 2015, **31**, 6298–6305.
- 54 A. Mikkelsen, J. Wojciechowski, M. Rajňák, J. Kurimský, K. Khobaib, A. Kertmen and Z. Rozynek, *Materials*, 2017, **10**, 329.
- 55 W. Thielicke and E. Stamhuis, *J. Open Res. Software*, 2014, **2**, e30.
- 56 N. Estrada, *Phys. Rev. E*, 2016, **94**, 062903.
- 57 A. Lazarus, H. C. B. Florijn and P. M. Reis, *Phys. Rev. Lett.*, 2012, **109**, 144301.
- 58 J. A. Lanauze, L. M. Walker and A. S. Khair, *J. Fluid Mech.*, 2015, **774**, 245–266.
- 59 D. Vella, P. Aussillous and L. Mahadevan, *Europhys. Lett.*, 2004, **68**, 212–218.
- 60 P. Erni, H. A. Jerri, K. Wong and A. Parker, *Soft Matter*, 2012, **8**, 6958–6967.
- 61 R. Allan and S. Mason, *Proc. R. Soc. London, Ser. A*, 1962, **267**, 45–61.
- 62 W. B. Smythe, *Static and dynamic electricity*, Hemisphere Publishing, 79 Madison Avenue, New York, NY10016, USA, 1988.
- 63 L. C. Davis, *Jpn. J. Appl. Phys.*, 1992, **72**, 1334–1340.
- 64 S. Nudurupati, M. Janjua, P. Singh and N. Aubry, *ASME Dyn. Syst. Control Conf., Proc.*, 2009, **10**, 159–167.
- 65 X.-D. Pan and G. H. McKinley, *J. Colloid Interface Sci.*, 1997, **195**, 101–113.
- 66 S. Torza, R. Cox and S. Mason, *Philos. Trans. R. Soc., A*, 1971, **269**, 295–319.
- 67 S. Lishchuk and I. Halliday, *Phys. Rev. E: Stat., Nonlinear, Soft Matter Phys.*, 2009, **80**, 016306.
- 68 Zion-Research, Microencapsulation Market for Pharmaceuticals, Household Products, Agrochemicals, Food Additives and Other Applications: Global Industry Perspective, Comprehensive Analysis, Size, Share, Growth, Segment, Trends and Forecast, 2014–2020, Market Research Store, 2016.



Electronic Supplementary Material for

Particle-covered drops in electric fields: Drop deformation and surface particle organization

A. Mikkelsen,^{a†} K. Khobaib,^{a†} F. K. Eriksen,^b K. J. Måløy^b and Z. Rozynek^{a†}

^a Faculty of Physics, Adam Mickiewicz University, Umultowska 85, 61-614 Poznań, Poland. *E-mail: alexam@amu.edu.pl; Tel: +48 608 179 539

^b PoreLab, The Njord Centre, Department of Physics, University of Oslo, P.O. Box 1048, Blindern, N 0316, Oslo, Norway.

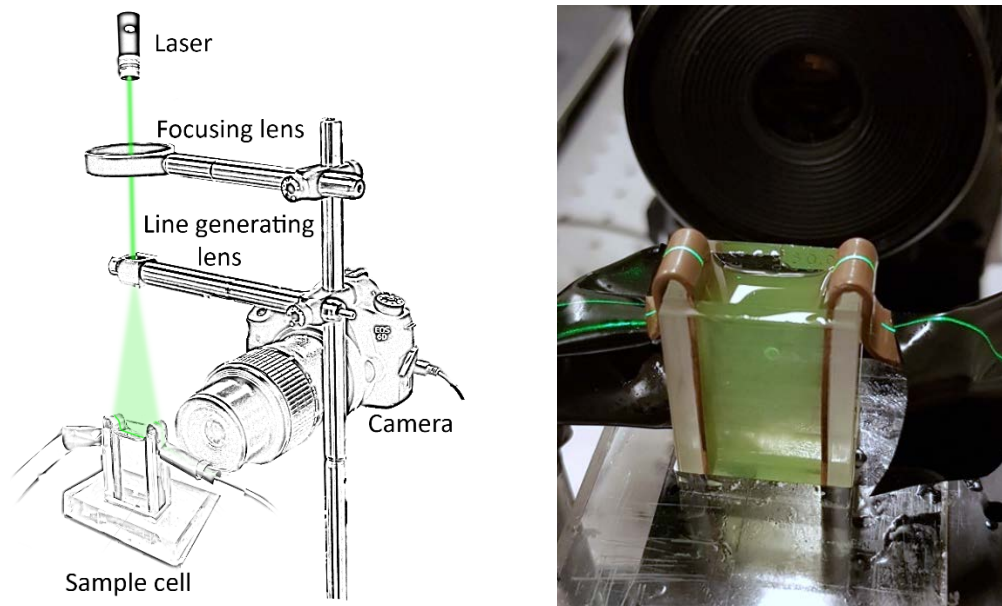


Fig. S1 (a) A schematic illustration and (b) a picture of the set-up used for estimating the electrohydrodynamic (EHD) flow velocities. EHD flowlines around drops were traced using particle image velocimetry (PIV). Fluorescent polyethylene particles (UVPMS-BY2-1.00, with average size of $35\ \mu\text{m}$, purchased from Cospheric LLC) were dispersed in castor oil (0.3% by weight) and poured in the sample cell. A $500\ \mu\text{m}$ thin sheet of particles were selected by focusing $532\ \text{nm}$ laser light (COM-09906-5mW laser, purchased from SparkFun Electronics) from above the sample cell through a laser line generator lens. During the experiments, the laser sheet was always aligned in the middle of the drop (which was positioned in the middle of the sample cell) and oriented along the electric field direction, and perpendicular to the view direction of the microscope.

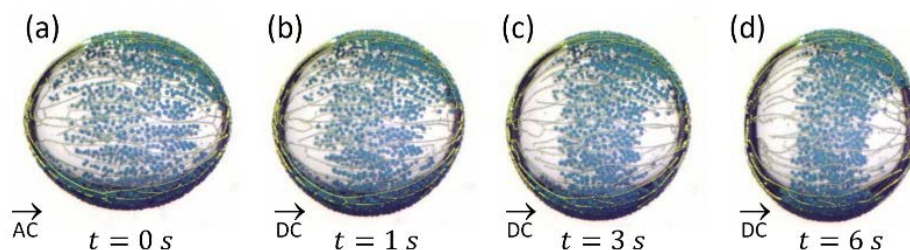


Fig. S2 Manipulation of particles by switching the electric field frequency from (a) $200\ \text{Hz}$ to (b-d) $0\ \text{Hz}$. Silicone oil drop covered by a mix of $15\ \mu\text{m}$ Ag-coated spheres and $50\ \mu\text{m}$ polyethylene (PE) particles. Blue PE particles are here used to qualitatively observe the presence or absence of EHD flows. (a) At AC fields, the PE particles do not move towards the drop electric equator, are loosely packed, and confined by the structured conductive particles. This is a direct confirmation that the EHD flows are completely suppressed at an electric field frequency of $200\ \text{Hz}$. (b-d) As the electric field frequency is switched back to $0\ \text{Hz}$, the induced EHD liquid flows convect the PE particles towards the electric equator of the drop.

Paper IV

Opening and closing of particle shells on droplets via electric fields
and its applications

Z Rozynek, K Khobaib and A Mikkelsen

ACS Appl. Mater. Interfaces **11**, 22840–22850 (2019)

Opening and Closing of Particle Shells on Droplets via Electric Fields and Its Applications

Zbigniew Rozynek,^{*,§,†} Khobaib Khobaib,[§] and Alexander Mikkelsen[§]

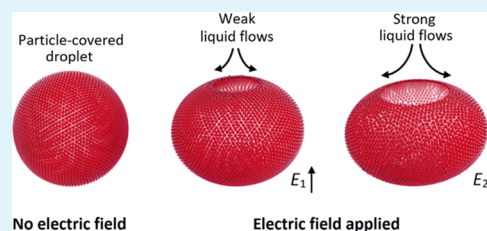
[§]Faculty of Physics, Adam Mickiewicz University, Uniwersytetu Poznańskiego 2, Poznań 61-614, Poland

[†]Harvard John A. Paulson School of Engineering and Applied Sciences, Harvard University, Cambridge, Massachusetts 02138, United States

Supporting Information

ABSTRACT: Active, tunable, and reversible opening and closing of particle shells on droplets may facilitate chemical reactions in droplets and enable various small-scale laboratory operations, including online detection, measurement, and adjustment of droplet liquid. Manipulating various types of particle shells in a controlled manner requires new routes. This work provides a new strategy for controlling the spatial arrangement of particle-covered oil droplets using electric fields that expands the application of responsive droplets beyond the abovementioned examples. The behavior of stimulated particle-covered droplets is exploited in multiple ways: to form an active smart device, fabricate Janus and patchy shells, create an online diagnostic tool, and produce a tool for fundamental studies. Electric fields are used here to manipulate particle films on oil droplets through the synergetic action of droplet deformation and electrohydrodynamic liquid flows. First, the effects of electric field strength and liquid viscosity on droplet deformation, surface particle arrangements, and dynamics are examined in detail. Then three examples of applications of responsive particle-covered droplets are demonstrated. Our results show that the reversible opening and closing of the droplet's shells, composed of various types of particles, can be conveniently achieved through electric fields, opening up a new possibility for applications in optics, clinical diagnostics, microfluidics, and material engineering.

KEYWORDS: particle film, responsive droplets, liquid–liquid interface, curved interface, assembly, electric field, smart structure



1. INTRODUCTION

Responsive materials are designed materials that have one or more properties that can be changed in a controlled fashion by external stimuli, for example, mechanical stress,¹ electric or magnetic fields,^{2–4} and changes in pH,^{5,6} temperature,⁷ or light intensity.⁸ These materials play an increasing role in our modern society and have been widely researched. This is because such materials may compose structures or devices that exhibit “smart” behavior, that is, shape changing,⁹ self-healing,^{10–12} self-sensing, self-diagnostic,^{13–15} and self-actuating.¹⁶ Many commercially available products have responsive materials to provide a smart response, such as switchable windows,¹⁷ battery power indicators,¹⁸ wound dressing,¹⁹ eyeglass frames,²⁰ and stent grafts.²¹ Responsive materials can also be used to perform various laboratory operations^{22–24} or manufacture new materials, for example, through additive manufacturing²⁵ or field-driven assembly.^{26–28} In this work, we created a responsive material of soft matter—an emulsion droplet covered with microparticles—and stimulated it by an electric field to form an active smart structure, facilitate simple laboratory operations, and manufacture new materials.

Particle-covered droplets are responsive materials with various functionalities controlled by external stimuli. Applications of these materials include self-healing,²⁹ mechanical strain detection,³⁰ or targeted drug delivery.³¹ Particle-covered droplets can be stimulated with electric or magnetic fields.

Such field-responsive droplets have proven to be convenient for controlling flows in microfluidic channels,^{32,33} producing hetero- and homogeneous particle shells,^{34,35} increasing the efficiency of Pickering emulsion fabrication,³⁶ droplet actuation,^{37,38} and manipulating particles at droplet interfaces.^{39,40} Here, we use electric fields to simultaneously change the shape of the droplet and control the spatial arrangement of particles at the droplet interface. Doing this forms an opening in the particle shell with an easily controllable size. This remarkable ability of particle-covered droplets to be reversibly opened and closed under the action of an electric field is here exploited in multiple ways: to form a miniaturized optical diaphragm with an adjustable aperture, to buckle armored droplets and fabricate droplets with Janus and patchy shells by manipulating droplet liquid, as an online diagnostic tool for the detection of inner liquid, and as a tool in fundamental studies, for example, in the study of the mechanical properties of thin particle films.

The opening and closing of particle shells on droplets have been studied by several researchers. Zhao et al.⁴¹ used magnetic force to pull a magnetic particle layer toward a magnet to open the particle shell and unarmor the droplet.

Received: March 23, 2019

Accepted: May 30, 2019

Published: May 30, 2019

This phenomenon was later used in miniature chemical reactors⁴² to promote the coalescence of otherwise stable and protected droplets and for the online detection and measurements of liquid marbles.⁴³ Zang et al.⁴⁴ demonstrated similar handling of particle shell coating. They used ultrasound to levitate particle-covered water droplets and to form a cavity on the particle shells. Our novel route for opening and closing particle-covered droplets is distinctively different. It works for droplets covered with various types of resistive (electrically weakly conductive) nano- or microparticles either magnetic or non-ferromagnetic (including most polymeric and ceramic particles, clay mineral particles, and silica particles), although droplets covered with more conductive particles (e.g., silver microparticles) subjected to an electric field acquire a dipole moment, which is in the opposite direction to the electric field. Thus, the droplet stretches along the electric field direction, and the electrohydrodynamic (EHD) flows cannot be induced as the electric poles of the droplet are electrically short-circuited.³⁹ The method can be straightforwardly implemented, for example, in microfluidic chips or microelectromechanical systems (MEMS). Unlike the otherwise elegant ultrasonic approach,⁴⁴ our electric approach can also be readily scaled up without requiring a complex experimental setup.

Our method for particle film manipulation involves the synergetic action of droplet deformation (induced by electric stress) and EHD liquid flows (see Figure 1).⁴⁵ When a silicone

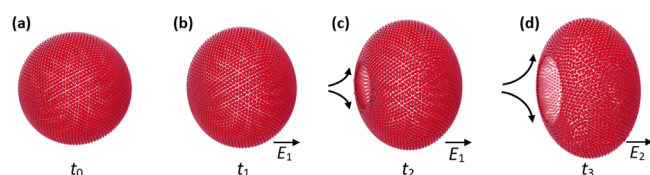


Figure 1. Schematics of particle shell opening. A droplet with the surface particles is viewed at a 30° angle with respect to the electric field direction, which is horizontal. Application of an electric field to (a) the initially spherical droplet densely covered with particles results in (b) its deformation due to the electric stress. (c) The induced EHD flows convect particles away from the droplet's electric pole, thereby forming an opening in the particle layer. (d) After application of a stronger electric field, the droplet deforms more, allowing the opening to grow in size and the EHD flows to strengthen, which is indicated by the longer curved arrows.

oil droplet with particles is suspended in castor oil and subjected to a uniform dc electric field, free charges (ionic impurities in oils) accumulate at the droplet's interface. Such a droplet acquires a dipole moment that leads to its deformation. Depending on the electrical properties of the oils and particles, the droplet can obtain either an oblate or a prolate shape.³⁹ With the particles used in this study, the particle-covered droplets compress along the electric field's direction to form an oblate shape. The magnitude of the droplet deformation primarily depends on the electric field strength. In addition to droplet deformation, EHD liquid flows can be induced at the droplet's surface. However, for droplets fully covered with particles, the EHD liquid flows cannot be generated because the particles in the shell are jammed or too densely packed.³⁹ To enable EHD flows, the particle coverage must be reduced; we achieved this by deforming the droplet and increasing the droplet's surface area. The induced EHD flows convect surface particles away from the droplet's electric pole, thereby forming an opening in the particle layer.

The first part of this paper presents how electric field strength influences the steady-state magnitude of the droplet's deformation, as well as particle arrangements on droplet interfaces. We quantified droplet deformation and the opening area at the droplet's electric pole as a function of the electric field strength. Our applications of the knowledge gained from these fundamental studies are presented in the second part of the manuscript.

2. MATERIALS AND METHODS

2.1. Experimental Setup. A schematic illustration of the setup used for the fundamental studies is shown in Figure 2a. The setup consisted of a sample cell (10 mm × 10 mm × 30 mm) placed on a mechanical xyz translational stage, a signal generator (SDG1025, SIGLENT Technologies), a high-voltage bipolar amplifier (10HVA24-BP1, HVP High Voltage Products GmbH), two digital microscopes (AM7115MZTL, Dino-Lite) for front and side viewing (perpendicular and parallel to the electric field direction), and a PC for recording movies and images. The sample cell was made of glass, with two of the inside walls coated with a conductive indium tin oxide (ITO) layer, constituting electrodes. From the voltage amplifier, a high-voltage signal was provided to the sample cell via two crocodile clips attached to the ITO-coated glass electrodes (as presented in Figure 2b). On the inside of one of the ITO-coated glass walls, we glued an O-ring (with outer diameter of ~4 mm, inner diameter of ~2.5 mm, and thickness of ~1 mm) in the center. The experimental setup was used in experiments presented in Figures 2c,d, 5a, 6, and 8 and Figures S2 and S6. In other experiments, we used a sample cell made of glass walls with only one wall (bottom) coated with conductive ITO. For the experiments presented in Figure 5b–e, we used a plate electrode, whereas for the experiment in which we demonstrated the use of electric fields in diagnostics of particle-covered droplets, we used a rod-shaped electrode (Figure 7, Figures S4 and S5). Both the plate electrode and the rod-shaped electrode were inserted from above and immersed in castor oil.

2.2. Materials. Silicone oil (VWR Chemicals, Rhodorsil 6678.1000, electrical conductivity ~5 pS·m⁻¹, relative permittivity ~2.8, density ~0.96 g·cm⁻³, and viscosity ~50 mPa·s, all measured at 25 °C) droplets were formed in castor oil (Sigma-Aldrich 83912, electrical conductivity ~60 pS·m⁻¹, relative permittivity ~4.7, density ~0.96 g·cm⁻³, and viscosity ~750 mPa·s, all measured at 25 °C). The interfacial tension between the two oils was around 4.5 mN·m⁻¹.⁴⁶ The droplets were covered with spherical nanoparticles or microparticles: silica, dyed polyethylene, and paramagnetic particles purchased from Cospheric, USA (SiO2MS-2.0, size ~250 nm, density ~2 g·cm⁻³; GPMS-0.98, size ~20 μm; REDPMS-0.98, size ~50 μm; GPMS-0.98, size ~90 μm; each particle type had density ~0.98 g·cm⁻³; BKPMS-1.2, size ~50 μm; density ~1.2 g·cm⁻³); Li-fluorohectorite clay particles from Corning Inc., USA (size 1–30 μm; density ~2.8 g·cm⁻³); and Laponite clay particles from Laponite Inc., USA (size 0.5–10 μm; density ~2.5 g·cm⁻³). The three-phase contact angle of PE particles at the silicone oil droplet–castor oil interface was 65 ± 5°, referenced against castor oil, which indicates that the PE particles had slightly higher affinity toward silicone oil. Unlike silica nanoparticles (a few orders of magnitude smaller than PE with a measured contact angle of 20 ± 7°), the PE microparticles bound strongly to the silicone oil–castor oil interface. Therefore, they did not detach from the droplet's surface when subjected to EHD liquid flows during the experiments.

2.3. Preparation of Particle-Covered Droplets. Particle-covered silicone oil droplets were made in castor oil. Initially, we filled a sample cell with castor oil. Next, we prepared dispersions by adding particles (particle concentrations are listed in Table S1) to silicone oil and mixed them by vigorous hand shaking (several seconds) followed by an ultrasonic bath treatment for 5 min. We then formed a dispersion droplet in castor oil using a regular mechanical pipette. When the droplet was made in castor oil, the majority of the particles were located inside the droplet. The particles could be brought to the droplet's surface via mechanical stirring and droplet

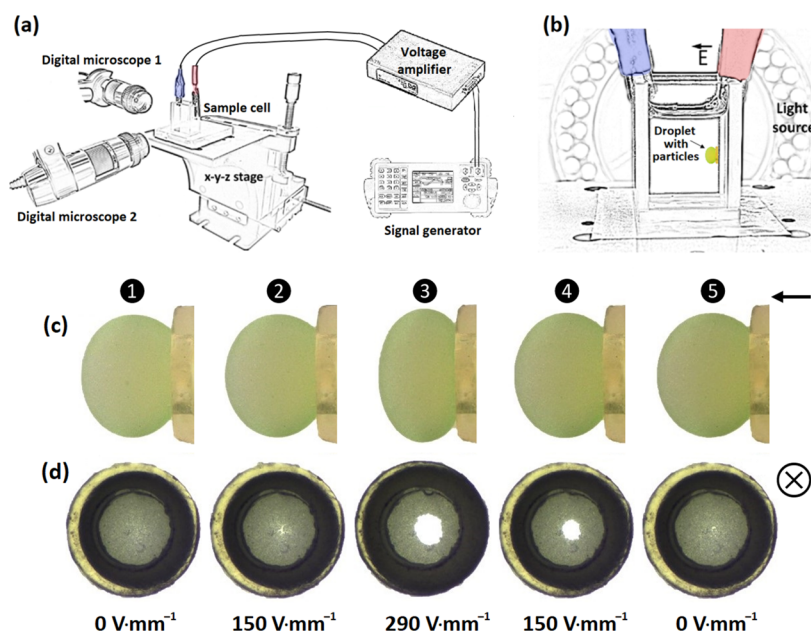


Figure 2. (a) Schematic illustration of the setup used for the fundamental studies. The setup consisted of a sample cell placed on a mechanical xyz translational stage, two digital microscopes for front and side viewing, a signal generator, and a voltage amplifier for generating a high-voltage dc electric signal, which was provided to the cell via two crocodile clips. (b) The sample cell was made of glass, with two of the walls coated with electrically conductive ITO layers. The transparent ITO-covered glass electrodes allowed for observation in a direction along the electric field. Droplets with or without particles were docked in an O-ring that was fastened to one of the conductive walls of the sample cell. The electric field direction is indicated by the arrow. Silicone oil droplet (~ 3 mm) covered with PE particles (~ 20 μm) viewed (c) perpendicular and (d) parallel to the electric field direction. The droplet was surrounded with castor oil and docked in an O-ring that was fastened to one of the electrodes. In the presence of a dc electric field, the electric stress deformed the droplet. As a result, the droplet's surface area increased, allowing particles to unjam and EHD flows to arise. The EHD flows conveyed particles away from the droplet's electric pole, forming a particle-free area. See also the corresponding [Movie S2](#). The symbols indicate the direction of the electric field.

deformation, through particle sedimentation, or with the use of external fields.^{47–49} Here, we used direct current (dc) electric fields to enhance the transportation of particles toward the surface (for more details, see our previous work⁴⁶). In fact, the utilization of electric fields went beyond the mere role of bringing particles to the surface of a droplet—the convective electrohydrodynamic liquid flows enabled the formation of a monolayer film composed of densely packed particles arranged in a nearly hexagonal geometry (see [Figure S1](#)). [Movie S1](#) presents the entire process of forming a droplet covered with densely packed particles.

As mentioned before, in some experiments, particle-covered droplets were docked in an O-ring that was fastened to one of the glass electrodes (see [Figure 2b](#)). The main reason for using this setup was to keep the droplet in one place and to facilitate experimental observations. Additionally, the setup enabled observation (in the direction along the electric field) of the surface particle arrangement by keeping one region of the droplet particle-free throughout the entire experiment. Particle-covered droplets were docked in the O-ring through the following steps: First, we attached a pure silicone oil droplet (~ 2.5 mm) to the O-ring so that nearly half of the droplet was inside the O-ring. We then brought a silicone oil droplet covered with PE particles (particle coverage of $\sim 75\%$ of the droplet's surface area) in close proximity to the pure silicone oil droplet. When a dc electric field was applied, the droplets electrocoalesced. The resulting coalesced droplet was entirely covered with particles on the side in contact with the castor oil, and there were no particles on the droplet's surface inside the O-ring. Such droplets were then studied in electric fields. In other experiments ([Figures 5b–e](#), [7](#)), the particle-covered droplets (with a particle coverage of $\sim 80\%$) were placed on the bottom of the sample cell.

2.4. Particle Image Velocimetry Experiments. The liquid flow fields formed around a droplet through the application of electric fields were studied through particle image velocimetry (PIV) experiments. PE particles (~ 20 μm) were added to the castor oil

and used to trace EHD flows around a droplet covered with red PE particles (~ 50 μm). A movie of the particle movement was recorded from a view perpendicular to the electric field direction. From the movie, an image was saved for each second. The frames were then compared and analyzed using PIVlab (v. 1.41, MATLAB toolbox), which yielded flow velocities for each interrogation area (the images were split into a number of interrogation areas of 64×64 pixels, which were then individually cross-correlated with the previous image to obtain displacement vectors). We then used MATLAB (v. R2017b, Math Works) to plot the flow velocities and Adobe Photoshop (v. 19.0, Adobe Systems) to edit the PIV image.

2.5. Experiments Demonstrating Possible Applications.

Using silicone oil droplets covered with PE particles, we demonstrated that a particle-covered droplet can be used as a millimeter-sized diaphragm with an adjustable aperture ([Figure 6](#)). The droplet was illuminated with laser light (class III laser pointer, wavelength 532 nm and diameter 0.5 mm) through the center of the droplet in the direction along the electric field lines. A dc electric field of strength between 0 and 260 $\text{V}\cdot\text{mm}^{-1}$ was applied to open and close the “shutter” (see [Figure S3](#) for a sketch of the setup).

In the experiment presented in [Figure S5](#), we demonstrated the possible usage of the method as a diagnostic tool. We made a conducting floor in a plastic cuvette (10 mm \times 10 mm \times 45 mm) by gluing a copper electrode to the bottom of the cuvette. Three droplets (~ 3 mm) were placed on the bottom electrode of the cuvette at equal distances. A rod-shaped electrode (stainless steel) was then placed at the center of and above one of the droplets. The distance between the rod-shaped electrode and the electrode at the bottom of the sample cell was ~ 4 mm. We used an electric field of 400 $\text{V}\cdot\text{mm}^{-1}$ to open the particle shell near the rod-shaped electrode. To show scalability of the method, we substituted the conductive rod with a flat copper electrode and placed 16 droplets of similar size (~ 2 mm) on the bottom electrode ([Figure Sd](#)). The distance between the two plate electrodes was ~ 6 mm, and the droplets were subjected to a dc

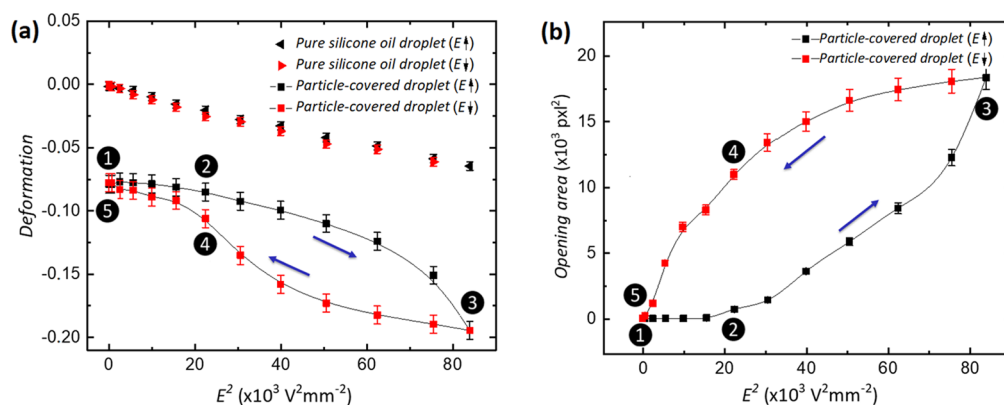


Figure 3. (a) Magnitude of steady-state deformations of a silicone oil droplet with and without PE particles plotted as a function of E^2 . (b) Opening area at the electric pole of a silicone oil droplet covered with PE particles vs E^2 . The arrows indicate whether the electric field was increased or decreased.

electric field ($\sim 325 \text{ V}\cdot\text{mm}^{-1}$). To observe the dynamics of all the droplets, we set the camera at an angle ($\sim 30^\circ$) and recorded movies.

3. RESULTS AND DISCUSSION

The central idea of the method presented here is combining the electrodeformation of particle-covered droplets with particle assembly facilitated by EHD flows, as illustrated in Figure 1. Initially, the interfacial particles are densely packed, jammed, and arranged in slightly disordered hexagons (Figure 1a). To initiate an opening in the particle shell, an electric field is applied. The electric stress deforms the droplet (Figure 1b), thereby increasing the droplet's surface area and decreasing particle coverage. The particles are then temporarily loosely arranged, and the EHD flows are induced. These flows convect particles away from the droplet's electric pole, thereby forming an opening in the particle layer. The convected particles are packed densely within the particle shell (Figure 1c). When the electric field strength is increased, the droplet deforms more, allowing the opening to grow in size and the EHD flows to strengthen (Figure 1d). This opening in the shell can be completely healed by decreasing the electric field strength. This process is reversible as long as the particles do not detach from the droplet's surface, for example, by applying a strong electric field.

3.1. Opening and Closing of the Particle Shell: Experimental Realization. To realize this opening-closing approach in the experiment, we designed the experimental setup (Figure 2a,b) and employed a silicone oil droplet ($\sim 3 \text{ mm}$) covered with polyethylene (PE) particles ($\sim 20 \mu\text{m}$). The droplet was surrounded with castor oil and docked in an O-ring that was fastened to an electrode. The main reason for using the O-ring was to ease the experimental observations. In the absence of an electric field, the droplet covered with PE particles was slightly aspherical (see Figure 2c). The droplet's asphericity indicates that, initially, the shell was composed of jammed particles. The droplet was then subjected to an electric field. We increased the electric field strength stepwise from 0 to $290 \text{ V}\cdot\text{mm}^{-1}$ and then decreased it stepwise to $0 \text{ V}\cdot\text{mm}^{-1}$ (see also the corresponding Movie S2). At each step, the electric field strength was maintained until a steady state (droplet deformation and/or particle arrangement) was observed.

Each time we increased the electric field strength, the magnitude of the droplet's deformation also increased. However, in weak electric fields, that is, up to $\sim 125 \text{ V}\cdot\text{mm}^{-1}$, the particle layer remained densely packed; therefore,

the EHD flows could not be induced. A previous study has reported that EHD flows induced around a droplet are greatly suppressed when the droplet is fully covered with particles.³⁹ Indeed, we could not detect any EHD flows at the droplet's surface and outside the droplet. At stronger electric fields, the droplet deformed more, and the surface area became large enough to allow the surface particles to unjam. During unjamming, the PE particle layer underwent a solid-to-liquid transition (as reported elsewhere⁵⁰), as the cohesive forces between the PE particles are very small. Now, the EHD flows onset and moved particles at the droplet's interface. In Figure S2, we show an example of the EHD flowlines around a particle-covered droplet, including the flow direction and a velocity map. The direction of the flow is determined by the electrical conductivities and dielectric properties of the fluids.^{51,52} For the system studied here, the flows guided the surface particles from the droplet's electric pole to its electric equator where the particles formed a densely packed ribbon-like structure. As a consequence, an opening area (particle-free area) developed at the droplet's electric pole, which increased in area with the applied electric field strength (Figure 2d). The particles' convection by the EHD flows is a dynamic process, and the timescale depends on several parameters, including electric field strength and liquid viscosity (described in greater detail in the next section).

In Figure 3, we present the quantitative data of the qualitative results shown in Figure 2c,d. Both the magnitude of the droplet's deformation and the opening area were plotted against the square of the applied electric field strength. The inset numbers in the plots correspond to the images presented in Figure 2. Droplet deformation is here defined as $D = (d_{\parallel} - d_{\perp}) / (d_{\parallel} + d_{\perp})$, where d_{\parallel} and d_{\perp} are the droplet axes parallel and perpendicular to the electric field direction, respectively.

The initial magnitude of deformation was around -0.08 (Figure 3a), which indicates that the droplet was in an arrested state and that the PE particle layer was jammed. We also observed that the droplet deformation was nonlinear to E^2 ; that is, the droplet deformation increased progressively with the electric field. That is because it cost less energy to deform a droplet more. Changes in the droplet's surface area were quantified by measuring the opening area in the region at the droplet's electric pole (Figure 3b).

Interestingly, both the deformation magnitude of the particle-covered droplet and the opening area exhibited hysteresis—that is, although the droplet eventually acquired

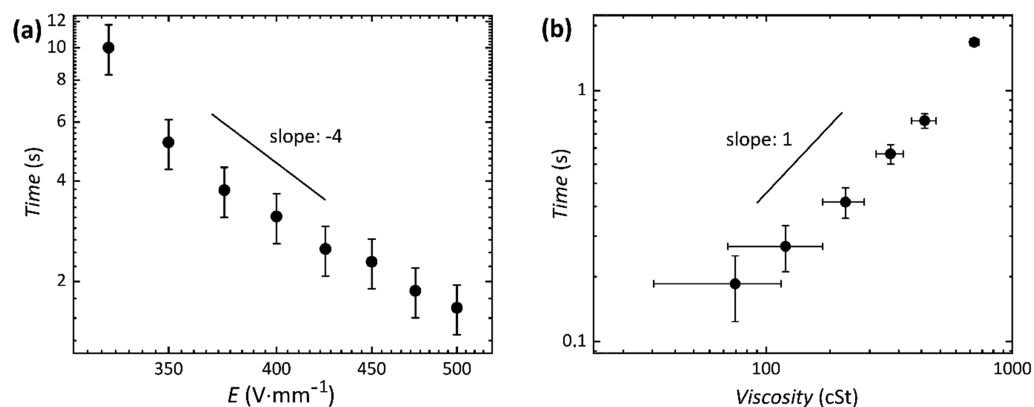


Figure 4. (a) Log–log plot of the time required to obtain an opening area A_{c1} (of around 55000 square pixels) at a silicone oil droplet (~ 3.2 mm) covered with PE particles (~ 20 μm) as a function of the applied electric field strength. (b) Time for the particle-free area at the droplet's pole to reach A_{c2} (of around 45000 square pixels) vs viscosity of the surrounding oil. A silicone oil droplet (~ 3.5 mm) covered with PE particles (~ 90 μm) is surrounded with castor oil and subjected to an electric field of strength 250 $\text{V}\cdot\text{mm}^{-1}$. To change the viscosity of the castor oil, the oil was heated to different temperatures. See also the corresponding [Movies S4](#) and [S5](#).

its initial state when the electric field was gradually reduced, the deformation and opening-area curves were not retraced. Because we collected the data in steady-state situations, the hysteresis loops must be time-independent, that is, not caused by a dynamic lag. By using a pure silicone oil droplet as a reference, we also ruled out any potential influence of the experimental conditions on the hysteresis loops. We subjected the pure silicone oil droplet (size of ~ 3 mm, docked in the O-ring) to the same electric field strengths and measured the droplet deformation. There was no hysteresis curve for the pure silicone oil droplets, and any differences in the deformation magnitudes (between the data points from increasing and decreasing electric fields) were within error bars (Figure 3a). We can therefore conclude that the hysteresis curves were caused neither by docking the droplets in the O-ring nor by the experimental procedures.

The deformation versus E^2 curve (Figure 3a) resembles a stress–strain hysteresis curve of a viscoelastic material in which the work done by the material in returning to its original shape is less than the work done by the deforming force. Particle monolayers at liquid interfaces have elastic, as well as granular, character.⁵³ We therefore expect viscous dissipations in our system through particle rearrangements when the droplet is compressed and the particle layer reassembles through EHD convective flows. This is actually observed in the experiment presented in [Movie S3](#). As was demonstrated by Mikkelsen et al.,⁵⁴ Vella et al.,⁵⁵ and Jambon-Puillet et al.,⁵⁶ particles forming a monolayer film have solid-like properties with elasticity given by the surface tension of the liquid–air interface (or interfacial tension between liquids)⁵⁷ and/or the capillary interactions between particles.⁵⁸ Even though the strength of the interaction between PE particles is very low and the particle shell is only slightly cohesive, it cost energy to disintegrate the particles and obtain a small opening. Rane and co-authors⁵⁹ studied the emergence of shape hysteresis of liquid marbles under compressive deformation. They concluded that the origin of the hysteresis can be a confluence of particle interlocking (cohesive interactions between particles), particle impregnation into the liquid surface, and restructuring in the particle shell, as we noted above. However, to draw the definitive conclusion, we suggest further experimental and theoretical investigations.

3.2. Dynamics of Particle Layers Subjected to an Electric Field. To study the effect of the electric field on the expansion of particle layers at droplet interfaces, we subjected particle-covered droplets to a dc electric field of strength 325–500 $\text{V}\cdot\text{mm}^{-1}$. The electric field was only applied until the opening area at the droplet (A_{c1}) reached an arbitrarily defined value of ~ 55000 square pixels. A larger area for A_{c1} was not considered to prevent droplet breakup and/or particle detachment from the interface due to strong liquid shearing. Particle-covered droplets in bulk fluids have also been reported to exhibit electrorotation when subjected to strong electric fields (≥ 250 $\text{V}\cdot\text{mm}^{-1}$).⁶⁰ However, for the field strengths used in our experiments, we did not observe electrorotation. This is because the droplet was docked in an O-ring. When we increased the strength of the applied electric field, the time to open particle shells decreased (Figure 4a). For example, when an electric field of strength 325 $\text{V}\cdot\text{mm}^{-1}$ was applied, it took ~ 10 s for the opening area to reach A_{c1} . When the droplet was subjected to a field of strength 500 $\text{V}\cdot\text{mm}^{-1}$, the opening area reached A_{c1} after only ~ 2 s (see also the corresponding [Movie S4](#)). Remarkably, the rate of particle shell opening scales as E^{-4} .

We also investigated how the viscosity of the fluids affected the rate of particle shell opening. We decreased the viscosity of the fluids by heating the oils from 23 to 60 $^{\circ}\text{C}$. When the viscosity of the oils was decreased, we observed that the particles moved faster and that the opening area reached the defined threshold area A_{c2} (~ 45000 square pixels) in a shorter time. When the temperature of the oils was 23 $^{\circ}\text{C}$, it took around 2 s for the opening area to reach A_{c2} . This time was reduced to around 0.2 s when the temperature of the fluids was set to 60 $^{\circ}\text{C}$. Figure 4b shows the time required for the particle-free area at the droplet's electric pole to reach A_{c2} , plotted as a function of the viscosity of castor oil. The particles are transported away from the droplet's electric pole by being moved together with liquids. The other forces that may act on particles, for example, gravitational force or electrostatic forces (dielectrophoresis, electrophoresis), are insignificant here. Thus, the particles are moved faster at lower viscosities because the velocity of the EHD flows increases, which is inversely proportional to the viscosity of liquids. We note that the temperature increase may affect the interfacial tension and thus the three-phase contact angle. However, in our experi-

ments on particle shell opening and closing conducted at elevated temperatures, we did not observe any differences in physical behavior of the shell in comparison to the experiment performed at room temperature.

3.3. Method Capability. Our approach for opening and closing particle shells can be used for droplets covered with various types of particle materials (Figure 5). The particle

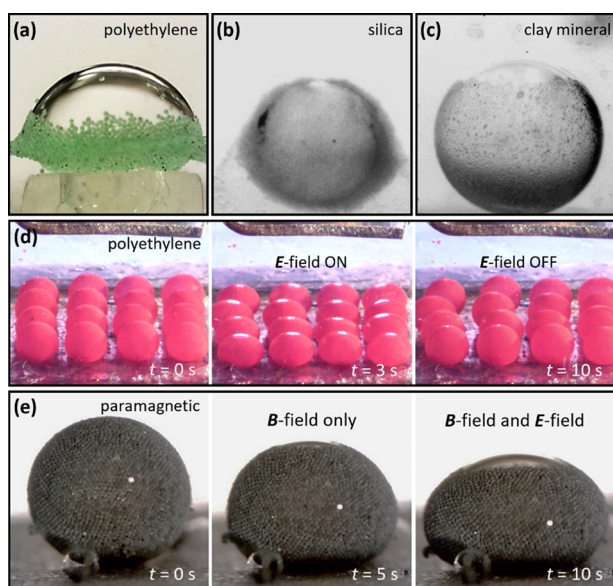


Figure 5. (a) Because PE particles are strongly bound to the droplet's interface, it is possible for the large opening in the particle shell. (b) EHD flows caused silica particles to detach from the droplet's surface, as the particles have high affinity to castor oil and do not bind strongly to the interface. (c) Opening in a weakly electrically conductive clay particle shell. (d) Sixteen droplets (~ 3 mm) placed between two flat electrodes. A dc electric field of strength $325 \text{ V}\cdot\text{mm}^{-1}$ was applied in the vertical direction. All droplets deformed and obtained similar opening areas. After the electric field was turned off, the droplets relaxed back to their initial shape and the opening in particle shells vanished. (e) Demonstration of the synergetic action of magnetic and electric fields.

shells should preferably be composed of particles strongly bound to the droplet's interface, especially if large openings are of concern. The particle binding energy to the droplet's interface is proportional to the particle surface area and the three-phase contact angle.⁶¹ We found that large PE particles ($\sim 90 \mu\text{m}$) with a high three-phase contact angle ($\sim 65^\circ$) did not detach from the surface of a silicone oil droplet even when a strong electric field ($500 \text{ V}\cdot\text{mm}^{-1}$) was applied and the particle shell crumpled through folding (Figure 5a). For such a droplet, we could open the particle shell so that nearly the entire droplet hemisphere was uncovered. This is because the particle shell folded. After the electric field was turned off, the compressed particle shell unfolded and covered the entire droplet again.

We observed a different situation for a droplet covered with small and hydrophilic silica particles ($\sim 250 \text{ nm}$). Although the silica particles did not bind well to the oil droplet's interface, we succeeded in creating a silica particle-covered droplet (Figure 5b). When the silica particle shell opened, many particles detached from the interface and resided in the castor oil. Weak particle binding is not a problem specific for our method. The magnetic field approach presented by Zhao et

al.⁴¹ also requires particles to adsorb well to the droplet's surface, and in general, strong particle binding is required for particle manipulation at liquid interfaces (particle structuring, assembly, or motion) and Pickering droplet manipulation (translation, rotation, or alignment).^{62,63} For droplets covered with polyethylene, weakly conductive clay particles (Figure 5c), and polyethylene-paramagnetic composite particles (Figure 5e), we opened particle shells without losing particles. Addition of particles to the droplet interface may change the magnitude of the interfacial tension. In our previous study,⁵⁰ we estimated the (effective) interfacial tension to change by around 40 and 10% when droplets were covered with clay mineral and polyethylene particles, respectively. This, in turn, affects the droplet's resistance to deformation,⁶⁴ although we can compensate for that by simply increasing (or decreasing) the electric field strength.

In our opening-closing experiments, we used droplets with diameters spanning from $200 \mu\text{m}$ to 5 mm . In principle, our method should also work for smaller particle-covered droplets. Droplet deformation is proportional to the droplet size and scales as E^2 . Stronger electric fields are thus required for smaller droplets to obtain the same deformation as larger droplets. From a theoretical point of view, it should be possible to manipulate particles on droplets as small as several micrometers. However, working with such small droplets imposes technical difficulties and makes the method less usable.

The electric field mechanism for manipulation of surface particles is also effective for multiple droplets. For the purpose of demonstration, we used a flat electrode to observe simultaneous rearrangements of interfacial particles on 16 droplets (Figure 5d). The droplets ($\sim 3 \text{ mm}$) were placed on the bottom electrode and subjected to a dc electric field of strength $325 \text{ V}\cdot\text{mm}^{-1}$ in the vertical direction. We observed that all droplets deformed and obtained similar opening areas at the pole of the droplets. Small differences in the opening area were caused by differences in the initial droplet shapes—that is, some of the droplets were slightly aspherical because of higher particle concentration. After 3 s, the electric field was turned off, the droplets relaxed into a spherical shape, and the particles formed jammed shells again.

Interestingly, our electric method can be coupled with the magnetic method.⁴¹ We made a droplet ($\sim 2 \text{ mm}$) covered with paramagnetic particles ($\sim 50 \mu\text{m}$) and positioned it on a metal electrode (Figure 5e). A stable opening was formed in the paramagnetic particle shell 5 s after a strong neodymium disc magnet (the intensity of the magnetic field was measured to be around 0.1 T) was placed under the electrode. However, the magnetic force alone was not sufficiently strong to create a large opening in the shell. By also applying an electric field ($250 \text{ V}\cdot\text{mm}^{-1}$), additional electric force deformed the droplet further and created a larger opening at the droplet surface. The synergetic action of magnetic and electric fields could be useful, for example, for droplet stabilization and positioning in a desired place; that is, we observed that the particle-covered droplet could be translated without any damage by simply moving the magnet under the electrode.

3.4. Applications for Controlled Opening and Closing of Particle Layers at Droplet Interfaces. When viewed along the direction of the electric field, the process shown in Figure 2d visually resembles the expansion and contraction of a human eye's pupil or an optical diaphragm. This inspired us to demonstrate the use of particle-covered droplets as a

millimeter-sized diaphragm with an adjustable aperture for controlling the light passage. As done in the previous experiments, we docked a particle-covered silicone oil droplet in an O-ring attached to one of the ITO-coated electrodes. Additionally, we illuminated the droplet with a laser light (see Figure S3). The sample cell was filled with castor oil, and the laser light was centered in the middle of the droplet. The droplet shape was nearly spherical in the absence of an electric field. Surface particles covered the entire interface of the droplet except the part inside the O-ring. As a result, very little light passed through the droplet (see the left panel of Figure 6a). When the droplet was subjected to a dc electric field of

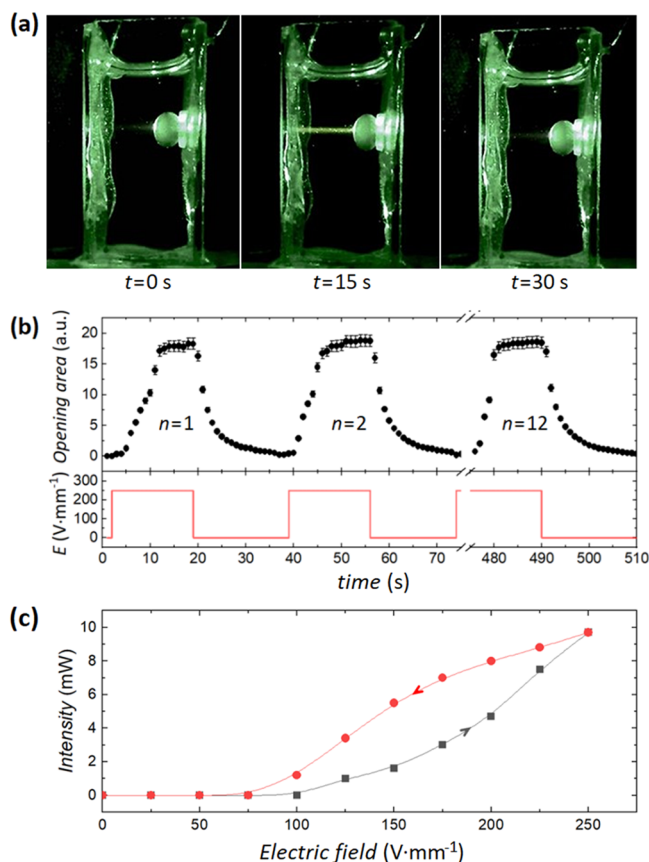


Figure 6. (a) Silicone oil droplet (~ 3.5 mm) covered with PE particles (~ 50 μm) viewed perpendicular to the electric field direction, which was horizontal. During the whole experiment, a laser light illuminated the center of the droplet. After the electric field was turned on, particles moved away from the droplet's electric pole and the laser light was able to pass through the droplet. (b) Opening area (particle-free area at the droplet's electric pole) and strength of the applied electric field as a function of time. The opening and closing process of the particle layer was repeated several times. (c) Changes in light intensity passing through a particle-covered droplet as a function of electric field strength. See also the corresponding Movie S6.

strength 250 $\text{V}\cdot\text{mm}^{-1}$, an opening in the particle film was formed at the droplet's electric pole, and the laser light could pass through the droplet (middle panel of Figure 6a). The droplet relaxed to a spherical shape after we turned off the electric field, and the particles covered the entire droplet again. Consequently, the laser light was blocked again (see also the corresponding Movie S6). We found that the opening-closing process was fully reversible and durable (Figure 6b).

Quantitative data for the light intensity as a function of electric field strength are shown in Figure 6c.

In the next experiment, we demonstrate that the method enables manipulation of droplet liquid without harming the particle shell. For this, we used a stainless-steel needle (outer diameter of 0.5 mm) that had a dual function. It worked as an electrode allowing formation of an opening in a particle shell and was used to remove/add liquid from/to a droplet. In the experiments, the needle was at a fixed dc potential of around 500 V. In Figure 7a–e, we show that the opening formed and grew in size as the electrode was lowered approaching a droplet. At such moderate voltage, it was possible to make a large enough opening to insert the needle into the droplet avoiding touching the particles. Too low electric potential was insufficient to form a large opening and too high electric tension caused the droplet to break apart (see Figure S4). As the surface of the droplet at its electric pole nearest to the needle-electrode has the electric potential as the electrode, the droplet is repelled for that electrode. The droplet deformation is balanced by the surface tension, and at some point, the electrode is able to reach the droplet's surface. This allows for adjustment of the droplet volume. We took advantage of it to form a buckled particle shell and a patchy shell. We formed a silicone oil droplet (~ 2 mm) covered with PE particles (50 μm) and placed it on a conductive bottom of the sample cell (Figure 7f). Then we applied voltage to the electrode and lowered it down to make an opening (Figure 7g) through which the needle was inserted into the droplet (Figure 7h). Next, we removed around one quarter of the initial volume of the droplet liquid (Figure 7i) and moved the electrode upward. After the electrode was removed from the droplet, we switched off the electric field. Because the surface area of the droplet decreased while the particle number stayed unchanged, the particle shell buckled and remained stable (Figure 7j). In the last decade, buckled armored droplets have been widely studied. This is because they are considered to hold promise for a variety of applications including drug delivery systems and biomimetic design of functional surfaces.^{65,66}

We made another spherical silicone oil droplet covered with PE particles (Figure 7), but this time, we added a portion of a dispersion of black dyed PE particles in silicone oil. In the same manner as before, we inserted a needle-electrode (Figure 7l) and added the dispersion (Figure 7m). Next, the electrode was lifted (Figure 7n), and the electric field was switched off. The droplet returned to the spherical shell, and particles relaxed covering the entire surface. The resulting droplet had a small patch made of black PE particles (Figure 7o). Droplets with patchy shells can be used for fabricating patchy capsules by interlocking (e.g., sintering) particles. Such structures combine the functionalities provided by permeable shells and those offered by Janus (patchy) particles. For example, due to specific interactions between their domains, patchy capsules can align and orient when subjected to external fields and self-assemble into suprastructures to produce light and hollow scaffolds.⁶⁷ When used as microcapsules, a patch can be used, for example, to anchor the capsule to the site of a target and also enable triggered release in a specific direction.³⁴ We note that the demonstrated route for formation of droplets with buckled and patchy shells is not high-throughput but it can be used for production of individual droplets with different physicochemical properties.

The method for particle shell opening and closing could be also possibly used to inspect the interior content of particle-

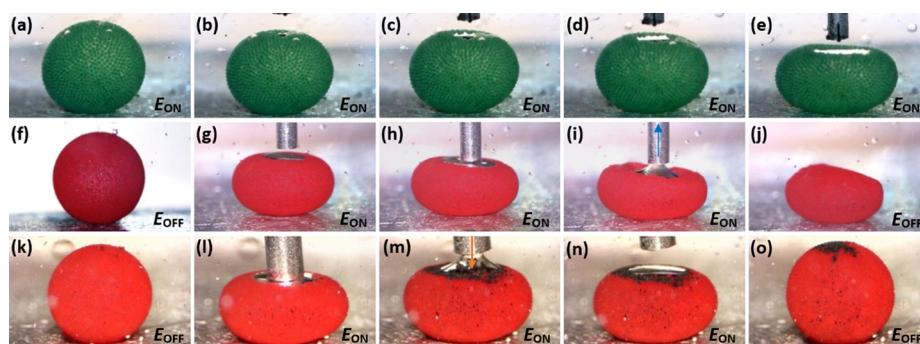


Figure 7. The method enables manipulation of droplet liquid without harming the particle shell. Three silicone oil droplets (~ 2 mm) were covered with PE particles (green ~ 100 μm , red ~ 50 μm) and placed on the conductive bottom of the sample cell. (a–e) A stainless-steel needle (outer diameter of 0.5 mm) is at an electric potential of around 500 V. The opening formed in the particle shell and grew in size as the electrode was lowered approaching the droplet. The droplet deformation is balanced by the surface tension, and at some point, the electrode is able to reach the droplet's surface. This allows for adjustment of the droplet volume and makes (f–j) a droplet with a buckled shell or (k–o) a droplet with a patchy shell by adding a small amount of dispersion of black dyed PE particles in silicone oil.

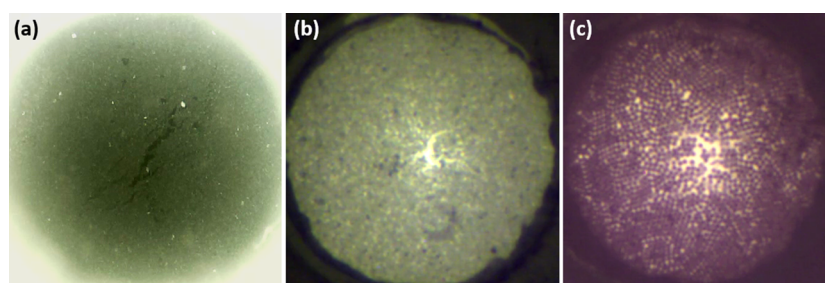


Figure 8. Opening of shells composed of particles with different cohesive forces. The droplets covered with particles were viewed along the electric field direction. (a) A particle film composed of Li-fluorohectorite clay mineral particles (size ~ 5 μm) fractures at an electric field strength of around 125 $\text{V}\cdot\text{mm}^{-1}$. (b) A similar electric field applied to a droplet covered with 20 μm PE particles resulted in formation of a small opening with short branches. (c) 50 μm PE particles separate very easily from one another, and the particle layer “liquifies”.

covered droplets, as we demonstrated in Figure S4. Such an online diagnostic method can be used, for example, in microfluidic systems, droplet-based microfluidics, or MEMS for studying the content of Pickering droplets. Zhao et al.⁴³ have recently demonstrated that online detection can be realized on magnetic liquid marbles by using magnetic fields to manipulate magnetic particles at interfaces. The authors performed electrochemical and optical measurements of a droplet through an opening in the magnetic particle shell. As presented in Section 3.3, our method works for various types of nonmagnetic particle shells and is also applicable to electrically weakly conductive particles with magnetic properties (such as demonstrated paramagnetic particles in Figure 5e).

The electric field method can also be used as a tool for fundamental studies. As an example, in Figure 8a–c, we present the study on the fracturing of particle shells on curved interfaces. We prepared three droplets covered with particle shells, each shell composed of particles with different strengths of the particle–particle cohesive interactions. After the particle-covered silicone oil droplets were docked in the O-ring, we applied an electric field (increasing its strength stepwise by 25 $\text{V}\cdot\text{mm}^{-1}$) to each droplet and observed the formation of an opening. In all cases, the observable feature on particle shells emerged at $E = 150$ $\text{V}\cdot\text{mm}^{-1}$. A particle film composed of Li-fluorohectorite clay mineral particles (size ~ 5 μm) fractured through one main crack (Figure 8a). The clay mineral particles adhered to each other strongly due to the presence of small amounts of water (in the clay) and formed a

thin two-dimensional elastic film that fractured under the load. Unlike the clay mineral particle shell, the shell made of 50 μm PE particles liquified. Because the attractive interactions between particles were weak, they separated very easily from one another forming only small aggregates (Figure 8c). It is known that the cohesive strength between particles increases with decreasing particle size. Indeed, this is what we observed experimentally—that is, the attractive interactions between 20 μm PE particles were slightly stronger than those for 50 μm PE particles. Application of an electric field for the droplet covered with 20 μm PE particles resulted in formation of a small opening with short fracturing branches (Figure 8b). When a stronger electric field was applied (>200 $\text{V}\cdot\text{mm}^{-1}$) to each of the droplets, large openings of similar size were formed with a circular shape without any fracturing features.

Nagri et al.⁶⁸ studied theoretically the deformation and failure of curved colloidal crystal shells formed on spheres. Their results highlighted the role of crystal defects in controlling mechanical stability and plastic rearrangements of the shell. Experimental realization would support the authors' findings, and the electric method demonstrated here can be used for this purpose—as a noncontact indenter—to study and understand the stability of curved colloidal or granular crystal and amorphous particle shells under load. Mechanical properties of particle layers can also be investigated through crumpling experiments, as demonstrated in Figure S6 and Movie S8.

4. CONCLUSIONS

We found that electric fields, through EHD convective flows and droplet electrodeformation, can structure particles at droplet interfaces to make an opening in particle shells formed on the droplets. The size of the opening can be actively controlled by tuning the strength of the electric field, and we have shown that it is intimately linked to the magnitude of droplet deformation. We have demonstrated that the time to open and close a particle layer on a droplet—that is, how fast EHD flows move particles at the droplet interface—depends on the applied electric field strength and the viscosity of the oils. The strong relationship between the electric field strength and the timescale for particle arrangement enables fast switching between states (from a closed to open particle shell) in just milliseconds. The possibilities to easily tailor both the size of the opening and dynamics of the opening-closing process via noninvasive electric fields make the particle-covered droplet a suitable responsive material for a wide range of applications. Indeed, we have shown that particle-covered droplets subjected to an electric field can function as a millimeter-sized diaphragm (e.g., to be incorporated into optical systems or used in robotics). The presented electric route allows manipulation of droplet liquid without harming its particle shell (for making droplets with buckled or patchy shells) or as an online diagnostic tool (e.g., for studying the content of Pickering droplets). Because the opening-closing method is easy to implement and operate, we expect it to find additional applications, for example, in microfluidic systems or MEMS. Moreover, the mechanism can also be used as a tool in fundamental research, for example, to study the mechanical properties of particle layers through crumpling experiments or to investigate fracturing of cohesive films. We envision that the presented mechanism for opening and closing particle films on oil droplets could also be used to control the colors of materials through structural manipulation (structural coloration) and to produce anisotropic functional structures, such as patchy shells and particles, or porous structures, for example, for cell-based applications.^{69,70}

■ ASSOCIATED CONTENT

Supporting Information

The Supporting Information is available free of charge on the ACS Publications website at DOI: 10.1021/acsami.9b05194.

Particle concentration in silicone oil; images of silicone oil droplet covered with PE particles, particle-covered droplet subjected to an electric field, an electrode inserted in the droplet, and inspecting the interior of the droplet; laser experiment setup; crumpling of a particle film (PDF)

Silicone oil droplet covered with polyethylene red particles (REDPMS-0.98, average size $\sim 50 \mu\text{m}$ and density $\sim 0.98 \text{ g}\cdot\text{cm}^{-3}$) were made inside the castor oil using a micropipette. The particles were transported at the silicone oil droplet interface by applying a dc electric field of strength $200 \text{ V}\cdot\text{mm}^{-1}$ (AVI)

A polyethylene green particle (GPMS-0.98, average size $\sim 20 \mu\text{m}$ and density $\sim 0.98 \text{ g}\cdot\text{cm}^{-3}$)-covered silicone oil droplet (diameter $\sim 3 \text{ mm}$) immersed in castor oil and docked in a nonconductive O-ring (outer diameter of $\sim 4 \text{ mm}$, inner diameter of $\sim 2.5 \text{ mm}$) that was fastened to an ITO-coated electrode. The droplet was subjected to a dc electric field. The electric field strength increased

stepwise from 0 to $290 \text{ V}\cdot\text{mm}^{-1}$ and then decreased stepwise to $0 \text{ V}\cdot\text{mm}^{-1}$. The movie was sped up 50 times (AVI)

A polyethylene red particle (REDPMS-0.98, average size $\sim 50 \mu\text{m}$ and density $\sim 0.98 \text{ g}\cdot\text{cm}^{-3}$)-covered silicone oil droplet (diameter $\sim 2.5 \text{ mm}$) immersed in castor oil and placed on a flat copper electrode at the bottom of a sample cell. A plate electrode was immersed in the castor oil from above. The droplet was subjected to a dc electric field of strength $250 \text{ V}\cdot\text{mm}^{-1}$. The movie was sped up 5 times and looped twice. The closing of the shell in the movie is actually an opening of the shell played in reverse (AVI)

A polyethylene green particle (GPMS-0.98, average size $\sim 20 \mu\text{m}$ and density $\sim 0.98 \text{ g}\cdot\text{cm}^{-3}$)-covered silicone oil droplet (diameter $\sim 3.2 \text{ mm}$) immersed in castor oil and docked in a nonconductive O-ring that was fastened to an ITO-coated electrode. The droplet was subjected to a dc electric field of strengths $325\text{--}475 \text{ V}\cdot\text{mm}^{-1}$, and the electric field was applied until the particle-free area at the drop pole reached the defined value A_{c1} (~ 55000 square pixels). The movie was sped up 2 times (AVI)

A polyethylene green particle (GPMS-0.98, average size $\sim 90 \mu\text{m}$ and density $\sim 0.98 \text{ g}\cdot\text{cm}^{-3}$)-covered silicone oil droplet (diameter $\sim 3.5 \text{ mm}$) immersed in castor oil and docked in a nonconductive O-ring that was fastened to an ITO-coated electrode. The viscosity of the castor oil was changed by heating the oils from 23 to $50 \text{ }^\circ\text{C}$. The silicone oil droplet was subjected to a dc electric field of strength $250 \text{ V}\cdot\text{mm}^{-1}$ until the opening area at the electric pole reached A_{c2} (~ 45000 square pixels). The movie was sped up 2 times (AVI)

A polyethylene green particle (GPMS-0.98, average size $\sim 20 \mu\text{m}$ and density $\sim 0.98 \text{ g}\cdot\text{cm}^{-3}$)-covered silicone oil droplet (diameter $\sim 3.5 \text{ mm}$) immersed in castor oil and attached to a nonconductive O-ring (outer diameter of $\sim 4 \text{ mm}$, inner diameter of $\sim 2.5 \text{ mm}$) that was fastened to an ITO-coated electrode. The droplet was subjected to a dc electric field of strength $260 \text{ V}\cdot\text{mm}^{-1}$. During the whole experiment, the droplet was illuminated with laser light (wavelength 532 nm , diameter $\sim 0.5 \text{ mm}$, intensity 30 mW) at the center of the droplet (AVI)

A polyethylene red particle (REDPMS-0.98, average size $\sim 50 \mu\text{m}$ and density $\sim 0.98 \text{ g}\cdot\text{cm}^{-3}$)-covered silicone oil droplet (diameter $\sim 3 \text{ mm}$) immersed in castor oil and placed on a flat copper electrode at the bottom of a sample cell. A metal rod, constituting a second electrode, was placed at the center above the droplets and subjected to a dc electric field of strength $400 \text{ V}\cdot\text{mm}^{-1}$. The movie was sped up 2 times (AVI)

A Laponite particle (purchased from Laponite Inc., in the form of a fine white powder)-covered silicone oil droplet (diameter $\sim 5 \text{ mm}$) immersed in castor oil and attached to a nonconductive O-ring (outer diameter of $\sim 4 \text{ mm}$, inner diameter of $\sim 2.5 \text{ mm}$) that was fastened to an ITO-coated electrode. The droplet was subjected to an electric field of strength $0\text{--}360 \text{ V}\cdot\text{mm}^{-1}$ (frequency 0.5 Hz). When the electric field strength was increased from 340 to $360 \text{ V}\cdot\text{mm}^{-1}$, the particle film crumpled through one main vertical fold. The movie was sped up 2 times (AVI)

AUTHOR INFORMATION

Corresponding Author

*E-mail: zbiroz@amu.edu.pl

ORCID

Zbigniew Rozynek: 0000-0002-0785-7088

Author Contributions

Z.R. initiated the project. Z.R., K.K., and A.M. designed all the experiments. K.K. performed the experiments, and Z.R. assisted in the experiments with results presented in Figures 2, 4, 5a, and 8 and Figures S1 and S5, while A.M. assisted in the experiments with results presented in Figures 5d and 6 and Figure S2 and contributed to data analysis and presentation. Z.R. performed the experiments with results presented in Figures 5b,c,e and 7 and Figures S4 and S6. All authors took part in discussions on the finalization of the manuscript. Z.R. administered the submission and the review process.

Notes

The authors declare no competing financial interest.

ACKNOWLEDGMENTS

Z.R. acknowledges financial support from the Polish-U.S. Fulbright Commission through the Fulbright scholarship. Z.R. and K.K. were supported by the Polish National Science Centre through the OPUS Program (2015/19/B/ST3/03055). A.M. acknowledges financial support from the European Union's Horizon 2020 Research and Innovation Framework Program under the M. Skłodowska-Curie grant agreement no. 752896.

REFERENCES

- (1) Murali, P.; Polcawich, R. G.; Trolier-McKinstry, S. Piezoelectric Thin Films for Sensors, Actuators, and Energy Harvesting. *MRS Bull.* **2009**, *34*, 658–664.
- (2) Heczko, O.; Sozinov, A.; Ullakko, K. Giant field-induced reversible strain in magnetic shape memory NiMnGa alloy. *IEEE Trans. Magn.* **2000**, *36*, 3266–3268.
- (3) Alameh, Z.; Yang, S.; Deng, Q.; Sharma, P. Emergent magnetoelectricity in soft materials, instability, and wireless energy harvesting. *Soft Matter* **2018**, *14*, 5856–5868.
- (4) Spaggiari, A.; Castagnetti, D.; Golinelli, N.; Dragoni, E.; Scire` Mammano, G. Smart materials: Properties, design and mechatronic applications. *Proc. Inst. Mech. Eng., Part L* **2017**, *233*, 734–762.
- (5) Alexander, C. Temperature- and pH-responsive smart polymers for gene delivery. *Expert Opin. Drug Deliv.* **2006**, *3*, 573–581.
- (6) Ju, G.; Cheng, M.; Shi, F. A pH-responsive smart surface for the continuous separation of oil/water/oil ternary mixtures. *NPG Asia Mater.* **2014**, *6*, No. e111.
- (7) Sun, L.; Huang, W. M.; Cheah, J. Y. The temperature memory effect and the influence of thermo-mechanical cycling in shape memory alloys. *Smart Mater. Struct.* **2010**, *19*, No. 055005.
- (8) Iqbal, D.; Samiullah, M. Photo-Responsive Shape-Memory and Shape-Changing Liquid-Crystal Polymer Networks. *Materials* **2013**, *6*, 116–142.
- (9) Li, Y.; Rios, O.; Keum, J. K.; Chen, J.; Kessler, M. R. Photoresponsive Liquid Crystalline Epoxy Networks with Shape Memory Behavior and Dynamic Ester Bonds. *ACS Appl. Mater. Interfaces* **2016**, *8*, 15750–15757.
- (10) Zhang, F.; Ju, P.; Pan, M.; Zhang, D.; Huang, Y.; Li, G.; Li, X. Self-healing mechanisms in smart protective coatings: A review. *Corros. Sci.* **2018**, *144*, 74–88.
- (11) Bekas, D. G.; Tsirka, K.; Baltzis, D.; Paipetis, A. S. Self-healing materials: A review of advances in materials, evaluation, characterization and monitoring techniques. *Compos. Part B-Eng.* **2016**, *87*, 92–119.

(12) Aïssa, B.; Therriault, D.; Haddad, E.; Jamroz, W. Self-Healing Materials Systems: Overview of Major Approaches and Recent Developed Technologies. *Adv. Mater. Sci. Eng.* **2012**, *1*–17.

(13) Konsta-Gdoutos, M. S.; Aza, C. A. Self sensing carbon nanotube (CNT) and nanofiber (CNF) cementitious composites for real time damage assessment in smart structures. *Cem. Concr. Compos.* **2014**, *53*, 162–169.

(14) Rana, S.; Subramani, P.; Fanguero, R.; Correia, A. G. A review on smart self-sensing composite materials for civil engineering applications. *Aims Mater. Sci.* **2016**, *3*, 357–379.

(15) Wang, Z. L. Piezotronic and Piezophototronic Effects. *J. Phys. Chem. Lett.* **2010**, *1*, 1388–1393.

(16) Wang, Y.; Runnerstrom, E. L.; Milliron, D. J. Switchable Materials for Smart Windows. In *Annu. Rev. Chem. Biom. Vol 7*; Prausnitz, J. M., Ed.; 2016; p 283–304.

(17) Andreau-Wiedenmaier, A.; Bouny, E.; Giron, J.; Jousse, D.; Labrot, M.; Letocart, P.; Mercks, H. Electrically switchable privacy glass pane for glazing of e.g. vehicle, has two transparent electrically conductive layers on either sides of liquid crystal layer, embedded between respective transparent dielectric layers. EP2128688-A1; DE102008026339-A1; DE102008032904-A1.

(18) Burroughs, J. R.; Okain, A. N.; O'Kain, A. N. Battery with strength indicator-includes in-line switch depressible to complete circuit to place indicator across cell terminals. US5015544-A; WO9213368-A1; EP569354-A1; JP6503441-W; BR9107195-A; EP569354-A4; CA2101077-C; EP569354-B1; DE69132881-E; US40506-E; US39703-E.

(19) Siniaguine, O.; Kachiguina, E. Self-adaptive and optionally also otherwise adaptable wound dressing. US 09681990, Jun 20 2017, 2017.

(20) Rochford, R. A.; Best, M. Eyeglasses and frames therefor. US 09134544, Sep 15 2015, 2015.

(21) Bogue, R. Smart materials: a review of capabilities and applications. *Assembly Autom.* **2014**, *34*, 16–22.

(22) Gurkan, U. A.; Tasoglu, S.; Akkaynak, D.; Avci, O.; Unluisler, S.; Canikyan, S.; Maccallum, N.; Demirci, U. Smart interface materials integrated with microfluidics for on-demand local capture and release of cells. *Adv. Healthcare Mater.* **2012**, *1*, 661–668.

(23) Al-Kaidy, H.; Kuthan, K.; Hering, T.; Tippkötter, N. Aqueous Droplets Used as Enzymatic Microreactors and Their Electromagnetic Actuation. *J. Visualized Exp.* **2017**, *1*–6.

(24) Chen, Z.; Zang, D.; Zhao, L.; Qu, M.; Li, X.; Li, X.; Li, L.; Geng, X. Liquid Marble Coalescence and Triggered Microreaction Driven by Acoustic Levitation. *Langmuir* **2017**, *33*, 6232–6239.

(25) Boydston, A. J.; Cao, B.; Nelson, A.; Ono, R. J.; Saha, A.; Schwartz, J. J.; Thrasher, C. J. Additive manufacturing with stimuli-responsive materials. *J. Mater. Chem. A* **2018**, *6*, 20621–20645.

(26) Tavacoli, J.; Heuvingh, J.; Du Roure, O. Assembly Modulated by Particle Position and Shape: A New Concept in Self-Assembly. *Materials* **2017**, *10*, 1291.

(27) Knaapila, M.; Romoen, O. T.; Svåsand, E.; Pinheiro, J. P.; Martinsen, Ø. G.; Buchanan, M.; Skjeltorp, A. T.; Helgesen, G. Conductivity enhancement in carbon nanocone adhesive by electric field induced formation of aligned assemblies. *ACS Appl. Mater. Interfaces* **2011**, *3*, 378–384.

(28) Feng, X.; Tousley, M. E.; Cowan, M. G.; Wiesenauer, B. R.; Nejati, S.; Choo, Y.; Noble, R. D.; Elimelech, M.; Gin, D. L.; Osuji, C. O. Scalable fabrication of polymer membranes with vertically aligned 1 nm pores by magnetic field directed self-assembly. *ACS Nano* **2014**, *8*, 11977–11986.

(29) Sanders, P.; Young, A. J.; Qin, Y.; Fancey, K. S.; Reithofer, M. R.; Guillet-Nicolas, R.; Kleitz, F.; Pamme, N.; Chin, J. M. Stereolithographic 3D printing of extrinsically self-healing composites. *Sci. Rep.* **2019**, *9*, 388.

(30) Burel, C. A.; Alsayed, A.; Malassis, L.; Murray, C. B.; Donnio, B.; Dreyfus, R. Plasmonic-Based Mechanochromic Microcapsules as Strain Sensors. *Small* **2017**, *13*, 1–7.

- (31) Bollhorst, T.; Rezwan, K.; Maas, M. Colloidal capsules: nano- and microcapsules with colloidal particle shells. *Chem. Soc. Rev.* **2017**, *46*, 2091–2126.
- (32) Wu, J.; Wen, W.; Sheng, P. Smart electroresponsive droplets in microfluidics. *Soft Matter* **2012**, *8*, 11589–11599.
- (33) Ray, A.; Varma, V. B.; Jayaneel, P. J.; Sudharsan, N. M.; Wang, Z. P.; Ramanujan, R. V. On demand manipulation of ferrofluid droplets by magnetic fields. *Sensor. Actuat. B-Chem.* **2017**, *242*, 760–768.
- (34) Rozynek, Z.; Józefczak, A. Patchy colloidosomes - an emerging class of structures. *Eur. Phys. J.-Spec. Top.* **2016**, *225*, 741–756.
- (35) Studart, A. R.; Shum, H. C.; Weitz, D. A. Arrested Coalescence of Particle-coated Droplets into Nonspherical Supracolloidal Structures. *J. Phys. Chem. B* **2009**, *113*, 3914–3919.
- (36) Rozynek, Z.; Bielas, R.; Józefczak, A. Efficient formation of oil-in-oil Pickering emulsions with narrow size distributions by using electric fields. *Soft Matter* **2018**, *14*, 5140–5149.
- (37) Bormashenko, E.; Pogreb, R.; Balter, R.; Gendelman, O.; Aurbach, D. Composite non-stick droplets and their actuation with electric field. *Appl. Phys. Lett.* **2012**, *100*, 151601–4.
- (38) Zhao, Y.; Xu, Z.; Parhizkar, M.; Fang, J.; Wang, X.; Lin, T. Magnetic liquid marbles, their manipulation and application in optical probing. *Microfluid. Nanofluid.* **2012**, *13*, 555–564.
- (39) Mikkelsen, A.; Khobaib, K.; Eriksen, F. K.; Måløy, K. J.; Rozynek, Z. Particle-covered drops in electric fields: drop deformation and surface particle organization. *Soft Matter* **2018**, *14*, 5442–5451.
- (40) Cui, M.; Emrick, T.; Russell, T. P. Stabilizing liquid drops in nonequilibrium shapes by the interfacial jamming of nanoparticles. *Science* **2013**, *342*, 460–463.
- (41) Zhao, Y.; Fang, J.; Wang, H.; Wang, X.; Lin, T. Magnetic liquid marbles: manipulation of liquid droplets using highly hydrophobic Fe₃O₄ nanoparticles. *Adv. Mater.* **2010**, *22*, 707–710.
- (42) Xue, Y.; Wang, H.; Zhao, Y.; Dai, L.; Feng, L.; Wang, X.; Lin, T. Magnetic liquid marbles: a “precise” miniature reactor. *Adv. Mater.* **2010**, *22*, 4814–4818.
- (43) Zhao, Y.; Xu, Z.; Niu, H.; Wang, X.; Lin, T. Magnetic Liquid Marbles: Toward “Lab in a Droplet”. *Adv. Funct. Mater.* **2015**, *25*, 437–444.
- (44) Zang, D.; Li, J.; Chen, Z.; Zhai, Z.; Geng, X.; Binks, B. P. Switchable Opening and Closing of a Liquid Marble via Ultrasonic Levitation. *Langmuir* **2015**, *31*, 11502–11507.
- (45) Saville, D. A. Electrohydrodynamics: The Taylor-Melcher leaky dielectric model. *Annu. Rev. Fluid Mech.* **1997**, *29*, 27–64.
- (46) Dommersnes, P.; Rozynek, Z.; Mikkelsen, A.; Castberg, R.; Kjerstad, K.; Hersvik, K.; Fossum, J. O. Active structuring of colloidal armour on liquid drops. *Nat. Commun.* **2013**, *4*, 2066–8.
- (47) Yeo, E.; Son, M.; Kim, K.; Kim, J. H.; Yoo, Y. E.; Choi, D. S.; Kim, J.; Yoon, S. H.; Yoon, J. S. A study on arrangement characteristics of microparticles in sedimentation on flat and round substrates. *Appl. Phys. Lett.* **2017**, *111*, 264101.
- (48) Nudurupati, S.; Janjua, M.; Aubry, N.; Singh, P. Concentrating particles on drop surfaces using external electric fields. *Electrophoresis* **2008**, *29*, 1164–1172.
- (49) Mikkelsen, A.; Wojciechowski, J.; Rajňák, M.; Kurimský, J.; Khobaib, K.; Kertmen, A.; Rozynek, Z. Electric Field-Driven Assembly of Sulfonated Polystyrene Microspheres. *Materials* **2017**, *10*, 329.
- (50) Mikkelsen, A.; Dommersnes, P.; Rozynek, Z.; Gholamipour-Shirazi, A.; Carvalho, M. D. S.; Fossum, J. O. Mechanics of Pickering Drops Probed by Electric Field-Induced Stress. *Materials* **2017**, *10*, 436.
- (51) Salipante, P. F.; Vlahovska, P. M. Electrohydrodynamics of drops in strong uniform dc electric fields. *Phys. Fluids* **2010**, *22*, 112110.
- (52) Teigen, K. E.; Munkejord, S. T. Influence of surfactant on drop deformation in an electric field. *Phys. Fluids* **2010**, *22*, 112104.
- (53) Cicuta, P.; Vella, D. Granular character of particle rafts. *Phys. Rev. Lett.* **2009**, *102*, 1–4.
- (54) Mikkelsen, A.; Dommersnes, P.; Fossum, J. O. Electric Stress-Induced Slip Lines in Jammed Particle Monolayers. *Rev. Cub. Fis.* **2016**, *33*, 47–49.
- (55) Vella, D.; Aussillous, P.; Mahadevan, L. Elasticity of an interfacial particle raft. *Europhys. Lett.* **2004**, *68*, 212–218.
- (56) Jambon-Puillet, E.; Josserand, C.; Protière, S. Wrinkles, folds, and plasticity in granular rafts. *Phys. Rev. Mater.* **2017**, *1*, No. 042601.
- (57) Bormashenko, E.; Whyman, G.; Gendelman, O. Elastic Properties of Liquid Surfaces Coated with Colloidal Particles. *Adv. Cond. Matter. Phys.* **2015**, *2015*, 1–6.
- (58) Kralchevsky, P. A.; Nagayama, K. Capillary interactions between particles bound to interfaces, liquid films and biomembranes. *Adv. Colloid Interface Sci.* **2000**, *85*, 145–192.
- (59) Rane, Y.; Foster, E.; Moradiafrapoli, M.; Marston, J. O. Compressive deformation of liquid marbles. *Powder Technol.* **2018**, *338*, 7–16.
- (60) Dommersnes, P.; Mikkelsen, A.; Fossum, J. O. Electrohydrodynamic propulsion of counter-rotating Pickering drops. *Eur. Phys. J.-Spec. Top.* **2016**, *225*, 699–706.
- (61) Levine, S.; Bowen, B. D.; Partridge, S. J. Stabilization of emulsions by fine particles I. Partitioning of particles between continuous phase and oil/water interface. *Colloids Surf.* **1989**, *38*, 325–343.
- (62) Amah, E.; Shah, K.; Fischer, I.; Singh, P. Electrohydrodynamic manipulation of particles adsorbed on the surface of a drop. *Soft Matter* **2016**, *12*, 1663–1673.
- (63) Nudurupati, S.; Janjua, M.; Singh, P.; Aubry, N. Effect of parameters on redistribution and removal of particles from drop surfaces. *Soft Matter* **2010**, *6*, 1157–1169.
- (64) Zang, D.; Chen, Z.; Zhang, Y.; Lin, K.; Geng, X.; Binks, B. P. Effect of particle hydrophobicity on the properties of liquid water marbles. *Soft Matter* **2013**, *9*, 5067–5073.
- (65) Sicard, F.; Striolo, A. Buckling in armored droplets. *Nanoscale* **2017**, *9*, 8567–8572.
- (66) Gu, C.; Botto, L. Buckling vs. particle desorption in a particle-covered drop subject to compressive surface stresses: a simulation study. *Soft Matter* **2018**, *14*, 711–724.
- (67) Rozynek, Z.; Mikkelsen, A.; Dommersnes, P.; Fossum, J. O. Electroformation of Janus and patchy capsules. *Nat. Commun.* **2014**, *5*, 3945.
- (68) Negri, C.; Sellerio, A. L.; Zapperi, S.; Miguel, M. C. Deformation and failure of curved colloidal crystal shells. *PNAS* **2015**, *112*, 14545–14550.
- (69) Urano, S.; Fukuda, T.; Emoto, A. Fabrication of high-density array of barnacle-like porous structures using polystyrene colloidal particle monolayer and poly(vinyl alcohol) coating. *Colloids Surf., A* **2017**, *522*, 408–415.
- (70) Lee, S. H.; Jeong, H. E.; Park, M. C.; Hur, J. Y.; Cho, H. S.; Park, S. H.; Suh, K. Y. Fabrication of hollow polymeric microstructures for shear-protecting Cell-Containers. *Adv. Mater.* **2008**, *20*, 788–792.

NOTE ADDED AFTER ASAP PUBLICATION

This paper was published ASAP on June 11, 2019, with formatting errors in the Author Contributions paragraph. The corrected version was reposted on June 12, 2019.

Opening and Closing of Particle Shells on Droplets via Electric Fields and its Applications

Zbigniew Rozynek,^{†§*} Khobaib Khobaib,[§] and Alexander Mikkelsen[§]

[†]Harvard John A. Paulson School of Engineering and Applied Sciences, Harvard University, Cambridge, MA 02138, USA

[§] Faculty of Physics, Adam Mickiewicz University, Umultowska 85, Poznań 61-614, Poland

*Corresponding author: zbiroz@seas.harvard.edu

Table S1. Particle concentration in silicone oil.

Figure	Particles	Concentration	Droplet size
Fig. 2	green PE (20 μm)	~ 3 w/w%	~ 3.0 mm
Fig. 4a	green PE (20 μm)	~ 3 w/w%	~ 3.2 mm
Fig. 4b	green PE (90 μm)	~ 10 w/w%	~ 3.5 mm
Fig. 5a	green PE (90 μm)	~ 10 w/w%	~ 3.5 mm
Fig. 5b	silica (250 nm)	~ 35 w/w%*	~ 0.2 mm
Fig. 5c	Li-fluorohectorite (~ 5 μm)	~ 30 w/w%*	~ 0.5 mm
Fig. 5d	red PE (50 μm)	~ 7 w/w%	~ 3.0 mm
Fig. 5e	paramagnetic (50 μm)	~ 12 w/w%	~ 2.0 mm
Fig. 6	red PE (50 μm)	~ 7 w/w%	~ 2.0 mm
Fig. 7a	green PE (100 μm)	~ 10 w/w%	~ 2.0 mm
Fig. 7b	red PE (50 μm)	~ 7 w/w%	~ 2.0 mm
Fig. 7c	red PE (50 μm)	~ 7 w/w%	~ 2.0 mm
Fig. 8a	Li-fluorohectorite (~ 5 μm)	~ 25 w/w%*	~ 3.0 mm
Fig. 8b	green PE (20 μm)	~ 3 w/w%	~ 3.0 mm
Fig. 8c	red PE (50 μm)	~ 9 w/w%	~ 3.0 mm
Fig. S1	red PE (50 μm)	~ 7 w/w%	~ 1.8 mm
Fig. S2	red PE (50 μm)	~ 11 w/w%	~ 3.0 mm
Fig. S4	green PE (100 μm)	~ 10 w/w%	~ 2.0 mm
Fig. S5	red PE (50 μm)	~ 7 w/w%	~ 3.0 mm
Fig. S6	Laponite (~ 5 μm)	~ 25 w/w%*	~ 5.0 mm

*High concentration was used to prepare the dispersion that was centrifuged to remove particle agglomerates > 10 μm

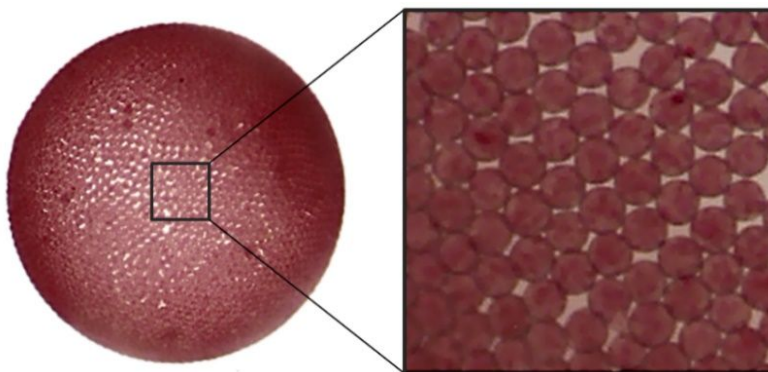


Figure S1. Particle-covered droplets were formed using a DC electric field. An example of a silicone oil droplet covered with PE particles (~ 50 μm). The particles (strongly capillary bound the droplet's surface) were arranged in a jammed, slightly disordered hexagonal structure as shown in the blow-up (see also **Movie S1**).

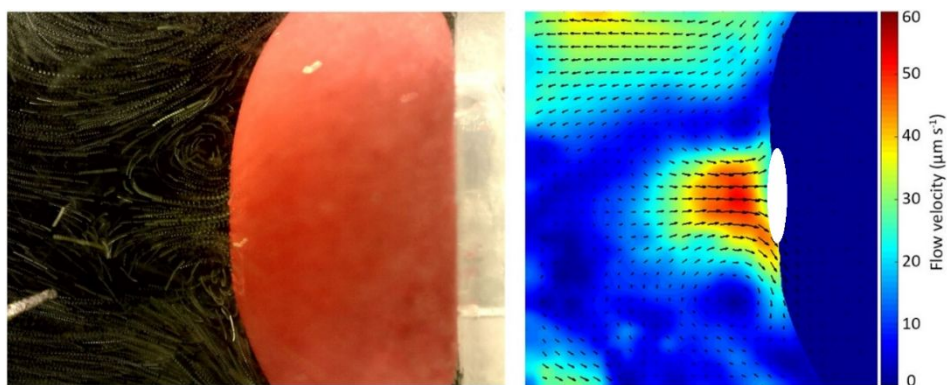


Figure S2. (left) Experimentally observed hydrodynamic streamlines outside a particle-laden droplet while subjected to an electric field of strength $260 \text{ V}\cdot\text{mm}^{-1}$. PE particles ($\sim 20 \text{ }\mu\text{m}$) were used as tracer particles in the surrounding castor. The sample cell was filled with castor oil and the droplet ($\sim 3 \text{ mm}$) covered with PE particles ($\sim 50 \text{ }\mu\text{m}$) was attached to an O-ring (fastened at one electrode). The image was composed by overlapping several images captured over a period of 20 seconds. (right) The corresponding particle image velocimetry image shows the flow velocity map. The white area represents the size of the opening in the particle layer.

By performing particle image velocimetry (PIV) experiments, we measured the magnitude and direction of EHD flows quantitatively outside the droplet's electric pole. PE particles ($\sim 20 \text{ }\mu\text{m}$) were suspended in castor oil and used as tracer particles (see the left panel of **Figure S2**). When we applied a DC electric field, the particles followed the electric field-induced flows outside the droplet's electric pole. The flow directions and velocities for a droplet subjected to an electric field of strength $260 \text{ V}\cdot\text{mm}^{-1}$ are visualized in the right panel of **Figure S2**. The flow fields demonstrate how the surface particles on the droplet are carried away from the droplet's electric pole by the flow. Two vortices are located close to the droplet interface, and the flow velocity is fastest closer to the droplet's electric pole (magnitude around $50 \text{ }\mu\text{m}\cdot\text{s}^{-1}$). The flows outside the droplet were measured after the droplet had reached a steady-state deformation and no further structuring of the particle layer was observed.

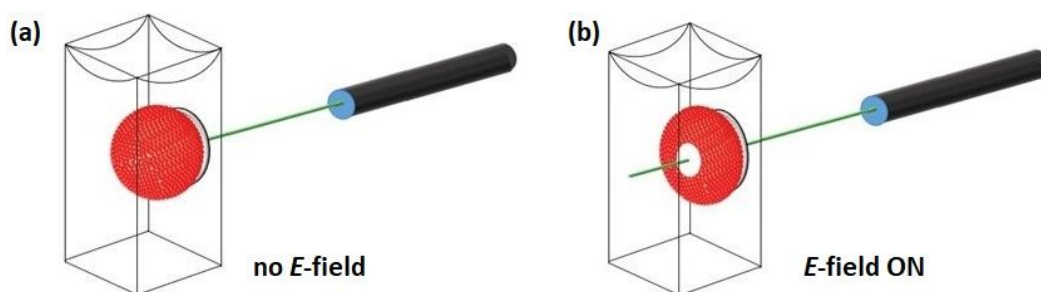


Figure S3. (a,b) Experimental setup for a laser experiment. A sample cell ($10 \text{ mm} \times 10 \text{ mm} \times 30 \text{ mm}$) was made of glass with two of the inside walls coated with a conductive indium tin oxide (ITO) layer, constituting electrodes. An O-ring of size 4 mm was fastened on the inside of the sample cell to one of the electrodes. The sample cell was filled with castor oil, and a silicone oil droplet covered with PE particles was docked in the O-ring. The droplet was illuminated with laser light (class III laser

pointer, of wavelength 532 nm, intensity 30 mW, and diameter 0.5 mm) through its center along the electric field. DC electric field of strength between 0 and $260 \text{ V}\cdot\text{mm}^{-1}$ were applied to open and close the particle layer at the droplet interface.



Figure S4. An electrode inserted into the PE particle covered silicone oil droplet ($\sim 2 \text{ mm}$). High electric tension ($\sim 1 \text{ kV}$) applied to the electrode caused the droplet to violently break apart.

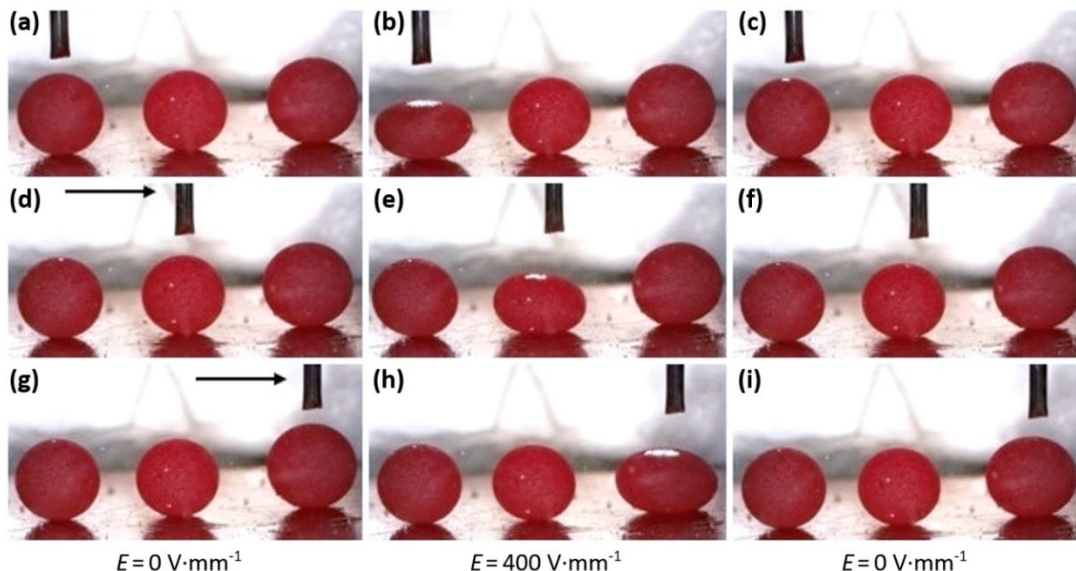


Figure S5. (a–i) Procedure of inspecting the interior content of particle-covered droplets. Three silicone oil droplets ($\sim 3 \text{ mm}$) were covered with PE particles and placed on a flat electrode in the bottom of the sample cell. A metal rod was used as the second electrode and placed at the center above one of the droplets. Under the application of an electric field (strength $400 \text{ V}\cdot\text{mm}^{-1}$ in vertical direction), the PE particles moved away from the droplet's electric pole and formed an opening in the particle shell that enabled inspection of the inside liquid. See also the corresponding **Movie S7**.

We made three particle-covered droplets ($\sim 3 \text{ mm}$) and placed them on an electrode at the bottom of a sample cell that was filled with castor oil. Above the droplets, we placed a conductive rod-shaped electrode that could move relative to the droplets. Initially, the three droplets were entirely covered with PE particles (**Figure S5a**). A non-uniform DC electric field of strength $\sim 400 \text{ V}\cdot\text{mm}^{-1}$ was then generated in the vertical direction. The configuration of the electrodes set up a local electric field that only deformed and induced flows around the droplet positioned between the electrodes. Consequently, the PE particles at the interface of that particular droplet moved away from the droplet's electric pole, forming an opening in the particle shell (**Figure S5b**). Next, we turned off the electric field (**Figure S5c**) and placed the electrode above a second droplet (**Figure S5d**). The electric field was then reapplied to form an opening in the PE particle shell (**Figure S5e**). The same procedure was repeated for the last droplet (**Figure S5g–i**). See also the corresponding **Movie S7**.

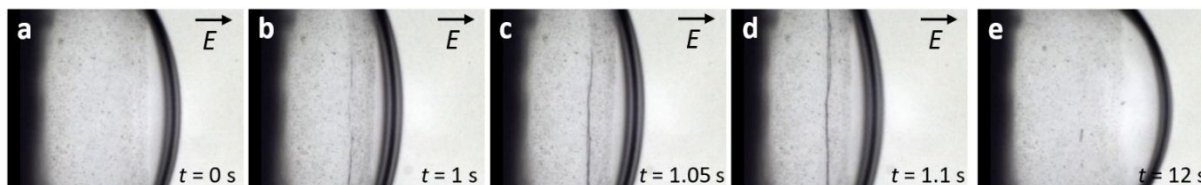


Figure S6. Crumpling of a particle film composed of Laponite clay particles (size $\sim 5 \mu\text{m}$) formed on a silicone oil droplet. **(a)** The particle-covered droplet was subjected to an electric field (horizontal direction) of strength $340 \text{ V}\cdot\text{mm}^{-1}$. **(b–d)** When the electric field strength was increased to $360 \text{ V}\cdot\text{mm}^{-1}$, the particle film crumpled through one main fold. **(e)** The particle layer unfolded after the electric field was turned off. See also the corresponding **Movie S8**. The electric field (through EHD liquid flows) can be used to study mechanical properties of particle films, such as the elasticity and bending stiffness.

Movie S1. Silicone oil droplet covered with polyethylene red particles (REDPMS-0.98, average size $\sim 50 \mu\text{m}$ and density $\sim 0.98 \text{ g}\cdot\text{cm}^{-3}$) were made inside the castor oil using a micropipette. The particles were transported at the silicone oil droplet interface by applying a DC electric field of strength $200 \text{ V}\cdot\text{mm}^{-1}$.

Movie S2. A polyethylene green particle (GPMS-0.98, average size $\sim 20 \mu\text{m}$ and density $\sim 0.98 \text{ g}\cdot\text{cm}^{-3}$)–covered silicone oil droplet (diameter $\sim 3 \text{ mm}$) immersed in castor oil and docked in a nonconductive O-ring (outer diameter of $\sim 4 \text{ mm}$, inner diameter of $\sim 2.5 \text{ mm}$) that was fastened to an ITO-coated electrode. The droplet was subjected to a DC electric field. The electric field strength increased stepwise from 0 to $290 \text{ V}\cdot\text{mm}^{-1}$ and then decreased stepwise to $0 \text{ V}\cdot\text{mm}^{-1}$. The movie was sped up 50 times.

Movie S3. A polyethylene red particle (REDPMS-0.98, average size $\sim 50 \mu\text{m}$ and density $\sim 0.98 \text{ g}\cdot\text{cm}^{-3}$)–covered silicone oil droplet (diameter $\sim 2.5 \text{ mm}$) immersed in castor oil and placed on a flat copper electrode at the bottom of a sample cell. A plate electrode was immersed in the castor oil from above. The droplet was subjected to a DC electric field of strength $250 \text{ V}\cdot\text{mm}^{-1}$. The movie was sped up 5 times and looped twice. The closing of the shell in the movie is actually an opening of the shell played in reverse.

Movie S4. A polyethylene green particle (GPMS-0.98, average size $\sim 20 \mu\text{m}$ and density $\sim 0.98 \text{ g}\cdot\text{cm}^{-3}$)–covered silicone oil droplet (diameter $\sim 3.2 \text{ mm}$) immersed in castor oil and docked in a nonconductive O-ring that was fastened to an ITO-coated electrode. The droplet was subjected to a DC electric field of strengths $325\text{--}475 \text{ V}\cdot\text{mm}^{-1}$, and the electric field was applied until the particle-free area at drop pole reached the defined value A_{c1} ($\sim 55,000$ square pixels). The movie was sped up 2 times.

Movie S5. A polyethylene green particle (GPMS-0.98, average size $\sim 90 \mu\text{m}$ and density $\sim 0.98 \text{ g}\cdot\text{cm}^{-3}$)–covered silicone oil droplet (diameter $\sim 3.5 \text{ mm}$) immersed in castor oil and docked in a nonconductive O-ring that was fastened to an ITO-coated electrode. The viscosity of the castor oil was changed by heating the oils from $23 \text{ }^\circ\text{C}$ to $50 \text{ }^\circ\text{C}$. The silicone oil droplet was subjected to a DC electric field of strength $250 \text{ V}\cdot\text{mm}^{-1}$ until the opening area at the electric pole reached A_{c2} ($\sim 45,000$ square pixels). The movie was sped up 2 times.

Movie S6. A polyethylene green particle (GPMS-0.98, average size $\sim 20 \mu\text{m}$ and density $\sim 0.98 \text{ g}\cdot\text{cm}^{-3}$)–covered silicone oil droplet (diameter $\sim 3.5 \text{ mm}$) immersed in castor oil and attached to a nonconductive O-ring (outer diameter of $\sim 4 \text{ mm}$, inner diameter of $\sim 2.5 \text{ mm}$) that was fastened to an ITO-coated electrode. The droplet was subjected to a DC electric field of strength $260 \text{ V}\cdot\text{mm}^{-1}$. During the whole experiment, the droplet was illuminated with laser light (wavelength 532 nm , diameter $\sim 0.5 \text{ mm}$, intensity 30 mW) at the center of the droplet.

Movie S7. A polyethylene red particle (REDPMS-0.98, average size $\sim 50 \mu\text{m}$ and density $\sim 0.98 \text{ g}\cdot\text{cm}^{-3}$)–covered silicone oil droplet (diameter $\sim 3 \text{ mm}$) immersed in castor oil and placed on a flat copper electrode at the bottom of a sample cell. A metal rod, constituting a second electrode, was placed at the center above the droplets and subjected to a DC electric field of strength $400 \text{ V}\cdot\text{mm}^{-1}$. The movie was sped up 2 times.




Movie S8. A Laponite particle (purchased from Laponite Inc., in the form of a fine white powder)–covered silicone oil droplet (diameter $\sim 5 \text{ mm}$) immersed in castor oil and attached to a nonconductive O-ring (outer diameter of $\sim 4 \text{ mm}$, inner diameter of $\sim 2.5 \text{ mm}$) that was fastened to an ITO-coated electrode. The droplet was subjected to an electric field of strength $0\text{--}360 \text{ V}\cdot\text{mm}^{-1}$ (frequency 0.5 Hz). When the electric field strength was increased from 340 to $360 \text{ V}\cdot\text{mm}^{-1}$, the particle film crumpled through one main vertical fold. The movie was sped up 2 times.

Paper V

Particle-covered droplet and a particle shell under compressive electric stress

K Khobaib, T Hornowski and Z Rozynek

Phys. Rev. E **103**, 062605 (2021)

Particle-covered droplet and a particle shell under compressive electric stressKhobaib Khobaib ¹, Tomasz Hornowski ¹ and Zbigniew Rozynek ^{1,2,*}¹*Faculty of Physics, Adam Mickiewicz University, Uniwersytetu Poznańskiego 2, 61-614 Poznań, Poland*²*PoreLab, The Njord Centre, Department of Physics, University of Oslo, Blindern, N-0316 Oslo, Norway*

(Received 15 October 2020; revised 19 March 2021; accepted 20 May 2021; published 8 June 2021)

Understanding of the behavior of an individual droplet suspended in a liquid and subjected to a stress is important for studying and designing more complex systems, such as emulsions. Here, we present an experimental study of the behavior of a particle-covered droplet and its particle shell under compressive stress. The stress was induced by an application of a DC electric field. We studied how the particle coverage (φ), particle size (d), and the strength of an electric field (E) influence the magnitude of the droplet deformation (D). The experimental results indicate that adding electrically insulating particles to a droplet interface drastically changes the droplet deformation by increasing its magnitude. We also found that the magnitude of the deformation is not retracable during the electric field sweeping, i.e., the strain-stress curves form a hysteresis loop due to the energy dissipation. The field-induced droplet deformation was accompanied by structural and morphological changes in the particle shell. We found that shells made of smaller particles were more prone to jamming and formation of arrested shells after removal of an electric stress.

DOI: [10.1103/PhysRevE.103.062605](https://doi.org/10.1103/PhysRevE.103.062605)**I. INTRODUCTION**

Droplets covered by granular or colloidal particles have recently been actively studied from the perspective of both the fundamental and the applied sciences. They are considered as suitable materials to be used in the food technology [1], drug delivery [2], cosmetics [3], biomedical applications [4], and oil industry [5]. Particle-covered droplets have characteristics that make them useful also for fabricating adaptive structures [6,7], porous materials [8], colloidal photonic crystals [9], and responsive microcapsules with homogenous [10,11] or heterogeneous particle shells [12,13]. Moreover, the particle-covered droplets can be used as experimental model systems for studying different phenomena taking place on curved liquid-liquid interfaces, for example, particle assembly [14], ordering [15], mixing [16], as well as particle-layer buckling [17].

In many research areas, knowledge of the stability and mechanics of an individual particle-covered droplet is essential, e.g., for the efficient fabrication of Pickering emulsions [18], for designing emulsions with controlled stability [19,20], and, in general, for the further development of the above mentioned research fields. In this context, several research groups have studied theoretically and experimentally the deformation [21–24], relaxation [25,26], dynamics [27], and mechanical properties of particle-laden droplets [28,29]. Experiment-

tal methodologies involved in research on particle-covered droplets include compressive strain [25,30], atomic force microscopy [31], as well as ultrasonic and magnetic methods [32,33]. Another approach for studying the properties of particle-laden droplets is the application of an electric field (E field).

E fields have demonstrated to be an adaptable method for studying particle-droplet stability [20], electrorotation [16,22], as well as steady-state [34,35] and transient deformations [36–38]. In this paper, we use an E field to study the behavior of a particle-covered oil droplet and its particle shell under induced electric stress. In the oil-oil systems, an E field can be used to generate the electric stresses that either compress or stretch a particle-covered droplet depending on physical parameters of the fluids and particles (e.g., electrical conductivity and dielectric properties), and the parameters of an applied E field (frequency and strength). For example, a particle-covered droplet subjected to a DC E field can compressively deform, whereas an application of an AC E field to the same droplet may stretch it [6]. Here, we wished to investigate a particle-covered droplet under compressive stress. Therefore, we chose to use a uniform DC E field and work with a three-phase system comprising an electrically weakly conductive silicone oil droplet covered by electrically insulating microparticles and suspended in slightly more electrically conductive castor oil. In such a system, the E field causes free ions with opposite charges (impurities in the oils) to accumulate at the two hemispheres of the particle-covered droplet. Electric stress is induced at the hemispheres when the E field acts on these charges, and it compresses the droplet that eventually acquires an oblate geometry, i.e., the longest droplet axis is perpendicular to the E field.

Many experimental and theoretical studies have been conducted on this type of deformation. Initially, the majority

*Corresponding author: zbiroz@amu.edu.pl

Published by the American Physical Society under the terms of the [Creative Commons Attribution 4.0 International](https://creativecommons.org/licenses/by/4.0/) license. Further distribution of this work must maintain attribution to the author(s) and the published article's title, journal citation, and DOI.

of the studies concerned particle-free droplets. The theory on the droplet deformation and relaxation (after reducing E -field strength) was established a long time ago [39] and has since been further developed [37,40–43]. Thus, the influence of liquids' electrical properties and parameters of the E field on the mechanics of pure droplets is now well described. Much less is known about the deformation of particle-covered droplets, although, lately the knowledge gap has been narrowing by the works of several research groups [6,24,34–36,44]. However, in all these research contributions the particle-covered droplets were studied in a narrow range of E -field strengths. This is because the particle-covered droplets suspended roughly in the middle of the sample cell and unattached to any surface could freely translate and rotate in the presence of an E field. Thus, at moderate strengths of E fields (above $\sim 150 \text{ V mm}^{-1}$) a particle-covered droplet begins electrorotating, which prevents researching on the droplet deformation at higher E -field strengths. In the research presented here, we solve this problem by docking a droplet into an O-ring washer attached to one of the walls of the sample cell. In this way the droplet is held in place preventing: (i) its motion in the sample cell due to the presence of convective flows of liquid in the cell and (ii) its electrorotation as well as easing the experimental observations. Therefore, we can study the behavior of a droplet and its particle shell subjected to much greater E -field strengths ($\sim 300 \text{ V mm}^{-1}$).

There is also little knowledge about the influence of particle coverage on the droplet deformation. In this paper, we investigate thoroughly this correlation. Another subject of consideration is the relaxation of the particle-covered droplets. Numerous research articles deal with the relaxation kinetics [25,35,44,45]. Lately, several works have been published on the behavior of the particle shell after removal of the external force. The research concerned particle jamming (leading to formation of stable nonspherical droplets), particle shell buckling, and structural changes [46–49]. In our previous work on opening and closing of particle shells on droplets, we found that the magnitude of the droplet deformation was nonretractable and exhibited hysteresis, and the particle shell underwent structural and morphological changes [46]. Rane *et al.* [30] reported hysteresis in deformation of liquid marbles during the mechanical compression and decompression. They attributed the presence of the hysteresis to the interlocking and rearrangement of particles at the droplet interface. Monteux *et al.* [50] and Xu *et al.* [51] also demonstrated the hysteresis effect by volume compression and expansion of the droplet, and they attributed the slow rearrangement due to the particles aggregation at the droplet interface.

Different mechanisms of droplet compression and decompression were used in the four above mentioned works, and the force on a particle-covered droplet was exerted in a different way. This has certain consequences. For example, during the mechanical compression of a droplet by two flat slabs, the particles in the shell become loosely packed. Whereas, in the method presented here and in our previous work [46], the particles are kept tight during the application of the E field, which may result in buckling of the shell. Due to the limited understanding of our previous result, we decided to conduct further research.

Thus, in this paper, our objectives are to show: (i) how the particle coverage, particle size, and the strength of the E field influence the magnitude of steady-state deformation of a droplet with a particle shell; and (ii) how the particle size and the strength of the E field affect the recovery of a particle shell and the arrangements of the surface particles.

II. EXPERIMENTAL SETUP AND MATERIALS

The experimental setup consisted of an optical acrylic cuvette ($10 \times 10 \times 30 \text{ mm}^3$) used as a sample cell with two copper plates that constituted electrodes, a signal generator (SDG1025, SIGLENT Technologies), a high voltage amplifier for generating a direct current electric signal (10HVA24-BP1, HVP High Voltage Products GmbH), and a digital microscope (AM7315MZT, Dino-Lite) for viewing perpendicular to the direction of the applied E field. A schematic illustrating the experimental setup is shown in Figs. 1(a) and 1(b). A plastic washer (outer diameter 4.0 mm, inner diameter 2.3 mm, and thickness 0.4 mm) was glued to one of the copper electrodes (at its center). The washer was used to hold a droplet in place, i.e., prevent: (i) its motion in the sample cell in the presence of convective flows of liquid and (ii) its rotation [22]. The presence of the washer influenced only slightly (by less than 15%) the magnitude of the droplet deformation (see Fig. S1 of the Supplemental Material [52]). We, therefore, do not take it into account in the data analysis and discussion. In the experiments with results presented in Figs. 8 and 9, we used a cell made of glass with two glass walls coated by an electrically conductive indium tin oxide (ITO) layer.

Polyethylene particles (WPMS-0.98, size $\sim 3 \mu\text{m}$, density $\sim 0.98 \text{ g cm}^{-3}$; GPMS-0.98, size $\sim 18 \mu\text{m}$, density $\sim 0.98 \text{ g cm}^{-3}$; BLPPMS-1.00, size $\sim 30 \mu\text{m}$, density $\sim 1.00 \text{ g cm}^{-3}$; REDPMS-0.98, size $\sim 50 \mu\text{m}$, density $\sim 0.98 \text{ g cm}^{-3}$; GPMS-0.98, size $\sim 100 \mu\text{m}$, density $\sim 0.98 \text{ g cm}^{-3}$; electrical conductivity $\sim 10^{-15} \text{ S m}^{-1}$, purchased from Cospheric LLC) and clay mineral particles (Li fluorohectorite, size $\sim 5 \mu\text{m}$; density $\sim 2.8 \text{ g cm}^{-3}$, Corning, Inc., USA) were used to make a monolayer shell on a silicone oil (VWR Chemicals, Rhodorsil® 6678.1000, density 0.96 g cm^{-3} , electrical conductivity $\sim 10 \text{ pS m}^{-1}$, relative permittivity $\sim 2.6\text{--}2.9$ at 25°C , and viscosity 50 mPa s) droplet formed in castor oil (Sigma-Aldrich 83912, density 0.961 g cm^{-3} at 25°C , electrical conductivity $\sim 60 \text{ pS m}^{-1}$, relative permittivity $\sim 4.6\text{--}4.8$ at 25°C , and viscosity 750 mPa s). The interfacial tension between the two immiscible oils was around 4.5 mN m^{-1} .

III. FORMATION OF PARTICLE-COVERED DROPLETS AND EXPERIMENTAL PROCEDURES

We used an E -field approach (see Ref. [7]) to form a monolayer particle shell on the surface of a silicone oil droplet. Initially, silicone oil dispersion of polyethylene (PE) particles was prepared using a specific particle concentration required to form a particle-covered droplet of a certain size and a desired particle coverage. The dispersion was ultrasonicated for 5 min to avoid particle aggregating, and, subsequently, a dispersion droplet was formed (using a regular mechanical pipette) in a cuvette filled with castor oil. Next, an E field

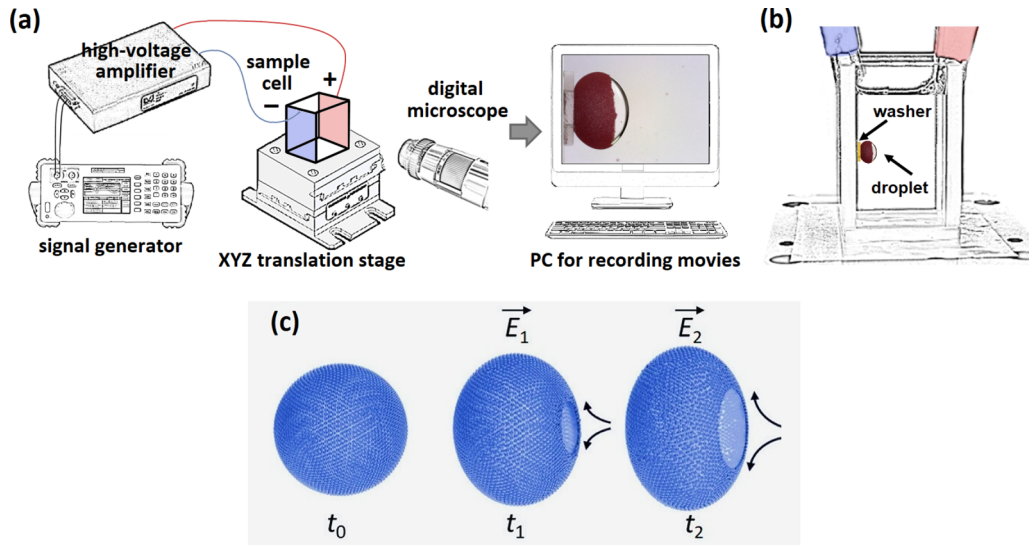


FIG. 1. (a) and (b) Schematics illustrating the experimental setup, which consisted of a digital microscope for viewing perpendicular to the direction of the applied E field, a sample cell placed on a mechanical XYZ translational stage, a signal generator, and a voltage amplifier for generating a high-voltage electric signal, which is provided to the electrodes inserted inside the sample cell. (c) Schematics of particle shell opening: A droplet with the surface particles is viewed at a 30° angle with respect to the E -field direction, which is horizontal. Application of an electric field (E_1) to the initially spherical droplet (t_0) densely covered with particles results in its deformation due to the electric stress. The induced EHD flows convect particles away from the droplet's electric pole thereby forming an opening in the particle layer. After application of a stronger electric field (E_2), the droplet deforms more, allowing the opening to grow in size, and the EHD flows to strengthen (indicated by the longer curved arrows).

($\sim 200 \text{ V mm}^{-1}$) was applied so that the particles in the bulk liquid of the dispersion droplet were guided toward the droplet's interface by electrostatic force. As the particles reached the surface of the droplet, they were carried toward the electric equator of that droplet by the E -field induced liquid flows. It took several minutes for all particles to get onto the interface and eventually form a packed particle monolayer. The particles were irreversibly trapped at the droplet interface by capillary forces as the thermal energy is a few orders of magnitude smaller than that stemming from the capillary interaction for microparticles [48]. The droplet was then docked in an O-ring washer to prevent its motion in the sample cell and ease the experimental observations. To avoid particles inside the ring, we first docked a pure silicone oil droplet and then brought the particle-covered droplet and let it electrocoalesce. To adjust the droplet volume and the particle coverage, some of the silicone oil was extracted from the droplet using a micropipette. This spherical particle-covered droplet was then studied in an E field, which was in the horizontal direction.

When a particle-free droplet or a droplet covered with PE particles is subjected to a direct current E field, free charges (ionic impurities in oils) accumulate at the droplet's interface. This results in the generation of the electric stress that deforms the droplet, thereby increasing the droplet's surface area and decreasing the particle coverage. The steady-state deformation of the droplet due to the electric stress is given by the Melcher-Taylor model [53],

$$D = \frac{9r_0\epsilon_0\epsilon_{\text{ex}}E_0^2}{16\gamma S(2+R)^2} \left[S(R^2+1) - 2 + 3(RS-1) \frac{2\lambda+3}{5\lambda+5} \right], \quad (1)$$

where $R = \frac{\sigma_{\text{in}}}{\sigma_{\text{ex}}}$, $S = \frac{\epsilon_{\text{ex}}}{\epsilon_{\text{in}}}$, $\lambda = \frac{\mu_{\text{ex}}}{\mu_{\text{in}}}$, and R , S , and λ are the conductivity, dielectric constant, and viscosity ratios, ϵ_{ex} is the dielectric constant of the surrounding fluid, r_0 is the radius of the droplet, and γ is the interfacial surface tension between the droplet and the exterior fluid. The subscript “ex” represents the exterior fluid (castor oil), whereas the subscript “in” represents the interior fluid which is the droplet (silicone oil). In the system studied here, the electric stress compresses the droplet, therefore, the magnitude of the deformation has a negative sign if the deformation is described as $D = (d_{\parallel} - d_{\perp}) / (d_{\parallel} + d_{\perp})$, where d_{\parallel} and d_{\perp} are the droplet's axes parallel and perpendicular to the E -field direction, respectively. However, in all our plots we use the absolute value of D . Application of the E field also results in the induction of the electrohydrodynamic (EHD) flows. In the case of the particle-covered droplets, these flows convect particles away from the droplet's electric pole, forming a particle-free area there. The convected particles pack densely within the particle shell. When the E -field strength is increased, the droplet deforms more, allowing the particle-free area to grow in size and the EHD flows to strengthen as presented in Fig. 1(c).

In our experiments, we varied the E -field strength and the particle coverage as well as the droplet size and studied changes in the magnitude of the droplet's deformation by estimating the major and minor lengths of the droplet using GRAPHS software. We limited the E -field strength to 285 V mm^{-1} because at stronger E fields (above $\sim 300 \text{ V mm}^{-1}$) particles detached irreversibly from the droplet's surface. The particles coverage was also estimated through image analysis of the droplets. We define here the particle coverage of the droplets as $\varphi = S/A$, where S is the

surface area of the particle film and A is the surface area of the droplet with excluded part of the droplet in the washer. Thus, the value of the particle coverage as defined here is in the range from 0 to around 1.0. $\varphi = 0$ defines the silicone oil droplet without particles, and $\varphi = 1$ defines the silicone oil droplet fully covered by the PE particles.

IV. PARTICLE IMAGE VELOCIMETRY EXPERIMENTS

The flowlines around droplets were traced using particle image velocimetry (PIV). Fluorescent PE particles (UVPMS-BY2-1.00, size of $\sim 35 \mu\text{m}$, Cospheric LLC) were dispersed in castor oil (0.3% by weight) and poured in the sample cell. A $500\text{-}\mu\text{m}$ thin sheet of particles was selected by focusing a 532-nm laser light (COM-09906-5 mW, SparkFun Electronics) from above the sample cell through a laser line generator lens (Powell lens), similar as in the experiment presented in Ref. [6]. During the experiments, the laser sheet was always aligned in the middle of the drop, oriented along the E -field direction, and perpendicular to the view direction of the microscope (see Fig. S2 in the Supplemental Material [52]). Movies (5 fps) were recorded for each experiment with a 1920×1080 -pixel resolution (1 pixel $\sim 6.2 \mu\text{m}$). Twenty-five sequential frames were then compared and analyzed using PIVLAB (v.1.41, MATLAB toolbox application), yielding flow velocities for each interrogation area (the frames were split into a number of interrogation areas of size 64×64 pixels, which were then individually cross-correlated with the previous frame to obtain displacement vectors). MATLAB (v.R2017b, MathWorks) was then used to plot the flow velocities.

V. RESULTS

General concept of the experiments: In all the experiments we used a tabletop experimental setup, which consisted of a sample cell with two electrodes, a source of a high voltage DC signal, and a digital microscope for viewing either parallel or perpendicular to the direction of the applied E field. A schematic illustrating part of the experimental setup is shown in Figs. 1(a) and 1(b). Application of a DC E field results in a compressive electric stress that acts on particle-covered droplet deforming it. When the droplet deforms, its surface area increases leading to unjamming of particles in a shell. This, in turn, enables the induction of the EHD flows. In our system, these flows convect particles away from the droplet's electric pole, forming a particle-free area there. The convected particles pack densely within the particle shell. When the E -field strength is increased, the droplet deforms more, allowing the particle-free area to grow in size and the EHD flows to strengthen as presented in Fig. 1(c).

A. Influence of particle coverage on the droplet deformation and emergence of its hysteresis

We began our research with studying the influence of particle coverage on the magnitude of steady-state droplet deformation at different strengths of an E field. We prepared seven silicone oil droplets ($\sim 4 \text{ mm}$) covered by the PE particles ($\sim 50 \mu\text{m}$), each droplet with different particle coverage. We also used a particle-free droplet as a reference. Initially, in the absence of the E field, the droplets were

spherical. Application of the E field induced electric stress on the droplets and resulted in their deformation, i.e., all droplets developed an oblate shape. The strength of the E field was increased stepwise from 0 V mm^{-1} to 285 V mm^{-1} and then decreased in the same manner to 0 V mm^{-1} . At each step, the E -field strength was increased by 15 V mm^{-1} and maintained until a steady state (droplet's deformation and particle arrangement) was observed. The difference in the droplet deformation can be easily observed qualitatively, especially at strong E fields, for example, at 285 V mm^{-1} as presented in Fig. 2(a). The droplets with higher particle coverage deform more. In Figs. 2(b)–2(d), we present the quantitative data from the experiments, which reveal the nonobvious behavior of particle-covered droplets.

In Fig. 2(b), the magnitude of droplet deformation is plotted against the square of the E -field strength. As expected, the magnitude of the deformation of the pure silicone oil droplet scales as E^2 at weak E fields (up to around $15 \text{ kV}^2 \text{ mm}^{-2}$) and follows Taylor's theory [39,54]. At stronger E fields, the curve becomes nonlinear and bends downward. The reason for this nonlinearity is the surface-charge convection (not included in Taylor's theory) due to the EHD liquid flows making it more difficult to deform the droplet into more oblate shape as explained and experimentally presented in Refs. [40–42,55]. The curve for the pure silicone oil droplet is entirely retraceable when the E field is decreased back to zero, i.e., the data points (\blacklozenge) overlap when sweeping the E field up and down.

A different situation is observed for the droplet covered with particles. The magnitude of the deformation is not retraceable (i.e., there are different values of the deformation depending on the direction of change of the E -field strength) and the curves form a hysteresis loop (will come back to that later). In addition, the magnitude of droplet deformation is sensitive to particle coverage. In general, the deformation is greater with the increased particle coverage. In Fig. 2(c), we plot the deformations measured at the strongest E field used in the experiment (285 V mm^{-1}) versus the particle coverage (φ). It can be seen that the magnitude of the deformation does not change much for the droplets with low particle coverage but increases sharply at higher particle coverages.

There are possibly two reasons for this: (i) As more of the droplet's surface is covered by particles, the charge convection may be depleted due to the reduced strength of EHD flows leading to accumulation of a larger amount of free charges on the droplet's surface. This, in turn, results in stronger electrical stress acting on the droplet. In addition, (ii) the effective electrical conductivity of the droplet interface may decrease (because the PE particles are several orders of magnitude less conductive than silicone oil [44]), leading to the greater electrical contrast between the particle-covered silicone oil droplet and castor oil and, thus, enhancing the compressive electric stress acting on the droplet. We conducted experiments and performed calculations to confront the above statements.

In Fig. 3, we present the results of PIV experiments performed on a silicone oil droplet with PE particle particles ($\sim 50 \mu\text{m}$) at different particle coverages subjected to a DC E field of 170 V mm^{-1} . The results from the PIV experiments confirm that the induced EHD flows at droplet interfaces are

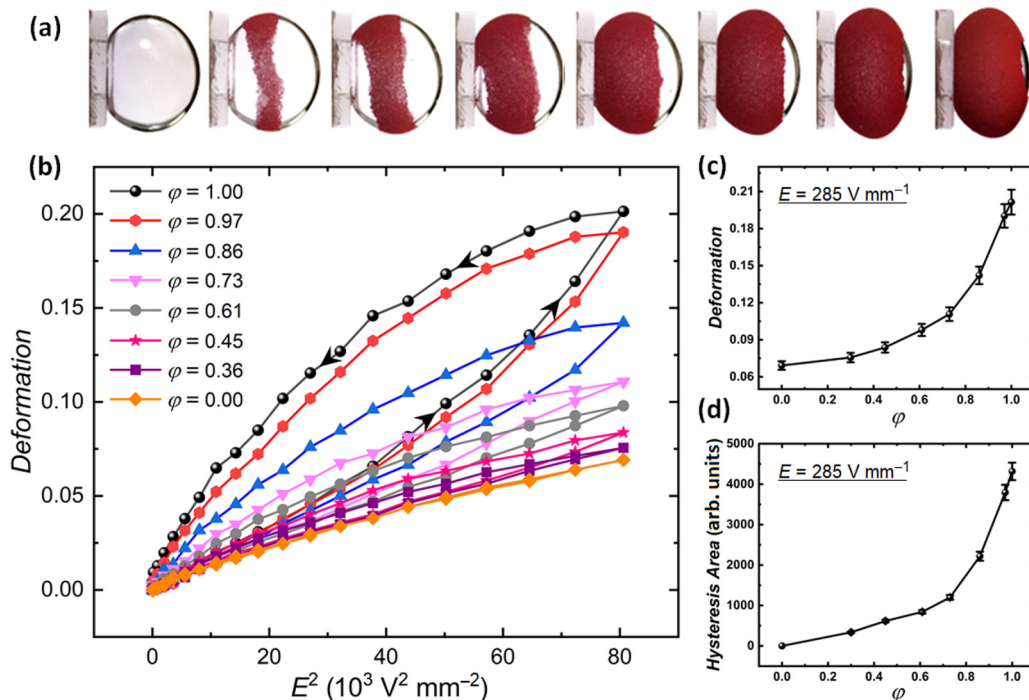


FIG. 2. (a) Silicone oil droplets with different particle coverages (ϕ) subjected to E -field strength of 285 V mm^{-1} . The diameter of each droplet is $\sim 4 \text{ mm}$, and the size of the PE particles is $\sim 50 \mu\text{m}$. (b) Steady-state deformation of droplets plotted as a function of the square of the applied DC E field. The E field was increased stepwise from 0 to 285 V mm^{-1} and then decreased stepwise to 0 V mm^{-1} . The black arrows represent the E -field sweep direction. (c) The magnitude of the droplet deformation and (d) the hysteresis area of the droplet deformation at $E = 285 \text{ V mm}^{-1}$ plotted as a function of particle coverage.

indeed greatly reduced by adding surface particles. When the particle coverage was increased from 0.25 to around 0.9 (droplet nearly fully covered by particles), the maximum EHD

flow velocity decreased from around 130 to nearly $0 \mu\text{m s}^{-1}$, verifying that the straining flows surrounding a silicone oil droplet in castor oil are suppressed when the droplet is fully

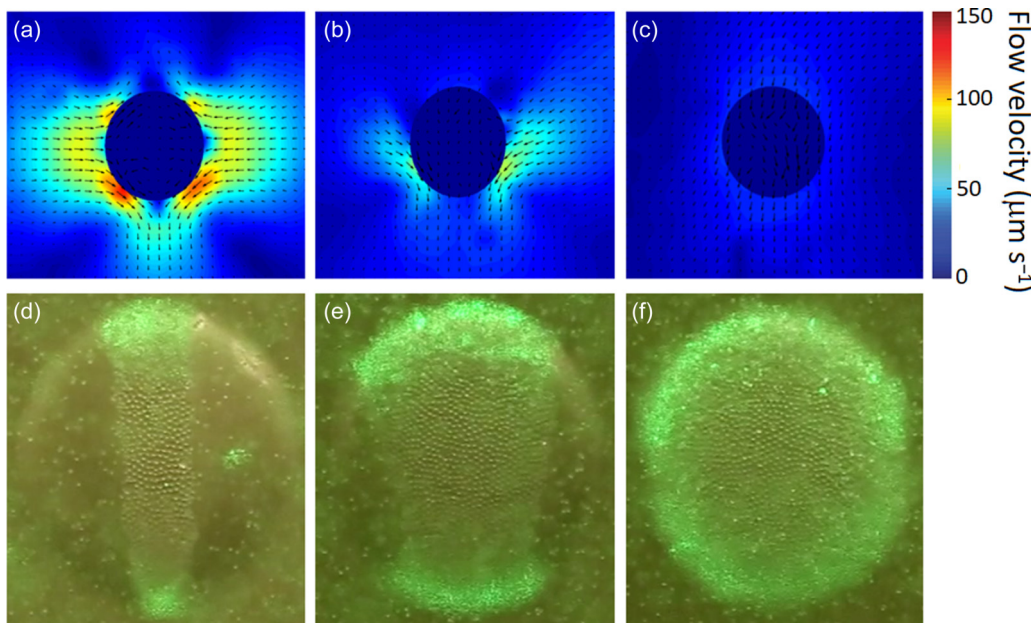


FIG. 3. (a)–(c) PIV images and (d)–(f) corresponding pictures of silicone oil droplets (diameter $\sim 2 \text{ mm}$) covered with PE particles (size $\sim 50 \mu\text{m}$). The droplets were formed in a dispersion of tracer particles ($\sim 35 \mu\text{m}$) in castor oil and subjected to an E -field strength of 170 V mm^{-1} (in the horizontal direction) yielding steady-state droplet deformations. The asymmetry of the flow fields in (a) and (b) was caused by a slow droplet sedimentation causing slightly nonuniform particle distribution (more particles on the top of a droplet). The particle coverage was (a) and (d) ~ 0.25 , (b) and (e) ~ 0.55 , and (c) and (f) ~ 0.9 .

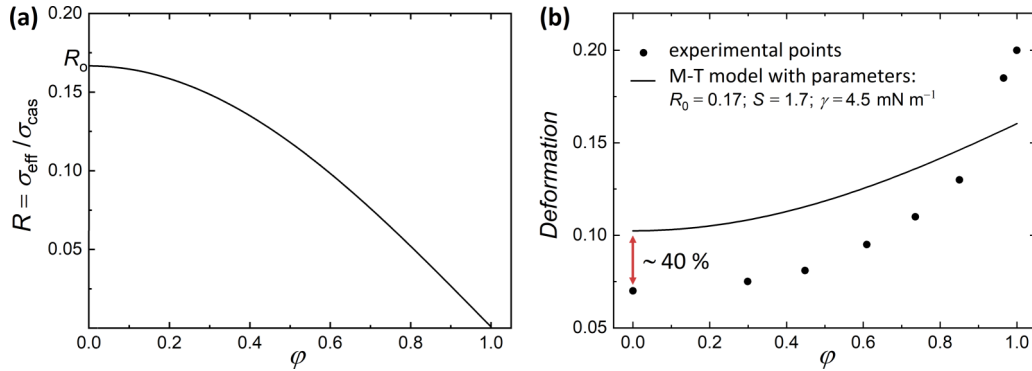


FIG. 4. (a) The electrical conductivity ratio (R) plotted as function of the particle coverage (φ). (b) The magnitude of the droplet deformation (D) plotted as a function of droplets' particle coverage. The solid line is obtained by using the Melcher-Taylor equation in which the trigonometric dependency for the effective electrical conductivity [see panel (a)] is included.

covered by the particles. This leads to the buildup of a greater number of charges at the droplet's interface, which, in turn, deforms the droplet more.

We will now estimate the change in the effective conductivity of the particle covered droplet and examine its effect on the magnitude of droplet's deformation. We recall that the EHD flows convect the particles towards the electric equator. Thus, by adding particles to the droplet's interface, the particle shell widens towards the droplet's electric pole. The contribution of the particles' conductivity to the effective electric conductivity of the droplet's interface is practically zero for those particles residing at the droplet's electric equator. We know that the surface charge density distribution on a droplet scales as $\cos(\theta)$ [55], where θ is the angle measured from the zenith direction. Therefore, the particles nearest to the droplet's electric pole should contribute the most to the change in the effective conductivity. We, thus, attempt to represent the effective conductivity by the cosine function,

$$\sigma_{\text{eff}}(\varphi) = \sigma_{\text{sil}} \cos\left(C_1 \frac{\pi}{2} \varphi\right), \quad (2)$$

where the prefactor $C_1 = 0.9999$ is introduced to obtain the finite value of the conductivity when $\varphi = 1$, which is here the conductivity of PE particles. For simplicity, we assumed that φ scales linearly with θ , and θ is in the range of $0-90^\circ$ for φ in the range of $0-1$. The calculated values of the conductivity ratio (R), using Eq. (2), are plotted in Fig. 4(a). Taking into account this trigonometric dependency in the Melcher-Taylor equation [Eq. (1)], we calculated values of $D(\varphi)$ and plotted them in Fig. 4(b) (see the solid black curve).

The theoretical results capture the upward bending trend with the particle coverage. Although, the magnitude of deformation is overestimated for φ values in the low range. This is what we expected: The Melcher-Taylor model does not take into account straining flows present at low particle coverage. The straining EHD flows affect the deformation by reducing its magnitude. As presented in Ref. [40] (see Fig. 7), the magnitude of droplet's deformation can be reduced by around 30% compared to that estimated from the Melcher-Taylor model. In our case the value of the droplet's deformation is smaller by around 40% compared to the calculated value. The reason for this could be the experimental procedure in which the droplet is docked into the washer. As mentioned before, docking the

droplet into the washer results in reduced magnitude of deformation by up to 15%. As the particle coverage increases, the difference between the experimental and the theoretical points decreases, and at high φ values, the magnitude of deformation is underestimated. This is because the Melcher-Taylor theory does not represent well such large deformations. In addition, the presence of surface particles may influence the surface tension. Ouriemi and Vlahovska [22] showed that the surface tension can be significantly reduced by adding particles to the droplet's interface, which resulted in the increased magnitude of the deformation. Overall, the tendency illustrated in Fig. 4(b) confirms the above stated hypothesis that the decreased effective electrical conductivity of the droplet interface enhances the compressive electric stress acting on the droplet. However, nontrivial numerical calculations would be needed to better represent the experimental data.

We also observed the emergence of the hysteresis loops as the particle coverage was increased [see Fig. 2(d)]. The hysteresis loop area does not change much for the droplets with low particle coverage. However, above coverage of around 0.65 the increase is sharp. The hysteresis loop is an indication of the energy dissipation. In the studied system, the energy can be dissipated through heat and viscous drag. The decoupling of these contributions and the estimation of the amounts of energy loss from the heat dissipation and the viscous drag is nontrivial and is beyond the scope of this paper. Nevertheless, we note that during the droplet compression and recovery, the particles relocate separately or through particle gliding and rotate dissipating the energy. In addition, (as it will be presented in the section Jamming of a particle shell) shells composed of smaller particles ($5 \mu\text{m}$ or smaller) undergo fracturing, which indicates that they form cohesive films, which may affect droplet's deformation and relaxation. We, therefore, decided to study this more closely by investigating the role of particle size on droplet deformation and relaxation.

B. Influence of particle size on droplet deformation and recovery of a particle shell

We performed an experiment with five silicone oil droplets ($\sim 4 \text{ mm}$), each covered with different sizes of PE particles (from 3 to $100 \mu\text{m}$). In the experiment, the E field was swept $0 \leftrightarrow 270 \text{ V mm}^{-1}$ in the same manner as in the previous

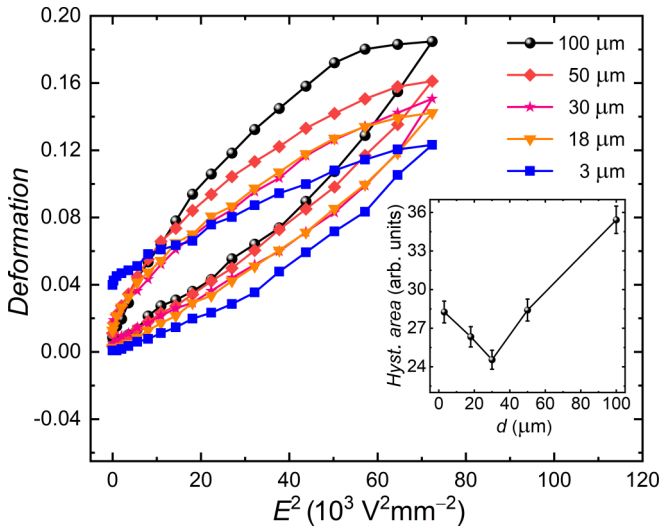


FIG. 5. Effect of the particle size on the hysteresis area of droplet deformation: Five silicone oil droplets (~ 4 mm), each covered with different sizes of PE particles (from 3 to 100 μm) subjected to E fields. The magnitude of steady-state deformation of the droplet plotted against the square of the E field that was increased stepwise from 0 to 270 V mm^{-1} and then decreased stepwise to 0 V mm^{-1} . The inset plot shows the estimated hysteresis area plotted against the particle size. The data reveal the threshold of particle size (30 μm), below which the hysteresis area grows due to the presence of residual deformation of a particle-covered droplet (when the E field is turned off).

experiment. The results presented in Fig. 5 show that the magnitude of droplet deformation is consistently lower for the droplet covered with the smaller particles at all E -field strengths.

This result was surprising for us—we expected the opposite trend, i.e., the magnitude of droplet deformation to be consistently lower for droplets covered with the bigger particles. We initially assumed that the tangential component of the electric stress (everywhere on the droplet’s interface, except the droplet’s electric pole and equator, the electric force acting on accumulated free charges has two components: normal and tangential) should be balanced by the bending stiffness of the elastic particle shell that would deform out of plane. In such a case, shells made of particles with larger diameter (d) should withstand greater electric stress as the bending stiffness (B) of a particle monolayer formed on liquid-liquid or liquid-air interface scales as $B \sim d^2$ [48,56]. However, after taking a closer look on what was happening with particles at the droplet’s electric pole (we viewed the droplet subjected to E fields with a direction along the E field), we understood that particle interlocking and/or rearranging had to play an important role. Particle shells made of small particles are typically more cohesive comparing to a shell formed of larger particles. Thus, it should be more difficult to rearrange particles during the compression and, hence, more difficult to deform the droplet covered by smaller particles.

The increased magnitude of the deformation for larger particles may also have an electric origin. Therefore, we decided to perform calculations and estimate the contribution of the particle size to the change in the electrical conductivity of

the droplet’s interface and, thus, to the magnitude of droplet deformation. The heterogeneous electrical characteristics of the particle-covered droplet, such as particle shell’s electrical conductivity and electrical conductivity of the droplet can be replaced by the equivalent homogeneous electrical conductivity σ_{eq} using the expression [57,58],

$$\sigma_{\text{eq}} = \sigma_{\text{PE}} \frac{2(1 - \beta)\sigma_{\text{PE}} + (1 + 2\beta)\sigma_{\text{sil}}}{(2 + \beta)\sigma_{\text{PE}} + (1 - \beta)\sigma_{\text{sil}}},$$

$$\beta = \left(1 - \frac{d}{2a}\right)^3, \quad (3)$$

where, d is the polyethylene particle diameter and a is the radius of the droplet.

According to Eq. (3), the conductivity ratio ($R = \sigma_{\text{eq}}/\sigma_{\text{cas}}$) decreases with the particle diameter as illustrated in Fig. 6(a). In Fig. 6(b), we plot the droplet deformation (subjected to the E -field strength of 270 V mm^{-1}) as a function of particle radius plotted using Melcher-Taylor’s equation [Eq. (1)] with the conductivity ratio. Although the deformation increases with the increase in particle radius, the calculated difference in the magnitude of deformations due to the particle size is much smaller than that observed experimentally (Fig. 5). Thus, the mechanical properties of the particle shell seem to dominate over the electric contribution or a different model has to be used than the membrane model [Eq. (3)].

As can be observed in Fig. 5, the strain-stress curve is not a complete hysteresis loop for the droplet covered with the smallest particles (3 and 18 μm). In the inset of Fig. 5, we plot the hysteresis area against the particle size. From that plot we learn that there is a particle size threshold below which, the hysteresis area grows due to the presence of residual deformation of a particle-covered droplet (when the E field is turned off). For better comprehension of the origin of this behavior, we performed experiments in which we studied the effect of different E -field strengths and particle sizes on a droplet’s deformation. Four droplets, each covered with particles of different average size ranging from 3 to 100 μm , were subjected to six E -field cycles, each cycle with a different maximum field strength.

In Figs. 7(a) and 7(b), we plotted the magnitude of droplet deformation against the square of the applied E field for two (out of four) droplets with shells composed of 100- and 3- μm PE particles, respectively. As expected, the hysteresis area increased with the increase of the E -field strength—the more work performed on the particle-covered droplet, the more energy is dissipated. However, when sweeping the E field down to zero the curves did not come back to their original points. This is particularly apparent for the droplet covered with the smallest particles [see Fig. 7(b)]. It turns out that the magnitude of the residual deformation ($\Delta D = d_r - d_i$, where d_i and d_r are the shapes of the initial droplet before application of the E field and the relaxed droplet after the sweeping cycle, respectively) depends on both the maximum E -field strength and the particle size. In Fig. 7(c), we plotted the residual deformation (ΔD) against the maximum strength of the E field applied during the sweeping. The results demonstrate that the magnitude of ΔD generally increases continuously with the increase in the maximum strength of the E field. The data for the three droplets for which we see the residual deformation is

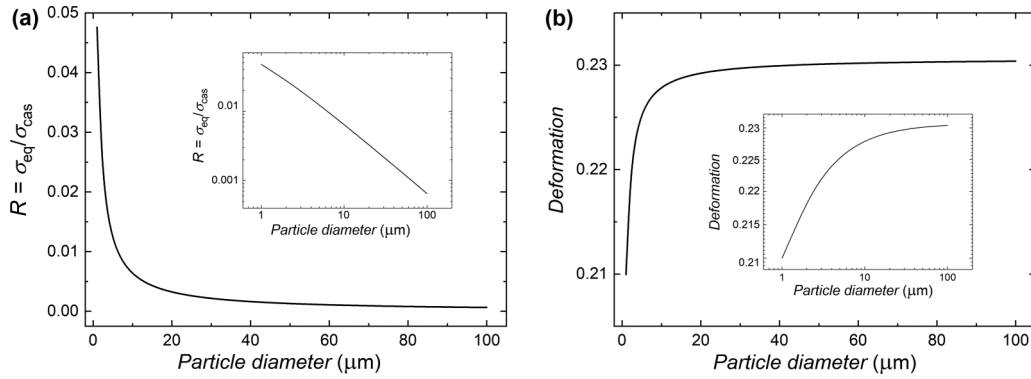


FIG. 6. (a) The electrical conductivity ratio (R) plotted as function of the particle diameter (d). The equivalent conductivity of the particles shell changes with the thickness of the film as expressed by Eq. (3). (b) The magnitude of the droplet deformation (D) is plotted as a function of the particle diameter (d). The inset figures in both panels are the log-log plots.

also presented in a log-log plot of ΔD versus D [see Fig. 7(d)]. The plot reveals that ΔD is ultimately proportional to D (the slope of 1 is included for a reference) within the used strengths of the E field. In addition, ΔD increases with the decrease in the particle size. This may indicate that the particles within the shell undergo structural changes and jam before the droplet fully relaxes. When lowering the E -field strength, the particles move on the curved surface back towards the droplet's electric pole. To be able to accommodate the particles and pack them densely, they need to move and rearrange without any restrictions. Otherwise, the particles jam and form an arrested

shell, preventing the droplet from returning to its spherical shape. We decided to further study the jamming of particles by viewing the droplet along the E -field direction.

C. Jamming of a particle shell

In Fig. 8, we present the results of an experiment on three droplets covered with PE particles of different sizes (diameter 3, 18, and 100 μm). The droplets (viewed along the E -field direction through transparent ITO electrodes) were subjected to $E = 180 \text{ V mm}^{-1}$ for around 1 min and after that the E

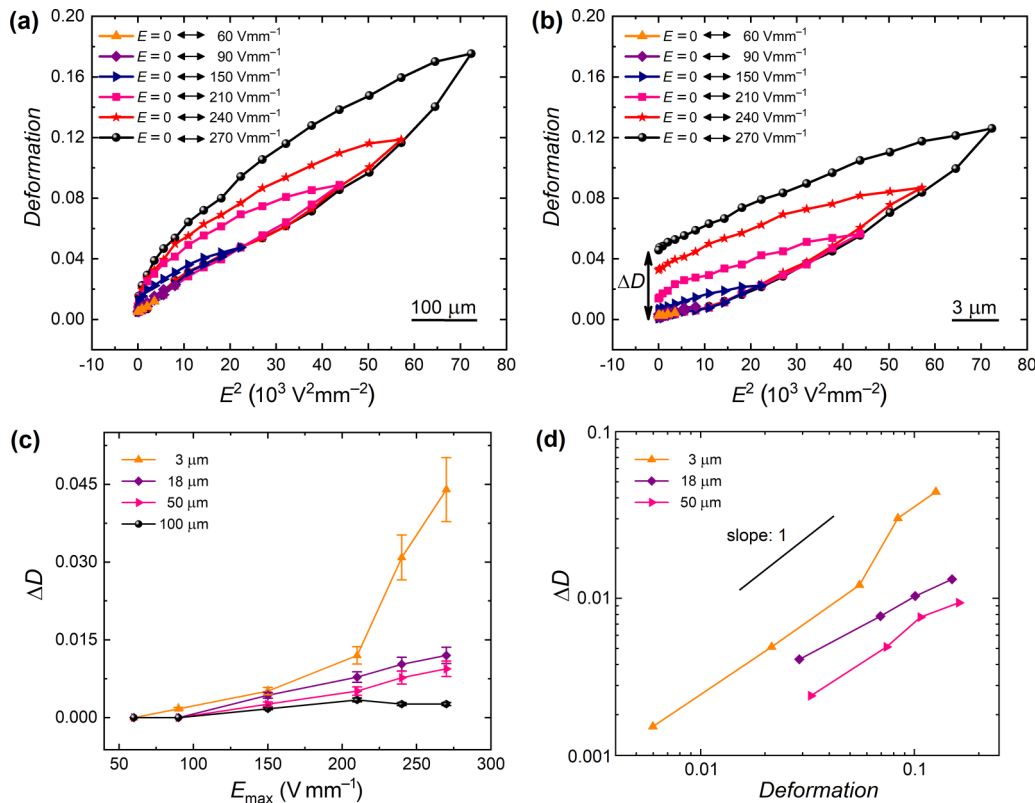


FIG. 7. Effect of the E field on the hysteresis area of droplet deformation: Droplets of diameter $\sim 4 \text{ mm}$ fully covered by PE particles with different particle sizes (a) $\sim 100 \mu\text{m}$ and (b) $\sim 3 \mu\text{m}$ were subjected to different E -field strengths for six cycles. (c) Residual deformation (ΔD) of the four particle-covered droplets plotted against the maximum E -field strength. (d) A log-log plot of ΔD versus D for the three droplets (covered with particles in the size range of 3–50 μm) for which the residual deformation is observed.

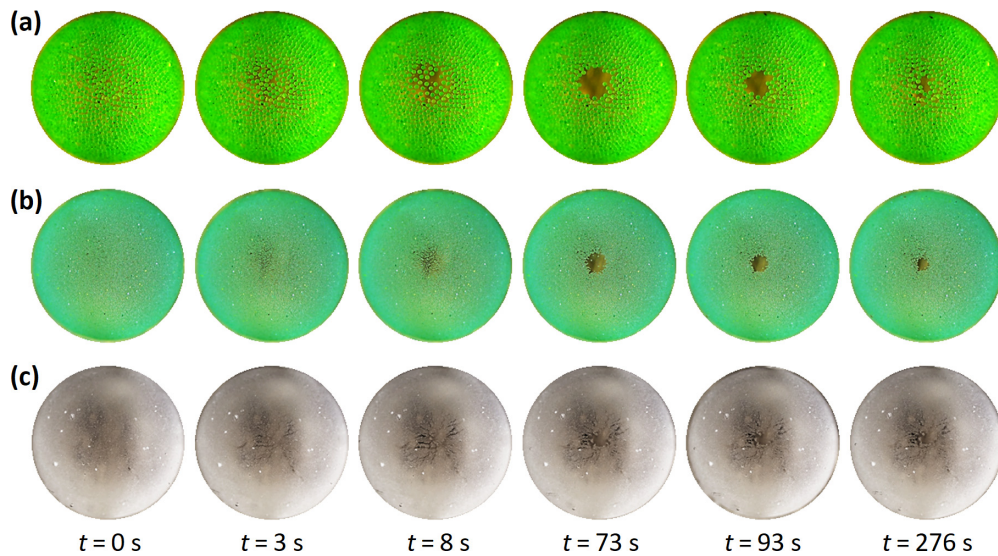


FIG. 8. Opening and closing of PE particle shells made of (a) $100\ \mu\text{m}$, (b) $18\ \mu\text{m}$, and (c) $3\ \mu\text{m}$. Initially at $t = 0\ \text{s}$, the particle shells were spherical in shape. Application of the E field of strength $180\ \text{V mm}^{-1}$ (up to $t = 73\ \text{s}$) resulted in (a) and (b) liquifying and (c) fracturing of a particle shell leading to formation of a hole at the droplet's electric pole. After the E field was turned off, the droplet relaxed back and opening area at pole decreased by around 75%, 50%, and 25% for the shells made of 100-, 18-, and 3- μm PE particles, respectively.

field was turned off enabling droplets to relax. As shown in Figs. 8(a) and 8(b), the application of the E field to the droplets covered with 100- and 18- μm PE particles resulted in formation of a small opening at the electric pole of each droplet. The particles separated very easily from one another, and the particle layer liquified. The openings had circular shapes without any fracturing features. After switching off the E field, the droplets relaxed returning nearly to the spherical shapes. The size of the opening was reduced by around 75%

and 50% for the shells made of 100- and 18- μm PE particles, respectively. The behavior of the shell composed of the smallest PE particles was different. Unlike the two other shells, the shell made of 3- μm PE particles fractured during the droplet compressive deformation [see Fig. 8(c)]. A small hole was formed in the particle shell that recovered very little (around 25%) after turning off the E field, leaving unhealed cracks. The reason for this could be the increased cohesive force between the particles (which is inversely proportional to particle

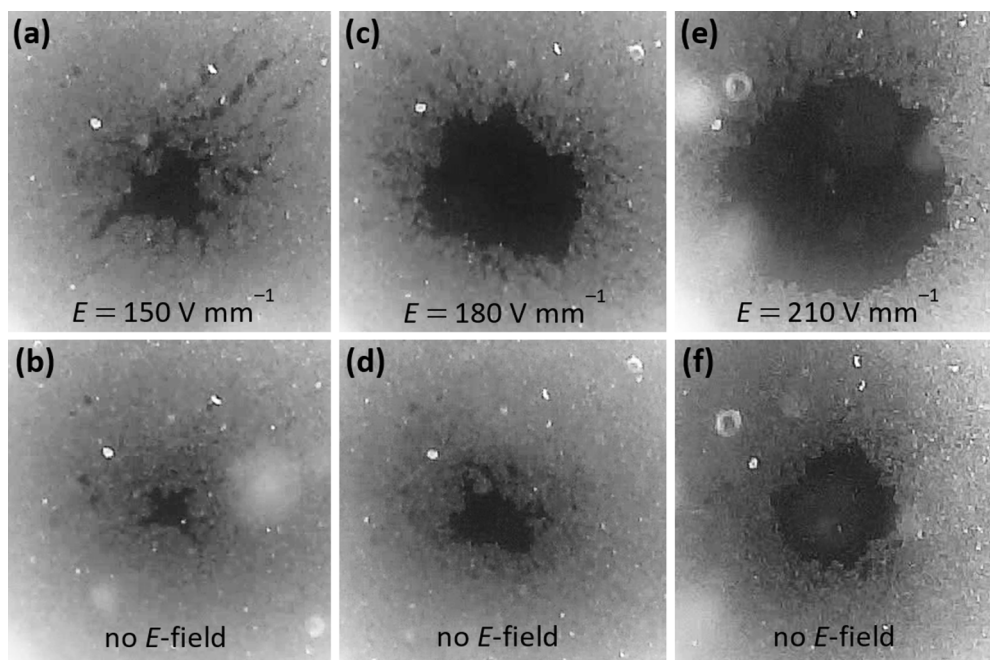


FIG. 9. Opening and closing of clay mineral particle shell under different E -field strengths. The camera view is along the direction of the applied E field. The droplet is subjected to an E -field strength of (a) $150\ \text{V mm}^{-1}$, (c) $180\ \text{V mm}^{-1}$, (e) $210\ \text{V mm}^{-1}$, and in panels (b), (d), and (f) the E field is turned off, respectively. See also the corresponding Movie S1 in the Supplemental Material [52].

size [59]) that prevents the individual particle's rearrangement during the droplet relaxation and/or the increase in packing density of particles forming the shell. We know from our previous experiments that clay mineral particles suspended in oils form cohesive films [52]. Therefore, we decided to perform an additional experiment in which we formed a clay mineral particles shell on a silicone oil droplet to compare its behavior with that of the PE particle shells.

In Fig. 9, we present the results of an experiment on a droplet covered with Li fluorohectorite clay mineral particles (average size $\sim 5 \mu\text{m}$) subjected to different E -field strengths ($150\text{--}210 \text{ V mm}^{-1}$). Typically, clay mineral particles adhere to each other strongly when suspended in oil due to the presence of small amounts of water (in the clay). Therefore, they form an elastic membrane that fractures under the load unlike a sheet made of noncohesive particles that liquefies under the load [60]. When a weak E field (150 V mm^{-1}) was applied, the clay particle shell fractured as shown in Fig. 9(a). The fracturing is similar to that observed for the shell made of the smallest ($3\text{-}\mu\text{m}$) PE particles presented in Fig. 8(c). At stronger E fields ($180\text{--}210 \text{ V mm}^{-1}$), the EHD flows ripped off small fragments of clay particle clusters and redistributed them within the droplet's surface and a nearly spherical opening was formed on the droplet's electric pole with a size depending on the strength of the E field (see Figs. 9(c) and 9(e) and Supplemental Material [52] Movie S1). After turning off the E field the particle-covered droplet relaxed. However, the droplet did not return to the initial spherical shape. Similar to the experiments with small PE particles [Figs. 7(b) and 8(c)], the clay mineral particles jammed and formed an arrested shell, leaving the hole in the particle shell. The size of the hole depended on the magnitude of the E field, i.e., the stronger the applied E fields, the larger the remaining hole in the shell after E field removal. The high cohesiveness between particles inhibits particle relocation when the droplet with the particle shell relaxes after turning off the E field. This, in turn, leads to particle jamming before the opening in the shell is healed.

VI. CONCLUSIONS

We used E fields to study the behavior of both a particle-covered droplet and a particle shell under compressive stress. Unlike the mechanical approaches (e.g., using a micropipette or a micromanipulator [61,62]), the E -field methods enable contactless application of stress and measurement of droplet deformation simultaneously with the examination of mechanical properties of the particle shell. We wondered how the particle coverage and the particle size as well as the strength of the E field influenced the magnitude of the droplet deformation. The experimental results indicate that adding particles to a droplet interface drastically changes the magnitude of the droplet deformation. With the PIV experiments we have shown that the straining flows were suppressed by the addition of particles to the droplet's surface, which, in turn, enabled for generation of greater electric stress acting on the droplet. We also performed theoretical calculations to capture the upward bending trend of the magnitude of droplet deformation as a function of the particle coverage. Our experimental results on the particle coverage dependency of the magnitude of deformation differ from those presented by Ouriemi and

Vlahovska [22]. The researchers observed that the magnitude of the droplet deformation becomes less sensitive to the particle coverage at high coverages. This is not the case here, i.e., the magnitude of deformation clearly increases with the particle coverage until the droplet is entirely covered. Perhaps, the difference in the observations originates from the fact that Ouriemi and Vlahovska studied deformation of droplets unattached to any surface and the measurements were performed in the narrower range of E -field strengths. This would require further investigations.

We also found that the magnitude of the deformation is not retraceable during the electric-field sweeping, i.e., the strain-stress curves form a hysteresis loop with the area increasing with the increase in the E -field strength. We observed that during the droplet compression and recovery, the particles relocate separately or through particle gliding and rotate dissipating the energy. The particle rotation and gliding were documented as contributing to the friction by Mikkelsen *et al.* [27]. In addition, shells composed of small particles fractured during the droplet compression, indicating that they form cohesive films, which greatly affected droplet's deformation and relaxation.

The smallest particles were more prone to jamming and formed arrested shells on relaxed droplets. Stable nonspherical droplets and bubbles created by the interfacial jamming of arrested shells have been studied by other researchers [12,29,63]. However, in many studies the jammed state was achieved by increasing the particle concentration (by addition of particles to the interface or coalescing particle-covered droplets). Here, the jamming occurs due to the change in the particle arrangement, whereas the particle concentration remains unchanged. We believe, that the electric method demonstrated here can be used as a noncontact indenter to study and understand the stability of curved colloidal or granular crystals and amorphous particle shells under load [64].

The results of our studies are important for developing an understanding of the mechanics and rheology of monolayered colloidal and granular shells formed on droplets (or other curved interfaces) and the surface particle organization as well as the behavior of particle-covered droplets probed by induced stress. We demonstrated that E -field-induced droplet deformation was accompanied by structural and morphological changes in the particle shell. This can be exploited in multiple ways, for example, to form and study buckled armored droplets and plastic rearrangements of the particle shell as well as to investigate fracturing of cohesive films on curved surfaces.

The results of our research go beyond the academic sphere and have practical relevance. For example, a particle-covered droplet can be used as a miniaturized optical diaphragm with an adjustable aperture [46]. Controlling reliably the light passage through such a diaphragm requires the knowledge on mechanical properties of a particle shell that opens and closes *via* application of an E field. With the results presented here, we can now better design such a responsive optical element.

To further extend the research presented here, we suggest the future experimental studies to investigate the influence of particle properties (e.g., electrical conductivity and particle packing) on the stability and mechanics of particle shells under E fields.

ACKNOWLEDGMENTS

This research was funded by the Polish National Science Centre through PRELUDIUM (Grant No. 2019/35/N/ST5/02821) and OPUS (Grant No. 2015/19/B/ST3/03055) and programmes. We also thank the Research Council of Norway for its support through the Centres of Excellence funding scheme, Project No. 262644.

K.K. initiated the project, designed, and performed all of the experiments. T.H. performed the theoretical calculations. K.K. authored the first draft of the paper. K.K., T.H., and Z.R. took part in discussions towards the finalization of the paper. All authors have read and agreed to the published version of the paper.

The authors declare no conflict of interest.

-
- [1] E. Dickinson, *Curr. Opin. Colloid Interface Sci.* **15**, 40 (2010).
- [2] T. Bollhorst, K. Rezwan, and M. Maas, *Chem. Soc. Rev.* **46**, 2091 (2017).
- [3] D. Venkataramani, A. Tsulaia, and S. Amin, *Adv. Colloid Interface Sci.* **283**, 102234 (2020).
- [4] C. L. G. Harman, M. A. Patel, S. Guldin, and G.-L. Davies, *Curr. Opin. Colloid Interface Sci.* **39**, 173 (2019).
- [5] J. Lee and T. Babadagli, *J. Dispers. Sci. Technol.* **41**, 2048 (2020).
- [6] A. Mikkelsen, K. Khobaib, F. K. Eriksen, K. J. Måløy, and Z. Rozynek, *Soft Matter* **14**, 5442 (2018).
- [7] P. Dommersnes, Z. Rozynek, A. Mikkelsen, R. Castberg, K. Kjerstad, K. Hersvik, and J. O. Fossum, *Nat. Commun.* **4**, 2066 (2013).
- [8] V. O. Ikem, A. Menner, T. S. Horozov, and A. Bismarck, *Adv. Mater.* **22**, 3588 (2010).
- [9] S. N. Yin, C. F. Wang, S. S. Liu, and S. Chen, *J. Mater. Chem. C* **1**, 4685 (2013).
- [10] J. Wang *et al.*, *Lab Chip* **17**, 1970 (2017).
- [11] R. Bielas, D. Surdeko, K. Kaczmarek, and A. Józefczak, *Colloids Surf., B* **192**, 111070 (2020).
- [12] Z. Rozynek, A. Mikkelsen, P. Dommersnes, and J. O. Fossum, *Nat. Commun.* **5**, 3945 (2014).
- [13] Z. Rozynek and A. Józefczak, *Eur. Phys. J. ST* **225**, 741 (2016).
- [14] V. N. Manoharan, *Science* **349**, 1253751 (2015).
- [15] W. T. Irvine, V. Vitelli, and P. M. Chaikin, *Nature (London)* **468**, 947 (2010).
- [16] Z. Rozynek, J. Banaszak, A. Mikkelsen, K. Khobaib, and A. Magdziarz, *Soft Matter* **17**, 4413 (2021).
- [17] F. Sicard and A. Striolo, *Nanoscale* **9**, 8567 (2017).
- [18] Z. Rozynek, R. Bielas, and A. Józefczak, *Soft Matter* **14**, 5140 (2018).
- [19] C. P. Whitby and E. J. Wanless, *Materials* **9**, 626 (2016).
- [20] K. Hwang, P. Singh, and N. Aubry, *Electrophoresis* **31**, 850 (2010).
- [21] J. K. Ferri, P. Carl, N. Gorevski, T. P. Russell, Q. Wang, A. Boker, and A. Fery, *Soft Matter* **4**, 2259 (2008).
- [22] M. Ouriemi and P. M. Vlahovska, *Langmuir* **31**, 6298 (2015).
- [23] C. Gu and L. Botto, *Soft Matter* **12**, 705 (2016).
- [24] R. B. Karyappa, S. D. Deshmukh, and R. M. Thakkar, *Phys. Fluids* **26**, 122108 (2014).
- [25] L. Becu and L. Benyahia, *Langmuir* **25**, 6678 (2009).
- [26] A. B. Pawar, M. Caggioni, R. Ergun, R. W. Hartel, and P. T. Spicer, *Soft Matter* **7**, 7710 (2011).
- [27] Y. Mei, G. Li, P. Moldenaers, and R. Cardinaels, *Soft Matter* **12**, 9407 (2016).
- [28] A. Mikkelsen, P. Dommersnes, and J. O. Fossum, *Rev. Cub. Fis.* **33**, 47 (2016).
- [29] M. Cui, T. Emrick, and T. P. Russell, *Science* **342**, 460 (2013).
- [30] Y. Rane, E. Foster, M. Moradiafrapoli, and J. O. Marston, *Powder Technol.* **338**, 7 (2018).
- [31] S. Y. Tan, R. F. Tabor, L. Ong, G. W. Stevens, and R. R. Dagastine, *Soft Matter* **8**, 3112 (2012).
- [32] D. Zang, J. Li, Z. Chen, Z. Zhai, X. Geng, and B. P. Binks, *Langmuir* **31**, 11502 (2015).
- [33] X. Liu *et al.*, *Science* **365**, 264 (2019).
- [34] M. S. Abbasi, H. Farooq, H. Ali, A. H. Kazim, R. Nazir, A. Shabbir, S. Cho, R. Song, and J. Lee, *Materials* **13**, 2984 (2020).
- [35] A. Mikkelsen, P. Dommersnes, Z. Rozynek, A. Gholamipour-Shirazi, M. d. S. Carvalho, and J. O. Fossum, *Materials* **10**, 436 (2017).
- [36] A. Mikkelsen, Z. Rozynek, K. Khobaib, P. Dommersnes, and J. O. Fossum, *Colloid. Surf., A* **532**, 252 (2017).
- [37] P. M. Vlahovska, *Annu. Rev. Fluid Mech.* **51**, 305 (2019).
- [38] Z. Rozynek, R. Castberg, A. Kalicka, P. Jankowski, and P. Garstecki, *Arch. Mech.* **67**, 385 (2015).
- [39] G. I. Taylor, *Proc. R. Soc.* **291**, 159 (1966).
- [40] D. Das and D. Saintillan, *J. Fluid Mech.* **810**, 225 (2017).
- [41] J. W. Ha and S. M. Yang, *Phys. Fluids* **12**, 764 (2000).
- [42] P. F. Salipante and P. M. Vlahovska, *Phys. Fluids* **22**, 112110 (2010).
- [43] D. Das and D. Saintillan, *J. Fluid Mech.* **914**, A22 A22,(2021).
- [44] M. Ouriemi and P. M. Vlahovska, *J. Fluid Mech.* **751**, 106 (2014).
- [45] P. Siahcheshm, F. Goharpey, and R. Foudazi, *Rheol. Acta* **57**, 729 (2018).
- [46] Z. Rozynek, K. Khobaib, and A. Mikkelsen, *ACS Appl. Mater. Interfaces* **11**, 22840 (2019).
- [47] Y. Xue, H. Wang, Y. Zhao, L. Dai, L. Feng, X. Wang, and T. Lin, *Adv. Mater.* **22**, 4814 (2010).
- [48] A. Mikkelsen and Z. Rozynek, *ACS Appl. Mater. Interfaces* **11**, 29396 (2019).
- [49] M. Kaganyuk and A. Mohraz, *Soft Matter* **16**, 4431 (2020).
- [50] C. Monteux, J. Kirkwood, H. Xu, E. Jung, and G. G. Fuller, *Phys. Chem. Chem. Phys.* **9**, 6344 (2007).
- [51] H. Xu, S. Melle, K. Golemanov, and G. Fuller, *Langmuir* **21**, 10016 (2005).
- [52] See Supplemental Material at <http://link.aps.org/supplemental/10.1103/PhysRevE.103.062605> for [brief description].
- [53] J. R. Melcher and G. I. Taylor, *Annu. Rev. Fluid Mech.* **1**, 111 (1969).
- [54] D. A. Saville, *Annu. Rev. Fluid Mech.* **29**, 27 (1997).
- [55] J. Q. Feng and P. Roy, *Proc. R. London, Ser A* **455**, 2245 (1999).

- [56] D. Vella, P. Aussillous, and L. Mahadevan, *Europhys. Lett.* **68**, 212 (2004).
- [57] A. Morshed, P. Dutta, M. R. Hossan, and R. Dillon, *Phys. Rev. Fluids* **3**, 103702 (2018).
- [58] M. Pavlin and D. Miklavcic, *Biophys. J.* **85**, 719 (2003).
- [59] H. Shi *et al.*, *KONA Powder Part. J.* **35**, 226 (2018).
- [60] Z. Rozynek, P. Dommersnes, A. Mikkelsen, L. Michels, and J. O. Fossum, *Eur. Phys. J.: Spec. Top.* **223**, 1859 (2014).
- [61] O. I. Vinogradova, O. V. Lebedeva, and B. S. Kim, *Annu. Rev. Mater. Res.* **36**, 143 (2006).
- [62] M. P. Neubauer, M. Poehlmann, and A. Fery, *Adv. Colloid Interface Sci.* **207**, 65 (2014).
- [63] A. B. Subramaniam, M. Abkarian, L. Mahadevan, and H. A. Stone, *Nature (London)* **438**, 930 (2005).
- [64] K. Khobaib, A. Mikkelsen, T. Vincent-Dispot, and Z. Rozynek, *Soft Matter* **17**, 5006 (2021).

SUPPORTING INFORMATION

A particle-covered droplet and a particle shell under compressive electric stress

Khobaib Khobaib¹, Tomasz Hornowski¹, Zbigniew Rozynek^{1,2}

¹ Faculty of Physics, Adam Mickiewicz University, Uniwersytetu Poznańskiego 2, Poznań 61-614, Poland;

² PoreLab, The Njord Centre, Department of Physics, University of Oslo, N-0316 Oslo, Norway;

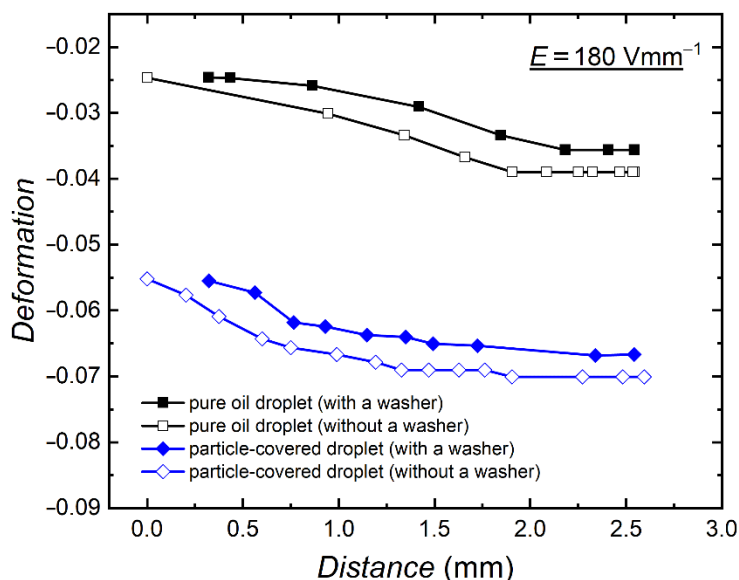


FIG. S1. Influence of the washer on the droplet's deformation: Pure droplet and 50- μm PE particle-covered droplet (diameter of around 3.5 mm) subjected to E -field strength of 180 V mm^{-1} . The droplets' deformation was studied at different distance in respect to the electrode (being a wall of the sample cell). Two sample cells were used: with and without a washer attached to the electrode. It can be seen that the presence of the washer influenced only slightly (by less than 15%) the magnitude of droplets' deformation.

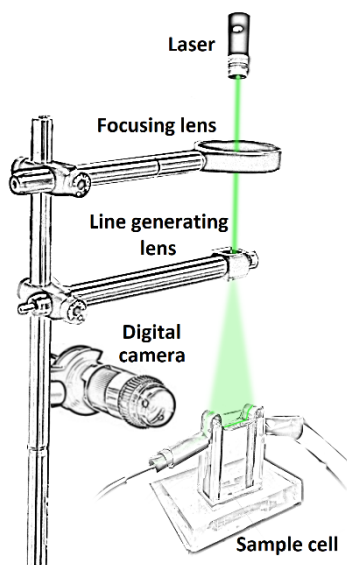


FIG. S2. Experimental setup to estimate flowlines around the droplet: The experimental setup consisted of a sample cell, a digital microscope to view flowlines around the droplet (perpendicular to the direction of the electric field), a 532-nm laser light (COM-09906-5mW laser, purchased from SparkFun Electronics), a lens for generating a 500- μm thin laser line by fanning out one-dimensional collimated beam. The laser sheet was aligned in the middle of the droplet and the droplet was placed in the centre of the sample cell.

Paper VI

Electrorotation of particle-coated droplets: from fundamentals to applications

Z Rozynek, J Banaszak, A Mikkelsen, K Khobaib and A Magdziarz

Soft Matter **17**, 4413–4425 (2021)



Cite this: *Soft Matter*, 2021, 17, 4413

Electrorotation of particle-coated droplets: from fundamentals to applications†

Z. Rozynek,^{ib}*^{ab} J. Banaszak,^a A. Mikkelsen,^{ib}^a K. Khobaib,^{ib}^a and A. Magdziarz,^{ib}^a

Electrically insulating objects immersed in a weakly conducting liquid may Quincke rotate when subjected to an electric field. Experimental and theoretical investigations of this type of electrorotation typically concern rigid particles and particle-free droplets. This work provides the basic features of electric field-induced rotation of particle-covered droplets that expand the current knowledge in this area. Compared to pure droplets, we show that adding particles to the droplet interface considerably changes the parameters of electrorotation. We study in detail deformation magnitude (D), orientation (β) and rotation rate (ω) of a droplet subjected to a DC E -field. Our experimental results reveal that both the critical electric field (for electrorotation) and the rotational rate depend on droplet size, particle shell morphology (smooth vs. brush-like), and composition (loose vs. locked particles). We also demonstrate the importance of the electrical parameters of the surface particles by comparing the behavior of droplets covered by (insulating) polymeric particles and droplets covered by (non-ohmic) clay mineral particles. The knowledge acquired from the electrorotation experiments is directly translated into practical applications: (i) to form arrested droplets with shells of different permeability; (ii) to study solid-to-liquid transition of particle shells; (iii) to mix particles on shells; and (iv) to increase the formation efficiency of Pickering emulsions.

Received 22nd January 2021,
Accepted 4th March 2021

DOI: 10.1039/d1sm00122a

rsc.li/soft-matter-journal

1 Introduction

Electric fields (E -fields) can rotate objects suspended in a liquid. There are several different mechanisms for electro-rotation, and these may employ either static or rotating E -fields.^{1–6} This work concerns rotation of particle-covered droplets that are subjected to a static and uniform E -field. The electrorotation studied here is similar to that described more than a century ago by Weiler and Quincke who observed rotation of electrically insulating particles immersed in a weakly conductive liquid.^{7,8}

In short, in the presence of an E -field, free charges (existing in the liquid in which a particle is immersed) accumulate at the surface of a particle and a dipole moment is induced. The direction of this electric dipole (with respect to the direction of the E -field) depends on the electrical properties of both the particle and the liquid, namely the dielectric constant (ϵ) and electrical conductivity (σ). More specifically, if the charge relaxation time of the particle ($\tau_p = \epsilon_p/\sigma_p$) is longer than that of the surrounding

liquid ($\tau_l = \epsilon_l/\sigma_l$), the induced dipole is opposite to the E -field direction. At large enough E -field strength, this configuration becomes unstable and the particle starts rotating in order to flip the direction of the induced dipole. The rotation is sustained if the particle's surface is continuously re-charged by the exterior fluid.

Many experimental and theoretical studies have been conducted on this type of electrorotation (often referred to as Quincke rotation). Initially, the majority of the studies concerned rigid particles. The theory on the rotation frequency of Quincke rotating particles was thus established a long time ago and has since been further developed.^{9–11} The influence of particle shape, size and electrical properties on the rotation rate and critical E -field (at which the rotation of solid particle begins) is now well described.^{12–14}

Meanwhile, several experimental and theoretical studies were performed on electrorotation of droplets.^{15–18} Unlike viscous droplets that deform very little, deformable droplets behave differently than rigid particles when subjected to E -fields.¹⁹ Because of the droplets' ability to deform and the existence of interfacial flow (not present in the case of a rigid body), their dynamics and electrorotation parameters differ from those of the rigid particles.²⁰ For example, the value of the critical E -field (for electrorotation) is typically much higher for droplets compared to that found for particles of the same size and electrical properties.²¹ Unlike a rigid particle, a rotating droplet may also tumble or undergo deformation while rotating

^a Faculty of Physics, Adam Mickiewicz University, Uniwersytetu Poznańskiego 2, 61-614 Poznań, Poland

^b PoreLab, The Njord Centre, Department of Physics, University of Oslo, Blindern, N-0316 Oslo, Norway. E-mail: zbiroz@amu.edu.pl

† Electronic supplementary information (ESI) available: Seven supplementary movies. See DOI: 10.1039/d1sm00122a



(depending on its viscosity).²² Theoretical descriptions of the electrorotation of particle-free droplets are challenging and often require numerical calculations.^{17,23–25} Despite the challenges, this two-phase liquid–liquid system has been well characterized. Much less is known about the electrorotation of droplets covered with particles, and the literature on this system is limited.

Adding particles to the surface of a droplet may significantly change the droplet's behavior and characteristics in E -fields, that is, it may alter the droplet's rheological and mechanical responses.^{26,27} A particle monolayer formed on the droplet's surface may affect the electrical properties of the droplet, and thus enhance or reduce the deformation magnitude of the droplet. Furthermore, the addition of particles suppresses electrohydrodynamic flows by immobilizing the droplet interface and therefore reducing charge convection.²⁸ Ouriemi and Vlahovska^{29,30} performed several experiments on particle-covered droplets and provided new insight into this research area and raised questions, for example on the role of important parameters (such as droplet size, particle type, and particle shell morphology and composition) affecting the electrorotation of particle-covered droplets or the fluid–solid transition of rotating particle shells. We address many of these questions in this work, and also go a step further by demonstrating new applications of electrorotation of particle-covered droplets.

There are several applications of Quincke rotating particles. It has been demonstrated that electrorotation of particles can change properties of that suspension, for example by lowering its effective viscosity or increasing electrical conductivity.^{31,32} Individual Quincke rotating particles are also used as rotors, motors, and micropumps,^{33–35} whereas large populations of electrorotating particles can self-organize into large-scale assemblies.³⁶ Particle rotation can also be used as a model system for studying, for example, collective swarming motion

and active matter.^{37–39} Nevertheless, just a few examples of applications of particle-covered droplets have been presented so far. These include studies on counter-rotating pairs of Pickering droplets and cooperative hydrodynamic propulsion of deformable rotors.⁴⁰ In this work, we demonstrate new uses of electrorotating droplets with particle shells, including their practical application.

2 Materials and methods

2.1. Experimental set-up

The experimental set-up consisted of a signal generator (SDG1025, SIGLENT Technologies), a high-voltage amplifier (20HVA24-BP1, HVP), a digital microscope (AM7315MZT, Dino-Lite) for viewing perpendicular to the direction of the applied E -field, a light source (KL 300 LED, Schott AG), a computer for collecting images and recording videos, and an optical glass cuvette (18 mm × 10 mm × 30 mm) used as a sample cell with two copper plates that constituted electrodes (with a gap of 15.4 mm). The sample cell was placed on a mechanical XYZ translation stage to ease its positioning relative to the optical path of the microscope. A schematic figure illustrating part of the experimental set-up is shown in Fig. 1a.

2.2. Materials

Castor oil (MA-220-1, density of $\sim 0.96 \text{ g cm}^{-3}$ at 25 °C, electrical conductivity of $\sim 50\text{--}100 \text{ pS m}^{-1}$, relative permittivity ~ 4.7 and kinematic viscosity of $\sim 750 \text{ cSt}$ at 25 °C) was purchased from Mareo, Poland. The oil has similar properties to the oil we previously used in our laboratory, that is, the castor oil purchased from Sigma-Aldrich (83912). Silicone oils (Rhodorsil Oils 47, with different viscosities in range 50–10000 cSt at 25 °C, density 0.96–0.97 g cm^{-3} at 25 °C, electrical conductivity of $\sim 5\text{--}10 \text{ pS m}^{-1}$, and

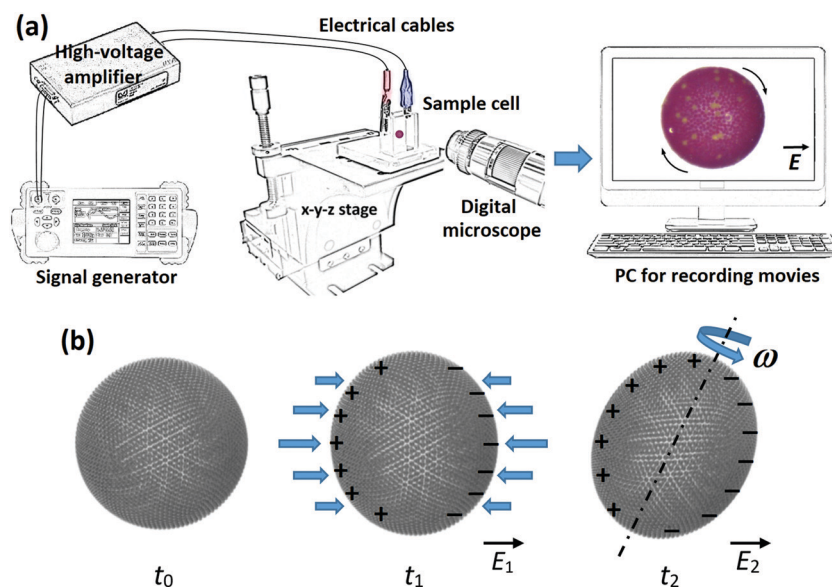


Fig. 1 (a) Schematic figure illustrating part of the experimental set-up. (b) A schematic illustrating the electric field-induced rotation of a particle-covered droplet. Application of an electric field (E_1) to the initially spherical droplet (t_0) results in its compressive deformation due to electric stress. After application of a stronger electric field (E_2), the droplet rotates with a rotation rate (ω).



relative permittivity ~ 2.8) were purchased from VWR Chemicals, USA. Castor oil and silicone oil are immiscible with an interfacial tension between them $\sim 4.5 \text{ mN m}^{-1}$. Polystyrene particles (PS, with a diameter of $\sim 10 \text{ }\mu\text{m}$ and $\sim 40 \text{ }\mu\text{m}$ and density of $\sim 1.05 \text{ g cm}^{-3}$) were bought from Microbeads AS, Norway. The surface of PS particles was modified as described in ref. 41 to change the three-phase contact angle and increase their affinity towards silicone oil so that the particles attach strongly to the oil–oil interface (as in the case of the PE particles). For the surface modification, the ratio of acrylate polymer surface modifier (FluoroPEL PFC 502AFA, Cytonix, USA) to methoxy-nonafluorobutane solvent was 1 : 300. The modified PS particles had density $\sim 1 \text{ g cm}^{-3}$, electrical conductivity $< 10^{-11} \text{ S m}^{-1}$, and relative permittivity ~ 2.6 . Clay mineral particles (Li-fluorohectorite, a synthetic 2 : 1 clay) were received from Prof. J.O. Fossum (NTNU, Trondheim, Norway). Similar clay particles were partially characterized in work.⁴² They were polydisperse in size, from hundreds of nm to $10 \text{ }\mu\text{m}$, density of $\sim 2.5 \text{ g cm}^{-3}$, electric conductivity $\sim 10^{-6} \text{ S m}^{-1}$ and dielectric constant ~ 6 . Polyethylene particles (PE, red coloured and cyan coloured, size of $\sim 50 \text{ }\mu\text{m}$ and density of $\sim 0.98 \text{ g cm}^{-3}$, and blue coloured, size of $\sim 50 \text{ }\mu\text{m}$, and cyan coloured, size of $\sim 30 \text{ }\mu\text{m}$, all with a density of $\sim 1 \text{ g cm}^{-3}$, electrical conductivity $< 10^{-12} \text{ S m}^{-1}$, and relative permittivity ~ 2.1) were purchased from Cospheric LLC, USA.

2.3. Formation of particle-covered droplets

We used an E -field approach (see ref. 43) to form a monolayer particle shell on the surface of a silicone oil droplet. Initially, a silicone oil dispersion of particles was prepared where the particle concentration was adjusted to form a particle-covered droplet of a certain size. A droplet with particles was formed (using a regular mechanical pipette) in a cuvette filled with castor oil. Next, an E -field ($\sim 200 \text{ V mm}^{-1}$) was applied to guide (by electrostatic force) the particles in the bulk liquid of the dispersion droplet toward the droplet's interface. The particles at the droplet interface were irreversibly trapped by capillary force, which in the case of microparticles is a few orders of magnitude greater than the thermal energy.⁴⁴ As the particles reached the surface of the droplet, they were carried toward the electric equator of that droplet by E -field-induced liquid flows. These flows moved particles within the droplet's surface, made them pack into a ribbon-like structure, which gradually widened and eventually (after $\sim 10 \text{ min}$) covered the droplet surface. The shell particles were arranged in a packed and nearly hexagonal structure. In the experiments with droplets covered by PS particles, we added a small amount (a few particles) of coloured PE particles to make it easier to track the particle position and estimate the rotation rate.

We also prepared a droplet covered with a Janus particle shell, *i.e.*, a heterogeneous shell composed of two different particle types (red and blue PE particles). Firstly, we formed two droplets partially covered with particles (around 70% coverage), one with red PE particles and the other one with blue PE particles using the same procedure as described above. The droplets were then mechanically brought into close proximity. Subjected to a DC E -field (200 V mm^{-1}), the droplets attracted

one to another and eventually coalesced forming a droplet with a heterogeneous monolayer shell comprising densely packed particles. This particle-covered droplet was used in the experiment on solid-to-liquid transition of a particle shell.

2.4. Experimental procedures

In our experiments on electrorotation of particle-covered droplets (and pure silicone oil droplets, as well as individual PE and PS particles, used as the reference data), we varied the E -field strength and droplet size, as well as the silicone oil viscosity, and studied (i) changes of the deformation magnitude of droplets, (ii) tilt angle, and (iii) rotation rate. The E -field was always applied in the horizontal direction. At weak E -fields, a particle-covered droplet deforms, and when stronger E -fields are applied the deformed droplet starts rotating, as sketched in Fig. 1b. The deformation is here defined as $D = |(d_1 - d_2)/(d_1 + d_2)|$, where d_1 and d_2 are the droplet minor and major axes, respectively. The tilt angle is measured between the major axis and the vertical direction, *i.e.*, its value is zero when the major axis is normal to the E -field direction.

In the experiments on electrorotation, the strength of the DC E -field was increased stepwise (0 – 835 V mm^{-1}) and each step was maintained for at least 1 minute. The deformation magnitude and rotation rate were calculated by averaging three data points collected at each E -field strength. The tilt angle values are presented using a candlestick chart, which shows the dynamic changes of the tilt values at each E -field strength. Red and blue colours indicate the decrease and increase of the absolute value of the tilt angle within one-minute measurement at a specific E -field strength. The errors included in some plots were estimated using standard deviation of the measurements. In several plots the error bars are omitted for figure clarity. The fundamental studies were followed by experiments demonstrating applications of the E -field method. The details on experimental procedures of these experiments are described in the paragraphs corresponding to the presented data. We used graphical software GIMP (v. 2.10) and Wondershare Filmora (v. 9.5) to edit collected pictures and movies.

3 Results

3.1. Electrorotation of a particle-covered droplet – fundamentals

A medium size droplet (diameter of $\sim 1 \text{ mm}$) of silicone oil (50 cSt) covered by PS particles ($40 \text{ }\mu\text{m}$) was subjected to an E -field. Initially, in the absence of the E -field, the droplet was spherical with a shell composed of densely packed particles. Application of weak E -fields ($< 225 \text{ V mm}^{-1}$) resulted in compressive deformation of the droplet, *i.e.*, the droplet deformed to an oblate shape (see images in Fig. 2a). At the time scale of the experiments conducted at weak fields ($\sim 1 \text{ min}$) we did not observe rotational motion of the droplet. Slow rotation of the particle-covered droplet was observed above 225 V mm^{-1} , and from $\sim 265 \text{ V mm}^{-1}$ the rotation rate increased nearly linearly with the increase of the E -field strength. The images in Fig. 2a show qualitatively the



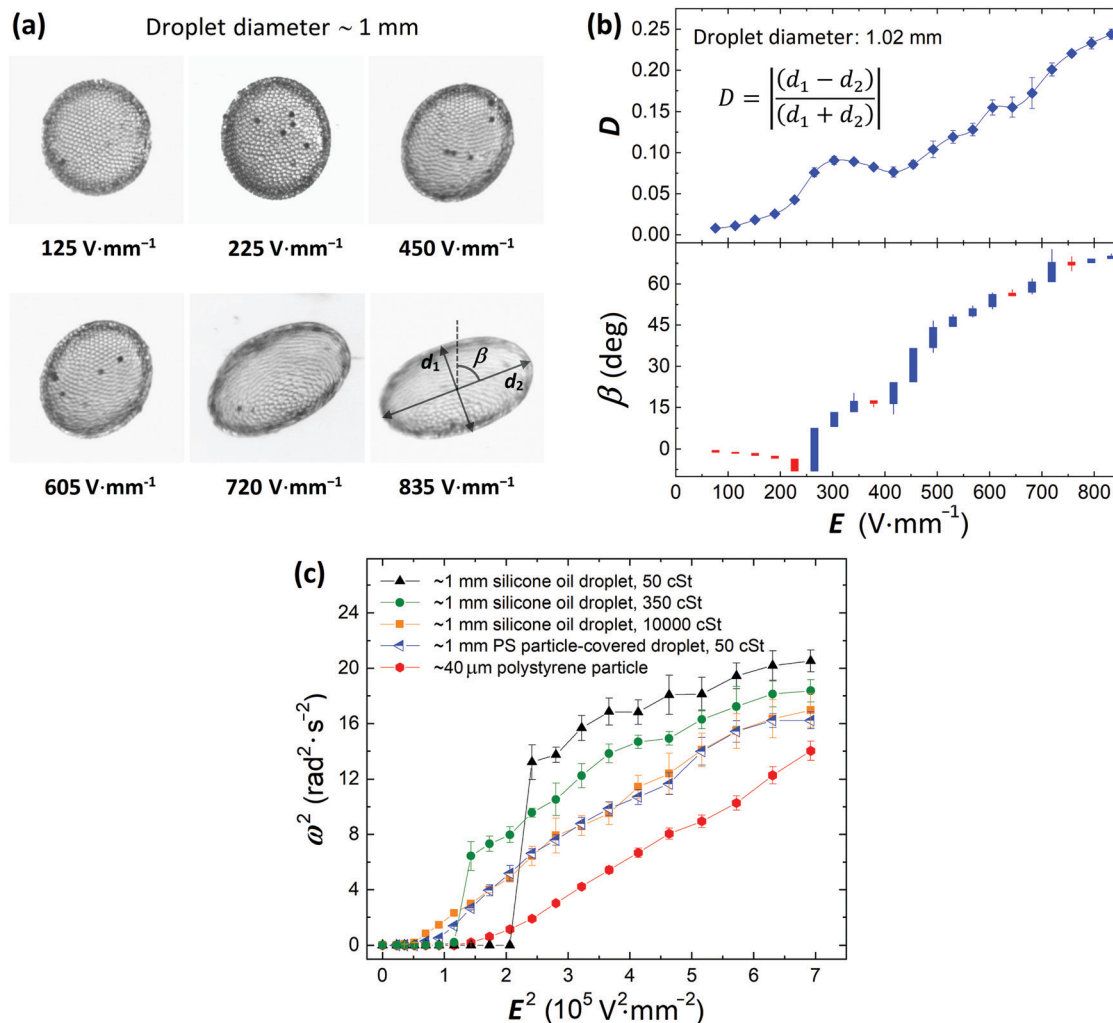


Fig. 2 (a) A silicone oil droplet (diameter of ~ 1 mm) covered by $40 \mu\text{m}$ PS particles and subjected to an E -field. The initially spherical droplet acquired an oblate shape at weak E -fields ($< 225 \text{ V mm}^{-1}$). As the strength of the E -field is increased, the droplet tilts more and rotates. (b) The deformation magnitude and the tilt angle plotted against the E -field strength. The absolute value of the tilt angle steadily increases with the increase of the E -field strength, though the tilt angle changed its sign at $E = 265 \text{ V mm}^{-1}$. The value of the tilt angle also changed in time even at a fixed E -field strength, which can be read from the candlestick chart. (c) The square of the rotation rate of the particle-covered droplet, a $40 \mu\text{m}$ PS particle, and three particle-free silicone oil droplets with different viscosities plotted as a function of the applied E -field squared.

deformation and orientation of the particle-covered droplet at different E -field strengths.

The quantitative analysis is presented in Fig. 2b where we plotted the magnitude of the droplet deformation and the tilt angle *versus* the E -field strength. At weak E -fields (at which droplet rotation was not observed), the magnitude of the deformation grew slightly faster than the square of the E -field strength (see Fig. S1 and the corresponding description for more details, ESI†). However, as the droplet started tilting and rotating, the magnitude of the deformation decreased locally leaving a bump in the D vs. E plot. The peak of this local bump is roughly in the place where the electroration of the droplet was clearly observed. A similar observation was made for clean droplets.¹⁷ As the E -field was further increased, both the magnitude of the deformation and the tilt angle steadily increased. At the strongest E -fields, the droplet rotated very fast ($\sim 4 \text{ rad s}^{-1}$), was stretched rather than being

compressively deformed. When the droplet deforms (while subjected to the E -field) and its surface area increases, the particle coverage decreases. We estimated (*via* image analysis) that the particle coverage for the spherical droplet (before application of the E -field) used in the experiment presented in Fig. 2 is around 0.83. At the strongest E -field, the deformation magnitude of the droplet was around 0.24. At this geometry, the droplet surface area increased by around 6% compared to the spherical geometry (deformation close to 0). With the increased surface the particle coverage decreased to around 0.78. The particles then had more room to move, and the droplet's rotational motion resembled tank-treading by appearance.

In Fig. 2c, we plotted the square of the rotation rate against the square of the E -field strength for the 1 mm PS particle-covered droplet (blue left-pointing triangles). As a reference, we also performed experiments on a single $40 \mu\text{m}$ PS particle and pure silicone oil droplets of three different viscosities: 50, 350



and 10 000 cSt. We chose to present the data in such a way (ω^2 vs. E^2) to find the correlation with the E -field strength and compare it with the classical description of rotating spherical particle, where the rotation rate scales as:^{17,35}

$$\omega^2 \propto E^2/E_Q^2, \text{ and } E_Q^2 = \frac{2\sigma_1\mu_1(R+2)^2}{3\epsilon_1^2(S-R)}, \text{ and } R = \frac{\sigma_p}{\sigma_1}, S = \frac{\epsilon_p}{\epsilon_1},$$

where μ is the viscosity, σ is the electrical conductivity, ϵ is the permittivity, and 'p' and 'l' denote particle and suspending liquid, respectively.

The data from the experiments on the particle-covered droplet and the pure silicone oil droplet with the highest viscosity almost overlap. This indicates that the particles forming a shell contribute greatly to the viscous effects slowing down the droplet rotation (by reducing the straining flows, see discussion in Section 4.3) as compared with the pure droplet of the same viscosity (that is 50 cSt). On the other hand, the presence of particles on the droplet's interface shifts the onset value of E -field at which the rotation begins. In the case of pure oil droplets, the charges that built up at the droplet interface are convected away by the electrohydrodynamic (EHD) flows generated by the E -field.²³ The charge convection is generally greater for droplets with lower viscosities, and therefore the onset value of E -field increases (see Fig. 2c). The EHD flows vanish when particles are added to the interface (see flow velocity maps in our work in ref. 28). The electric stress on a particle-covered droplet is therefore larger compared to that acting on the pure oil droplet of the same size and viscosity (at the same E -field strength) explaining why electroration of particle-covered droplets initiates at weaker E -field strengths compared to pure droplets (of the same viscosity).

Remarkably, the rotation rate of a particle-covered droplet is nearly identical to that of a high-viscosity droplet, and very

different from a PS particle. This observation suggests that there is a small change to the droplet's electric properties with the addition of particles. The difference between the critical E -field for the viscous droplet and particle-covered droplet is small and could be due to differences in deformation or a weak straining flow. However, these differences disappear once rotation sets in.

Moreover, we learned that the rotation data from the experiment on the single PS particle looks the most linear (Fig. 2c). The other curves look linear only at weak E -fields. At stronger fields, the curves consistently bend downward. This may indicate that the deformation of droplets (with or without particles) affects the rotation rate. We decided to further investigate this, and study droplets with different size, knowing that the droplet deformation is proportional to its size.^{28–30}

To study the influence of droplet size on electroration we prepared droplets with different diameters. We used silicone oil with a viscosity of ~ 50 cSt and PS particles (same parameters as in the previous experiments). Each droplet was subjected to an E -field that was increased stepwise from 0 to 835 V mm^{-1} . Each step was maintained for ~ 1 minute. In Fig. 3a we present pictures of four particle-covered droplets at four different E -field strengths. For the droplet dynamics see the corresponding Movie S1 (ESI[†]).

Our experiments show that at the same E -field strength, the smallest droplet deformed the least, whereas the largest droplet deformed the most (Fig. 3b). It is not trivial to precisely predict how the magnitude of deformation theoretically scales with the E -field. That is because the droplet's geometry changes from oblate to nearly prolate, the surface area of the droplet increases, and at the same time, the particle coverage changes when E -field strength is increased. From the data presented in Fig. 3b, we can see that D is roughly proportional to $d \cdot E^2$ within the studied range of E -field strengths, where d is the droplet

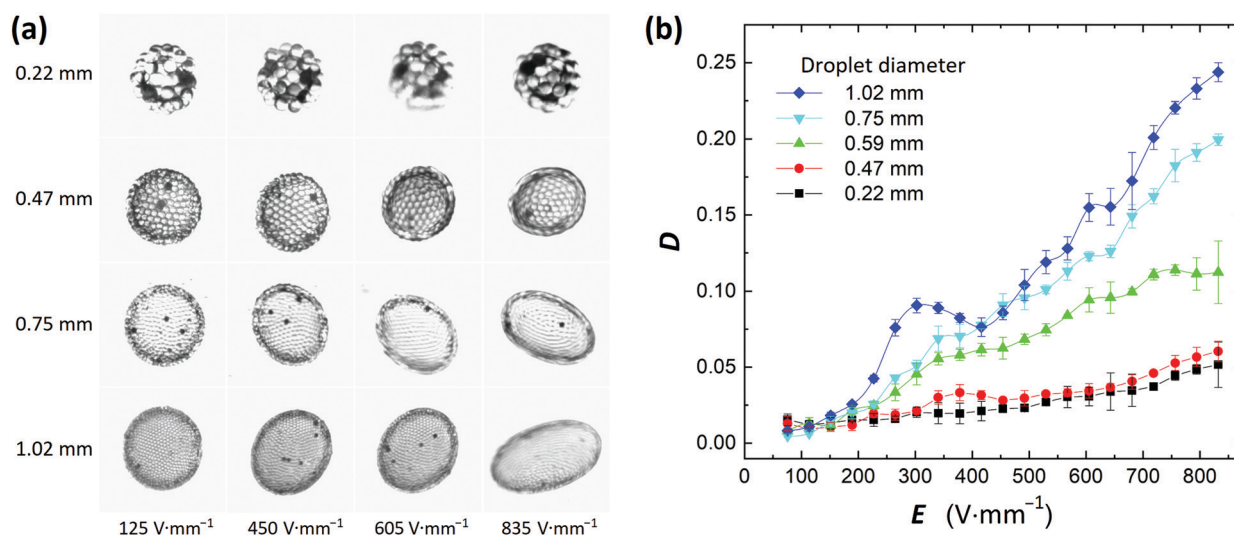


Fig. 3 (a) Images of four PS particle-coated droplets subjected to different E -field strengths. See also the corresponding Movie S1 (ESI[†]). (b) The magnitude of deformation is plotted against the E -field strength. D is roughly proportional to $d \cdot E^2$ within the studied range of E -field strengths, where d is the droplet diameter. There is also a characteristic bump in each data set, and the peak of the bump precedes the initiation of droplet rotation.



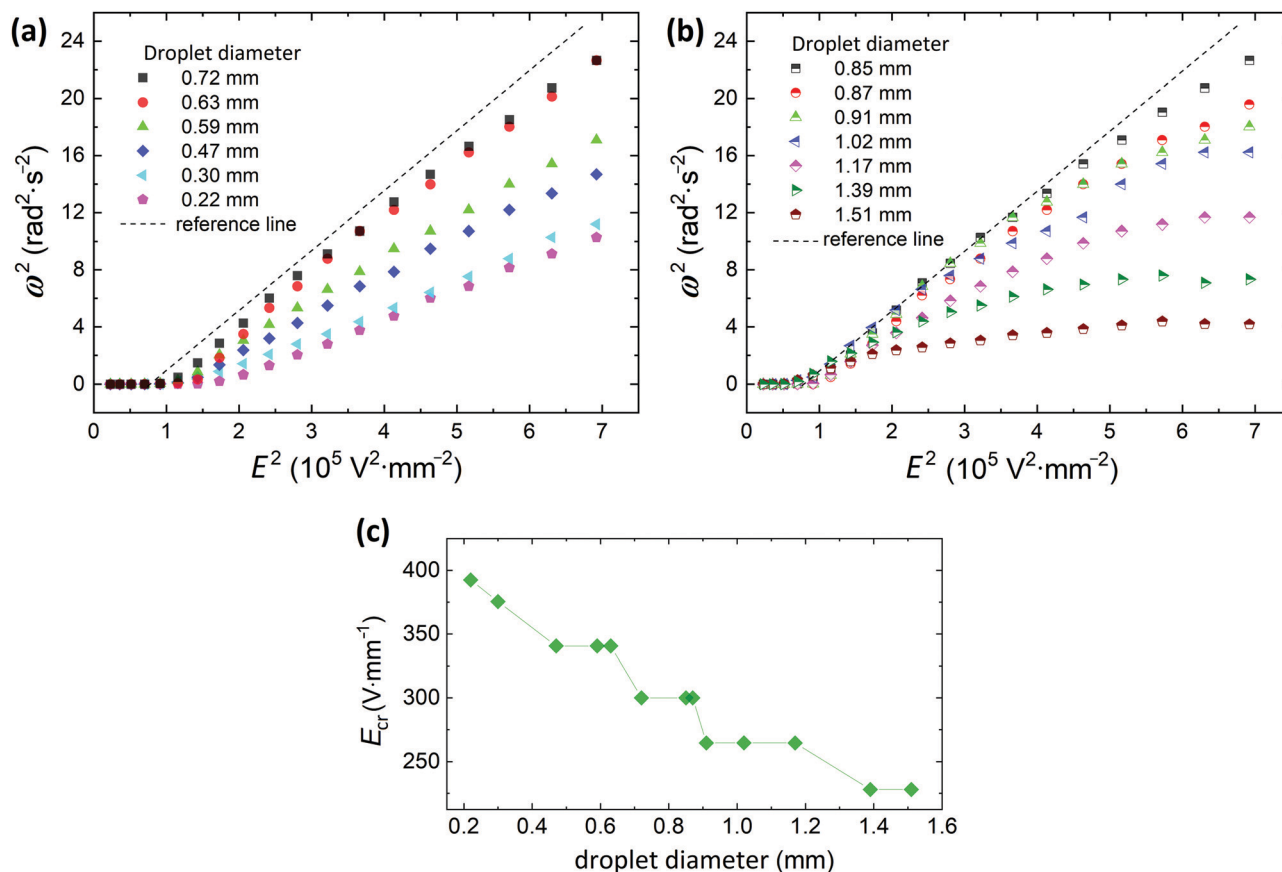


Fig. 4 Rotation rate of particle-covered droplets with a diameter of (a) 0.22–0.72 mm and (b) 0.85–1.51 mm. (b) The rotation rate consistently decreased and the curves deviated more from the linear trend (observed in panel (a)) with the increase of the droplet diameter. (c) Critical field (E_{cr}) at which the droplet started rotating plotted against the diameter of a droplet. The data series presented in panels (a and b) were also plotted in Fig. S2 (ESI[†]), where the argument values for each data series were normalized by the corresponding value of E_{cr} taken from panel (c).

diameter. This phenomenon can be exploited for applications as it will be demonstrated in Section 3.2 where particle rearrangement within the shell (by unjamming the particles) is possible above a certain value of D . In Fig. 3b we also observe the characteristic bump in all of the D vs. E plots. Similarly, to the experiment presented in Fig. 2b, the peak of the bump proceeds the initiation of droplet rotation. In Fig. 4a and b we plot ω^2 vs. E^2 for the all the studied droplets with PS particle shells. We split the data into two plots for better clarity, and also to highlight that the behavior of small droplets (below 0.8 mm) differs from that of larger droplets.

Interestingly, unlike the classical description of Quincke rotation of rigid particles (see the equations for ω and E_Q on the previous page), the rotation of the deformable particle-covered droplets is size-dependent, *i.e.*, both the rotation rate and the critical E -field for rotation are size-dependent (see also Fig. 4c). We therefore, use a different notation for the critical E -field for the onset of the rotation in our system, E_{cr} . Size-dependency of the critical E -field was theoretically shown to exist, for example, for insulating cylinder particles, and it originated from ion diffusion and electro-migration in the charge layer.¹¹ However, these phenomena prevail for small rotating objects, at least one order of magnitude smaller than

particle-covered droplets used in this study. Here, in the three-phase soft-matter system, the size-dependency of E_{cr} can originate from droplet deformation (similar as for clean droplets).²⁰ Larger particle-covered droplets are easier to deform, and thus initiate rotation at weaker E -fields. As shown in Fig. 4c, the $E_{cr}(d)$ is consistently decreasing with the droplet diameter (d).

To verify if the droplet deformation may cause E_{cr} shifting, we performed an experiment using a droplet with a rigid shell composed of sintered PS particles. The results are presented in Fig. 5a and b. Subjected to an E -field the droplet rotated without being deformed (see images in Fig. 5b). The critical field for electrorotation was found to be around 360 V mm^{-1} (the value is similar to that of an individual PS particle), far from the E_{cr} of a deformable droplet of similar diameter ($\sim 1.39 \text{ mm}$) covered by unsintered PS particles (which started rotating at $\sim 250 \text{ V mm}^{-1}$).

The experiment also shows that the rotation rate of the droplet with a rigid PS particle shell is roughly linearly proportional to the E -field strength. This is not the case for the deformable droplet covered with unsintered particles. The data points corresponding to the measurements of the deformable droplet band downward. The deviation from the linear trend is consistently greater for larger droplets, as presented in Fig. 4b. For example, the rotation rate of 0.85 mm particle-covered droplet follows the



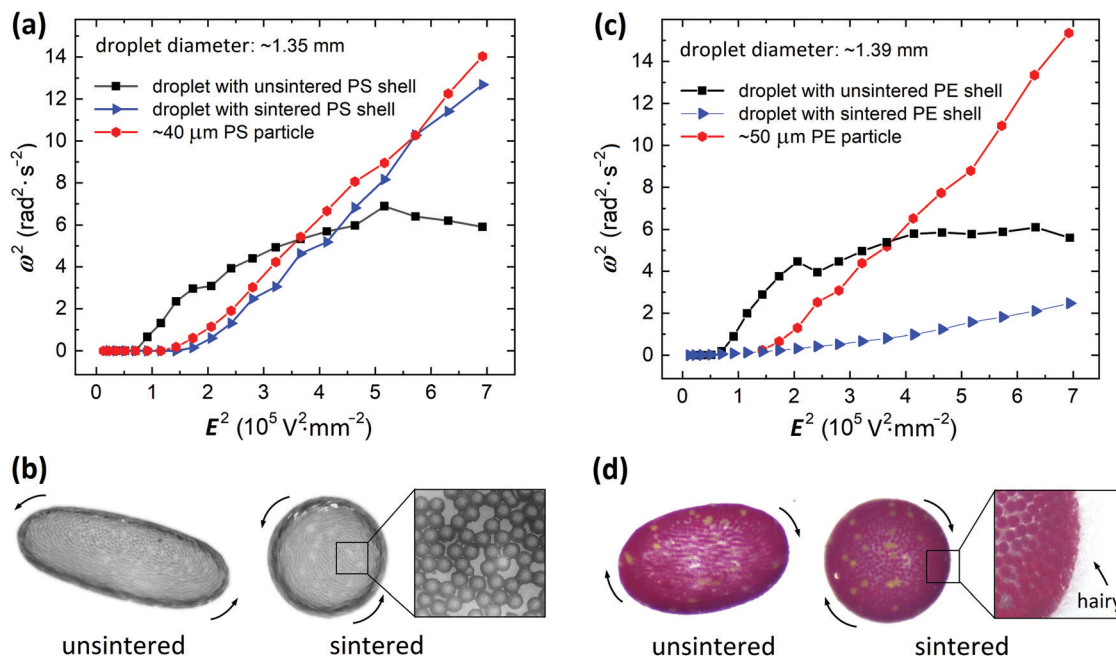


Fig. 5 Electrorotation of droplets with rigid and deformable shells composed of (a and b) PS particles and (c and d) PE particles. The rigid shells were made by joining particles through heating using a microwave oven. Characteristic necks between sintered PS particles are shown in the zoomed image in panel (b). During heating of the PE particle-covered droplet, hairy polymeric structures were formed sticking out of the shell, as presented in the zoomed image in panel (d). The change of the morphology of the PE particle shell formed on an oil droplet affected its rotation rate (see also corresponding Movie S2, ESI†).

linear trend up to around $3 \times 10^5 \text{ V}^2 \text{ mm}^{-2}$, the 1.02 mm droplet follows the trend to around $2 \times 10^5 \text{ V}^2 \text{ mm}^{-2}$, whereas the rotation rate of the largest droplet size of 1.51 mm is non-linear practically for all E -field strengths.

The rotation rate is also affected by the morphology of particle shells. In Fig. 5c and d we present the results from the experiments on electrorotation of PE particle-covered droplets with different morphologies of their shells. We prepared two droplets (diameter of ~ 1.39 mm) both covered by PE particles (50 μm). One of the droplets was heated in a microwave oven (600 W) for several seconds to partially melt the PE particles. This led to the fusing of the PE particles and the formation of a rigid shell. During the heating, brush or hairy-like shell was formed (see the zoomed image in Fig. 5d). The two particle-covered droplets were then subjected to an E -field. The droplet with hairy shell rotated significantly slower than the droplet with a smooth shell. We expect this is due to the increase of the magnitude of drag coefficient (see also the corresponding Movie S2, ESI†) and/or due to the changes of the effective electric properties of the particle shell. Kabir *et al.*⁴⁵ studied how the particle surface morphology affected the drag force acting on a particle. They measured the drag coefficient to be at least 20% higher for a hairy particle compared to that of a smooth surface, which is aligned with our anticipations. We observed that many hairs that initially (before electrorotating) protruded almost perpendicular to the particle shell were flattened due to the liquid drag as the droplet started spinning faster when the E -field was increased (see an analogous experiment with a tennis ball).⁴⁶ This change in the hair alignment should favor faster rotation of the shell. Indeed, the measured rotation rate for the hairy PE shell (blue triangles in

Fig. 5c) supports this (the rotation rate is accelerated with increasing E -field strength). The heating of PE particles that led to the formation of hairy structures could also affect the electric properties of the shell. This will have to be investigated in more detail.

Furthermore, the electrorotation of the particle-covered droplet can be affected by the electrical nature of the particles. To electrorotate an object immersed in a low conducting liquid it is required that the rotor's electrical conductivity (or dielectric constant, see the equation for Maxwell-Wagner relaxation time) is lower than that of the media fluid. An interesting situation happens when a shell on a droplet is composed of non-ohmic particles, *i.e.*, having a non-linear relationship between the electric current and the voltage. In Fig. 6, we present the results from an experiment, in which a silicone oil droplet (~ 0.7 mm) was covered by clay mineral particles. Subjected to an E -field of around 270 V mm^{-1} the droplet slowly rotated with a rotation rate of around 0.2 rad s^{-1} . The rotation rate was increased by increasing the E -field strength up to around 300 V mm^{-1} . However, at $E \sim 330 \text{ V mm}^{-1}$ the clay particle-covered droplet stopped rotating. The dipole moment of the droplet covered by the clay film flipped at $E > 330 \text{ V mm}^{-1}$. As a consequence, the E -field acting on the droplet stretched it along the E -field direction (see Fig. 6 and the corresponding Movie S3, ESI†).

3.2. Towards applications

In this section, we present examples of application of electrorotation of particle-covered droplets. In the first example, we demonstrate that the electrorotation enables fabrication of arrested droplets with different geometries and with shells



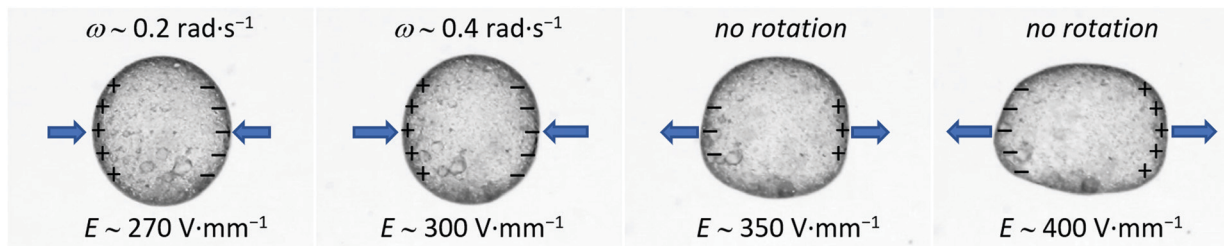


Fig. 6 A silicone oil droplet (50 cSt) covered by non-ohmic clay particles (Li-fluorohectorite). The droplet electrorotated in E -field range of around 270 to 330 V mm^{-1} . At stronger E -fields (e.g., 350 and 400 V mm^{-1}) the electric dipole induced on a droplet was flipped resulting in the droplet electrostretching (see also the corresponding Movie S3, ESI†). E -Field was applied horizontally, and the positive signal was on the left side of the droplet. The blue arrows indicate the direction of the electric stress acting on the droplet.

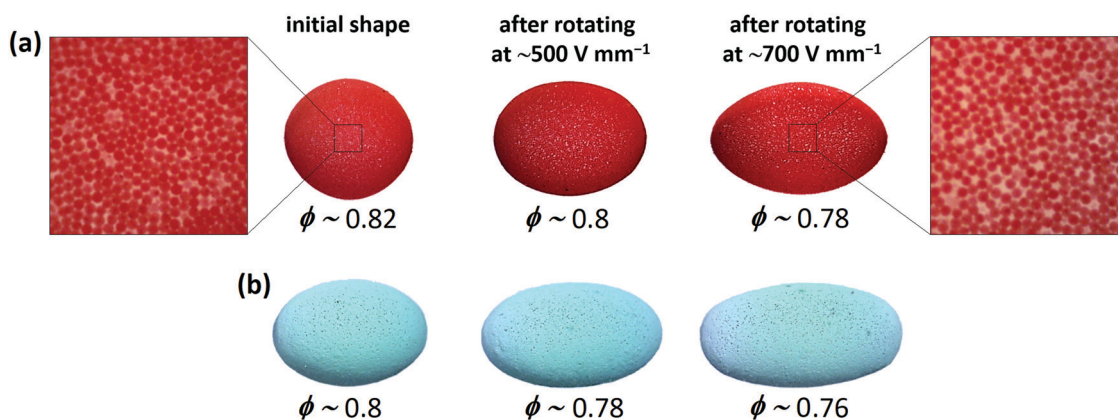


Fig. 7 Electrorotation used for making arrested droplets of different shapes and particle shells with various porosity. The change in particle coverage was estimated to be around 0.04 compared to the particle coverage of droplets before rotation. Droplets were covered by PE particles with a diameter (top) $\sim 50 \mu\text{m}$ and (bottom) $\sim 30 \mu\text{m}$.

having different porosity (or particle coverage). We prepared two silicone oil droplets covered with polyethylene (PE) particles. One droplet was initially spherical (Fig. 7a) and the other droplet was aspherical (Fig. 7b) made by coalescing two droplets, as shown in Fig. S3, (ESI†). To tune the shape of the droplets we electrorotated them at strong E -fields (500 and 700 V mm^{-1}) for a few seconds.

We know from fundamental studies that as a particle-covered droplet rotates at strong E -field, it also stretches and allows the particles in the shell to separate from one another. By turning off the E -field, the droplet relaxes and reduces its surface area thus forcing the particles to form a shell again. However, the particle-covered droplets did not return to their initial shapes, and the structure of their shells was more disordered and porous compared to that of the initial shells (as shown in Fig. 7 and Movie S4, ESI†). That happened because the particles did not have sufficient time to find optimal arrangements when the surface area decreased fast after switching off the E -field. We found that the application of stronger E -fields (e.g., 700 V mm^{-1}) resulted in formation of more elongated arrested droplets with more porous particle shells. We estimated that the particle coverage decreased by around 0.02 and around 0.04 when the droplets were stretched and rotated at 500 and 700 V mm^{-1} , respectively (compared to the particle coverage value of droplets before

electrorotation). The elongated droplets remained stable, *i.e.*, they did not change shape, and we did not observe particle rearrangements.

In the next experiment, we demonstrate how electrorotation can be utilized to mix particles and study solid to liquid transition of the particle layer. We performed an experiment on a droplet (diameter around 3 mm) covered with a Janus shell made of 50 μm PE particles (red and blue), suspended in castor oil, and subjected to different E -field strengths. Fig. 8 shows the time development of a Janus shell subjected to a weak (200 V mm^{-1}) and strong (400 V mm^{-1}) E -field. Subjected to the weak E -field, the droplet with the Janus shell rotated almost as a solid sphere being slightly deformed. The particles forming the shell were practically jammed and, therefore, could not mix. After 5 minutes and several rotations, the border separating the blue and red particles is still intact; confirming that the particle layer acts as a particle film. Subjected to the stronger E -field, the particle-covered droplet deformation was large enough ($D > 0.1$) for the particle film to liquefy. As seen in Fig. 8 (bottom row), the particles started to mix, and the border separating the two particle shells of different colour split up. Eventually, after several minutes of electrorotation, the particles were almost completely mixed.

To study the efficiency of electrorotation on particle mixing, we used droplets (diameter $\sim 2 \text{ mm}$) covered with a Janus shell



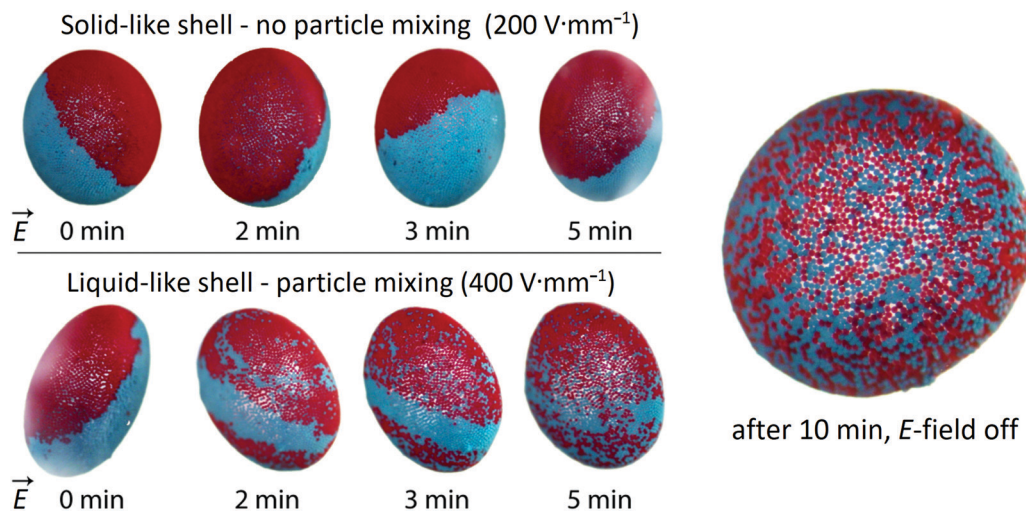


Fig. 8 A droplet with Janus shell in the weak E -field regime where it rotated as a solid shell with nearly jammed surface particles (top figures), and in the strong E -field regime where it tank-treaded with a flowing particle layer (bottom figures). The droplet was made out of 50 cSt silicone oil and was covered with 50 μm PE particles (red and blue). The E -field was in the horizontal direction as indicated by the arrows.

made of 50 μm PE particles (red and cyan). E -Fields of 260, 450 and 700 V mm^{-1} were applied during the experiments (see also Movie S5, ESI†). Images of the droplets (Fig. 9a–c) were captured as the droplets finished 3, 5, 10 and 40 revolutions (Rev). With this methodology, we could qualitatively compare the degree of particle mixing. We found that the efficiency of particle mixing depends on the E -field strength, *i.e.*, the particles mixed faster at

stronger fields. This is because droplets subjected to strong E -fields deform more and thus make more space at the droplet surface for particles to rearrange, and the particles at the surface move faster and may collide and pull on other particles. Moreover, we observed that the particle mixing depends on the droplet size (compare Fig. 9c and d). We also observed that the E -field strength at which solid-to-liquid transition and particle

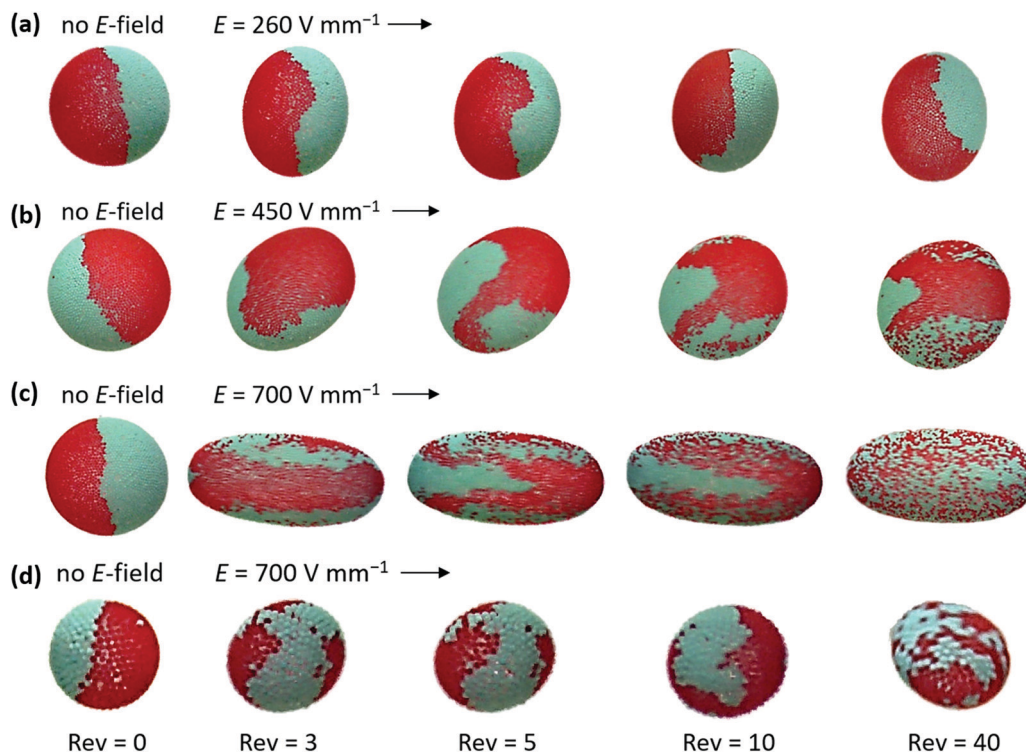


Fig. 9 Droplets with a diameter of (a–c) ~ 2 mm and (d) ~ 0.8 mm covered with 50 μm PE particles (red and cyan) forming a Janus shell. Fast particle mixing is facilitated by the application of stronger E -fields. The particles mix slower at the surface of the smaller droplet. See also the corresponding Movie S5 (ESI†).



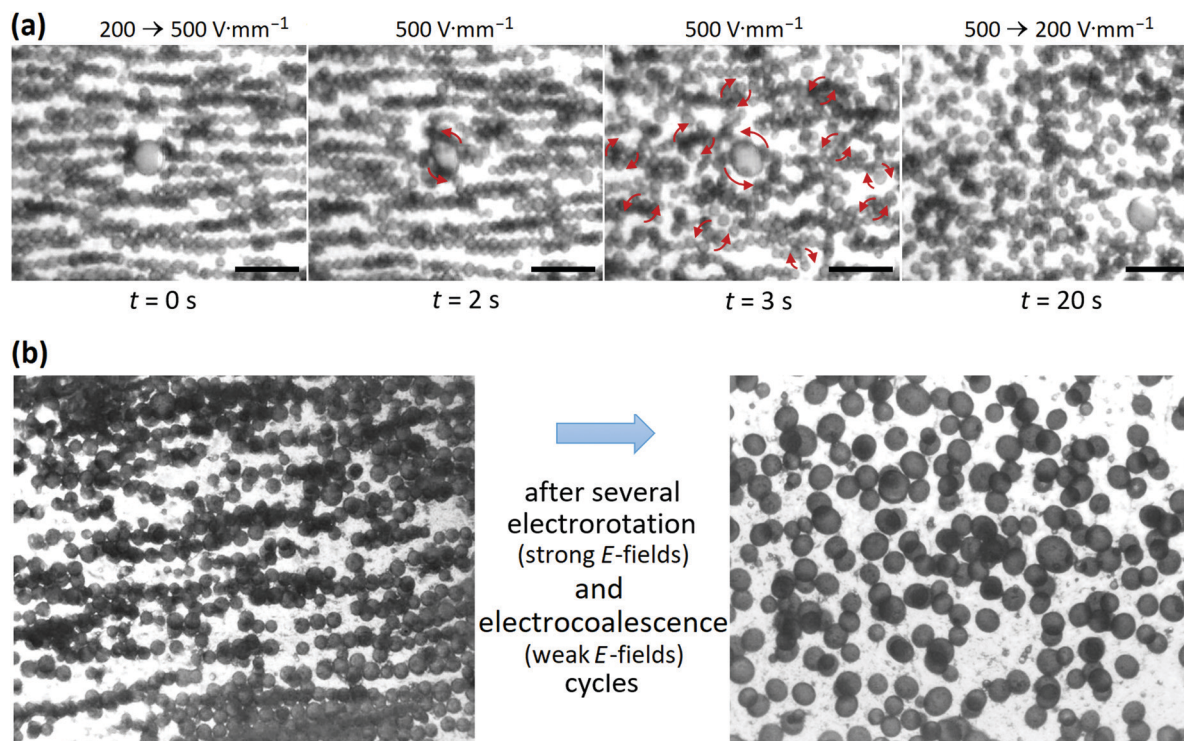


Fig. 10 Optical microscope images of emulsions droplets covered by $10\ \mu\text{m}$ PS particles. (a) An E -field of $500\ \text{V}\ \text{mm}^{-1}$ was applied for ~ 20 seconds to induce electrorotation of droplets and droplet clusters to help the clustered droplets to separate. See also the corresponding Movie S6 (ESI †). The scale bars are $1\ \text{mm}$. (b) Many droplets formed unwanted chain-like structures and clusters (left panel). Application of E -fields in an alternating fashion (weak \leftrightarrow strong) resulted in cluster disintegration and enabled the formation of separated emulsion droplets (see right panel) with an average diameter of $\sim 250\ \mu\text{m}$.

mixing initiates depends on the size of the surface particles. However, we do not have sufficient data to be conclusive on this point. Nevertheless, the data presented here should serve as an entry point for formulating theoretical models of the solid-to-liquid transition of particle shells and particle mixing induced by E -fields.

The knowledge gained from the experiments on individual droplets can be also very useful in studying and advancing more complex systems, such as emulsions. Recently, we were exploring the possibility offered by E -fields to fabricate Pickering emulsions through a limited coalescence approach.⁴⁷ We used E -fields to promote the attraction of droplets partially covered by particles. That enabled speeding up the droplets' coalescence that led to the formation of stable emulsion droplets, *i.e.*, densely covered by particles. However, during the Pickering emulsion formation, many droplets formed unwanted electrorheological chain-like structures often composed of particle-bridged droplets. This prevented completion of the Pickering emulsion maturing and caused the formation of droplet clusters.

In this example of the application of electrorotation phenomena, we demonstrate that the droplet chaining and clustering (see left panels in Fig. 10) can be prevented. During the formation of Pickering emulsion by E -field-assisted electrocoalescence, we cyclically (every 20 seconds) increased and decreased the E -field strength. In Fig. 10a, we present a sequence of optical microscopy images. These images were recorded within 20 seconds,

roughly in the middle of the process of fabricating a Pickering emulsion (that took ~ 30 min, see ref. 47 for a similar experiment showing the whole process of emulsion maturing). Switching between the critical E -field for rotation $E < E_{\text{cr}}$ and $E > E_{\text{cr}}$, enabled droplet coalescence at weak fields and destruction of droplet agglomerates at strong fields.

As presented in Fig. 10a, at strong E -field ($500\ \text{V}\ \text{mm}^{-1}$), droplets and droplet clusters started rotating and shearing the emulsion locally. These dynamics helped the clustered droplets to separate. The rotation of individual droplets and droplet clusters (before their destruction) is shown in the corresponding Movie S6 (ESI †). In Fig. 10b, the electrorotation of selected droplets is marked with red arrows. For the sake of image clarity, we only marked selected droplets. Before lowering the E -field strength back to $200\ \text{V}\ \text{mm}^{-1}$, nearly all droplets were separated and rotated individually. This procedure of alternating the strengths of the E -field resulted in the formation of a Pickering emulsion where the majority of droplets were densely covered by particles (see right panel in Fig. 10b).

Currently, we are also exploring how electrorotation could be used to produce oil-oil Pickering emulsions with nearly monodispersed Pickering droplet size. We use electrorotation to prevent droplet clustering and also split droplets at even stronger fields (three levels of E -field strengths are used) to coalesce them again with other droplets to even the particle concentration in each droplet. Once more, electrorotation is the key to efficient formation of stable particle emulsions.



4 Comments

4.1. Three-phase system

In our study, we mainly used droplets with polymeric shells composed of spherical microparticles (10–50 μm) as a model system. However, the presented methodology is not limited to droplets with this type of shell, as long as: (i) the particles' electrical properties fulfil the condition for electrorotation, and (ii) the particles are strongly bound to the oil–oil interface and do not detach when sheared during droplet rotation. In our laboratories, we performed several additional experiments with droplets as small as 100 μm and as large as 0.5 cm, using different types of particles, including poorly conductive kaolinite particles and silica particles, as well as polymeric particles, and these had a broad size range of 500 nm to 0.2 mm. In our experiments, we used castor oil as the surrounding liquid. However, as presented in several other studies, other combinations of liquids can also be used.^{15,48}

4.2. Electric field parameters

In the experiments presented here, we used DC E -fields between 0 to 835 V mm^{-1} because stronger E -fields resulted in a break-up of the largest droplet (*i.e.*, the particle-covered droplet with a diameter of around 1.51 mm). However, in principle, smaller droplets (*e.g.*, a diameter of 100 μm) can be exposed to E -fields far above a few kV mm^{-1} because they deform less, as presented in Fig. 3b, and thus break up at stronger E -fields compared to larger droplets. Also, droplets with higher viscosities than those used here can be subjected to stronger E -fields, as their characteristic time of deformation may be smaller than the charge build-up time.

We noted that there is a major difference in droplet behaviour depending on how the E -field is applied, that is, whether the strong E -field is reached instantly or gradually. The instant application of a strong E -field may cause significant deformation of a droplet accompanied by an irreversible detachment of particles from the droplet's surface (see Fig. S4 and Movie S7, ESI[†]). We also observed that when the E -field was increased gradually, the particle-covered droplets tumbled less compared to particle-covered droplets exposed to sharply changing E -field strengths. Because the droplet's behaviour at each E -field strength was studied for short time (~ 1 minute), we cannot conclusively state whether a steady shape is reached. However, the data collected for the experiment on particle mixing indicates that the steady shape (and tilt angle) can be achieved after several minutes of electrorotation (see Movie S5, ESI[†]). We also noted that the direction of the Quincke rotation can be changed by flipping the E -field direction.

As presented in Fig. 6, the fluorohectorite clay particles had interesting electrical characteristics limiting the electrorotation at stronger E -fields so that the electrorotation was achieved only at the narrow E -field band (that is, for $270 \text{ V mm}^{-1} < E < 330 \text{ V mm}^{-1}$). We think that the bandwidth can be modified. The electrical properties of clay mineral particles depend on the type of clay used (fluorohectorite, LAPONITE[®], kaolinite, *etc.*), their water content, and also their size. Thus, by controlling these parameters one can design a particle-covered droplet with the desired E -field bandwidth of droplet electrorotation.

4.3. Straining flows

As we described in the Section 3.1, the size-dependency of E_{cr} (shown in Fig. 4c) originated from droplet deformation. The increased deformation increases the dipole strength, and thus decrease E_{cr} . On the other hand, when the droplet deforms (while subjected to the E -field) and its surface area increases, the particle coverage decreases, which enables formation of EHD flows. These straining flows may convect away the charge accumulated on the droplet's interface (especially relevant for low viscosity droplets) decreasing the strength of the electric dipole, which should lead to increased E_{cr} values. From our experimental data presented in ref. 28, we learnt that the straining flows created near the small opening in the particle shell (formed at the droplet's electric equator) are very weak compared to those formed around a particle-free droplet, and narrow (located only near to the opening). Therefore, we believe their contribution to the change of the E_{cr} value is negligible in our system. However, at larger droplet deformation (when a particle-covered droplet rotates), the straining flows may play a more significant role, for example, in particle mixing, as presented in Fig. 9.

5 Conclusions

We experimentally studied electrorotation of particle-covered droplets (and pure silicone oil droplets, as well as individual PE and PS particles, used as reference data) immersed in electrically more conductive castor oil. We showed that the addition of particles to the droplet interface changes the parameters of electrorotation compared to those of pure droplets and solid particles. The surface particles contributed to the viscous effects, slowing down the droplet rotation compared to the particle-free droplets, and their presence shifted the onset value of the critical E -field strength (at which the rotation begins). We also reported the presence of a second critical E -field (at which the rotation terminates) for the droplets covered by non-ohmic particles. We found that the rotation rate (ω) and the critical E -field for rotation (E_{cr}) depend on the size of particle-covered droplets, dissimilar to the macroscopic spherical particles for which the Quincke description is held. We also observed that both ω and E_{cr} depend on particle shell morphology and composition.

We have also presented new applications for Quincke rotation of particle-covered droplets. (i) We demonstrated that this electric phenomenon can be used to form arrested droplets with non-spherical shells. In the context of the stability and applications of particle-covered droplets (*e.g.*, constituting Pickering emulsions), it is important to understand their mechanical properties. Several research groups have studied the deformation, relaxation, and mechanical properties of particle-covered droplets.^{27,49,50} The majority of the research concern spherical droplets. However, very little is known about arrested droplets with non-spherical particle shells. The method presented here enables the formation of arrested droplets with controllable geometry and porosity, and thus, facilitates research, for example, on deformation, yielding, and crumpling of jammed particle shells formed on arrested droplets (that is ongoing research in our laboratories). (ii) We also introduced a novel experimental



approach for monitoring the dynamics of particles forming a monolayer on the surface of droplets by using a droplet covered with a Janus shell. This setup enabled particle tracing and direct visualization of the transition from solid-like rotation to the fluid-like tank-treading motion of a particle-covered droplet. (iii) Furthermore, we demonstrated that the electrorotation of deformable droplets permitted particle mixing on the interface of droplets and the formation of patchy particle shells. (iv) Finally, we showed that electrorotation can be used to facilitate efficient fabrication of Pickering emulsions.

Future experimental studies should investigate how particle properties, *e.g.*, their cohesiveness, particle packing, and particle coverage, affect the mechanics of particle shells and electrorotation of particle-covered droplets. The role of the straining flows in electrorotation of large-size particle-covered droplets should be investigated in more detail. It would also be interesting to study interactions of two or more deformable particle-covered droplets electrorotating in close proximity.

Author contributions

Z. Rozynek and A. Mikkelsen initiated the project. Z. Rozynek, A. Mikkelsen and J. Banaszak designed all experiments. J. Banaszak performed the experiments with results presented in Fig. 2–5 and Fig. S2 (ESI[†]). K. Khobaib performed the experiments with results shown in Fig. 7, 9 and Fig. S3 (ESI[†]). A. Mikkelsen performed the experiments with results presented in Fig. 8. Z. Rozynek performed the experiments with results presented in Fig. 6, 10 and Fig. S1, S4 (ESI[†]). Z. Rozynek wrote the first version of the manuscript. All authors took part in discussions towards the finalization of the manuscript. Z. Rozynek administered the submission and the review process.

Funding sources

A. Mikkelsen received funding from the European Union's Horizon 2020 Research and Innovation Framework Program under the M. Skłodowska-Curie grant agreement no. 752896. Z. Rozynek, J. Banaszak and K. Khobaib received funding from the Polish National Science Centre through OPUS and PRE-LUDIUM program (2015/19/B/ST3/03055 and 2019/35/N/ST5/02821). We thank the Research Council of Norway through its Centres of Excellence funding scheme, Project No. 262644.

Conflicts of interest

There are no conflicts of interest to declare.

References

- 1 Y. Hu, P. M. Vlahovska and M. J. Miksis, *Phys. Rev. E*, 2018, **97**, 013111.
- 2 A. I. Grachev, *Tech. Phys. Lett.*, 2018, **44**, 716–718.
- 3 T. Mochizuki, *ACS Omega*, 2018, **3**, 1031–1040.

- 4 Y. Dolinsky and T. Elperin, *Phys. Rev. E: Stat., Nonlinear, Soft Matter Phys.*, 2009, **79**, 026602.
- 5 P. García-Sánchez, Y. Ren, J. J. Arcenegui, H. Morgan and A. Ramos, *Langmuir*, 2012, **28**, 13861–13870.
- 6 Z. M. Sherman and J. W. Swan, *Phys. Rev. Lett.*, 2020, **124**, 208002.
- 7 W. Weiler, *Phys. Chem.*, 1893, 194–195.
- 8 G. Quincke, *Ann. Phys.*, 1896, **295**, 417–486.
- 9 T. B. Jones, *IEEE Trans. Ind. Appl.*, 1984, **20**, 845–849.
- 10 I. Turcu, *J. Phys. A: Math. Gen.*, 1987, **20**, 3301–3307.
- 11 F. Peters, L. Lobry, A. Khayari and E. Lemaire, *J. Chem. Phys.*, 2009, **130**, 194905.
- 12 Q. Brosseau, G. Hickey and P. M. Vlahovska, *Phys. Rev. Fluids*, 2017, **2**, 014101.
- 13 Y. Gu and H. Zeng, *Phys. Rev. Fluids*, 2017, **2**, 083701.
- 14 E. Lemaire and L. Lobry, *Phys. A*, 2002, **314**, 663–671.
- 15 S. Krause and P. Chandratreya, *J. Colloid Interface Sci.*, 1998, **206**, 10–18.
- 16 J. Q. Feng, *J. Colloid Interface Sci.*, 2002, **246**, 112–121.
- 17 H. He, P. F. Salipante and P. M. Vlahovska, *Phys. Fluids*, 2013, **25**, 032106.
- 18 A. N. Tyatyushkin, *Phys. Fluids*, 2017, **29**, 097101.
- 19 J.-W. Ha and S.-M. Yang, *Phys. Fluids*, 2000, **12**, 764–772.
- 20 P. F. Salipante and P. M. Vlahovska, *Phys. Fluids*, 2010, **22**, 112110.
- 21 P. F. Salipante and P. M. Vlahovska, *Phys. Rev. E: Stat., Nonlinear, Soft Matter Phys.*, 2013, **88**, 043003.
- 22 H. Sato, N. Kaji, T. Mochizuki and Y. H. Mori, *Phys. Fluids*, 2006, **18**, 127101.
- 23 D. Das and D. Saintillan, *J. Fluid Mech.*, 2017, **810**, 225–253.
- 24 D. Das and D. Saintillan, *J. Fluid Mech.*, 2017, **829**, 127–152.
- 25 E. Yariv and I. Frankel, *J. Fluid Mech.*, 2016, **788**, R2.
- 26 A. Mikkelsen, P. Dommersnes and J. O. Fossum, *Rev. Cubana Fis.*, 2016, **33**, 47–49.
- 27 L. Bécu and L. Benyahia, *Langmuir*, 2009, **25**, 6678–6682.
- 28 A. Mikkelsen, K. Khobaib, F. K. Eriksen, K. J. Måløy and Z. Rozynek, *Soft Matter*, 2018, **14**, 5442–5451.
- 29 M. Ouriemi and P. M. Vlahovska, *J. Fluid Mech.*, 2014, **751**, 106–120.
- 30 M. Ouriemi and P. M. Vlahovska, *Langmuir*, 2015, **31**, 6298–6305.
- 31 L. Lobry and E. Lemaire, *J. Electrostat.*, 1999, **47**, 61–69.
- 32 N. Pannacci, L. Lobry and E. Lemaire, *Phys. Rev. Lett.*, 2007, **99**, 094503.
- 33 M. S. Abbasi, R. Song, S. Cho and J. Lee, *Micromachines*, 2020, **11**, 942.
- 34 A. Jakli, B. Senyuk, G. Liao and O. D. Lavrentovich, *Soft Matter*, 2008, **4**, 2471–2474.
- 35 G. E. Pradillo, H. Karani and P. M. Vlahovska, *Soft Matter*, 2019, **15**, 6564–6570.
- 36 A. Zöttl and H. Stark, *J. Phys.: Condens. Matter*, 2016, **28**, 253001.
- 37 A. Bricard, J. B. Caussin, N. Desreumaux, O. Dauchot and D. Bartolo, *Nature*, 2013, **503**, 95–98.
- 38 S. Q. Lu, B. Y. Zhang, Z. C. Zhang, Y. Shi and T. H. Zhang, *Soft Matter*, 2018, **14**, 5092–5097.
- 39 D. Das and E. Lauga, *Phys. Rev. Lett.*, 2019, **122**, 194503.



- 40 P. Dommersnes, A. Mikkelsen and J. O. Fossum, *Eur. Phys. J.: Spec. Top.*, 2016, **225**, 699–706.
- 41 Z. Rozynek, M. Kaczmarek-Klinowska and A. Magdziarz, *Materials*, 2016, **9**, 679.
- 42 A. Mikkelsen, P. Dommersnes, Z. Rozynek, A. Gholamipour-Shirazi, M. D. S. Carvalho and J. O. Fossum, *Materials*, 2017, **10**, 436.
- 43 P. Dommersnes, Z. Rozynek, A. Mikkelsen, R. Castberg, K. Kjerstad, K. Hersvik and J. O. Fossum, *Nat. Commun.*, 2013, **4**, 2066.
- 44 A. Mikkelsen and Z. Rozynek, *ACS Appl. Mater. Interfaces*, 2019, **11**, 29396–29407.
- 45 A. M. R. Kabir, D. Inoue, Y. Kishimoto, J. Hotta, K. Sasaki, N. Kitamura, J. P. Gong, H. Mayama and A. Kakugo, *Polym. J.*, 2015, **47**, 564–570.
- 46 R. D. Mehta and J. M. Pallis, *Sports Eng.*, 2001, **4**, 177–189.
- 47 Z. Rozynek, R. Bielas and A. Józefczak, *Soft Matter*, 2018, **14**, 5140–5149.
- 48 A. Zakinyan, E. Tkacheva and Y. Dikansky, *J. Electrostat.*, 2012, **70**, 225–232.
- 49 H. Xu, S. Melle, K. Golemanov and G. Fuller, *Langmuir*, 2005, **21**, 10016–10020.
- 50 R. B. Karyappa, S. D. Deshmukh and R. M. Thaokar, *Phys. Fluids*, 2014, **26**, 122108.



Electronic Supplementary Material for

Electrorotation of particle-coated droplets: from fundamentals to applications

Z. Rozynek,^{a,b*} J. Banaszak,^a A. Mikkelsen,^a K. Khobaib,^a and A. Magdziarz^a

^aFaculty of Physics, Adam Mickiewicz University, Uniwersytetu Poznańskiego 2, 61-614 Poznań, Poland

^bPoreLab, The Njord Centre, Department of Physics, University of Oslo, Blindern, N-0316 Oslo, Norway

*Corresponding author: zbiroz@amu.edu.pl

Figure S1: At weak E-fields (up to around $250 \text{ V}\cdot\text{mm}^{-1}$), the deformation magnitude increased as power law of the electric field strength with an exponent slightly above 2. This is particularly apparent for larger droplets (with a diameter above 1 mm) that deform more than smaller droplets. During the droplet deformation, the surface area increases, thus more charges may accumulate on the droplet's interface contributing to the increase of the total electric stress acting on the droplet. At stronger electric field strengths (above around $400 \text{ V}\cdot\text{mm}^{-1}$), the magnitude of droplet deformation is roughly proportional to E^2 .

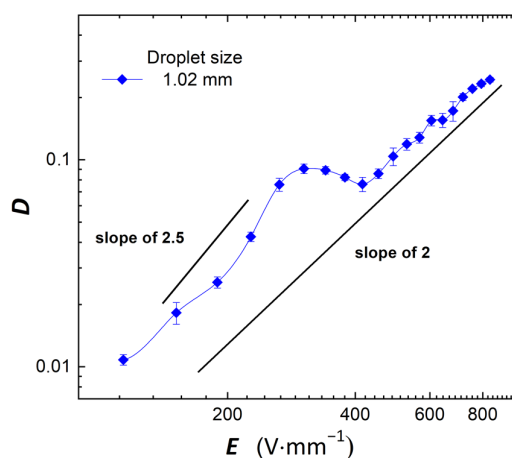


Fig. S1. A log-log plot of the deformation magnitude vs. the E -field strength.

Figure S2: It appears that the data for droplets smaller than 0.85 mm collapse and follow $\omega^2 \propto E^2/E_{cr}^2$ relationship. Though, the droplet rotation rate at high field strength (i.e., $E^2 \gg E_{cr}^2$) goes through a non-monotonic transition with increasing droplet size (above 0.72 mm).

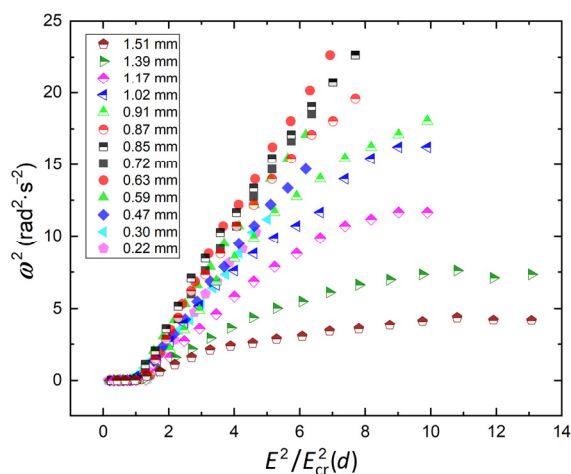


Fig. S2. Re-plotted data series presented in Fig. 3a,b. The argument values for each data series were normalized by the corresponding value of E_{cr} taken from panel Fig. 3c.

Figure S3: Two silicone oil droplets partly covered by 50- μm PE particles (left panel) coalesced to form an arrested Pickering droplet (right panel). The coalesced droplet had a jammed-particle layer that kept the droplet non-spherical even after the E -field was turned off.

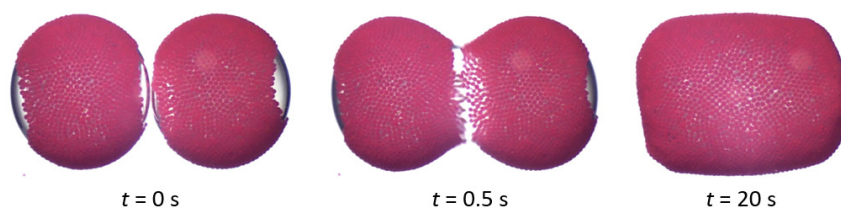


Fig. S3. (left) Two silicone oil droplets just before electrocoalescence and (right) the resulting coalesced droplet. The diameter of each original droplet was ~ 1.5 mm.

Figure S4: Two silicone oil (50 cSt) droplets (particle-free and particle-covered) formed in castor oil. Application of a strong E -field of around $850 \text{ V}\cdot\text{mm}^{-1}$ resulted in irreversible detachment of particles from the droplet's surface. The droplets were viewed through an optically transparent ITO electrode along the E -field direction.

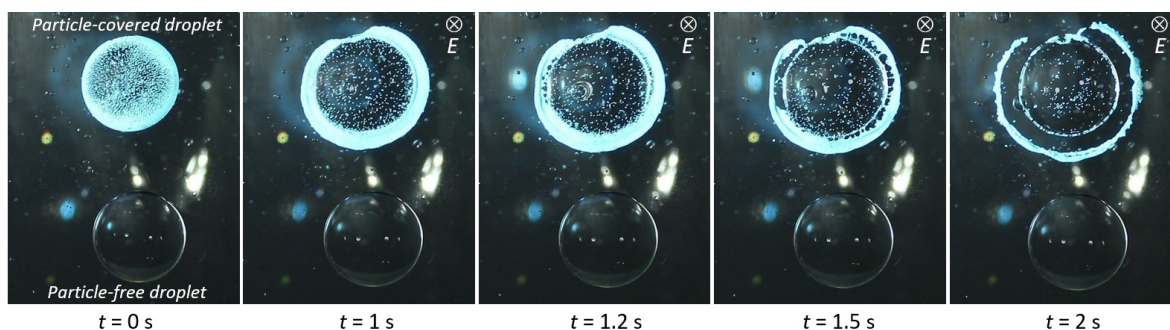


Fig. S4. Detachment of surface microparticles from a silicone oil droplet (diameter of ~ 1.7 mm). Application of a strong E -field of around $850 \text{ V}\cdot\text{mm}^{-1}$ caused the particles to crumple and eventually irreversibly detach from the surface of the droplet. The droplet is imaged parallel to the direction of the E -field through transparent electrodes. See also the corresponding **Movie S7**.

Movie S1. Four PS particle-covered droplets (diameter 0.22–1.02 mm) at different E -field strengths (125 – $835 \text{ V}\cdot\text{mm}^{-1}$).

Movie S2. Electrorotation of droplets (diameter of ~ 1.39 mm) with rigid and deformable shells composed of PE particles. The rigid shell was made by joining particles through heating using a microwave oven. During heating of a PE particle-covered droplet, hairy polymeric structures were formed sticking out of the shell. The droplet with a hairy shell rotated significantly slower than the droplet with a smooth shell owing to the increase of the magnitude of drag coefficient.

Movie S3. A silicone oil droplet (diameter of ~ 0.7 mm) covered by non-ohmic clay mineral particles (Li-fluorohectorite). Subjected to an E -field of $\sim 270 \text{ V}\cdot\text{mm}^{-1}$ the droplet slowly rotated with at a rate of around $0.2 \text{ rad}\cdot\text{s}^{-1}$. The rotation rate was increased by increasing the E -field strength up to $\sim 300 \text{ V}\cdot\text{mm}^{-1}$. However, at $E \sim 330 \text{ V}\cdot\text{mm}^{-1}$ the clay particle-covered droplet stopped rotating. The dipole moment on the droplet covered by the clay film flipped at $E \sim 330 \text{ V}\cdot\text{mm}^{-1}$, and thus, the E -field acted on a droplet by stretching it along the E -field direction.

Movie S4. Electrorotation used for changing shape of a droplet and porosity of its particle shell. A droplet covered with $50\text{-}\mu\text{m}$ PE particles electrorotate in E -field of 350 and $600 \text{ V}\cdot\text{mm}^{-1}$. The movie was sped up 4 times.

Movie S5. A droplet with diameter ~ 2 mm covered with $50\text{-}\mu\text{m}$ PE particles (red and cyan) forming a Janus shell subjected to $E = 700 \text{ V}\cdot\text{mm}^{-1}$. The movie was sped up 4 times and then 10 times.

Movie S6. Breaking the droplet agglomerates down to individual droplets. Optical microscope images of silicone oil emulsions droplets covered by $10\text{-}\mu\text{m}$ PS particles. Castor oil was used as a continuous medium. An E -field of $200 \text{ V}\cdot\text{mm}^{-1}$ was applied to promote electrocoalescence of droplets, whereas a stronger E -field of $500 \text{ V}\cdot\text{mm}^{-1}$ was applied to induce electrorotation of droplets and droplet clusters to help the clustered droplets to separate. The electric field was applied in horizontal direction, and the movie was sped up two times.

Movie S7. Detachment of surface microparticles from a silicone oil droplet (diameter of ~ 1.7 mm). Application of a strong field of $\sim 850 \text{ V}\cdot\text{mm}^{-1}$ caused the particle to crumple and eventually irreversibly detach from the surface of the droplet. The droplet is imaged parallel to the direction of the E -field through transparent electrodes.

Paper VII

Electric-field-induced deformation, yielding, and crumpling of jammed particle shells formed on non-spherical Pickering droplets

K Khobaib, A Mikkelsen, T Vincent-Dospital and Z Rozynek

Soft Matter **17**, 5006–5017 (2021)



Cite this: *Soft Matter*, 2021, **17**, 5006

Electric-field-induced deformation, yielding, and crumpling of jammed particle shells formed on non-spherical Pickering droplets†

K. Khobaib, ^a A. Mikkelsen, ^a T. Vincent-Dospital ^b and Z. Rozynek ^{*ab}

Droplets covered with densely packed solid particles, often called Pickering droplets, are used in a variety of fundamental studies and practical applications. For many applications, it is essential to understand the mechanics of such particle-laden droplets subjected to external stresses. Several research groups have studied theoretically and experimentally the deformation, relaxation, rotation, and stability of Pickering droplets. Most of the research concerns spherical Pickering droplets. However, little is known about non-spherical Pickering droplets with arrested particle shells subjected to compressive stress. The experimental results presented here contribute to filling this gap in research. We deform arrested non-spherical Pickering droplets by subjecting them to electric fields, and study the effect of droplet geometry and size, as well as particle size and electric field strength, on the deformation and yielding of arrested non-spherical Pickering droplets. We explain why a more aspherical droplet and/or a droplet covered with a shell made of larger particles required higher electric stress to deform and yield. We also show that an armored droplet can absorb the electric stress differently (*i.e.*, through either in-plane or out-of-plane particle rearrangements) depending on the strength of the applied electric field. Furthermore, we demonstrate that particle shells may fail through various crumpling instabilities, including ridge formation, folding, and wrinkling, as well as inward indentation.

Received 23rd January 2021,
Accepted 20th April 2021

DOI: 10.1039/d1sm00125f

rsc.li/soft-matter-journal

1 Introduction

Particles of nano- and micrometer size can strongly adhere to droplet interfaces,¹ forming a particle shell that changes the mechanical properties of the fluid droplet interface.^{2–4} Droplets densely covered with particles (referred to as Pickering droplets) constitute Pickering emulsions and Pickering emulsion gels,^{5–7} and can be used to produce particle capsules.^{8–10} Such emulsions and capsules are promising for many applications, particularly in the pharmaceutical and food industries,^{11–13} as well as in the oil industry and biofuel processing.^{14,15} Moreover, particle-covered droplets facilitate the fabrication of new materials^{16–18} and can be designed to form novel adaptive structures.^{19,20} Pickering droplets can also be used in basic research, *e.g.*, as model systems for mimicking the physical properties of red blood cells²¹ or for studying particle crystal growth and ordering or particle layer buckling on curved interfaces.^{22–26}

In many research areas, knowledge of the stability and mechanics of an individual Pickering droplet is essential, *e.g.*, for the efficient fabrication of Pickering emulsions,²⁷ for designing emulsions with controlled stability,^{28,29} and, in general, for the further development of the abovementioned research fields. Several research groups have studied theoretically and experimentally the deformation,^{30–34} relaxation,^{35,36} and mechanical properties of Pickering droplets.^{37,38} Most of the research concerns spherical droplets. Yet several studies exist on non-spherical Pickering droplets, investigating the droplets' fabrication,^{38–41} deformation, kinetic, relaxation, and rheological properties.^{42–45} However, little is known about arrested non-spherical particle shells subjected to stress. The experimental results presented here contribute to filling this gap in research. The objective of this study is thus to understand and describe the behavior of non-spherical Pickering droplets with jammed particle shells under stress.

We use an electric field (E-field) to induce a compressive electric stress on a Pickering droplet and study both qualitatively and quantitatively the droplet's response to the E-field. The questions of principal interest in this research were the following: (i) How does particle shell geometry affect the critical E-field strength required for arrested Pickering droplets to collapse? (ii) How do particle and droplet size affect the

^a Faculty of Physics, Adam Mickiewicz University, Uniwersytetu Poznańskiego 2, 61-614 Poznań, Poland. E-mail: zbiroz@amu.edu.pl

^b PoreLab, The Njord Centre, Department of Physics, University of Oslo, Blindern, N-0316 Oslo, Norway

† Electronic supplementary information (ESI) available: Eight supplementary movies. See DOI: 10.1039/d1sm00125f



collapsing mechanism of non-spherical Pickering droplets? (iii) How does the E-field strength affect the wrinkling and crumpling of particle shells? To answer these questions, we performed experiments on mm-size silicone oil droplets coated with electrically insulating polymeric microparticles suspended in castor oil and subjected to direct current (DC) E-fields.

Various E-field approaches have been demonstrated to be useful in investigating the deformation,^{34,46} electrorotation,³² propulsion,⁴⁷ and buckling⁴⁵ of Pickering droplets. Here, we use a static and uniform E-field to generate compressive stress *via* charge accumulation on the droplet's surface. Under a DC E-field, free charges (impurities in the oils) accumulate at the oil–oil interface. Depending on the electrical properties of the oils and particles, the Pickering droplet may acquire a dipole moment oriented either parallel or antiparallel with the E-field. In our experiments, we prepared Pickering droplets with an electrical conductivity smaller than that of the surrounding castor oil. The charge relaxation time ($\tau = \epsilon\epsilon_0/\sigma$, where ϵ is the relative dielectric permittivity, ϵ_0 is the vacuum permittivity, and σ is the electric conductivity) of castor oil is shorter than that of silicone oil, so the droplet acquires a dipole moment oriented antiparallel with the E-field. As a result, compressive stress is exerted on the Pickering droplet (see Fig. 1a), whose magnitude is controlled by the strength of the E-field. We used this compressive mode to study the mechanical properties of the particle shells.

2 Materials and methods

2.1. Materials

The particle-covered droplets used in our experiments were made of silicone oil (Rhodorsil Oils 47, with electrical conductivity $\sigma_{\text{in}} \sim 10 \text{ pS m}^{-1}$, relative permittivity $\epsilon_{\text{in}} \sim 2.8$, density $\rho_{\text{in}} \sim 0.96 \text{ g cm}^{-3}$ at 25 °C, and viscosity $\sim 50 \text{ mPa s}$ at 25 °C) and polyethylene (PE) particles with diameters between around 2 and 100 μm (Cospheric LLC, with electrical conductivity $\sigma_{\text{pe}} < 1 \times 10^{-15} \text{ S m}^{-1}$, relative permittivity $\epsilon_{\text{pe}} \sim 2.3$, and density $\rho_{\text{pe}} \sim 1.0 \text{ g cm}^{-3}$). Depending on particle size and the desired volume and shape of the droplets, the concentration of particles was between 8% and 12% by weight (see ref. 27 for the formula for

obtaining densely packed spherical shells). Castor oil (Sigma-Aldrich 83 912, with electrical conductivity $\sigma_{\text{ex}} \sim 100 \text{ pS m}^{-1}$, relative permittivity $\epsilon_{\text{ex}} \sim 4.7$, density $\rho_{\text{ex}} \sim 0.96 \text{ g cm}^{-3}$, and viscosity $\sim 750 \text{ mPa s}$ at 25 °C) was used as an external fluid. Castor oil and silicone oil are immiscible, and the interfacial tension between them is $\sim 4.5 \text{ mN m}^{-1}$.

2.2. Experimental set-up

The experimental set-up consisted of a signal generator (SDG1025, SIGLENT Technologies Co, Ltd, China), a voltage amplifier (20HVA24-BP1, HVP High Voltage Products GmbH, Germany), a digital microscope (AM7315MZT, Dino-Lite, AnMo Electronics Corporation, Taiwan), a light source (KL 300 LED, Schott AG, Germany), a computer for collecting images and recording videos, and a sample cell (an optical glass cuvette of 15 mm \times 15 mm \times 30 mm) with two inserted copper plates that acted as electrodes. The sample cell was placed on a mechanical XYZ translation stage (LT3, Thorlabs, Sweden) to ease its positioning relative to the optical path of the microscope. The observation view of the microscope was always perpendicular to the E-field (which in all figures is in the horizontal direction). A schematic figure illustrating the experimental set-up is shown in Fig. 1b.

2.3. Formation of a non-spherical Pickering droplet

Castor oil was poured into a sample cell. Silicone oil and particles were measured by weight and then stirred together to make a dispersion. To form a dispersion droplet in the castor oil, we used a mechanical pipette. When a silicone oil droplet with particles was formed in the castor oil, most of the particles resided inside the droplet. To bring the particles to the droplet's interface, we used an E-field, as demonstrated in ref. 2 and 8. As soon as a particle reached the interface, it was transported toward the electric equator of the droplet by the convective motion of liquids (*i.e.*, induced electrohydrodynamic flows).^{48,49} Particles at the equator formed a densely packed particle film that widened as time passed and more particles reached the interface (typically taking a few minutes). The final particle packing and the coverage of the droplet's interface depended on the applied E-field and the particle concentration. Extensive details of the method can be found in our previous studies.^{19,50}

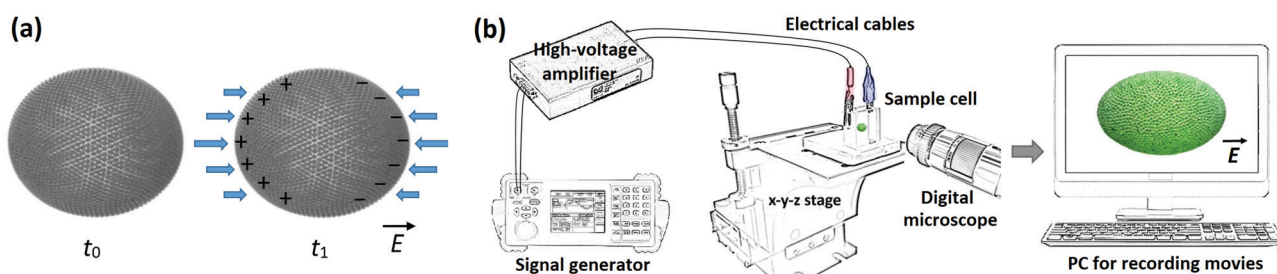


Fig. 1 (a) A schematic diagram illustrating the electric phenomena used in the experiments. A non-spherical Pickering droplet is initially stable when no E-field is applied (t_0). Application of an E-field (t_1) causes free charges (impurities in the oils) to accumulate at the droplet's interface. The action of the E-field on these charges yields electric stresses, which may deform and compress the droplet in various ways and with different dynamics (studied here in detail). (b) A schematic illustration of the set-up used in all the experiments. The set-up consisted of a signal generator, a voltage amplifier, a digital microscope with a perspective perpendicular to the direction of the E-field, a glass sample cell with copper electrodes placed on a mechanical XYZ translational stage, and a computer for data collection.



To make a stable non-spherical droplet with a jammed particle shell, we coalesced two spherical droplets that were initially almost fully covered with particles, as shown in Fig. S1 and Movie S1 (ESI[†]). To further tune the shape of the arrested Pickering droplet, we electrorotated it at an elevated DC E-field (between 500 and 800 V mm⁻¹). As the Pickering droplet rotated, it also stretched, allowing unjamming of the shell particles. By turning off the E-field, the droplet relaxed and reduced the area of its interface, thereby again inducing particle jamming and the formation of a shell. However, the structure of the shell was now more disordered and porous compared with the structure of the initial shell (see also ref. 51). We found that when the droplet was further stretched (by applying stronger E-fields), the particle shell that formed after switching off the E-field was more elongated and more porous. Finally, as a droplet with a new shape was formed, we used an AC E-field (e.g., 100 Hz, 300 V mm⁻¹) to align it with its major axis along the direction of the E-field. In the AC E-field, the droplet acquires a dipole moment oriented parallel with the E-field, so the droplet is stretched. Whenever it was necessary to make the droplet more ellipsoidal and symmetric, we further increased the strength of the AC E-field up to 1 kV mm⁻¹. In Movie S2 (ESI[†]), we provide an example of the electrorotation of a droplet in a DC E-field and an example of the aligning and shaping of a droplet in an AC E-field.

2.4. Image processing and estimation of the local curvature

Images taken in the experiment on the prolate-to-oblate shape transition of particle-covered droplets subjected to different E-field strengths (presented in Section 3.4) were processed using MATLAB[®] software and its Image Processing Toolbox[™]. On each image, the shape of the droplet (2D-projected onto our camera's focal plane) was first detected from the luminance contrast between the droplet and the background oil by using an automatic boundary tracing algorithm. We applied a running-average smoothing filter to the derived shapes to attenuate the sharp edges arising from the discrete representation of the droplets (i.e., due to the camera's pixel size). With a least-square method,⁵² we then inverted the circle equations that best fitted the various local portions of the obtained periphery of the droplet. We thus computed the local curvature along the droplet's shape as the inverse of the fitted circle's radius. For the MATLAB[®] code, see the ESI[†].

3 Results

3.1. E-Field-induced deformation and yielding

An arrested Pickering droplet made of silicone oil and 30 μm polyethylene (PE) particles was prepared in castor oil. The droplet was non-spherical with a deformation of ~0.2 (left inset image in Fig. 2). Deformation is defined as $D = (d_{\parallel} - d_{\perp}) / (d_{\parallel} + d_{\perp})$, where d_{\parallel} and d_{\perp} are the lengths of the droplet's axes parallel and perpendicular to the direction of the E-field, respectively. The application of an E-field resulted in the generation of compressive stress on the droplet. In weak

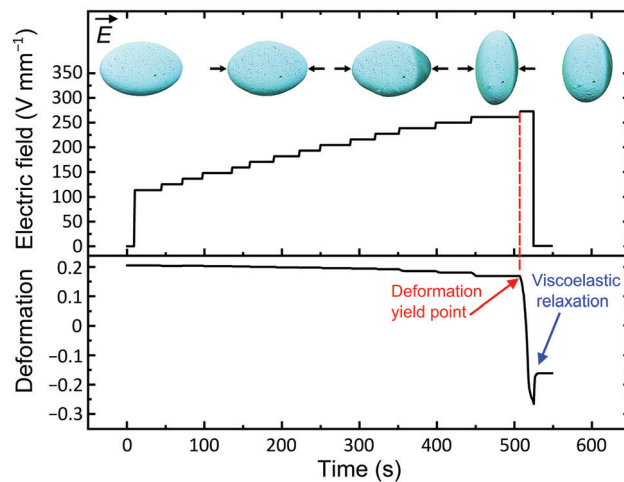


Fig. 2 E-Field-induced deformation of an arrested droplet with a jammed particle shell. Dynamic deformation of an arrested Pickering droplet made of silicone oil covered with 30 μm PE particles. Initially, the major and minor axes of the droplet were 3.9 and 2.6 mm, respectively (left inset image). The Pickering droplet was suspended in castor oil and subjected to a DC E-field that was stepwise increased. In the inserted images, the direction of the E-field was horizontal, and the arrows schematically indicate the compressive electric forces. See also corresponding Movie S3 (ESI[†]).

E-fields (less than 200 V mm⁻¹), we observed no change in the droplet's shape. However, in stronger E-fields, the droplet deformed and eventually yielded, which led to a prolate-to-oblate deformation transition.

The quantitative data are presented in Fig. 2, in which we plot the measured values of the droplet's deformation *versus* time and the strength of the applied E-field. As the E-field was stepwise increased from 0 to 225 V mm⁻¹, the magnitude of the droplet's deformation was mostly unchanged ($\Delta D \sim 0.01$). The elastic stress from the particle layer was sufficiently strong to withstand the electric stress, and the prolate shape of the droplet was undisturbed. At moderate E-field strengths (between 225 and 265 V mm⁻¹), we observed small changes in the droplet's deformation ($\Delta D \sim 0.03$). This deformation was caused by the rearrangement of particles; that is, the packing of the particles increased, and/or the particles deformed out-of-plane. At $E \sim 272$ V mm⁻¹, the droplet went through a prolate-to-oblate deformation transition. This E-field threshold is referred to as the critical yield point of the droplet, E_y . The droplet yielded when the total magnitudes of the applied electric stress and the capillary stress (originating from the surface tension between the liquids) were sufficiently large to overcome the mechanical resistance of the particle layer. This experiment demonstrates that the particle layer of an arrested Pickering droplet subjected to compressive electric stress resembles a Bingham plastic material. That is, it behaves like a solid material at low applied stresses and becomes liquid-like when the applied stress exceeds a yield stress point.

We noted that shortly before turning off the E-field (~520 s in Fig. 2), the droplet was compressed to such an extent that the particle layer unjammed. Nevertheless, as soon as the E-field was switched off, the droplet relaxed (D changed by ~0.1),



causing the particles to jam again; hence the main part of the oblate deformation remained. The inset images in Fig. 2 show how the arrested Pickering droplet was compressed from a prolate shape into an oblate geometry (see also Movie S3, ESI†). The arrows schematically indicate the direction of the electric forces that acted on the droplet.

The evolution of the Pickering droplet's deformation can also be studied with a test in which the droplet is subjected to an E-field of constant strength for a long time, rather than to an E-field that is stepwise increased. Such a bifurcation measurement requires more time and effort than the experiment presented above. However, it may provide more precise estimates of the values of the yield point and enables studying the deformation dynamics.

In Fig. 3, we present the results of a bifurcation experiment performed on a non-spherical PE particle-covered droplet studied at different E-field strengths (114–796 V mm⁻¹). At each E-field strength, the data were collected for up to two minutes. We re-shaped the droplet (see the procedure described in Section 2.3) before each experiment to obtain the same initial non-spherical geometry; that is, the minor axis is 2.5 mm and the major axis is 4.0 mm. In lower E-fields (up to 256 V mm⁻¹), the droplet's deformation was small, and the droplet reached a stable prolate state (shown in Fig. 3). This occurred because the applied electric stress was not strong enough to overcome the elastic energy of the particle shell, and the droplet stayed in a prolate shape. When the droplet was subjected to stronger E-fields; that is, $E \geq E_y = 257 \text{ V mm}^{-1}$, it deformed continuously from a prolate into an oblate shape.

We found that above the critical E-field strength, the prolate-to-oblate deformation transition time varied with the applied E-field strength. For example, at $E = 257 \text{ V mm}^{-1}$, the transition

took several seconds, whereas at $E = 796 \text{ V mm}^{-1}$ it took less than a second. While performing this experiment, we also observed that depending on the strength of the applied E-field, the electric stress was absorbed differently by the Pickering droplet (through in-plane or out-of-plane particle rearrangements). We investigate and discuss this observation in Section 3.4.

The value of the yield point obtained from the bifurcation test (257 V mm⁻¹) differs slightly from the value estimated from the first experiment in which the E-field strength was stepwise increased (272 V mm⁻¹). The difference may arise from applying different methodologies since in the experiment presented in Fig. 2, we changed the E-field strength in steps of $\sim 15 \text{ V mm}^{-1}$. It can also result from a difference in the initial geometry of the studied Pickering droplets (the initial droplet in the experiment presented in Fig. 3 was more elongated than the one shown in Fig. 2). We therefore decided to study the influence of the droplet's initial geometry on the deformation and yielding of a non-spherical Pickering droplet.

3.2. Effect of initial droplet geometry on deformation and yielding

We prepared five Pickering droplets with the same volume (within an error of less than 3%) but different shapes and subjected them to E-fields between 0 and 260 V mm⁻¹. Except for particle size (now 50 μm), the other parameters, such as particle material and oil type, were the same as in the experiments described in the previous section. Fig. 4a presents the deformation values plotted against the applied E-field strength for the Pickering droplets with different initial shapes (shown in the inset images of Fig. 4a). The results show that the more elongated Pickering droplets (with larger asphericity) yielded at higher E-field strengths. We here assumed that the droplets had an axisymmetric shape and that they were initially ellipsoidal. Thus, the asphericity (its degree) of the initial shape of a droplet can be defined by the local curvature at the droplet's electric pole, $\kappa = b/a^2$, where a and b are the minor and major semi-axes of an ellipsoid. In the inset of Fig. 4a, we normalized the data by dividing the argument values by $\sqrt{\kappa}$. All the data, except the values for the droplet that was initially the least deformed, collapsed into one master curve, indicating that $E_y \propto \sqrt{\kappa}$. The data points marked with up-pointing blue triangles (droplet no. 5) lay outside the master curve because this nearly spherical droplet began electrorotating at $E > 200 \text{ V mm}^{-1}$ (this phenomenon is explained in detail in ref. 51). As a result, a stronger E-field was required to compressively deform the droplet.

The droplets in Fig. 4a had different prolate asphericities but also different aspect ratios b/a . To exclude the role of the aspect ratio in the droplet's deformation and yielding (and to present the curvature dependence), we performed an additional set of experiments. We used three Pickering droplets of different volumes (10–23 mm³) but with the same aspect ratio $b/a \sim 1.8$ (see images in Fig. 4b). The droplets were subjected to E-fields of different strengths (increased stepwise). Again, we found that the value of E_y was higher for the particle shells with larger curvature

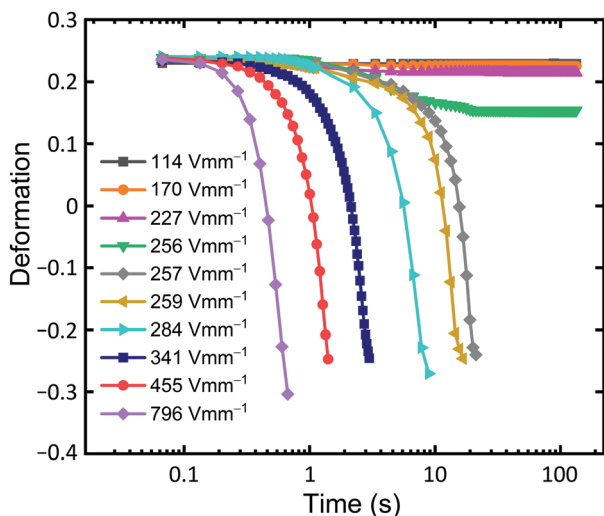


Fig. 3 Bifurcation measurement. Deformation dynamics of an arrested PE Pickering droplet (major axis = 4.0 mm, minor axis = 2.5 mm) covered with 30 μm PE particles under different DC E-field strengths. In weak E-fields, the particle shell deformed slightly but remained in a prolate-like shape. Above the critical E-field, the droplet changed its geometry continuously from a prolate into an oblate shape.



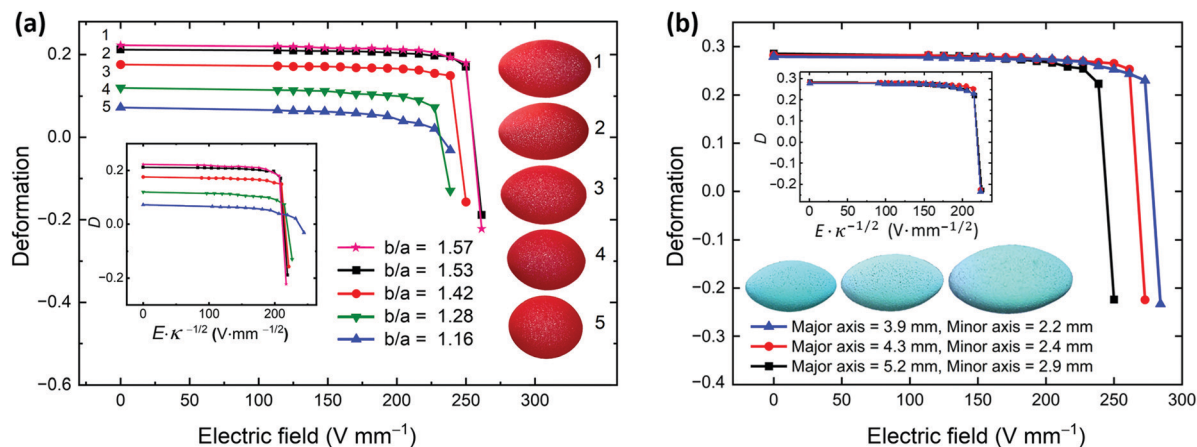


Fig. 4 Influence of the droplet's initial geometry on deformation and yielding. (a) Arrested non-spherical PE Pickering droplets made of 50 μm PE particles subjected to DC E-fields of different strengths. The initial droplet geometries varied, as shown in the inset images. (b) Arrested Pickering droplets with different volumes but with the same aspect ratio $b/a \sim 1.8$. The droplets (covered with 30 μm PE particles) were subjected to DC E-fields of different strengths (increased stepwise). In the inset, we plot the collapsed data.

values (see Fig. 4b). For example, the largest droplet yielded at $E \sim 250 \text{ V mm}^{-1}$, while the smallest droplet yielded at $E \sim 284 \text{ V mm}^{-1}$. In the inset of Fig. 4b, we plot D versus $E\kappa^{-1/2}$, and the collapsed data indicate that $E_y \propto \sqrt{\kappa}$.

3.3. Influence of particle size on deformation and yielding

In the next experiment, we study the effect of particle size on the mechanical properties of particle shells. We prepared non-spherical Pickering droplets covered with PE particles of sizes ranging from 2 to 100 μm . The initial shapes of all the droplets were similar, and they had similar volumes (within an error of less than 3%). The droplets were subjected to DC E-fields ranging from 0 to 285 V mm^{-1} . We found that the critical E-field for yielding (*i.e.*, deforming a droplet into an oblate shape) depended on the size of the particles on the droplet's interface (Fig. 5). For example, for a particle shell composed of 2 μm PE particles, the critical E-field was around $\sim 250 \text{ V mm}^{-1}$, whereas for a particle shell composed of 100 μm PE particles, the critical E-field was $\sim 285 \text{ V mm}^{-1}$. We found that the critical E-field scaled as $E_y \propto d^{0.04}$ (see inset plot in Fig. 5) for a Pickering droplet that was initially ellipsoidal with an aspect ratio $b/a \sim 1.5$.

Unlike elastic membranes on droplets/bubbles, shells made of particles can undergo structural changes; that is, the particles can change positions relative to their neighbours. This, in turn, helps to accommodate the applied stresses. In Movie S4 (ESI[†]), we demonstrate, with a few examples, how particles rearrange in-plane, enabling the droplet to change its shape.

Particle shells on curved interfaces may also deform by buckling through ridges, folds, or wrinkles.^{53–55} As we will show in the next section, the rate of compression will determine the buckling mode. In the experiment of which the results are shown in Fig. 5, we observed the formation of several bumps with small amplitudes. These bumps, observed typically at $E_y/2 < E < E_y$, were formed near the electric equator of the droplet. Their localization is not very symmetric, which could be the

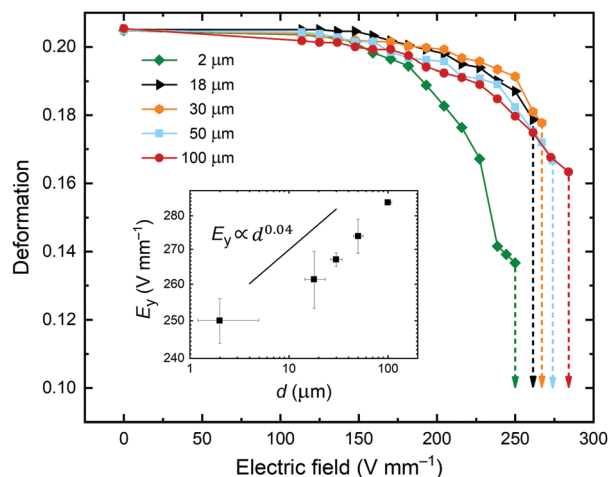


Fig. 5 Effect of particle size on droplet deformation. Deformation of silicone oil droplets covered with PE particles of sizes ranging from 2 to 100 μm . The magnitude of droplet deformation is plotted against the applied E-field. The major and minor axes of the droplets were 4.4 and 2.9 mm, respectively ($b/a \sim 1.5$). The value of E_y is plotted vs. the particle diameter. The standard deviation bars are estimated from two series of experiments. The dashed lines indicate the continuous prolate-to-oblate shape transition.

effect of the geometrical disorder in the particle shell. We note that the particles used in the experiments were slightly poly-dispersed. Thus, a geometrical disorder of particle positions perpendicular to the mean plane of the monolayer is expected. These geometrical deviations may contribute to the deformation of the particle shell by the mechanisms of the particle overlapping and disentanglement.⁵⁶ These phenomena may cause local out-of-plane deformations that result in the densification of the monolayer and a reduction in the surface area occupied by the particles. This, in turn, enables shape changes of a Pickering droplet.

In general, we observed less in-plane particle motion for bigger particles ($\geq 50 \mu\text{m}$) than for smaller particles.



Qualitatively, the behaviour of shells composed of bigger particles resembles that of a granular arch. Pitois *et al.*⁵⁶ studied the collapsing of armoured bubbles and droplets by deflation. They observed a transition in particle shell deformation depending on the ratio of particle size to droplet size. Like us, they found that droplets covered with small particles were easier to deform than those covered with larger particles.

Structured interfaces can also absorb compressive stress by the expulsion of material into one of the liquid phases.⁵⁷ We did not observe this process in the system studied here. The microparticles used in our experiments were rather large and therefore strongly bound to the silicone oil–castor oil interface (with a binding energy $\approx 10^4 k_B T$),⁵⁵ thus preventing particle expulsion.

3.4. Absorption of electric stress by the particle shell

As noted in Section 3.1, we observed that a Pickering droplet absorbed the electric stress differently depending on the strength of the applied E-field. To investigate this phenomenon further, we performed additional experiments to study the influence of both the compression dynamics and the particle size on the wrinkling of particle shells. The Pickering droplets used in the experiments were covered with PE particles of sizes ranging from 2 to 100 μm . The droplets had similar volumes and initial shapes. They were suspended in castor oil and subjected to E-fields of strengths 350, 700, and 1050 V mm^{-1} . Under these E-fields, the droplets continuously deformed from prolate into oblate shapes. When the weakest E-field (with a strength of 350 V mm^{-1}) was applied, the particle shells deformed slowly. The droplets deformed from a prolate into an oblate shape without an observable formation of wrinkles at their particle shells or irregular folds with small amplitudes (see Fig. 6a and Fig. S2, ESI†).

Slow compression of particle shells facilitate in-plane particle rearrangements analogous to the gliding of grain layers in granular flows.⁵⁸ In response to the compressive electric stress, the surface particles started to move relative to one another. We observed several slip lines appearing during shell compression. A similar phenomenon was observed and presented in ref. 37. Note that in stronger E-fields of 700 and 1050 V mm^{-1} , the particle shells deformed considerably faster (see Fig. 6b and c). Consequently, the particles did not have sufficient time to rearrange and thus deformed out-of-plane, forming more regular wrinkles. The wrinkles were formed perpendicular to the applied electric field, as the particle layer was compressed in the direction from the electric poles to the electric equator, as indicated by the arrows in Fig. 6c.

At the strongest E-field strength (1050 V mm^{-1}), we observed wrinkling of particle shells on all droplets (see Fig. 7 and corresponding Movie S6, ESI†). The wrinkling pattern can be quantified in terms of the wrinkling wavelength. Because the wrinkling wavelength is sensitive to the strain,⁵⁹ it had to be measured in such a way that we could compare the results of the droplets coated with particles of different sizes (which have a different deformations at different times). We decided to measure the wavelength of the wrinkles that were formed close to the electric equator of a droplet, at the time when the droplet was slightly oblate (see the droplets marked with the dashed rectangle in Fig. 7a–d), that is, when the wrinkles could be clearly observed. In Fig. 7e, we plot the wavelength values (λ) against the particle diameter d . We found that the wrinkling wavelength scaled roughly as $\lambda \propto \sqrt{d}$. Similar scaling behaviour was reported by researchers who studied wrinkling of particle monolayers formed on either flat liquid–air interfaces^{60,61} or liquid–liquid interfaces.⁵⁵

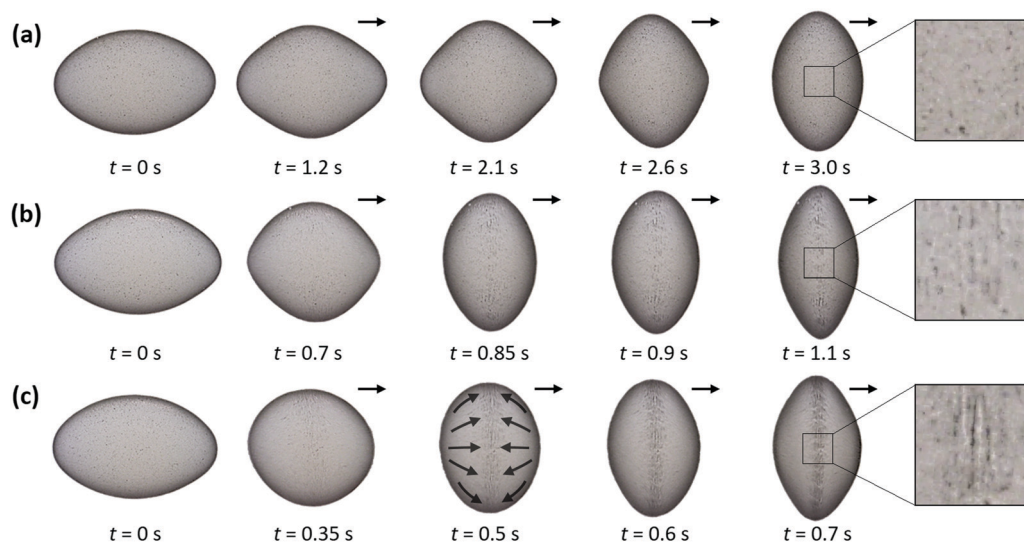


Fig. 6 Deformation of particle shells at different E-field strengths. Arrested droplets with PE particle shells composed of 2 μm PE particles. Initially, at $t = 0$ s, the particle shells were ellipsoidal, with a major axis of ~ 3.9 mm and a minor axis of ~ 2.6 mm. The particle-coated droplets were subjected to E-fields of strengths (a) 350, (b) 700, and (c) 1050 V mm^{-1} applied in the horizontal direction, as indicated by the arrows. In these E-fields, the droplets continuously deformed from prolate into oblate shapes. See also corresponding Movie S5 (ESI†).



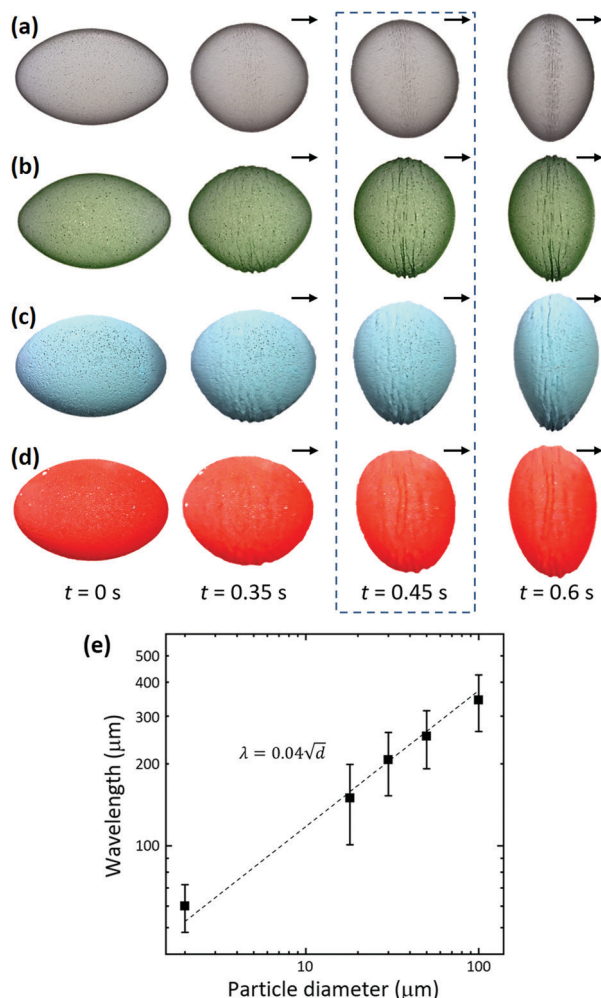


Fig. 7 Wrinkling of particle shells. Four droplets covered with PE particles of different diameters, (a) 2 μm, (b) 18 μm, (c) 30 μm, and (d) 50 μm, were subjected to an E-field of strength 1050 V mm⁻¹ applied in the horizontal direction, as indicated by the arrows. Initially, at t = 0 s, the particle shells were ellipsoidal, with a major axis of ~3.9 mm and a minor axis of ~2.6 mm. (e) A log–log plot of the measured crumpling wavelength of the deformed particle shells as a function of the particle size. See also Movie S6 (ESI†).

We fitted the data with the square root power function (dashed line in Fig. 7e) to compare our results with the results of other studies. We found that the wavelengths of the wrinkles ($\lambda = 0.04d^{0.5}$) were shorter than those reported for particle layers on flat interfaces. For example, $\lambda_v = 0.24d^{0.49}$ and $\lambda_j = 0.25d^{0.5}$ were reported by Vela *et al.*⁶¹ and Jambon *et al.*,⁶⁰ respectively. The shorter wavelengths observed for our particle shells are due to the curvature of the interface. Any deformation on a curved interface yields an additional strain contribution that increases the elastic energy of the particle layer, which in turn gives rise to shorter wavelengths. The wavelengths observed here are also shorter than those reported in our previous studies on particle shells formed on mm-sized droplets ($\lambda = 0.07d^{0.5}$).⁵⁵ This difference in wavelength is to be expected because a particle shell is strained more by compressive stress than by hoop stress, as demonstrated in ref. 55.

While performing the experiments on the Pickering droplets' prolate-to-oblate transition at various strengths of the E-field, another feature caught our interest. Depending on the compression dynamics (*i.e.*, the E-field strength), the particle-covered droplets underwent different shape transformations at the intermediate stages of the transition. In Fig. 8a, we present images of the experiment on Pickering droplets made of 2 μm particles (shown in Fig. 6). This time, we chose the frames of the recorded videos in such way that we could compare the droplets' shapes at similar stages of the prolate-to-oblate transition. Using the MATLAB software suite (see ESI† for the MATLAB code), we estimated the curvature values along the droplets' edges. The automatically detected droplets' contours, together with the calculated color-coded values of the curvature, were added to the experimental images.

The difference between the droplets' projected two-dimensional (2D) shapes is clearly seen in the middle column of Fig. 8a. The contour of the Pickering droplet subjected to the weakest E-field resembles a rhombus shape, whereas that of the Pickering droplet subjected to the strongest E-field is nearly spherical. A similar tendency was also observed for droplets covered by larger particles of 18–50 μm (see Fig. S3, ESI†).

We further computed the data to present the curvature distributions at different stages. The results are displayed using polar plots to properly appreciate the variations in curvature values along the polar angle (Fig. 8b) and bar plots to show the probability distribution (Fig. 8c). For the sake of image clarity, we show the data only at three characteristic times: before the application of the E-field, in the middle of the prolate-to-oblate transition, and just before the E-field was turned off. For the full analysis, see corresponding Movie S7 (ESI†).

The polar plots presented in Fig. 8b reveal how the curvature varies as a function of the direction. As expected, the maximum values of the curvatures of all three initial droplets (before the application of an E-field) align with the first principal curvature direction (see left panel in Fig. 8b). From the histogram shown on the left panel of Fig. 8c, we learn that the probability distribution of the curvature values is bimodal for all three droplets, with the major mode located at ~0.4 mm⁻¹.

After the E-field was applied, the Pickering droplets acquired distinctively different shapes. In the middle of the transition, the curvature variation along the polar angle is very different for the three Pickering droplets. The droplet that was compressed slowly (at $E = 350$ V mm⁻¹) developed a nearly bicone shape (a similar shape can also be observed when two liquid marbles coalesce *via* collision).⁶² The contour drawn around the droplet's 2D projection resembled a square, with maximum curvatures aligning in both principal polar directions and nearly flat regions in the ordinal directions. On the other hand, the Pickering droplet that was compressed very fast (subjected to $E = 1050$ V mm⁻¹) acquired an almost spherical shape. The contour drawn around that droplet's projection is almost a circle, and the curvature values are similar in all directions (see the middle panel of Fig. 8b, green line). Consequently, the probability distribution of the curvature also differs for each droplet. The distribution is almost uniform for the droplet



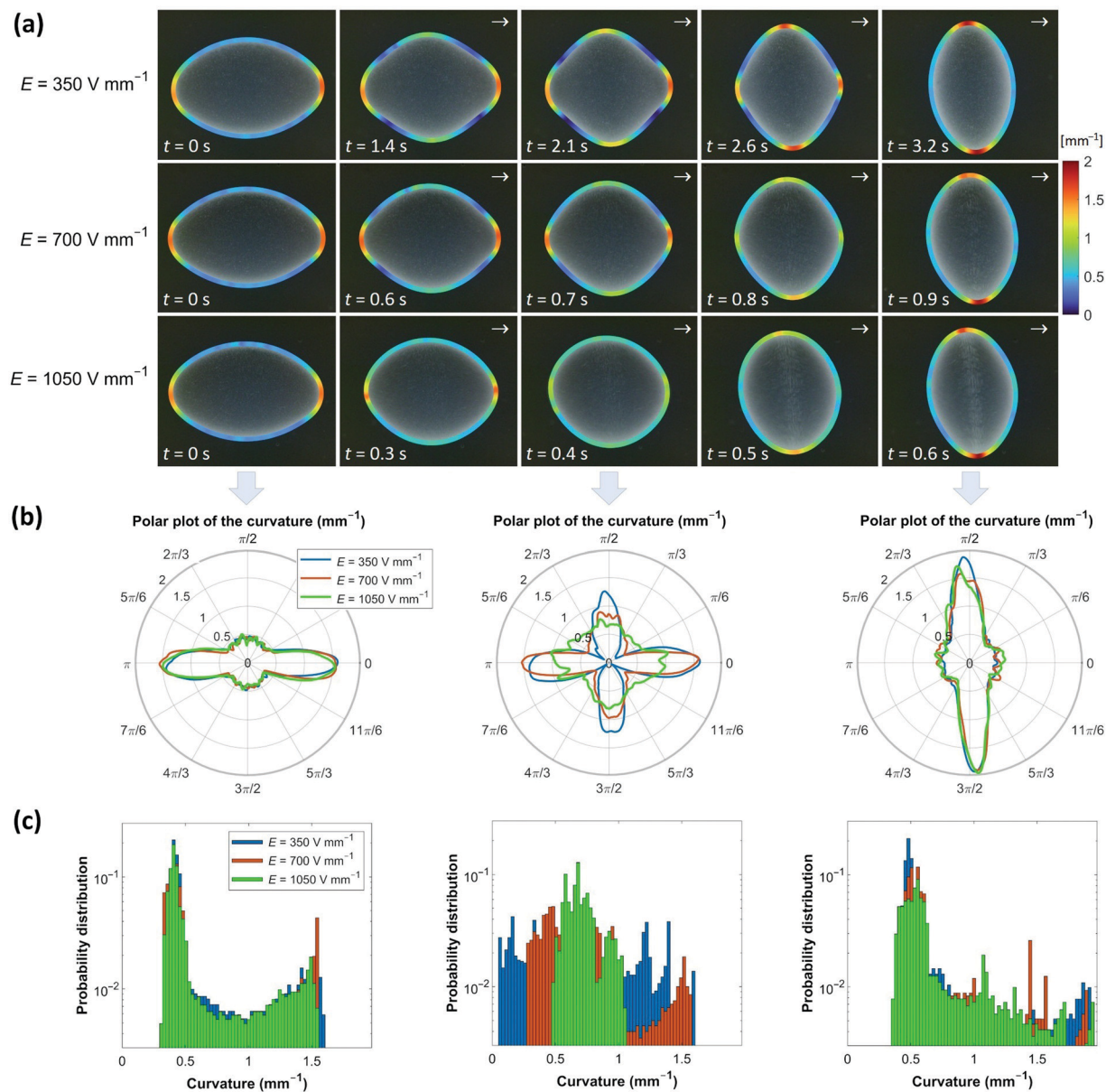


Fig. 8 Deformation of particle shells at different E-field strengths. Arrested droplets with particle shells made of $2 \mu\text{m}$ PE particles. The droplets were subjected to E-fields of strengths $350\text{--}1050 \text{ V mm}^{-1}$ applied in the horizontal direction, as indicated by the arrows. (a) Series of experimental images with added color-coded contours representing the values of the curvature (in mm^{-1}). The same color scale applies to all the images. (b) The estimated curvature values plotted against the 2D polar angle. (c) The curvature distributions are presented using bar charts. See also corresponding Movie S7 (ESI[†]).

subjected to the weakest E-field, whereas the histogram for the droplet subjected to the strongest E-field approaches a Dirac distribution centred at $\sim 0.7 \text{ mm}^{-1}$. Eventually, all the droplets obtained a similar oblate shape, and the data for the three droplets overlap again (see the right panels of Fig. 8b and c).

As already discussed, the slow compression of the particle shells enables in-plane particle rearrangements (possibly leading to a higher particle packing). This process costs less energy than the out-of-plane particle shell deformation and is therefore more favourable. Thus, in weak E-fields (just above E_y), the particle-coated droplet obtains a bicone-like shape when transitioning from a prolate into an oblate geometry. By contrast, the higher compression speeds (for a stronger E-field) allowed a deformation

with minimal time-dependent behaviour of the particles. The electric stress acting on the non-spherical Pickering droplets was absorbed mainly by the buckling of the particle shell buckling, as the particles had not enough time to rearrange themselves on the droplet's surface.

Let us now investigate, with a new set of experiments, how the initial shape of a Pickering droplet affects the morphologies of the wrinkles. We prepared Pickering droplets of equal volumes (within an error of less than 3%) but with different geometries (see the images in the left column of Fig. 9). The Pickering droplets were then subjected to an $E \sim 320 \text{ V mm}^{-1}$. We found that more elongated droplets deformed slower into an oblate shape than less elongated droplets (with time



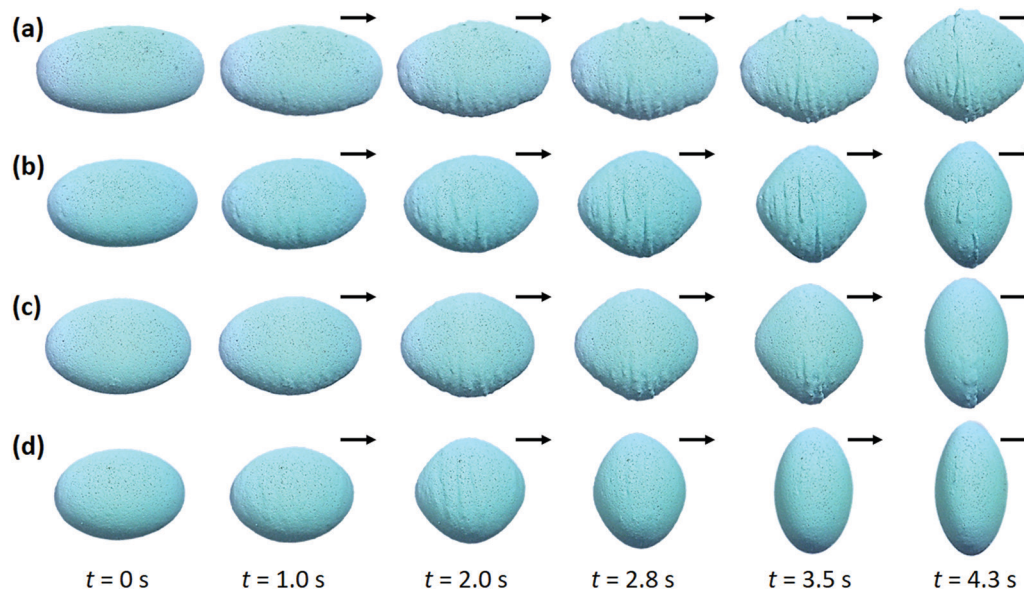


Fig. 9 Wrinkling of particle shells of different geometries. Droplets of equal volumes but different geometries were made of silicone oil covered with 30 μm PE particles. The different geometries of the Pickering droplets: (a) major axis = 4.6 mm, minor axis = 2.39 mm; (b) major axis = 4.12 mm, minor axis = 2.42 mm; (c) major axis = 3.98 mm, minor axis = 2.58 mm; and (d) major axis = 3.6 mm, minor axis = 2.63 mm. The shells were subjected to a DC E-field of 320 V mm^{-1} applied in the horizontal direction, as indicated by the arrows.

measured from the application of the E-field to the moment that the droplet obtains an oblate geometry). In Fig. 3, we show that the prolate-to-oblate deformation time decreased when the difference $E - E_y$ increased, where E is the applied E-field strength and E_y is the E-field threshold at which the droplet yields. From the results shown in Fig. 4a, we also observed that more elongated droplets (of the same volume) yielded at higher E-field strengths owing to differences in rigidity stemming from differences in curvature. The difference $E - E_y$ is thus smaller for the more elongated droplets, explaining why they deform slower than more spherically shaped droplets (compare Fig. 9a and d).

During the deformation transition from a prolate into an oblate shape, the droplet's surface area (A) changed; it decreased in the first phase and then increased. The change in surface area (ΔA) was greater for Pickering droplets that were initially more elongated than for droplets that were initially more spherical. Thus, the particle shells formed on the elongated droplets crumpled, with many clear folds with large amplitudes (Fig. 9a and b), to accommodate this large change in surface area during the shape transition. The shells formed on less elongated droplets (Fig. 9c and d) formed rather irregular and less apparent folds and ridges. In general, the buckled structures are not very symmetric, which we believe is the effect of the geometrical disorder in the particle shell.

3.5. Deformation of asymmetric shells formed on droplets

In Sections 3.2 and 3.3, we studied the effect of the initial droplet geometry and particle size on the deformation and yielding of a Pickering droplet. We concluded that a more aspheric droplet and/or a droplet covered with a shell made of larger particles required higher electric stress (*i.e.*, a stronger

E-field) to deform and yield than a droplet that is more spherical and/or covered with a shell made of smaller particles. Here, we study asymmetric Pickering droplets with a homogeneous shell (composed of one particle type) and a heterogeneous shell (consisting of two parts with different particle types).

In the first case, we prepared an asymmetric Pickering droplet with a homogeneous shell by coalescing two droplets of different sizes (~ 1.6 and 2.7 mm). One part of the shell was more curved than the other part (see Fig. 10a). Subjected to an E-field of 300 V mm^{-1} , the particle shell folded at the right part of the shell. This result is consistent with our experimental data presented in Section 3.2 since the shell yielded at the less curved side of the particle shell.

We also prepared three Pickering droplets with a heterogeneous shell. The shells were composed of white 2 μm PE particles and red 50 μm PE particles (Fig. 10b), red 50 μm PE particles and white 2 μm PE particles (Fig. 10c), and green 100 μm PE particles and white 2 μm PE particles (Fig. 10d). The droplets were slightly rounder on one side (the right side of the images in Fig. 10b and c). We designed one droplet with bigger particles on the more spherical part of the shell (Fig. 10b), while for the other droplet, the bigger particles were on the most aspherical part of the shell (Fig. 10c). The Pickering droplets were subjected to an E-field of 300 V mm^{-1} (above the critical E-field for yielding). At this E-field strength, the particle layer on both Pickering droplets folded at the more spherical part of the shell, regardless of whether this part of the shell was composed of smaller or larger particles. The result indicates that the difference in mechanical properties of the shell (frictional and/or elastic), as determined by particle size, is too small to be dominating. Thus, for such asymmetrically



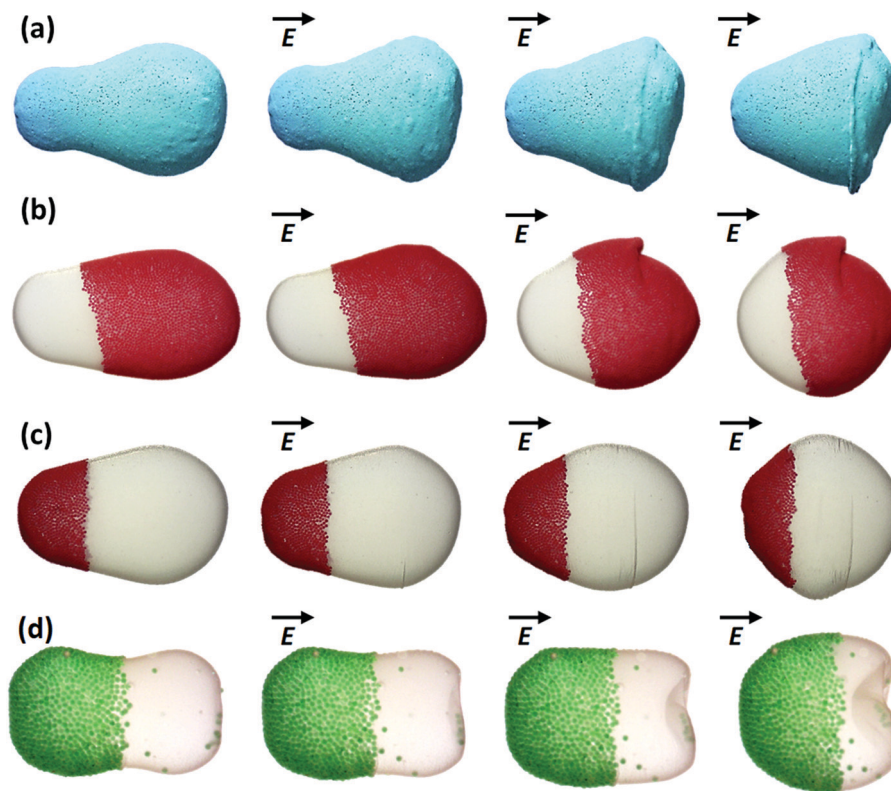


Fig. 10 Asymmetric Pickering droplets subjected to electric stress. (a) A homogeneous shell was made of blue 30 μm PE particles. (b–d) Heterogeneous particle shells were composed of (b) white 2 μm PE particles and red 50 μm PE particles, (c) red 50 μm PE particles and white 2 μm PE particles, and (d) green 100 μm PE particles and white 2 μm PE particles. The Pickering droplets were subjected to an E-field of 300 V mm^{-1} . The particle shells deformed through (a–c) one main fold or *via* (d) inward indentation. The direction of the E-field was horizontal, as indicated by the arrows. During compression, a vertical inward fold was formed at the right part of the heterogeneous shells. See Movie S8 (ESI \dagger) for a video of the deformation dynamics.

shaped Pickering droplets, the geometry of the particle shell (*i.e.*, its curvature) prevails over the mechanical properties of the particle shell.

In Fig. 10a–c, the particle shells deformed through one main fold. However, the droplet's deformation may also proceed through inward indentation. In Fig. 10d, we show the deformation of an aspherical peanut-like shell. Initially, before the application of the electric stress, the right part of the shell was flat. Subjected to an E-field, this flat part bent inward forming a concave cup-like shape. In the system studied here, the electric stress acts on the entire shell, with its magnitude distributed unevenly along the polar angle. However, the strongest force (in the normal direction to the shell surface) acts on the droplet's electric pole. Thus, it can be assumed (with some approximation) that the experiment with the electric field resembles the indentation tests of ellipsoidal shells.^{63,64} For a capsule with a thin shell (fulfilling the requirement $t_h/r \ll 1$, where r is the radius and t_h is the thickness), the axial stiffness of the shell scales proportionally to the curvature κ . As the shell is nearly flat on the right side of the arrested droplet, $\kappa \rightarrow 0$, and the electric stress near the electric pole is balanced only by capillary forces and the pressure difference across the droplet's interface, whereas there is a nearly zero contribution from the elasticity of the particle shell. This explains why the right part of the shell bent inward.

4 Conclusions

In a three-phase system consisting of silicone oil, castor oil, and electrically insulating particles, the application of a DC E-field resulted in the generation of stress acting compressively on a Pickering droplet. We used such an E-field to study the deformation, yielding, and crumpling of non-spherical particle shells formed on droplets. Our experimental results show that both the initial geometry and the size of the droplets, as well as the size of the particles, influence the deformation and yielding of non-spherical Pickering droplets. For example, a more aspheric droplet and/or a droplet covered with larger particles required higher electric stress (*i.e.*, a stronger E-field) to yield and to deform from a prolate into an oblate geometry. We also investigated the crumpling of particle shells and observed that a Pickering droplet absorbed the electric stress differently depending on the strength of the applied E-field. That is, slow compression of particle shells facilitated in-plane particle rearrangements that promoted the formation of ridges, whereas fast compression resulted in the formation of wrinkles on the particle shells. Interestingly, the Pickering droplets acquired distinctively different shapes when transiting from prolate into oblate geometries depending on the compression speed. Many studies have been devoted to the characterization of the rheological properties of particle-coated droplets



(and flat particle-coated interfaces). However, most experiments are limited to slow deformations. Our results contribute to a better understanding of the dynamic deformation of particle-laden interfaces with curvature.

We also found that particle shells formed on more elongated droplets crumpled with many clear folds with large amplitudes, as compared with shells formed on less elongated droplets. Moreover, the wrinkling wavelength of the particle monolayer also depended on the particle diameter, and it scaled as \sqrt{d} , meaning that a particle shell composed of bigger particles wrinkles at a higher wavelength. This confirms again that wrinkling phenomena show universal scaling behavior, as proposed by Cerda and Mahadevan in their article on the physics of wrinkling.⁶⁵ Finally, we studied the absorption of electric stress by asymmetric Pickering droplets. We found that particle shells can deform either through folding or through inward indentation.

Given the limited knowledge of the mechanics of non-spherical Pickering droplets probed by E-fields, we hope to have provided an entry point for further theoretical and experimental studies. Future experimental studies should investigate how particle properties, such as electrical conductivity, dielectric permittivity, cohesiveness, particle packing, and particle disorder, affect the stability and mechanics of Pickering droplets subjected to E-fields. It would also be interesting to study the particle rearrangements in detail (e.g., by microstructure characterization using microscope images of a zoomed-in region) during the deformation of the particle shells. This would surely help to better understand the microstructural mechanisms underlying particle shell deformation (similar to studies on arrested coalescence of Pickering emulsion droplets).⁴² This research can also be extended to investigations of the effect of the morphology of droplet stabilizers, such as different particle shapes⁶⁶ and particle mixtures (as in experiments with liquid marbles),⁶⁷ on the viscoelastic properties of arrested Pickering droplets with jammed particle shells.

Author contributions

Z. Rozynek and A. Mikkelsen initiated the project and performed preliminary experiments. K. Khobaib performed all the actual experiments of which the results are presented in Fig. 2–10. T. Vincent-Dospital contributed to the curvature data presentation (Fig. 8 and Fig. S3, ESI[†]). K. Khobaib wrote the first version of the manuscript. All authors took part in discussions that helped finalize the manuscript.

Funding sources

This work was supported by the Polish National Science Centre through the OPUS (2015/19/B/ST3/03055) and PRELUDIUM (2019/35/N/ST5/02821) programs. A. Mikkelsen received funding from the European Union's Horizon 2020 Research and Innovation Programme under Marie Skłodowska-Curie Grant Agreement No. 752896. We also thank the Research

Council of Norway for its support through the Centres of Excellence Funding Scheme, Project No. 262644.

Conflicts of interest

There are no conflicts of interest to declare.

References

- 1 B. P. Binks, *Curr. Opin. Colloid Interface Sci.*, 2002, **7**, 21–41.
- 2 A. Mikkelsen, P. Dommersnes, Z. Rozynek, A. Gholamipour-Shirazi, M. D. S. Carvalho and J. O. Fossum, *Materials*, 2017, **10**, 436.
- 3 A. D. Dinsmore, M. F. Hsu, M. G. Nikolaides, M. Marquez, A. R. Bausch and D. A. Weitz, *Science*, 2002, **298**, 1006–1009.
- 4 C. Zeng, H. Bissig and A. D. Dinsmore, *Solid State Commun.*, 2006, **139**, 547–556.
- 5 Y. Yang, Z. Fang, X. Chen, W. Zhang, Y. Xie, Y. Chen, Z. Liu and W. Yuan, *Front. Pharmacol.*, 2017, **8**, 287.
- 6 R. Aveyard, B. P. Binks and J. H. Clint, *Adv. Colloid Interface Sci.*, 2003, **100–102**, 503–546.
- 7 M. N. Lee, H. K. Chan and A. Mohraz, *Langmuir*, 2012, **28**, 3085–3091.
- 8 Z. Rozynek, A. Mikkelsen, P. Dommersnes and J. O. Fossum, *Nat. Commun.*, 2014, **5**, 3945.
- 9 T. Bollhorst, K. Rezwan and M. Maas, *Chem. Soc. Rev.*, 2017, **46**, 2091–2126.
- 10 A. M. Bago Rodriguez and B. P. Binks, *Curr. Opin. Colloid Interface Sci.*, 2019, **44**, 107–129.
- 11 T. Kubiak, J. Banaszak, A. Józefczak and Z. Rozynek, *ACS Appl. Mater. Interfaces*, 2020, **12**, 15810–15822.
- 12 Q. Sun, Y. Du, E. A. H. Hall, D. Luo, G. B. Sukhorukov and A. F. Routh, *Soft Matter*, 2018, **14**, 2594–2603.
- 13 E. M. Shchukina, M. Graham, Z. Zheng and D. G. Shchukin, *Chem. Soc. Rev.*, 2018, **47**, 4156–4175.
- 14 B. L. Peng, L. C. Zhang, J. H. Luo, P. M. Wang, B. Ding, M. X. Zeng and Z. D. Cheng, *RSC Adv.*, 2017, **7**, 32246–32254.
- 15 C. Herrera, D. Fuentealba, I. T. Ghampson, C. Sepulveda, J. L. García-Fierro, R. I. Canales and N. Escalona, *Catal. Commun.*, 2020, **144**, 106092.
- 16 L. Wei, S. Yan, H. Wang and H. Yang, *NPG Asia Mater.*, 2018, **10**, 899–911.
- 17 J. Guo, B. L. Tardy, A. J. Christofferson, Y. Dai, J. J. Richardson, W. Zhu, M. Hu, Y. Ju, J. Cui, R. R. Dagastine, I. Yarovsky and F. Caruso, *Nat. Nanotechnol.*, 2016, **11**, 1105–1111.
- 18 V. O. Ikem, A. Menner and A. Bismarck, *Langmuir*, 2010, **26**, 8836–8841.
- 19 P. Dommersnes, Z. Rozynek, A. Mikkelsen, R. Castberg, K. Kjerstad, K. Hersvik and J. Otto Fossum, *Nat. Commun.*, 2013, **4**, 2066.
- 20 Z. Rozynek, K. Khobaib and A. Mikkelsen, *ACS Appl. Mater. Interfaces*, 2019, **11**, 22840–22850.
- 21 V. Kozlovskaya, J. F. Alexander, Y. Wang, T. Kuncewicz, X. Liu, B. Godin and E. Kharlampieva, *ACS Nano*, 2014, **8**, 5725–5737.



- 22 W. T. Irvine, V. Vitelli and P. M. Chaikin, *Nature*, 2010, **468**, 947–951.
- 23 V. N. Manoharan, *Science*, 2015, **349**, 1253751.
- 24 C. J. Burke, B. L. Mbanganga, Z. Wei, P. T. Spicer and T. J. Atherton, *Soft Matter*, 2015, **11**, 5872–5882.
- 25 F. Sicard and A. Striolo, *Nanoscale*, 2017, **9**, 8567–8572.
- 26 J. Hegemann, S. Knoche, S. Egger, M. Kott, S. Demand, A. Unverfehrt, H. Rehage and J. Kierfeld, *J. Colloid Interface Sci.*, 2018, **513**, 549–565.
- 27 Z. Rozynek, R. Bielas and A. Józefczak, *Soft Matter*, 2018, **14**, 5140–5149.
- 28 C. P. Whitby and E. J. Wanless, *Materials*, 2016, **9**, 626.
- 29 K. Hwang, P. Singh and N. Aubry, *Electrophoresis*, 2010, **31**, 850–859.
- 30 J. K. Ferri, P. Carl, N. Gorevski, T. P. Russell, Q. Wang, A. Boker and A. Fery, *Soft Matter*, 2008, **4**, 2259–2266.
- 31 M. K. Mulligan and J. P. Rothstein, *Langmuir*, 2011, **27**, 9760–9768.
- 32 M. Ouriemi and P. M. Vlahovska, *Langmuir*, 2015, **31**, 6298–6305.
- 33 C. Gu and L. Botto, *Soft Matter*, 2016, **12**, 705–716.
- 34 A. Mikkelsen, Z. Rozynek, K. Khobaib, P. Dommersnes and J. O. Fossum, *Colloids Surf., A*, 2017, **532**, 252–256.
- 35 L. Becu and L. Benyahia, *Langmuir*, 2009, **25**, 6678–6682.
- 36 A. B. Pawar, M. Caggioni, R. Ergun, R. W. Hartel and P. T. Spicer, *Soft Matter*, 2011, **7**, 7710–7716.
- 37 A. Mikkelsen, P. Dommersnes and J. O. Fossum, *Rev. Cubana Fis.*, 2016, **33**, 47–49.
- 38 M. M. Cui, T. Emrick and T. P. Russell, *Science*, 2013, **342**, 460–463.
- 39 S. A. F. Bon, S. D. Mookhoek, P. J. Colver, H. R. Fischer and S. van der Zwaag, *Eur. Polym. J.*, 2007, **43**, 4839–4842.
- 40 P. Dahiya, M. Caggioni and P. T. Spicer, *Philos. Trans. R. Soc., A*, 2016, **374**, 20150132.
- 41 P. Dahiya, A. DeBenedictis, T. J. Atherton, M. Caggioni, S. W. Prescott, R. W. Hartel and P. T. Spicer, *Soft Matter*, 2017, **13**, 2686–2697.
- 42 Z. Y. Xie, C. J. Burke, B. Mbanganga, P. T. Spicer and T. J. Atherton, *Soft Matter*, 2019, **15**, 9587–9596.
- 43 M. Kaganyuk and A. Mohraz, *Soft Matter*, 2017, **13**, 2513–2522.
- 44 C. Hao, Z. Xie, T. J. Atherton and P. T. Spicer, *Langmuir*, 2018, **34**, 12379–12386.
- 45 R. B. Karyappa, S. D. Deshmukh and R. M. Thaokar, *Phys. Fluids*, 2014, **26**, 122108.
- 46 A. Mikkelsen, K. Khobaib, F. K. Eriksen, K. J. Måløy and Z. Rozynek, *Soft Matter*, 2018, **14**, 5442–5451.
- 47 P. Dommersnes, A. Mikkelsen and J. O. Fossum, *Eur. Phys. J.: Spec. Top.*, 2016, **225**, 699–706.
- 48 G. I. Taylor, A. D. McEwan and L. N. J. D. Jong, *Philos. Trans. R. Soc., A*, 1997, **291**, 159–166.
- 49 D. A. Saville, *Annu. Rev. Fluid Mech.*, 1997, **29**, 27–64.
- 50 Z. Rozynek, P. Dommersnes, A. Mikkelsen, L. Michels and J. O. Fossum, *Eur. Phys. J.: Spec. Top.*, 2014, **223**, 1859–1867.
- 51 Z. Rozynek, J. Banaszak, A. Mikkelsen, K. Khobaib and A. Magdziarz, *Soft Matter*, 2021, DOI: 10.1039/D1SM00122A.
- 52 I. Kåsa, *IEEE Trans. Instrum. Meas.*, 1976, **IM-25**, 8–14.
- 53 C. Gu and L. Botto, *Soft Matter*, 2018, **14**, 711–724.
- 54 M. Ouriemi and P. M. Vlahovska, *J. Fluid Mech.*, 2014, **751**, 106–120.
- 55 A. Mikkelsen and Z. Rozynek, *ACS Appl. Mater. Interfaces*, 2019, **11**, 29396–29407.
- 56 O. Pitois, M. Buisson and X. Chateau, *Eur. Phys. J. E: Soft Matter Biol. Phys.*, 2015, **38**, 48.
- 57 V. Garbin, *Curr. Opin. Colloid Interface Sci.*, 2019, **39**, 202–211.
- 58 T. G. Drake, *J. Geophys. Res.*, 1990, **95**, 8681–8696.
- 59 H. Jiang, D.-Y. Khang, J. Song, Y. Sun, Y. Huang and J. A. Rogers, *Proc. Natl. Acad. Sci. U. S. A.*, 2007, **104**, 15607–15612.
- 60 E. Jambon-Puillet, C. Josserand and S. Protière, *Phys. Rev. Mater.*, 2017, **1**, 042601.
- 61 D. Vella, P. Aussillous and L. Mahadevan, *Europhys. Lett.*, 2004, **68**, 212–218.
- 62 J. Jin, C. H. Ooi, D. V. Dao and N. T. Nguyen, *Soft Matter*, 2018, **14**, 4160–4168.
- 63 A. Lazarus, H. C. Florijn and P. M. Reis, *Phys. Rev. Lett.*, 2012, **109**, 144301.
- 64 D. Vella, A. Ajdari, A. Vaziri and A. Boudaoud, *Phys. Rev. Lett.*, 2012, **109**, 144302.
- 65 E. Cerda and L. Mahadevan, *Phys. Rev. Lett.*, 2003, **90**, 074302.
- 66 B. Madivala, J. Franssaer and J. Vermant, *Langmuir*, 2009, **25**, 2718–2728.
- 67 S. Azizian, S. Fujii, M. Kasahara, H. J. Butt and M. Kappl, *Adv. Powder Technol.*, 2019, **30**, 330–335.



Electronic Supplementary Material for

Electric-field-induced deformation, yielding, and crumpling of jammed particle shells formed on non-spherical Pickering droplets

K. Khobaib,^a A. Mikkelsen,^a T. Vincent-Dospital,^b and Z. Rozynek^{a,b*}

^a Faculty of Physics, Adam Mickiewicz University, Uniwersytetu Poznańskiego 2, 61-614 Poznań, Poland

^b PoreLab, The Njord Centre, Department of Physics, University of Oslo, P. O. Box 1048, Blindern, N-0316 Oslo, Norway

Fig. S1 demonstrates the creation of homogeneous and non-homogeneous arrested Pickering droplets by droplet coalescing. Two silicone oil droplets partly covered with particles coalesced to form an arrested Pickering droplet. The shape of the final coalesced droplet is determined by the particle surface coverage of the two original droplets. In **Fig. S1**, the particle concentration of the original droplets varied from ~8 to ~12 wt%. As a result, we obtained Pickering droplets of different shapes, including a spherical shape (**Fig. S1a**), a slightly aspherical shape (**Fig. S1b**), a rectangle-like shape (**Fig. S1c**), and a peanut-like shape (**Fig. S1d**). The coalesced droplet in **Fig. S1a** was not completely covered with particles (two openings can be seen at the electric poles of the droplet). That is, the particle layer was not in a jammed state, and the particles had some space available to rearrange. The other coalesced Pickering droplets had jammed particle layers that kept the droplet in a non-spherical shape also after the E -field was turned off. Owing to particle rigidity (the particles cannot be deformed, and it costs energy to move particles out of plane), the particle layer resisted the retracting force stemming from the surface tension of the droplet.

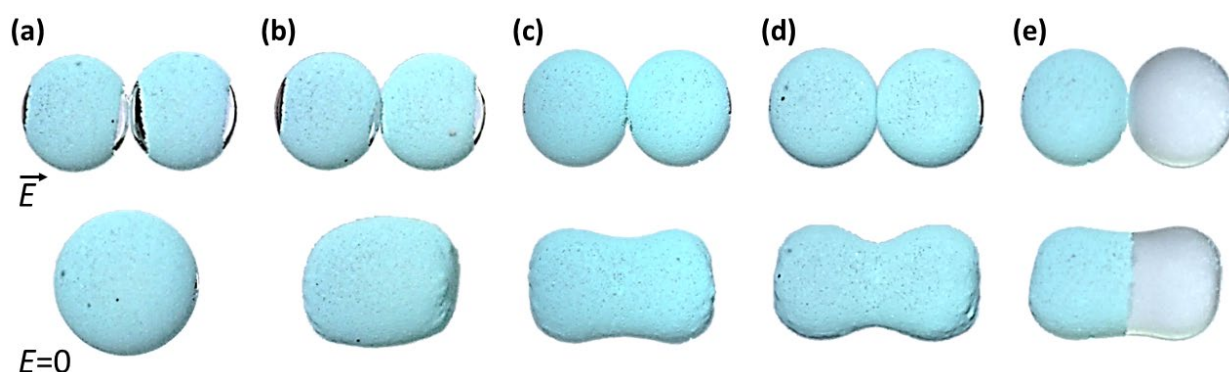


Fig. S1. Pickering droplets with different shapes made by electrocoalescence. The droplets just before electrocoalescence are presented in the top row, whereas the coalesced droplets are shown in the bottom row. The original particle concentrations on the two original droplets were (a) ~8 wt%, (b) ~9 wt%, (c) ~10 wt%, and (d) ~11 wt%. Blue 30- μm PE particles were used to form homogenous shells (a-d). (e) An example of a Janus shell composed of PE particles of two different sizes: blue 30- μm PE particles and white 2- μm particles. The original particle concentrations of the two original droplets were ~10 and ~12 wt% for the blue and white particles, respectively. The size of each original droplet was ~2.0 mm. See also corresponding **Movie S1**.

Fig. S2 demonstrates that at a weak E -field (350 V mm^{-1}), droplets deformed from a prolate into an oblate shape without an observable formation of wrinkles at their particle shells or with irregular folds with small amplitudes. Slow compression of particle shells facilitated in-plane particle rearrangement analogous to the gliding of grain layers in granular flows. In response to compressive electric stress, the surface particles started to move relative to one another. We observed several slip lines appearing during shell compression.

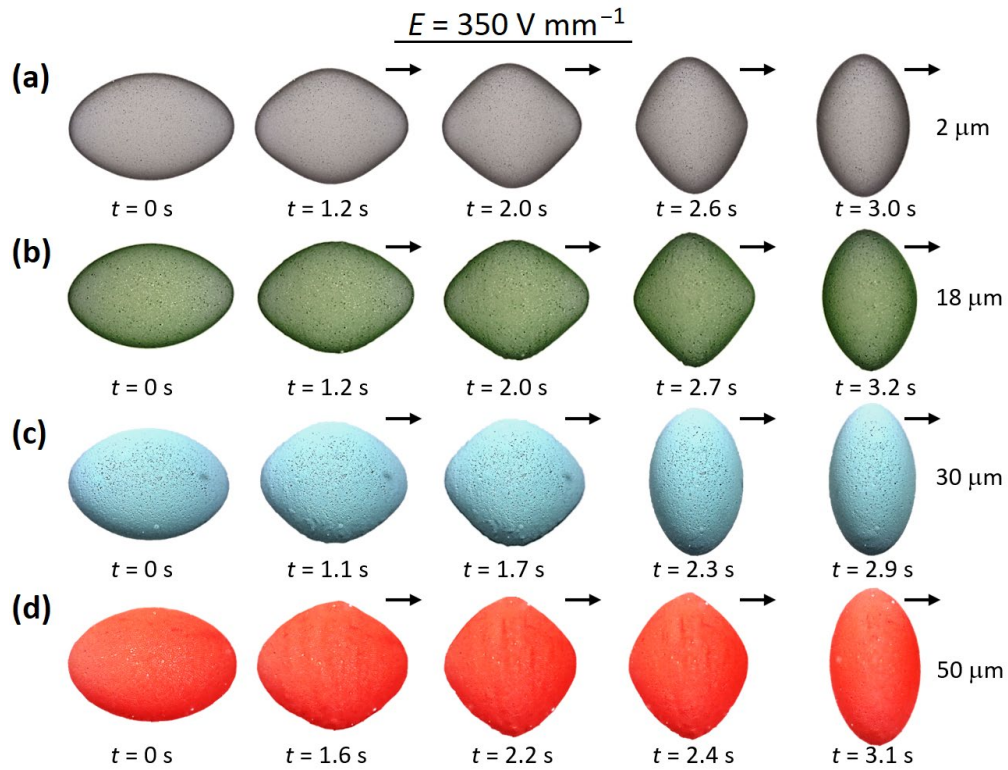


Fig. S2. Deformation of particle shells at different E -field strengths. Arrested droplets with PE particle shells made of (a) 2- μm , (b) 18- μm , (c) 30- μm and (d) 50- μm PE particles. Initially, at $t = 0 \text{ s}$, the particle shells were ellipsoidal with a major axis of 3.9 μm and a minor axis of 2.6 μm . Electric field applied in horizontal direction.

In **Fig. S3**, we show that depending on the compression dynamics (i.e., E -field strength) the particle-covered droplets undergo different shape transformations at the intermediates during the prolate-to-oblate shape transition. The difference between the droplets' projected two-dimensional (2D) shapes is clearly seen (especially in the middle column of the figure). The contours of the Pickering droplets subjected to the weakest E -field (350 V mm^{-1}) resembles a rhombus shape, whereas that of the Pickering droplet subjected to the strongest E -field (1050 V mm^{-1}) are nearly spherical.

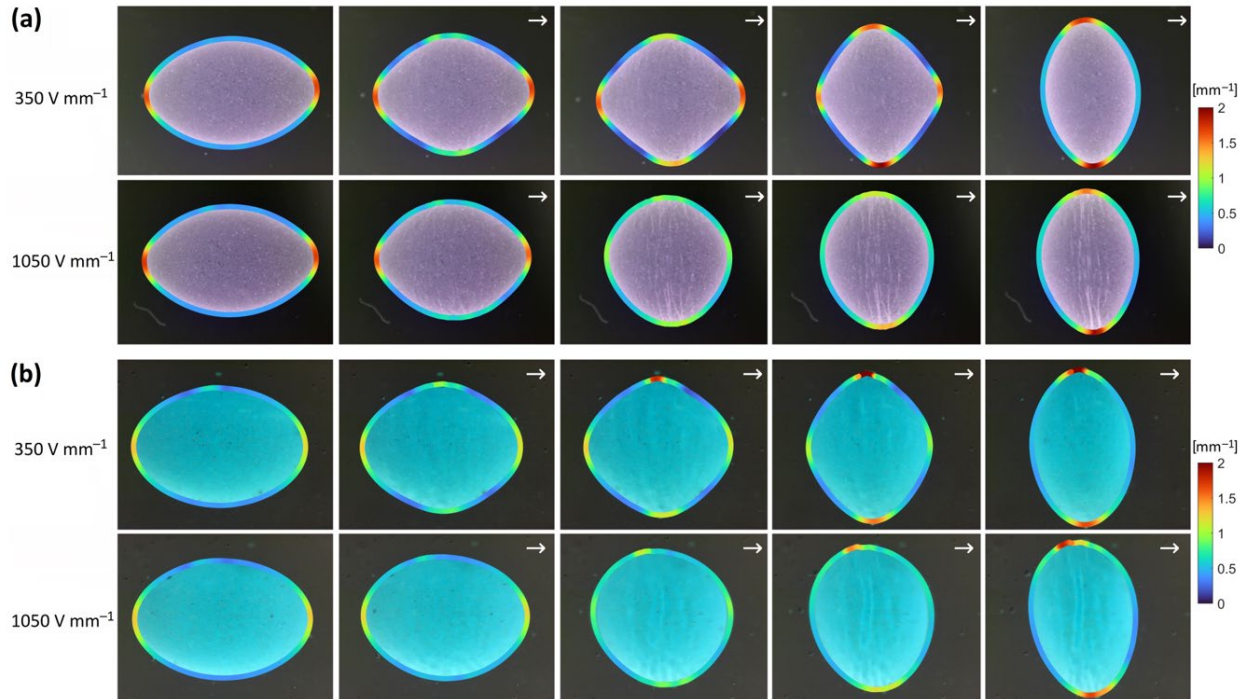


Fig. S3. Deformation of particle shells at different E -field strengths. Series of experimental images with added color-coded contours representing values of the curvature. Arrested droplets with particle shells made of **(a)** $18 \mu\text{m}$ and **(b)** $50 \mu\text{m}$ particles. The droplets were subjected to E -fields of strengths 350 and 1050 V mm^{-1} . The droplets subjected to the stronger E -field are more round at the intermediates compared to those subjected to the weak E -field. Note: The Pickering droplet with $50 \mu\text{m}$ particles wrinkles with the wrinkling amplitude of several pixels, which was picked up by the software that affected the shape of the contours.

Movie S1. Collection of movies demonstrating the preparation of Pickering droplets with different shapes. In each movie, two silicone oil droplets with surface particles undergo electrocoalescence subjected to a DC E -field of strength 170 V mm^{-1} . The resultant shape of the droplet depends on the initial particle coverage. The movie is sped up 2 times.

Movie S2. Preparation of ellipsoidal particle shells by using DC and AC E -fields. An ellipsoidal particle shell is prepared by the electrorotation of a Pickering droplet in a DC E -field, followed by the aligning of the droplet (with its longest axis along the direction of the E -field) and the shaping of the droplet using an AC E -field (100 Hz).

Movie S3. E -field-induced deformation of arrested droplets with jammed particle shells. A silicone oil droplet covered with $30\text{-}\mu\text{m}$ PE particles was suspended in castor oil and subjected to a DC E -field that was stepwise increased. The applied E -field and the deformation of the droplet are plotted against time.

Movie S4. Particle in-plane rearrangement. Droplets with shells made of $2 \mu\text{m}$, $30 \mu\text{m}$, and $100 \mu\text{m}$ PE particles under electric stress. Each movie is recorded with a reverse playback and is sped up two times.

Movie S5. Deformation of non-spherical Pickering droplets subjected to different E -field strengths. Three arrested droplets (with similar volume and initial shape) covered by $2\text{-}\mu\text{m}$ PE particles are subjected to E -fields of strengths 350 , 700 , and 1050 V mm^{-1} . Under these E -field strengths, the droplets continuously deformed from prolate into oblate shapes but with different dynamics.

Movie S6. Crumpling of particle shells. Four droplets covered by PE particles of different diameters $2\text{--}50 \mu\text{m}$ were subjected to E -field of strength 1050 V mm^{-1} . Initially, at $t = 0 \text{ s}$, the particle shells were ellipsoidal with a major axis of $\sim 3.9 \text{ mm}$ and a minor axis of $\sim 2.6 \text{ mm}$. The movies were slowed down four times.

Movie S7. Shape transformations of a Pickering droplet under different speed of compression. Arrested droplets (with similar volume and initial shape) covered by $2\text{-}\mu\text{m}$ PE particles were subjected to E -fields of strengths $350\text{--}1050 \text{ V mm}^{-1}$. Series of experimental images with added color-coded contours representing values of the curvature are shown on the top row. The estimated curvature values are plotted against the 2D polar angle, and the curvature distributions are presented using bar charts.

Movie S8. Asymmetric Pickering droplets under electrical stress. A homogeneous particle shell is prepared by the coalescence of 1.6- and 2.7-mm silicone oil droplets covered with blue $30\text{-}\mu\text{m}$ PE particles. Three different types of heterogeneous particle shells are prepared by the coalescence of silicone oil droplets covered with white $2\text{-}\mu\text{m}$ and red $50\text{-}\mu\text{m}$ PE particles, and green $100\text{-}\mu\text{m}$ and white $2\text{-}\mu\text{m}$ PE particles. The asymmetrical particle shells are subjected to an E -field of strength $\sim 300 \text{ V mm}^{-1}$.

MATLAB code

```
% Curvature computation around a Pickering Droplet / Matlab Code

clc; clear; close all

%% Extra function (index wrapping)
wrapN = @(x, n) (1 + mod(x-1, n));

%% Parameters
image_file = 'name.jpg';
T = 0.41; % Threshold for the detection of the droplet's boundary (0<T<1)
sm = 20; % Number of points for the average smoothing filterering of the boundary
k = 50; % Number of data points to fit local circles to the boundary

%% Charge image and compute droplet boundary
I = imcomplement(imread(image_file));
% imshow(I)
BW = im2bw(I,T);
% imshow(BW)

dim = size(BW);
col = round(dim(2)/2)-90;
row = min(find(BW(:,col)));
boundary = bwtraceboundary(BW,[row, col],'N');

%% Smoothing
boundary(:,2) = smooth(boundary(:,2),sm);
boundary(:,1) = smooth(boundary(:,1),sm);

%% Compute curvature
n = length(boundary(:,2));
curv = NaN*zeros(1,n);

%% Fitting Circles, Kasa Method (1976)
for i=1:n
    if ((i+k <= n) && (i-k >= 1))
        [xc,yc,R] = Kasa(boundary(i-k:i+k,2),boundary(i-k:i+k,1));
    elseif i+k > n
        [xc,yc,R] = Kasa([boundary(i-k:n,2);boundary(1:wrapN(i+k,n),2)],[boundary(i-k:n,1);boundary(1:wrapN(i+k,n),1)]);
    elseif i-k < 1
        [xc,yc,R] = Kasa([boundary(wrapN(i-k,n):n,2);boundary(1:i+k,2)],[boundary(wrapN(i-k,n):n,1);boundary(1:i+k,1)]);
    end
    curv(i)=1/R;
end

%% Conversion to mm
pixsize = 0.00405;
curv = curv/pixsize;

%% Plotting
figure(1)
set(gcf, 'Position', get(0, 'Screensize'));
set(gcf,'color','w');

subplot(1,3,1)
imshow(I)
hold on;
scatter(boundary(:,2),boundary(:,1),20,curv,'filled');
colorbar
```

```

colormap('turbo')
caxis([0,2])
title({'Approximate curvature (mm-1)'})

%%% QCing the last fitted circle
% hold on
% viscircles([xc yc],R);

xc=mean(boundary(:,2)); yc=mean(boundary(:,1));
Theta=atan2(-(boundary(:,1)-yc),(boundary(:,2)-xc));
subplot(1,3,2)
polarplot(Theta,curv,'linewidth',2)
rlim([0 0.008/pixsize])
title('Polar plot of the curvature (mm-1)')

subplot(1,3,3)
h1=histogram(curv,'FaceAlpha',1,'Normalization','probability');
h1.BinWidth = 0.0001/pixsize;
xlim([0,0.008/pixsize]); ylim([0.003,0.3]);
set(gca,'YScale','log')
title('Curvature probability distribution (mm-1)')

%%% Extra functions
function [xcenter,ycenter,radius] = Kasa(xdata,ydata)

% I. Kasa, "A curve fitting procedure and its error analysis",
% IEEE Trans. Inst. Meas., Vol. 25, pages 8-14, (1976)

Mat=[xdata ydata ones(size(ydata))]\[-(xdata.^2+ydata.^2)];
xcenter = -Mat(1)/2;
ycenter = -Mat(2)/2;
radius = sqrt((Mat(1)^2+Mat(2)^2)/4-Mat(3));

end

```


Paper VIII

Mechanical properties of particle-covered droplets probed by
non-uniform electric field

K Khobaib and T Hornowski

In preparation

Mechanical properties of particle-covered droplets probed by non-uniform electric field

Khobaib Khobaib* and Tomasz Hornowski

Faculty of Physics, Adam Mickiewicz University, Uniwersytetu Poznańskiego 2, Poznań 61-614, Poland

*Corresponding author: khokho@amu.edu.pl

ABSTRACT: Particle-covered droplets are used in many fundamental studies and practical applications. For many applications, it is important to understand the mechanics of such droplets subjected to external stresses induced, for example, by electric field (E -field). Several research groups have studied the deformation and stability of droplets subjected to uniform E -fields. However, little is known about the behaviour of particle-laden droplets in non-uniform E -field. Here, we present the results of studies on the deformation of silicone oil droplet coated by an electrically insulating particle shell suspended in castor oil. Such droplet deforms compressively under DC E -field. We create E -fields with different intensities and field gradients by changing the shape of the signal electrode and its position in respect to the stationary plate-shaped electrode. The experimental results on the droplet deformation are compared with the theoretical calculations obtained through modelling of the distribution of non-uniform electric field around cylindrical electrode using the finite element method. We find quite good agreement between experimental results and theoretical predictions, for droplet deformations, especially for moderate electric potentials, up to 1 kV.

KEYWORDS: droplet deformation, electric potential, electrode geometry, non-uniform electric field

1. Introduction

Understanding the mechanical and rheological properties of droplets (pure or covered by particles) subjected to external stresses is important for many practical applications, including fabrication of emulsions [1–3]. The deformation of a droplet is often investigated, as it is an essential parameter for a variety of industrial applications such as inkjet printing [4], droplet separation in microfluidic systems [5], de-emulsification [6,7], biological cell systems [8] and enhanced oil recovery [9]. Besides investigating the behavior of pure droplets, particle-covered droplets are also a subject of fundamental studies. That is because droplets with a particle shell are important for technological aspects such as food products [10], pharmaceutical products [11], cosmetics [12], biocatalysts [13], cell printing [14], biodiesel production [15], and drug delivery [16,17].

Typically, the mechanical and rheological properties of droplets are investigated by using mechanical compression [18–20], hydrodynamic shear flow [21,22] or magnetic [23] and electric fields [24]. Electric field approaches have proven to be useful as a non-contact method for studying droplets' response to an external stress [24–28]. Usually, a homogenous electric field is used to generate the electric stress, and many works on droplets subjected to a uniform electric field have been published [25,29–32].

37 The literature is less extensive on the subject concerning the use of non-uniform electric
38 fields and includes the following contributions: Ahn [33], Yao [34], Mhatre [35] and Song [36]
39 *et al.* investigated the deformation and motion of silicone oil and water droplets in a non-
40 uniform electric field both theoretically and experimentally. Feng [37] performed a
41 theoretical analysis of a deformable fluid particle in a non-uniform electric field. Deshmukh
42 and Thaokar [38] studied the deformation and breakup of a leaky dielectric droplet in a leaky
43 dielectric fluid in an axisymmetric quadrupole electric field). Our goal is to fill the gap in this
44 research area by demonstrating how electrode geometry affects the droplet's deformation.
45 We focus on the effect of electrode size, droplet size and the spacing between the electrodes
46 on the magnitude of the droplet deformation. In our experiments, we used different sizes of
47 top electrodes (from pin- to plate-shaped electrodes), whereas the flat bottom electrode
48 remained the same for all the experiments. The experimental data was compared with
49 theoretical results obtained through the finite element analysis.

50 **2. Materials and experimental method**

51 **2.1. Materials**

52 Particle-covered droplets were made out of silicone oil (VWR Chemicals, Rhodorsil
53 6678.1000, viscosity ~ 50 mPa·s, density ~ 0.96 g·cm⁻³, relative permittivity ~ 2.8 , and
54 electrical conductivity ~ 5 pS·m⁻¹) and polyethylene particles (Cospheric LLC, REDPMS-0.98
55 45–53 μ m, electrical conductivity $\sim 10^{-15}$ S·m⁻¹, relative permittivity
56 ~ 2.1 and density ~ 0.98 g·cm⁻³). First, we dispersed the polyethylene (PE) particles in silicone
57 oil, and then using a mechanical pipette we formed a droplet of dispersion inside castor oil
58 (Sigma-Aldrich 83912, viscosity ~ 750 mPa·s, density ~ 0.96 g·cm⁻³, relative permittivity ~ 4.7 ,
59 and electrical conductivity ~ 100 pS·m⁻¹). In the formed droplet, most of the PE particles
60 resided inside the droplet. In order to bring the particles to the silicone oil-castor oil interface
61 we used an E -field, as described in ref. [39]. Once the particles reached the interface, they
62 strongly bound to it with the binding energy $\sim 10^4 k_B T$.

63 **2.2. Experimental method**

64 The experimental setup consisted of a signal generator (SDG1025, SIGLENT), a high-
65 voltage bipolar amplifier (10HVA24-BP1, HVP High Voltage Products GmbH), a digital
66 microscope (AM7115MZTL, Dino-Lite Digital Microscope) for observation at an angle ($\sim 20^\circ$)
67 perpendicular to the direction of the applied E -field, a light source, a PC for recording movies,
68 and an optical acrylic cuvette (15 mm \times 15 mm \times 30 mm) used as a sample cell. The sample

69 cell was placed on a mechanical XYZ translation stage (LT3, Thorlabs, Sweden) to ease its
70 positioning relative to the optical path of the microscope. The bottom wall of the cell was
71 made of a glass coated indium tin oxide (ITO) thin layer and it served as an electrode. The
72 signal electrode was placed above a particle-covered droplet (inserted from the open top of
73 the sample cell and immersed in castor oil). For the signal electrode, we used materials with
74 different shapes: a pin electrode (diameter 0.1 mm), a cylindrical electrode (diameter
75 ranging from 0.6 mm to 3 mm) and a plate electrode. A high-voltage bipolar signal was
76 provided to the sample cell via two crocodile clips attached to the top and bottom
77 electrodes. The distance between the electrodes (h) was adjusted according to the
78 experimental need. A stainless-steel O-ring was attached to the conductive bottom of the
79 sample cell (at its center) to hold the droplet in place and to prevent its electrorotation—a
80 phenomenon that occurs in strong E -fields [40].

81 **2.3. Particle image velocimetry (PIV) experiment**

82 Electrohydrodynamic flows (EHD) induced around a particle-covered droplet and near the
83 tip of a non-planar electrode were traced using particle image velocimetry (PIV). Blue PE
84 particles (Cospheric LLC, BLPPMS-1.00, size $\sim 30\ \mu\text{m}$, and density $\sim 1.00\ \text{g}\cdot\text{cm}^{-3}$) used as tracer
85 particles were dispersed in castor oil and poured in the sample cell. A silicone oil droplet (~ 4
86 mm) coated with $50\text{-}\mu\text{m}$ PE particles was suspended in the dispersion medium and docked
87 into a conductive O-ring. Electric tension of different intensities (1.3–2.6 kV) was provided
88 to the signal electrode, which resulted in generation of liquid flows in the system. We
89 recorded movies at a speed of 10 frames/s and a resolution of 1280×960 using a digital
90 microscope (AM7115MZTL, DINO-LITE). Three hundred sequential frames were extracted
91 from each movie and used to generate flow field maps using MATLAB® software (v.R2017b,
92 MathWorks®) and its Particle Image Velocimetry Toolbox™.

93 **2.4. Droplet deformation**

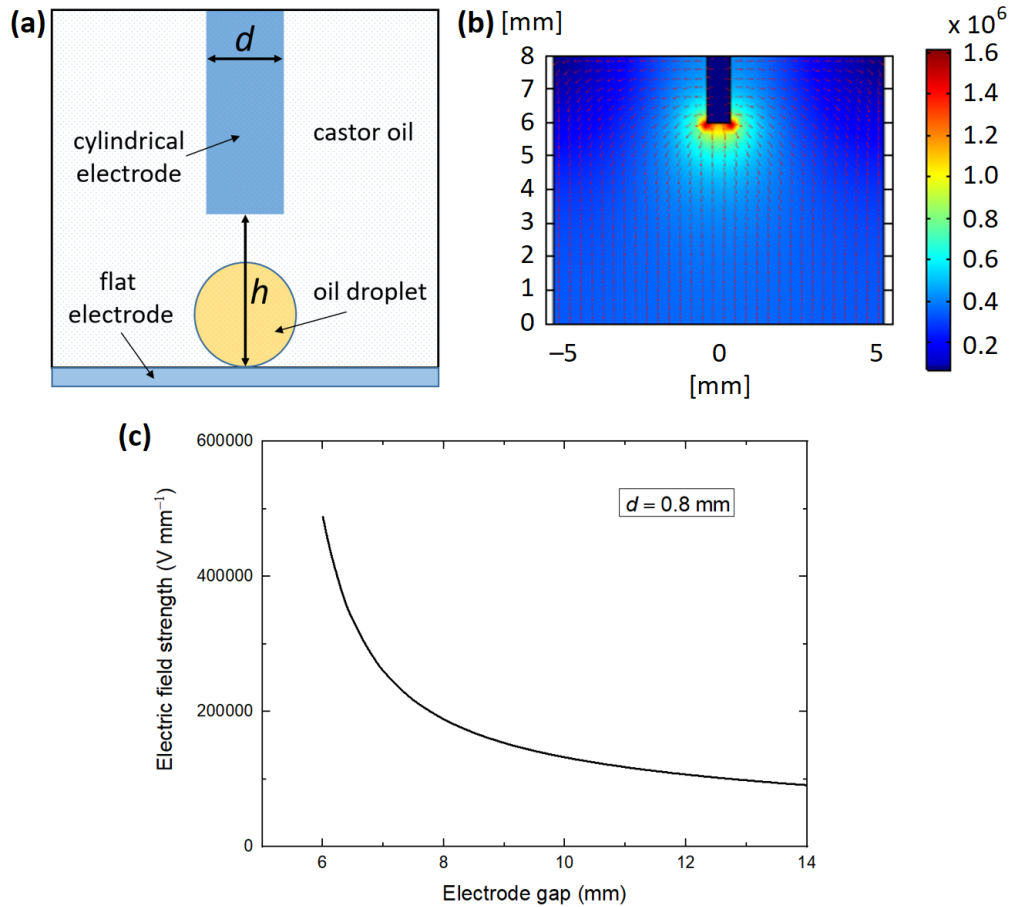
94 Taylor [41] introduced the leaky dielectric model that was later developed by Melcher
95 and Taylor [42] to describe the EHD deformation of weakly conducting droplets suspended
96 in another conducting medium under an applied electric field. The model is based on the
97 assumption that the free charges build up at the droplet's interface, resulting in the
98 generation of compressive electric stress, which, in turn, deforms the droplet. The
99 magnitude of droplet deformation depends on the stability between surface tension (γ) and
100 normal stress ($\epsilon_{ex} \cdot E_0^2$) and is given by

101
$$D = \left(\frac{d_{\parallel} - d_{\perp}}{d_{\parallel} + d_{\perp}} \right) = \frac{9r_0 \varepsilon_0 \varepsilon_{ex} E_0^2}{16\gamma S(2+R)^2} [S(R^2 + 1) - 2 + 3(RS - 1) \frac{2\lambda + 3}{5\lambda + 5}] \quad (1)$$

102 where d_{\parallel} and d_{\perp} are the droplet axes parallel and perpendicular to the direction of the
 103 applied electric field, respectively, ε_0 is the vacuum permittivity, ε_{ex} is the permittivity of the
 104 surrounding liquid, r_0 is the radius of the droplet, the dimensionless numbers R , S and λ are
 105 the conductivity, dielectric constant, and viscosity ratios which are defined as: $R = \frac{\sigma_{in}}{\sigma_{ex}}$;
 106 $S = \frac{\varepsilon_{ex}}{\varepsilon_{in}}$; $\lambda = \frac{\mu_{ex}}{\mu_{in}}$. We are aware that the model is applicable only for small deformations and for
 107 a droplet placed in a uniform field. However, we will use it here for a coarse estimation of
 108 the droplet deformation.

109 **2.5. Modelling of the electric field distribution using the finite element method**

110 The configuration of cylinder-plate electrode under consideration is shown in **Fig. 1 (a)**.
 111 The cylindrical electrode of diameter d is placed perpendicular to a plate electrode at
 112 distance h . The diameter d , and the filled with castor oil gap h between the electrodes are
 113 the parameters which define the geometry and determine the electric field strength.



114
 115 **Figure 1. (a)** The configuration of the cylinder-plate electrode system with a particle-covered droplet placed on
 116 the bottom of the container. **(b)** Electric field intensity around the cylindrical electrode, $U = 3$ kV, $h = 6$ mm,
 117 $d = 0.7$ mm. **(c)** Electric field intensity along the gap axis $U = 1300$ V, $d = 0.8$ mm.

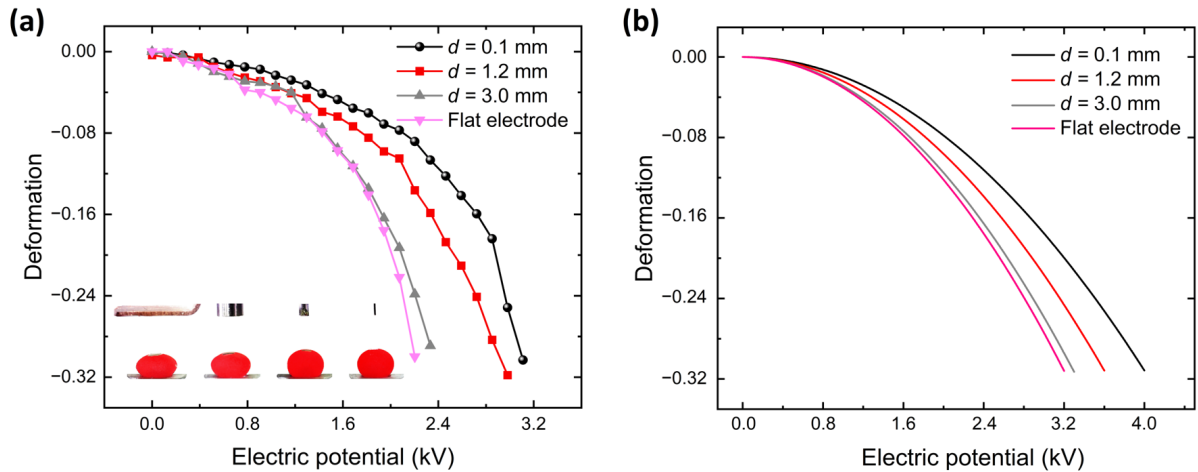
118 The electric field or potential distribution may only change in the radial direction,
119 perpendicular to the plate electrode along the gap. Therefore, the task may be reduced into
120 a two-dimensional axisymmetric problem. For the modelling of electric field distribution, we
121 used COMSOL Multiphysics v.5.5 software package. The surface plot of the electric field
122 strength distribution across the electrode gap is shown in **Fig. 1 (b)**. An example of the
123 calculated variation of the electric field intensity across the gap, for a given electrode size of
124 0.8 mm is shown in **Fig. 1 (c)**. The values of electric field strength for different electrode
125 configurations and electric potentials were treated as the input values to the Melcher-
126 Taylor equation (**eq. 1**).

127 **3. Results and Discussion**

128 **3.1. Effect of electrode geometry on droplet deformation**

129 The droplet deformation under a uniform electric field was studied in previous works
130 [25,26,43]. In this study we investigate the deformation of a droplet influenced by both
131 uniform and non-uniform electric fields created by the different electrode geometries. We
132 prepared a silicone oil droplet (~4.4 mm) covered with 50 μm PE particles and the droplet
133 was suspended in castor oil and docked into a stainless-steel O-ring attached to the
134 conductive bottom of the sample cell. A signal electrode was placed at a fixed electrode
135 distance (~8 mm) and electric potential was increased stepwise (0–3.2 kV). At each step, the
136 electric potential was increased ~0.13 kV and we waited for 1 minute to reach the steady-
137 state droplet deformation and particle rearrangement. Four different sizes of the top
138 electrodes were used: a plate electrode, cylindrical electrodes (diameter 1.2 mm, and 3.0
139 mm) and a pin electrode (diameter 0.1 mm). The electrodes are shown in the inset image in
140 **Fig. 2 (a)**, in which a droplet is subjected to an electric potential of ~2.2 kV.

141 In **Fig. 2**, the magnitude of droplet deformation is plotted as a function of electric
142 potential. The result demonstrates that the deformation magnitude is consistently higher for
143 the uniform electric field in comparison with the non-uniform electric field. We also
144 compared the experimental result with the theoretical prediction by using the Melcher-
145 Taylor equation (see **eq. (1)**). We calculated the deformation magnitude for different
146 electrode geometries and plotted it as a function of applied electric potential (see **Fig. 2 (b)**).



147

148

149

150

151

Figure 2. Electrode geometry effect on the magnitude of the droplet deformation. A particle-covered droplet (diameter 4.4 mm) was placed at the conductive bottom of the sample cell. The electric potential was increased stepwise. Four different sizes of the top electrodes were used (see inset images) and were placed at the fixed distance of 8 mm. **(a)** Experimental and **(b)** theoretical data of the magnitude of the droplet deformation.

152

153

154

155

156

157

158

159

160

161

162

163

164

165

166

The theoretical results show good qualitative agreement with the experimental results and demonstrate that the deformation magnitude depends on both the applied electric potential and the electrode geometry. This is because at a constant electrode distance (~ 8 mm), the electric field strength increases more strongly with the applied electric potential in the uniform than in the non-uniform field. The result also demonstrates that in a non-uniform electric field, the deformation magnitude decreases with the decrease of the electrode diameter and deforms the least with the electrode of the smallest diameter (~ 0.1 mm). Ahn *et al.* [33] studied the droplet charging characteristic under different electrode configurations. They suggested that at a fixed electrode distance, when the cross-sectional area of the electrode becomes much smaller than the diameter of the droplet, the charge decreases at the droplet interface. Luo *et al.* [44] explained the electric field distribution in a non-uniform electric field. They reported that at a constant electrode distance the electric field is the strongest at the tip of the electrodes and becomes considerably weaker when it reaches the plate electrode. Our experimental data are in good agreement with their observation.

167

168

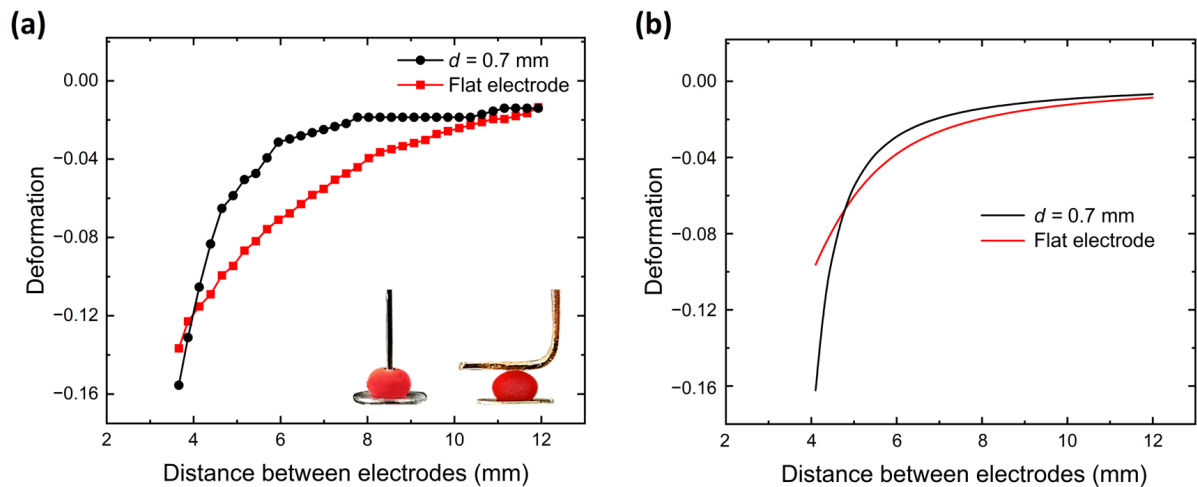
169

170

171

After understanding the effect of electrode geometry on droplet deformation at a fixed electrode distance, we decided to further study the deformation by minimizing the gap between the electrodes to the point when the electrodes touch the droplet. In **Fig. 3**, we estimated the magnitude of droplet deformation both experimentally and theoretically. The droplet is subjected to a fixed DC electric potential of ~ 0.8 kV through two different sizes of

172 the top electrodes' (i) cylindrical electrode (diameter 0.7 mm), and (ii) plate electrode. At
 173 such a low voltage, it was possible to touch the droplet with the top electrodes without
 174 harming the particle shell. Initially, the cylindrical electrode was placed above the droplet at
 175 a distance of ~ 11.9 mm from the bottom electrode. The strength of the electric field was
 176 increased stepwise by moving down (~ 0.26 mm) the top electrode. We found that in up to
 177 ~ 6 mm of electrode distance the magnitude of the droplet deformation with the cylindrical
 178 electrode increased more slowly ($\Delta D \sim 0.03$) compared to the plate electrode ($\Delta D \sim 0.07$)
 179 (see **Fig. 3 (a)**). With further decrease of the distance between the electrodes, i.e. below ~ 6
 180 mm, the magnitude of the droplet deformation with the cylindrical electrode started to
 181 increase steeply, but the deformation magnitude was still smaller than with the plate
 182 electrode. However, when the top electrode nearly touched the droplet (below ~ 4 mm of
 183 electrode distance), the droplet deformed strongly with the cylindrical electrode and crossed
 184 the magnitude of the deformation curve with the plate electrode. The theoretical result also
 185 showed a similar crossing point on the magnitude of the droplet deformation curve when
 186 the electrodes touched the droplet (see **Fig. 3 (b)**). This is due to stronger field intensity at
 187 the tip of the electrode [33], which creates higher compressive electric stress on the droplet.

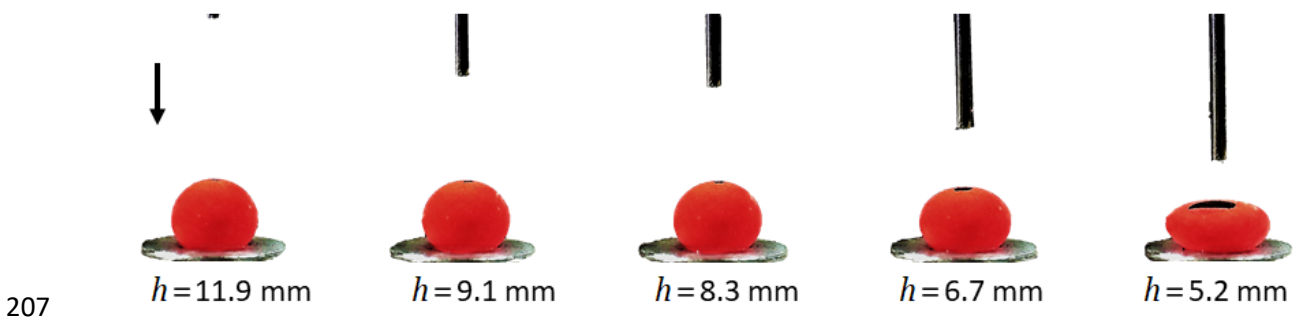


188

189 **Figure 3.** Deformation of silicone oil droplet (~ 4.3 mm) covered with $50\text{-}\mu\text{m}$ PE particles plotted as a function
 190 of the distance between electrodes. The droplet is placed at the conductive bottom of the sample cell. A
 191 stainless-steel cylindrical electrode with diameter of ~ 0.7 mm, and a plate electrode used as a top electrode
 192 are at a fixed DC potential of ~ 0.80 kV. The electric field strength was increased stepwise by minimizing the
 193 distance between the electrodes. The magnitude of the droplet deformation is estimated **(a)** experimentally
 194 and **(b)** theoretically.

195 3.2. Electric potential-induced deformation of the particle shell

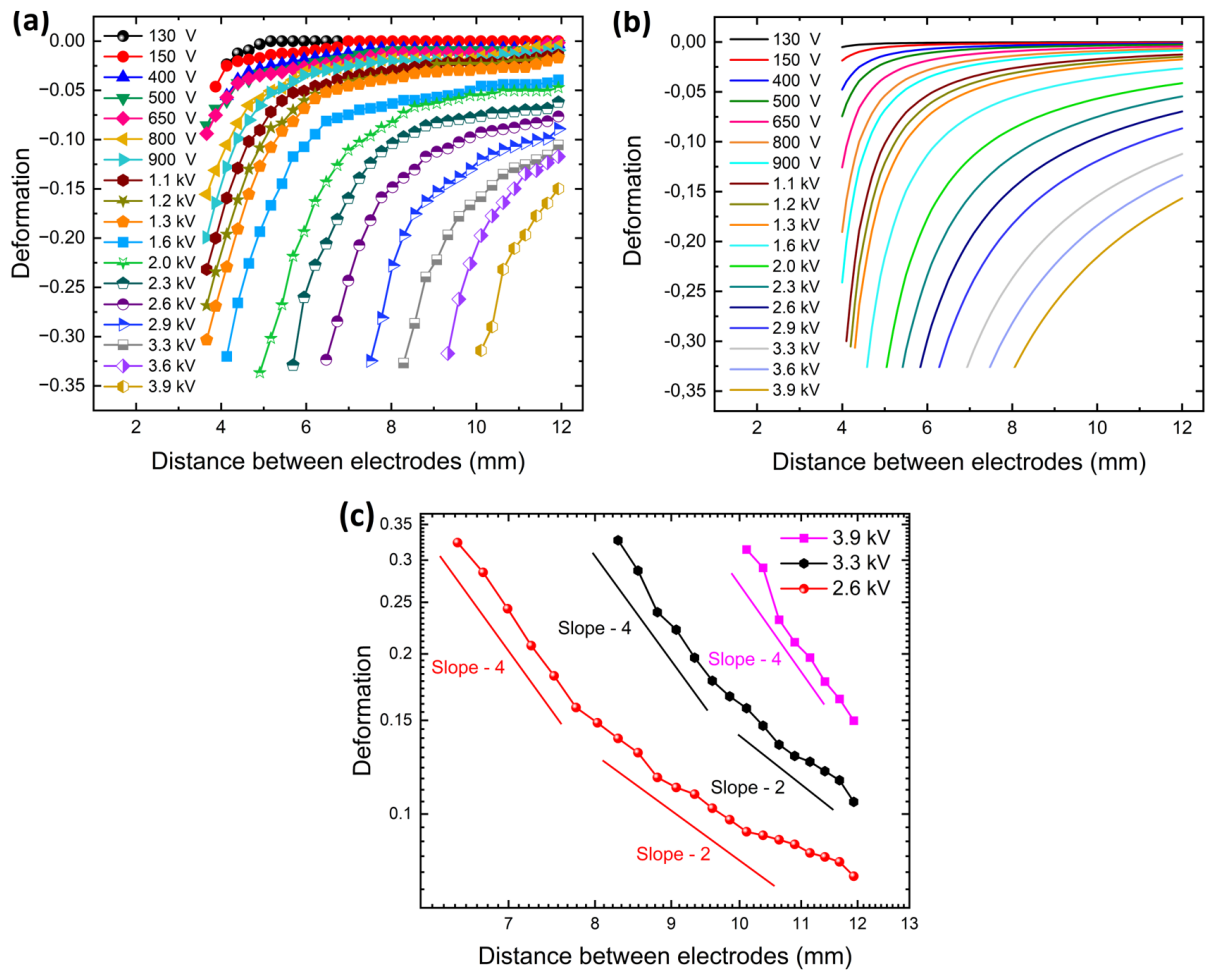
196 In this experiment, we prepared a silicone droplet (~ 4.3 mm) covered by the 50- μm PE
197 particles placed in castor oil and subjected to a non-uniform DC electric field. The droplet
198 was subjected to an electric field by applying a constant DC voltage of ~ 130 V to ~ 3.9 kV.
199 Initially, the cylindrical electrode was placed at a distance of ~ 11.9 mm from the bottom
200 electrode. The strength of the electric field was increased stepwise by moving down the top
201 electrode in a similar manner to what we presented in the previous experiment. At constant
202 electric potential, with each step of minimizing the electrode distance, the magnitude of the
203 droplet deformation and the opening area at the electric pole increased (see **Fig. 4**). This is
204 due to the increase of electric field strength with the lowering of the electrode distance,
205 thereby resulting in a higher magnitude of droplet deformation. In **Fig. 5** and **Fig. 6**, we
206 present the quantitative data of the observation shown in **Fig. 4**.



208 **Figure 4.** A silicone oil droplet (size ~ 4.3 mm) covered with 50- μm PE particles was placed inside the castor oil
209 and attached to the conductive bottom of the sample cell through a stainless-steel O-ring. A cylindrical
210 electrode (diameter ~ 0.7 mm) was used as a top electrode and connected with an electric potential of ~ 2 kV.
211 The strength of the electric field was increased by lowering the top electrode.

212 In **Fig. 5(a)**, the magnitude of the droplet deformation is plotted as a function of the
213 distance between the electrodes. We also estimated theoretically the magnitude of droplet's
214 deformation at different electric potentials by using equation (1), see **Fig. 5(b)**. Although the
215 magnitude of the droplet deformation was smaller theoretically, the result showed good
216 qualitative agreement with the experimental result. At lower electric potential, e.g. 130 V
217 and 250 V, the droplet was un-deformed with decreases of the electrode distance up to ~ 4.9
218 mm and ~ 6.7 mm, respectively. This is because the total magnitude of the applied electric
219 stress was not large enough to overcome the elasticity of the particle layer. At higher electric
220 potential, the magnitude of the droplet deformation was increased slowly and steadily with
221 the decrease of the electrode distance, and follows Taylor's theory [41] up to the critical

222 distance (h_c) (here, h_c refers to the gap between the electrodes, where the deformation
 223 curve bent downward). At electric potential 650 V, the droplet deformed with slope ~ -2 , up
 224 to $h_c \approx 4.4$ mm. With further decrease of the electrode distance, the deformation magnitude
 225 increased steeply, and the curve bent downwards with slope -4 . When the droplet was
 226 subjected to electric potential from 130 V to 3.9 kV, the critical distance shifted to the larger
 227 electrode distance (see **Fig. 5(c)**). In our previous work [45], we also observed such strong
 228 $D(h)$ relationship for droplet deformation $D > 0.1$. For such large deformations the
 229 Taylor model is invalid, as the droplet becomes highly nonspherical.

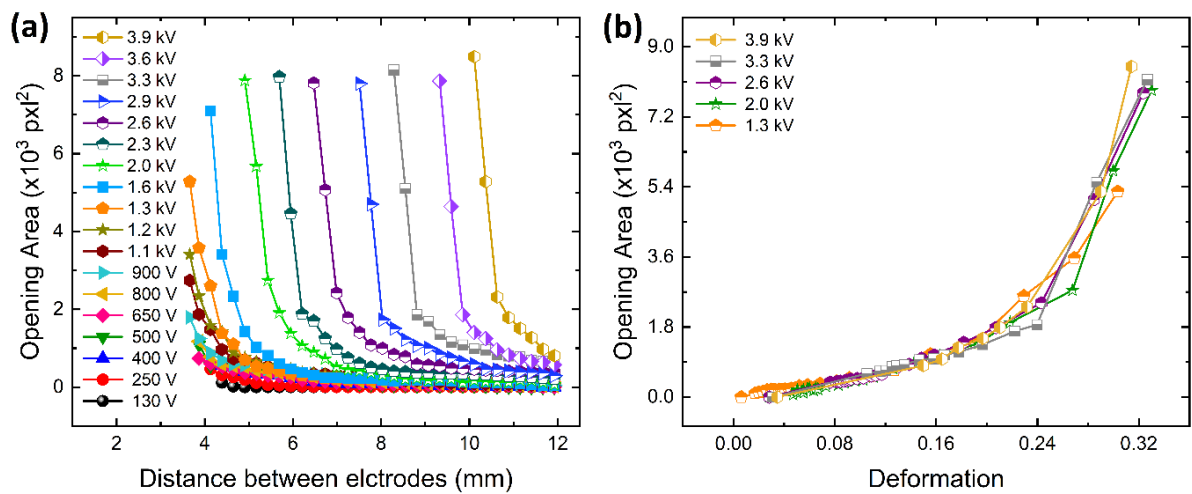


230

231 **Figure 5.** (a) Steady state deformation of silicone oil droplet (diameter ~ 4.3 mm) covered with $50\text{-}\mu\text{m}$ PE
 232 particles plotted as a function of the distance between the electrodes. (b) The magnitude of the droplet
 233 deformation is calculated theoretically at different electric potentials (0.4–3.3 kV). (c) Log-log plot of droplet
 234 deformation at electric potential 2.6 kV, 3.3 kV and 3.9 kV.

235 In **Fig. 6(a)**, we plotted the opening area at the droplet pole as a function of the electrode
 236 distance. At lower electric potential, e.g. 130 V and 250 V, no opening area was observed at
 237 the droplet electrical pole until the gap between the electrodes was ~ 4.9 mm and ~ 6.7 mm,

238 respectively. This is because the droplet was un-deformed (see **Fig. 5(a)**), the particles
 239 formed a jammed monolayer at the droplet surface. However, at a stronger electric potential
 240 (above ~ 250 V), the droplet started deforming, and the magnitude of the deformation
 241 increased with the lowering of the top electrode. Thus, the total area of the droplet
 242 increased, allowing the particle layer to unjam. The unjamming of the particle layer
 243 underwent a solid-to-liquid transition and the EHD flows were generated at the fluid-fluid
 244 interface. The flows were directed from the droplet poles to the droplet equator, thereby
 245 forming an opening area at the droplet pole. The opening became wider with the higher
 246 deformation magnitude. The size of the opening area at the droplet's pole should be
 247 proportional to the change in the total area of the droplet after deformation, assuming that
 248 the particle packing of the particles forming the shell is not altered. To crosscheck our
 249 experimental results (**Fig. 5(a)** and **Fig. 6(a)**), we plotted the opening area at the droplet pole
 250 as a function of the absolute value of the droplet deformation at different electric potentials
 251 (1.3 kV to 3.9 kV). We found that the data at the different electric potentials were
 252 overlapping. This confirms that our experimental results are correct and under the same
 253 applied electric stress the opening area at the droplet pole depends on the change in the
 254 total area of the droplet, and that the particle packing in the shell remains similar.



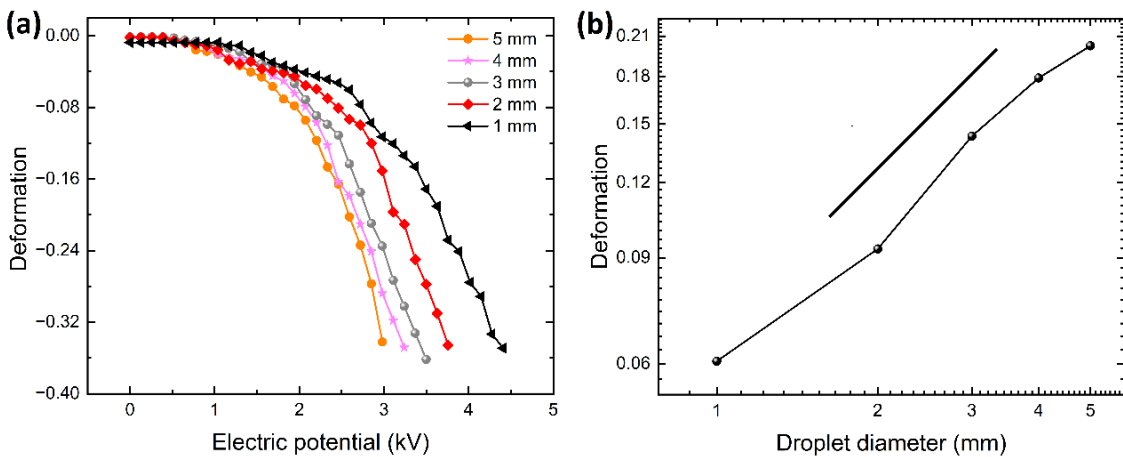
255
 256 **Figure 6. (a)** The opening area of the particle layer at the electric pole of the silicone oil droplet covered with
 257 50- μm PE particles plotted as a function of the distance between the electrodes. **(b)** The opening area at the
 258 electric pole of the particle-covered droplet plotted as a function of the absolute value of the droplet
 259 deformation.

260 **3.3. Effect of droplet size on deformation**

261 To study the influence of the droplet size on the magnitude of the deformation, we
 262 prepared five droplets with different diameters ranging from 1 to 5 mm covered with 50- μ m
 263 PE particles and subjected to an electric potential. The strength of the electric potential was
 264 increased stepwise from 0 to 4.4 kV with the cylindrical electrode (diameter \sim 0.6 mm). The
 265 result presented in **Fig. 7(a)** shows that the magnitude of droplet deformation is consistently
 266 higher for the larger droplet at all electric potentials. This is expected as the magnitude of
 267 droplet deformation is proportional to the droplet size, as a result of the Laplace pressure.
 268 The Laplace pressure of a liquid droplet is written as:

269
$$\Delta P = P_i - P_o = 2 \frac{\sigma}{R} \quad (\Delta P \propto \frac{1}{R}) \quad (2)$$

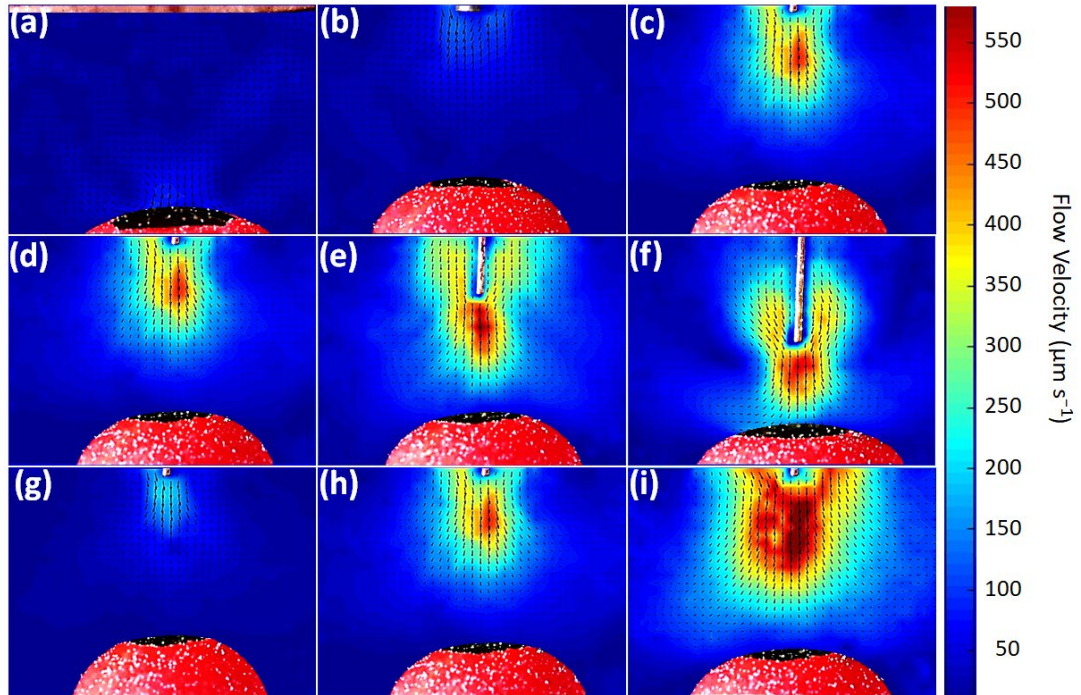
270 where σ is the surface tension at the droplet interface, R is the radius of the droplet, P_i and
 271 P_o are the pressures inside and outside of the droplets, respectively. The value of the outside
 272 pressure (P_o) is the same for all the droplets, whereas the inside pressure (P_i) increased with
 273 the decrease of droplet size. Therefore, higher electric potential is required to deform the
 274 smallest droplet. From the data presented in **Fig. 8(a)**, the magnitude of the droplet
 275 deformation is plotted as a function of the droplet diameter at electric potential of 2.6 kV,
 276 **Fig. 7(b)**. The result demonstrates that the value of the droplet deformation increased with
 277 the size of the droplet. The black line on the log-log plot represents a slope of 1, which shows
 278 a good agreement with the inversely proportional relationship between the Laplace pressure
 279 and the size of the droplet.



280
 281 **Figure 7.** Silicone oil droplet with different diameters (1 to 5 mm) covered with 50- μ m PE particles formed in
 282 castor oil. The distance between the cylindrical electrode (diameter 0.6 mm) and the bottom (plate shape)
 283 electrode is \sim 7 mm. **(a)** The magnitude of the droplet deformation plotted as a function of the electric
 284 potential. The potential was increased stepwise. **(b)** The log-log plot of the droplet deformation (at electric
 285 potential 2.6 kV) as a function of droplet diameter.

286 **3.4. Particle image velocimetry (PIV) analysis with different electrode geometries**

287 In previous experiments, we studied the effect of electrode geometry, distance between the
288 electrodes and different applied electric potential on the magnitude of droplet deformation.
289 Here, we study such effects on the magnitude and direction of the EHD flows by performing
290 the particle image velocimetry (PIV) experiment. In this experiment, we prepared a ~4 mm
291 silicone oil droplet covered with 50 μm PE particles and a DC electric potential was related
292 to different electrode geometries.



293
294 **Figure 8.** PIV images of a ~4 mm silicone oil droplet covered with 50- μm PE particles and placed at the
295 conductive bottom of the sample cell. **(a–f)** The droplet was subjected to a fixed DC electric potential of 2.0 kV.
296 **(a–c)** Electric potential was applied through three different electrode geometries, i.e. plate electrode,
297 cylindrical electrode (diameter ~0.6 mm), and a pin electrode (diameter ~0.1 mm), at a fixed electrode
298 distance of ~7 mm. **(d–f)** The strength of the electric field was varied by changing the distance between the
299 electrodes **(d)** $h = 7$ mm, **(e)** $h = 6$ mm, and **(f)** $h = 5$ mm. **(g–i)** The droplet was subjected to different strengths
300 of DC electric potential, i.e. 1.3 kV, 2.0 kV and 2.6 kV, respectively, at a fixed electrode distance of ~7 mm.

301 Our previous experimental data (**Fig. 2**, **Fig. 3** and **Fig. 5**) are consistent with the PIV
302 results. In **Fig. 8(a–c)**, the droplet was subjected to an electric potential of strength 2 kV with
303 three different sizes of the top electrodes, i.e. plate electrode, cylindrical electrode
304 (diameter 0.6 mm) and a pin electrode (diameter 0.1 mm). The results of the PIV experiments
305 confirm that the EHD flows are greatly influenced by the geometry of the electrodes. When
306 the top electrode was changed from plate to pin electrode, the flow velocity at the tip of the

307 electrodes was increased from nearly $0 \mu\text{m s}^{-1}$ to $\sim 150 \mu\text{m s}^{-1}$. We also noticed that in the
308 non-uniform electric field (pin/cylindrical-plate electrode configuration), the magnitude of
309 the EHD flow velocity changed with the distance of the electrodes, e.g. in the pin electrode
310 the flow velocity near the droplet decreased to $\sim 50 \mu\text{m s}^{-1}$, whereas in the uniform electric
311 field (plate-plate electrode configuration) the flow increased about $\sim 150 \mu\text{m s}^{-1}$ around the
312 droplet. This is because in the uniform electric field the field distribution was constant in the
313 system and the EHD flow velocity around the droplet depended on the particle coverage (for
314 more details see [26]), whereas in the non-uniform electric field the field strength was
315 strongest at the tip of the electrode, resulting in a maximum flow, and it became weaker
316 when it reached the droplet [44]. In **Fig. 8(d–f)**, we kept the fixed DC electric potential of 2.0
317 kV and changed the distance between the electrodes. When the distance was decreased
318 from 7 mm to 5 mm, the EHD flow velocity at the tip of the electrode increased from ~ 500
319 $\mu\text{m s}^{-1}$ to $\sim 550 \mu\text{m s}^{-1}$. In **Fig. 8(g–i)**, we kept the electrode distance fixed and the droplet
320 was subjected to different DC electric potentials (1.3–2.6 kV). We found that EHD flow at the
321 tip of the electrode was weaker at the lower electric potential, e.g. 1.3 kV, and the flow
322 velocity was $\sim 200 \mu\text{m s}^{-1}$. When the potential was increased to 2.6 kV the flow velocity
323 increased to $\sim 550 \mu\text{m s}^{-1}$. This is because when we minimized the space between the
324 electrodes or increased the electric potential, the surface charge density increased around
325 the pin electrode, resulting in stronger EHD flow velocity.

326 **4. Conclusions**

327 In this study, the deformation of particle-covered droplets was analyzed according to the
328 distance between the electrodes and their geometry. It was found that at a constant
329 electrode distance, the magnitude of the droplet deformation was strongest with the plate
330 electrode, whereas the weakest deformation was observed with the pin electrode.
331 Interestingly, we found the crossing point on the magnitude of the deformation curve with
332 two different sizes of electrodes when it touched the droplet. To compare our experimental
333 results with our theoretical calculation, we also estimated the magnitude of the droplet
334 deformation by using the Taylor model for different electrode geometries. The results show
335 good qualitative agreement with the experimental results, but the magnitude of the droplet
336 deformation is consistently smaller than the corresponding experimental results. This is

337 because the Taylor model does not account for the effect of surface charge convection,
338 which affects the magnitude of the droplet deformation by reducing it.

339 In another experiment we studied the structuring of the particles at the droplet interface
340 in a non-uniform electric field and created an opening area at the interface. The size of the
341 opening area can be controlled by changing the electrode distance as well as the applied
342 electric potential. We also showed that the opening area directly depends on the magnitude
343 of the droplet deformation. In the PIV experiment we found that the EHD flow is strongly
344 influenced by the geometry of the electrodes, the space between the electrodes, as well as
345 the applied electric potential. In the case of the non-uniform electric field, the strongest EHD
346 flow was observed around the tip of the pin electrode, whereas the weakest flow was found
347 around the droplet. But in the uniform electric field, the flow was stagnant around the plate
348 electrode (top electrode), whereas near the droplet it became stronger.

349 The findings of our studies are important for applications in electro-coalescence as well
350 as electro-emulsification. They are also important for designing electrodes for droplet-based
351 microfluidic systems. We expect that our work will influence further studies on the effect of
352 a non-uniform electric field on EHD deformation of particle-covered droplets.

353 **Acknowledgments**

354 This research was funded by the Polish National Science Centre through PRELUDIUM
355 (2019/35/N/ST5/02821) and OPUS (2015/19/B/ST3/03055) programs.

356 **References**

- 357 [1] A. Fery and R. Weinkamer, *Polymer* **48**, 7221 (2007).
358 [2] C. L. Tucker Iii and P. Moldenaers, *Annual Review of Fluid Mechanics* **34**, 177 (2002).
359 [3] Y. Zhu, H. Gao, W. Liu, L. Zou, and D. J. McClements, *Journal of Texture Studies* **51**, 45 (2020).
360 [4] S. Wang, Y. Zhong, and H. Fang, *Journal of Fluid Mechanics* **869**, 634 (2019).
361 [5] Y. Chang, X. Chen, Y. Zhou, and J. Wan, *Industrial & Engineering Chemistry Research* **59**, 3916
362 (2020).
363 [6] F. Mostowfi, K. Khristov, J. Czarnecki, J. Masliyah, and S. Bhattacharjee, *Applied Physics Letters*
364 **90**, 184102 (2007).
365 [7] Y. Peng, T. Liu, H. Gong, and X. Zhang, *International Journal of Chemical Engineering* **2016**,
366 2492453 (2016).
367 [8] F. Fanalista *et al.*, *ACS Nano* **13**, 5439 (2019).
368 [9] P. Lele, A. H. Syed, J. Riordon, N. Mosavat, A. Guerrero, H. Fadaei, and D. Sinton, *Journal of*
369 *Petroleum Science and Engineering* **165**, 298 (2018).
370 [10] C. C. Berton-Carabin and K. Schroën, *Annual Review of Food Science and Technology* **6**, 263
371 (2015).
372 [11] C. Albert, M. Beladjine, N. Tsapis, E. Fattal, F. Agnely, and N. Huang, *J Control Release* **309**, 302
373 (2019).
374 [12] D. Terescenco, N. Hucher, C. Picard, and G. Savary, *International Journal of Cosmetic Science* **42**,
375 198 (2020).

- 376 [13] A. Heyse, C. Plikat, M. Grün, S. Delaval, M. Ansorge-Schumacher, and A. Drews, *Process*
377 *Biochemistry* **72**, 86 (2018).
- 378 [14] P. He, Y. Liu, and R. Qiao, *Microfluidics and Nanofluidics* **18**, 569 (2015).
- 379 [15] Y. Jiang, X. Liu, Y. Chen, L. Zhou, Y. He, L. Ma, and J. Gao, *Bioresource technology* **153**, 278 (2014).
- 380 [16] Y. Chevalier, M.-A. Bolzinger, and S. Briançon, (2015), pp. 267.
- 381 [17] S. M. Dieng, N. Anton, P. Bouriat, O. Thioune, P. M. Sy, N. Massaddeq, S. Enharrar, M. Diarra,
382 and T. Vandamme, *Soft Matter* **15**, 8164 (2019).
- 383 [18] M. P. Neubauer, M. Poehlmann, and A. Fery, *Advances in Colloid and Interface Science* **207**, 65
384 (2014).
- 385 [19] A. B. Subramaniam, M. Abkarian, L. Mahadevan, and H. A. Stone, *Langmuir* **22**, 10204 (2006).
- 386 [20] S. Y. Tan, R. F. Tabor, L. Ong, G. W. Stevens, and R. R. Dagastine, *Soft Matter* **8**, 3112 (2012).
- 387 [21] R. Finken, S. Kessler, and U. Seifert, *Journal of Physics: Condensed Matter* **23**, 184113 (2011).
- 388 [22] H.-H. Boltz and J. Kierfeld, *Physical Review E* **92** (2015).
- 389 [23] C. Wischnewski and J. Kierfeld, *Physical Review Fluids* **3**, 043603 (2018).
- 390 [24] A. Mikkelsen and Z. Rozynek, *ACS Applied Materials & Interfaces* **11**, 29396 (2019).
- 391 [25] A. Mikkelsen, P. Dommersnes, Z. Rozynek, A. Gholamipour-Shirazi, M. d. S. Carvalho, and J. O.
392 Fossum, *Materials* **10**, 436 (2017).
- 393 [26] A. Mikkelsen, K. Khobaib, F. K. Eriksen, K. J. Måløy, and Z. Rozynek, *Soft Matter* **14**, 5442 (2018).
- 394 [27] Z. Rozynek, J. Banaszak, A. Mikkelsen, K. Khobaib, and A. Magdziarz, *Soft Matter* (2021).
- 395 [28] Z. Rozynek, K. Khobaib, and A. Mikkelsen, *ACS Applied Materials & Interfaces* **11**, 22840 (2019).
- 396 [29] P. F. Salipante and P. M. Vlahovska, *Physics of Fluids* **22**, 112110 (2010).
- 397 [30] R. B. Karyappa, S. D. Deshmukh, and R. M. Thaokar, *Physics of Fluids* **26**, 122108 (2014).
- 398 [31] N. Benteitis and S. Krause, *Langmuir* **21**, 6194 (2005).
- 399 [32] D. Das and D. Saintillan, *Journal of Fluid Mechanics* **829**, 127 (2017).
- 400 [33] M. M. Ahn, D. J. Im, and I. S. Kang, *Analyst* **138**, 7362 (2013).
- 401 [34] Y. Yao, Y. Wang, and K. M. Beussman, *Microfluidics and Nanofluidics* **17**, 907 (2014).
- 402 [35] S. Mhatre and R. M. Thaokar, *Physics of Fluids* **25**, 072105 (2013).
- 403 [36] C. Song, Q. Chen, X. Wang, L. Wen, and T. Zheng, in *2015 IEEE 11th International Conference on*
404 *the Properties and Applications of Dielectric Materials (ICPADM)2015*, pp. 652.
- 405 [37] J. Q. Feng, *Physical Review E* **54**, 4438 (1996).
- 406 [38] S. D. Deshmukh and R. M. Thaokar, *Journal of Fluid Mechanics* **731**, 713 (2013).
- 407 [39] P. Dommersnes, Z. Rozynek, A. Mikkelsen, R. Castberg, K. Kjerstad, K. Hersvik, and J. Otto
408 Fossum, *Nature Communications* **4**, 2066 (2013).
- 409 [40] Z. Rozynek, J. Banaszak, A. Mikkelsen, K. Khobaib, and A. Magdziarz, *Soft Matter* **17**, 4413 (2021).
- 410 [41] G. I. Taylor, A. D. McEwan, and L. N. J. de Jong, *Proceedings of the Royal Society of London. Series*
411 *A. Mathematical and Physical Sciences* **291**, 159 (1966).
- 412 [42] J.R. Melcher and G.I. Taylor, *Annual Review of Fluid Mechanics* **1**, 111 (1969).
- 413 [43] A. Mikkelsen, Z. Rozynek, K. Khobaib, P. Dommersnes, and J. O. Fossum, *Colloids and Surfaces*
414 *A: Physicochemical and Engineering Aspects* **532**, 252 (2017).
- 415 [44] S. Luo, J. Schiffbauer, and T. Luo, *Physical Chemistry Chemical Physics* **18**, 29786 (2016).
- 416 [45] K. Khobaib, T. Hornowski, and Z. Rozynek, *Physical Review E* **103**, 062605 (2021).

Appendix I: List of other publications

1. Assembly of 1D granular structures from sulfonated polystyrene microparticles.
A Mikkelsen, A Kertmen, **K Khobaib**, M Rajňák, J Kurimský and Z Rozynek
Materials **10(10)**, 1212 (2017)

The above listed paper is not a part of this dissertation, but it was completed with my contributions in the laboratory during the time of my PhD work.

Appendix II: List of significant conference presentations

1. International Soft Matter Conference 2019, Edinburgh, UK, 03–07.05.2019, **poster presentation**: *Opening and closing of particle shells on droplets via electric fields and its applications.*
2. American Physical Society, March Meeting 2019, Boston, United States, 04–08.03.2019, **oral presentation**: *Active structuring of a particle film on a droplet's surface and examples of its applications.*
3. Jülich Soft Matter Days, Jülich, Germany, 20–23.11.2019, **poster presentation**: *Deformation of particle-laden droplets and controllable surface particle assembly by using electrohydrodynamic flows.*
4. 20th International Conference on Atomic, Molecular, Soft Matter and Biological Physics, Vienna, Austria, 14–15.06.2018, **oral presentation**: *Deformation of particle-laden droplet in viscous liquid under DC electric fields.*
5. NanoTech Poland International Conference & Exhibition, Poznań, Poland, 06–09.06.2018, **poster presentation**: *Deformation of particle laden droplets and controllable surface particle assembly by using electrohydrodynamics flow.*
6. 47th Winter School on Wave and Quantum Acoustics, Szczyrk, Poland, 26–28.02.2018, **poster presentation**: *Manipulation of microparticles in Oil droplets by ultrasonic and electric fields.*
7. 44. Zjazd Fizyków Polskich (44ZFP), Wrocław, Poland, 10–15.09. 2017, **poster presentation**: *Quincke rotation of particle laden drops.*
8. Danube Vltava Sava Polymer Meeting (DVSPM) 2017, Vienna, Austria, 05–08.09.2017, **oral presentation**: *Electric field-driven assembly of sulfonated polystyrene microspheres.*
9. NanoTech Poland International Conference & Exhibition, Poznań, Poland 01–03.06.2018, **oral presentation**: *Electric field-driven assembly of sulfonated polystyrene microspheres.*
10. International Winter School: The Geilo School 2017: Physics Inspired by Living Matter, Geilo, Norway, 20–30.03.2017, **poster presentation**: *Electric field-driven assembly of sulfonated polystyrene microspheres.*

Appendix III: List of awards and distinctions

1. Best presentation award at “International Conference on Atomic, Molecular, Soft Matter and Biological Physics”, Vienna, Austria
2. Scholarship from “UNIWERSYTET JUTRA” for 3-month internship in University of Oslo, Norway
3. Scholarship for PhD student at the Faculty of Physics, Adam Mickiewicz University, Poznań, (2017–2018)
4. Pro-quality scholarship, Adam Mickiewicz University, Poznań, (2017–2018)
5. Scholarship for PhD student at the Faculty of Physics, Adam Mickiewicz University, Poznań, (2018–2019)
6. Pro-quality scholarship, Adam Mickiewicz University, Poznań, (2018–2019)
7. Scholarship for PhD student at the Faculty of Physics, Adam Mickiewicz University, Poznań, (2019–2020)
8. Pro-quality scholarship, Adam Mickiewicz University, Poznań, (2019–2020)
9. Rector Scholarship for the best Ph.D. student at Adam Mickiewicz University (2019–2020)

Oświadczenie

Ja, niżej podpisany, Khobaib Khobaib, doktorant Wydziału Fizyki Uniwersytetu im. Adama Mickiewicza w Poznaniu oświadczam, że przedkładaną rozprawę doktorską pt.:

Experimental studies of particle-covered droplets in electric fields: Mechanical and rheological properties of droplets and interfacial particle organization

napisałem samodzielnie. Oznacza to, że przy pisaniu pracy, poza niezbędnymi konsultacjami, nie korzystałem z pomocy innych osób, a w szczególności nie zlecałem opracowania rozprawy lub jej istotnych części innym osobom, ani nie odpisywałem tej rozprawy lub jej istotnych części od innych osób.

Równocześnie wyrażam zgodę na to, że w sytuacji gdyby powyższe oświadczenie okazało się nieprawdziwe, decyzja o nadaniu mi stopnia naukowego doktora zostanie cofnięta.

Khobaib Khobaib

Khobaib Khobaib